Zolensky ME and McSween, HY Jr (1988) Aqueous alteration. *In* Meteorites and the Early Solar System (JF Kerridge, MS Matthews eds) Univ. of Arizona, Tucson, 114-143
Zolensky ME, Score R, Schutt JW, Clayton RN, Mayeda TK (1989a) Lea County 001, an H5 chondrite, and Lea County 002, an ungrouped type 3 chondrite. Meteoritics 24:227-232
Zolensky ME, Barrett R, Prinz M (1989b) Petrography and mineralogy of Yamato-86720 and Belgica-7904. 14th Symp Ant Meteorites 24-26
Zolensky ME, Barrett R, Prinz M (1989c) Petrography, mineralogy and matrix composition of Yamato-82162, a new CI2 chondrite (abstr). Lunar Planet Sci XXVI:1253-1254
Zolensky ME, Prinz M, Lipschutz ME (1991) Mineralogy and thermal history of Y-82162, Y-86720, B-7904. Abstr Symp Antarct Met 16:195-196
Zolensky ME, Hewins RH, Mittlefehldt DW, Lindstrom MM, Xiao X, Lipschutz ME (1992) Mineralogy, petrology and geochemistry of carbonaceous chondritic clasts in the LEW 85300 polymict eucrite. Meteoritics 27:596-604
Zolensky ME, Barrett T, Browning L (1993) Mineralogy and composition of matrix and chondrule rims in carbonaceous chondrites. Geochim Cosmochim Acta 57:3123-3148
Zolensky ME, Weisberg MK, Buchanan PC, Mittlefehldt DW (1996a) Mineralogy of carbonaceous chondrite clasts in HED achondrites and the Moon. Met Planet Sci 31:518-537
Zolensky ME, Ivanov AV, Yang V, Mittlefehldt DW, Ohsumi K (1996b) The Kaidun meteorite: Mineralogy of an unusual CM1 lithology. Meteoritics 31:484-493

Chapter 4

NON-CHONDRITIC METEORITES FROM ASTEROIDAL BODIES

David W. Mittlefehldt
C23/Basic and Applied Research Departnment
Lockheed Martin SMSS Company
Houston, Texas 77058

Timothy J. McCoy
MRC 119, Department of Mineral Sciences
National Museum of Natural History
Smithsonian Institution
Washington, DC 20560

Cyrena A. Goodrich
Abteilung Kosmochemie
Max-Planck-Institute für Chemie
Postfasch 3060
55020 Mainz, Germany

Alfred Kracher
Department of Geological Sciences
Iowa State University
Ames, Iowa 50011

INTRODUCTION

This chapter considers all meteorites which are of asteroidal origin and which do not contain members displaying classic chondritic textures (i.e. chondrules in a fine-grained matrix). This chapter forms a logical bridge between the previous chapter on chondrites, and the following chapters on lunar and martian rocks, the products of planetary differentiation. We cover a wide range of petrologic types including undifferentiated, but highly metamorphosed chondritic materials, melt-depleted ultramafic rocks, ultramafic and mafic cumulates, mafic melts, metallic cumulates and melts, and stony-irons composed of various materials. In addition, we will touch on several unique non-chondritic meteorites, and on achondritic clasts from chondrites that do not appear to be impact melts. Table 1 summarizes the major meteorite types covered in this chapter, gives a synopsis of the characteristic mineralogies and petrologies, and probable modes of origin. The mineralogy of all meteorite groups was reviewed by Rubin (1997).

The meteorites and meteorite groups covered here have experienced a wide range of planetary processes. At one extreme, we have rocks such as the acapulcoites, which seem to be simply ultra-metamorphosed chondritic material. It is debatable whether these rocks ever reached their solidi, although the textures suggest some mobilization of minimum melts in the Fe,Ni-FeS system. At the other extreme, we have rocks such as the eucrites, which are planetary basalts far removed in composition from that of their bulk parent body. We also have materials, such as the IIE irons, in which impact mixing, and possibly melting, must have played an important role. We have rocks, the aubrites, that were formed under such low oxygen fugacities that elements normally strongly lithophile in character, Ca and the rare earth elements (REE), behaved as chalcophile elements. Finally, some of the meteorite types exhibit curious mixtures of nebular and planetary properties, such as the lodranites and ureilites.

0275-0279/98/0036-0004$20.00

Table 1. Synopsis of petrologic characteristics of meteorite groups and modes of origin.

GROUP	MINERALOGY	PETROLOGY	LIKELY ORIGIN
magmatic irons, and pallasite and mesosiderite metal phase	kamacite, tetrataenite, martensite, awaruite troilite, schreibersite ± graphite	coarse-grained metal, generally exsolved	fractional crystallization of core
non-magmatic irons IAB, IIE, IIICD metal phase	kamacite, tetrataenite, martensite, awaruite troilite, schreibersite ± graphite	coarse-grained metal, generally exsolved	impact melting (?)
IAB-IIICD silicate inclusions, winonaites	olivine, orthopyroxene, clinopyroxene, sodic plagioclase, ultrametamorphism, partial melting, impact mixing troilite, metal, daubreilite, schreibersite, graphite		fine-grained equigranular
IIE silicate inclusions	olivine, pyroxene, sodic plagioclase, metal, troilite; orthopyroxene, sodic plagioclase; orthopyroxene, clinopyroxene, sodic plagioclase	chondritic to gabbroic to silica-alkali-rich	metamorphism, partial melting, melt migration, shock
pallasites, silicates	olivine, chromite ± low-Ca pyroxene	coarse-grained, rounded to angular	cumulates from core-mantle boundary
IVA silicate inclusions	silica ± orthopyroxene	coarse-grained, igneous	partial melting (?)
brachinites	olivine, augite, Fe-sulfide, ± orthopyroxene ± sodic plagioclase	medium- to coarse-grained equigranular	metamorphosed chondrite, partial melting residue
acapulcoites-lodranites	olivine, orthopyroxene, clinopyroxene, metal ± troilite ± sodic plagioclase	fine- to coarse-grained equigranular	ultrametamorphism, partial melting ± melt migration
ureilites	olivine, pyroxene (some combination of pigeonite, orthopyroxene, augite)	coarse-grained granular	partial melting residue
aubrites	enstatite, forsterite, sodic plagioclase, metal, numerous sulfides	breccias of igneous lithologies	melted and crystallized residues from partial melting
diogenites, eucrites, howardites	orthopyroxene, olivine, chromite; pigeonite, calcic plagioclase, silica	coarse-grained orthopyroxenites, gabbros, fine- to coarse-grained basalts, brecciated	cumulates, crystallized melts, impact mixing
angrites	Al-Ti-diopside, anorthite, calcic olivine	fine- to coarse-grained igneous	crystallized melts, cumulates (?)
mesosiderites	orthopyroxene, olivine, chromite, pigeonite, calcic plagioclase, silica, phosphates	breccias of igneous lithologies, impact melts	impact melted crustal igneous lithologies

Figure 1. Oxygen-isotope plot for non-chondritic meteorites from asteroidal sources. In all parts of this figure, unlabeled symbols are for several different meteorite types, which will be separated and labeled in subsequent parts. The terrestrial fractionation (TF) and Allende mixing (AM) lines are shown for reference. (a) The entire range in O-isotopic compositions, showing the distributions of anomalous irons (iron-an), Eagle Station pallasites (es-pal), and ureilites (urei). The anomalous irons Bocaiuva (B) and Tucson (T) discussed in the chapter are labeled. Silicate and chromite samples of the anomalous iron Mbosi are connected with a tie line. (b) Metal-rich meteorites and winonaites plot along three mass fractionation lines; the IAB and IIICD irons and winonaites (win) plot on one below the terrestrial fractionation line, and the IIE and IVA irons on lines at higher $\Delta^{17}O$. The closely related acapulcoites and lodranites (aca-lod) form a cluster with significant dispersion in $\Delta^{17}O$. Aubrites (aub) are the only non-chondritic asteroidal meteorites that fall on the terrestrial fractionation line. The anomalous irons Guin (G) and Sombrerete (S) discussed in the chapter are labeled. (c) This portion of the figure clearly shows the much greater dispersion in $\Delta^{17}O$ for the acapulcoites and lodranites compared to many other non-chondritic meteorites, such as the IIIAB irons, main-group pallasites (mg-pal) and brachinites (brac). The two pyroxene pallasites (py-pal) plot near two members of the acapulcoite-lodranite clan. The unique achondrite Divnoe is similar in O-isotopic composition to the IAB and IIICD irons and winonaite meteorites, but distinct from them in $\Delta^{17}O$. The unique achondrite LEW 88763 (L) and the IIIAB iron containing chondritic silicates Puente del Zacate (PZ) discussed in the chapter are labeled. (d) An extreme close-up view shows the general O-isotopic similarity of the IIIAB irons, main-group pallasites, howardites, eucrites and diogenites (HED), mesosiderites (mes), angrites (ang) and brachinites. The unique meteorite Enon also occupies this region of O-isotope space. All data are from Clayton and Mayeda (1996).

Figure 1 places the meteorites discussed here in O-isotope space. Many of the meteorite groups, especially those that exhibit the clearest signature of planetary style igneous processes, occupy a fairly narrow region of O-isotope space just below the

terrestrial fractionation line. However, overall, the non-chondritic meteorites occupy much of known solar system O-isotope space, and therefore have probably sampled parent bodies formed at various locations in the solar system.

The organization of this chapter is difficult to put in any single logical order. Logically, we should start where the last chapter left off, and discuss those meteorite groups that are closest to chondritic material, and work our way sequentially through more and more differentiated materials. This works well for the silicate-rich meteorites, but to some extent, the irons are quite distinct and do not fit in. Yet there are numerous interconnections between metallic and silicate materials; winonaites and IAB irons, and main-group pallasites and IIIAB irons, for example. Because of this, we will first discuss iron meteorite groups, presenting their petrologic and chemical characteristics. Armed with knowledge of the irons, we will then move on to tackle the achondrites and stony-irons.

There are a few conventions we will follow in this chapter. The Antarctic Meteorite Newsletter put out by the Office of the Curator at Johnson Space Center contains very basic mineralogical data that may be the only source of information for some poorly studied meteorites. Rather than fill the reference list with citations to these, we will refer to them in the body of the text, figure captions and tables as AMN X-Y, which means volume X, number Y of the newsletter. We use the definition of $\Delta^{17}O = \delta^{17}O - 0.52\,\delta^{18}O$ as given by Clayton (e.g. see Clayton and Mayeda 1996). We also here define mg# as molar 100*MgO/(MgO+FeO). When discussing modal mineralogy data, we will specify either wt % or vol % when it is known. If the author was not clear which was being used, we will opt for the nebulous %. Normalization to chondritic abundances are done using the CI values of Anders and Grevesse (1989). Finally, some mineral names are no longer officially recognized. We have used whitlockite instead of merrillite, and aluminian-titanian-diopside instead of fassaite throughout, regardless what was used in the original references.

IRON METEORITE GROUPS AND THE METAL PHASE OF STONY IRONS

General metallography and mineralogy

Metallic nickel-iron constitutes the largest mass proportion of extraterrestrial material available for study on earth. Among observed falls, however, iron meteorites account for only about 5%. Metallic meteorites are thus overrepresented in collections, because they are both durable and easy to recognize.

A typical iron meteorite consists mostly of metallic iron with 5 to 20% Ni, which is texturally continuous over the size of the meteorite, and contains various minor phases as inclusions. There are, however, individual exceptions to all of these features. Samples with up to 60% Ni are known, some meteorites are brecciated on a millimeter-to-centimeter scale, and a few objects are classified as metal-rich, even though they contain more sulfide than metal. However, no authenticated iron meteorite is known that contains less than 4% Ni. A thorough description of practically all iron meteorites known by the 1970s was presented by Buchwald (1975).

A number of meteorites consist partly of metallic iron and partly of silicates, and these are traditionally classified as stony-iron meteorites. In addition to the two major classes of stony-irons, pallasites and mesosiderites, some unusual individuals such as Lodran and Enon are often included in this category. However, the division between irons and stony-irons is somewhat arbitrary, since some iron meteorite breccias of group IAB contain as much silicate as mesosiderites, and some pallasites contain large silicate-

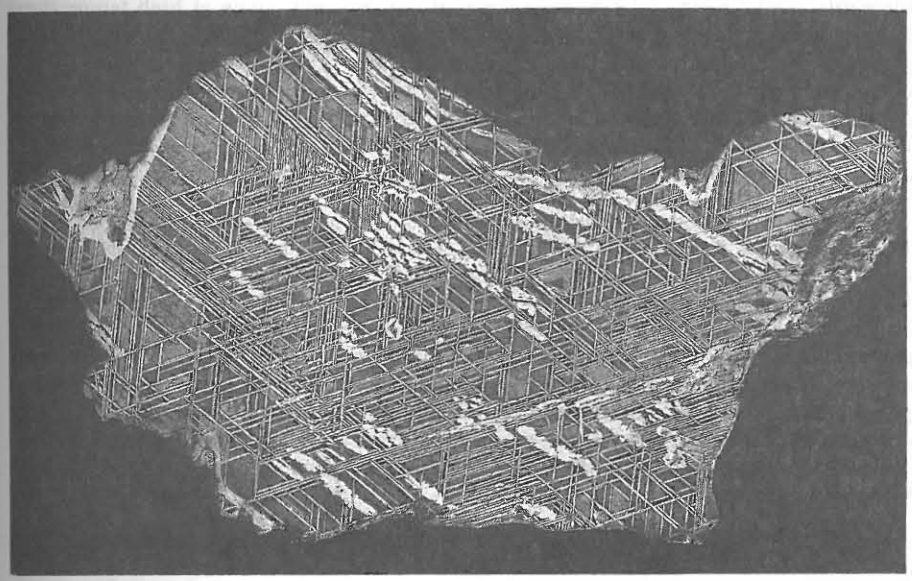

Figure 2. Photograph of a polished and etched slab of the Edmonton (Kentucky) IIICD iron meteorite, showing the Widmanstätten structure of a fine octahedrite (Of) with an average bandwidth of ~0.32 mm. The slab is 12 cm in its long dimension.

free areas of metal. Stony-irons and irons are sometimes collectively called "metal-rich meteorites" (Wasson 1974) to indicate that their metal content is higher than that of average solar system material.

The metallic phase of many iron meteorites shows a texture called the Widmanstätten pattern, an oriented intergrowth of body-centered cubic α-Fe,Ni, and high-Ni regions which consist of several phases (Fig. 2). The structure can be revealed by etching a well-polished sample with nital, a 2% solution of nitric acid in ethanol. The Widmanstätten pattern was discovered independently by G. Thompson and E.C. Howard in the first decade of the 19th century, some time prior to the eponymous Alois Beckh von Widmannstätten. Note that German literature, following the spelling of the proper name, uses "Widmannstätten" with "-nn-" whereas English literature always refers to "Widmanstätten structure" with a single "-n-."

The α-Fe,Ni phase, kamacite (known as ferrite in metallurgy), forms extensive lamellae with a Ni content <6%. A wide range of lamella widths is found among different meteorites, but within each one, the width of the kamacite lamellae is approximately constant. The more Ni-rich areas are generally referred to as taenite, but detailed study shows that these areas are complex mixtures of phases. A profile of the Ni content of taenite lamellae is generally M-shaped, with Ni contents close to 50% within a few micrometers of the kamacite interface, and much lower contents at the center of the lamellae. The 50% Ni region has subsequently been found to be an ordered, tetragonal phase of FeNi composition named tetrataenite (Clarke and Scott 1980). A sub-micron intergrowth of Ni-poor and Ni-rich phases called plessite is present within the taenite regions of more Ni-rich samples.

The formation of the Widmanstätten structure can be understood by considering the Fe-Ni phase diagram (Swartzendruber et al. 1991, Yang et al. 1996). Above about 800°C

meteoritic metal forms γ-Fe,Ni regardless of composition, since at high temperatures there is no miscibility gap. During slow cooling α-Fe,Ni precipitates along the {111} planes of the γ-Fe,Ni parent. Depending on the bulk Ni content, nucleation of α-Fe,Ni occurs between 500° and 800°C, the lower temperatures corresponding to higher Ni contents. The continuity of the Widmanstätten structure in many large meteorite samples indicates that at the high temperature stage the γ-Fe,Ni crystals reached sizes of tens of centimeters to meters.

Taenite has traditionally been considered to be γ-Fe,Ni with varying Ni content, except for minor regions of tetrataenite. Recent work by Yang et al. (1997a,b) has cast doubt on this generally accepted picture. Based on detailed studies of the Ni-rich lamellae, they have concluded that if γ-Fe,Ni is present at all, it is only of minor importance. Most of the original γ-Fe,Ni undergoes complex decomposition reactions at temperatures below 400°C. Areas with Ni contents between 30% and 50% are actually intergrowths of tetrataenite and a body-centered cubic phase referred to as α_2-Fe,Ni. This phase is structurally identical to martensite, but unlike industrial martensite it did not originate by fast cooling. A very thin layer of awaruite, $FeNi_3$, separates the tetrataenite regions from kamacite. The bulk of the kamacite lamellae is apparently unaffected by the low-temperature reactions in the taenite region.

This reinvestigation of the Ni-rich areas of the Widmanstätten pattern represents a drastic revision of the traditional picture of iron meteorite mineralogy, and its implications have not yet become clear. Since diffusion in Fe-Ni alloys is too slow at low temperatures for an experimental determination of equilibrium reactions, most of the Fe-Ni phase diagram below 400°C is actually based on the phases observed in iron meteorites (Reuter et al. 1988, Yang et al. 1996, 1997b). Although meteorites as a natural long-term experiment have considerably increased our knowledge of Fe-Ni phase relations, the element of circularity that is thereby introduced invites caution when the meteorite-derived phase diagram is used to interpret meteorite structures.

The characteristic Widmanstätten pattern thus consists of lamellae of kamacite, separated by Ni-rich lamellae composed of several phases. Because kamacite lamellae are oriented along octahedral planes, meteorites that show this structure are known as octahedrites. According to the width of their kamacite lamellae, octahedrites are further subdivided into coarsest (Ogg, bandwidths >3.3 mm), coarse (Og, 1.3–3.3 mm), medium (Om, 0.5–1.3 mm), fine (Of, 0.2–0.5 mm), and finest octahedrites (Off, <0.2 mm). Plessitic octahedrites (Opl) are transitional to ataxites. The bandwidth boundaries, based on classifications developed in the 19th century, were redefined by Buchwald (1975) in such a way that most chemically related meteorites now fall into the same structural class. A few iron meteorites do not fit this textural classification scheme, and are regarded to have an anomalous texture. Some of these are specimens in which the Widmanstätten pattern has been partly or wholly obliterated by reheating in space (e.g. Juromenha; see Fig. 116 in Buchwald 1975, p. 95).

Samples with very high Ni content undergo the γ-α transformation at such low temperatures that only small kamacite spindles but no continuous lamellae form, and the texture is only microscopically visible. These meteorites are known as ataxites, designated D, and most have bulk Ni contents of ≥15%.

Some iron meteorites with Ni contents below 6% consist almost entirely of kamacite and show no Widmanstätten pattern; they are called hexahedrites and are designated H. The name refers to the cubic (hexahedral) cleavage of α-Fe,Ni single crystals. Most hexahedrites belong to chemical group IIA.

Etched kamacite in both hexahedrites and octahedrites usually shows features called Neumann bands, which are mechanical twins on the {211} planes of α-Fe,Ni. Twinning is induced by shock, either due to collisions in space, or during atmospheric passage (Buchwald 1975). Neumann bands can be best seen on the large, continuous kamacite crystals of hexahedrites, from which the usually more conspicuous Widmanstätten pattern is absent.

The ubiquity of Neumann bands indicates that they are formed easily at relatively low levels of shock. Most iron meteorites, however, show evidence of higher levels of shock as well. Shock pressures >13 GPa lead to a transient transformation of α-Fe,Ni to the high pressure ε modification, which manifests itself as "hatched kamacite." Even more severely shocked samples often show signs of eutectic melting at the edge of troilite nodules, secondary reactions of metal with carbide and phosphide, and deformation and even partial obliteration of the Widmanstätten pattern.

In addition to forming Widmanstätten lamellae or (in Ni-rich samples) kamacite spindles, α-Fe,Ni also commonly nucleates at the interface of non-metallic inclusions. This morphology, called swathing kamacite, forms around inclusions of troilite, schreibersite, silicates, etc., as a continuous layer of kamacite, which can be twice as wide as the average width of Widmanstätten lamellae (Buchwald 1975, p. 89).

Mineralogy of accessory phases

Except for a few transitional cases, there is a visually obvious difference between two types of mineral occurrences in metal-rich meteorites: (a) a major non-metallic lithology in meteorites such as pallasites or iron-silicate breccias such as Woodbine, and (b) minor occurrences of non-metallic minerals that are accessory phases within the metallic lithology. Separate sections of this chapter are dedicated to the silicate portions of stony-irons and iron-silicate breccias.

Table 2 gives an overview of minerals associated with the metal phase. By far the most common non-metallic minerals are troilite, schreibersite, and graphite. The carbides cohenite or, less frequently, haxonite, are common in some groups. In a small number of meteorites, notably the large Canyon Diablo iron associated with Meteor Crater, Arizona, some graphite has been transformed into diamond and lonsdaleite, a hexagonal high-pressure polymorph (Frondel and Marvin 1967), due to shock. Some graphite has formed by decomposition of cohenite, but it is also found as rims around non-metallic inclusions in a morphology that suggests subsolidus exsolution from the metal. "Cliftonite" is a carbon occurrence with cubic morphology, but is crystallographically identical to graphite. Its shape is imposed by the cubic structure of the host metal.

Troilite, the hexagonal, practically stoichiometric (Fe:S mole ratio usually ≥0.98) modification of FeS, differs structurally from terrestrial pyrrhotite. Schreibersite, $(Fe,Ni)_3P$, occurs either as coarse irregular or skeletal inclusions, or as very small euhedral crystals in the shape of rods or platelets. The latter were originally thought to be a different mineral, and named "rhabdite," a name still used to refer to this particular morphology. The Ni content of troilite is generally negligible, but both schreibersite and cohenite, $(Fe,Ni)_3C$, contain appreciable amounts of Ni. When they are in equilibrium, cohenite contains less and schreibersite more Ni than the host metal.

Platelet-shaped inclusions of chromite, troilite, or both, are relatively common. They can reach cm in size, but are usually only a few μm thick. Known as Reichenbach lamellae, they are mostly oriented along cubic planes of the parent γ crystal (Buchwald 1975), and enveloped by swathing kamacite. Their morphology suggests exsolution from the host metal.

Table 2. Mineralogy of the metal phase of iron and stony iron meteorites.

Elements and alloys			
kamacite	α-Fe,Ni (<6% Ni)	1	
martensite*	α_2-Fe,Ni	1	
taenite*	Fe,Ni (>30% Ni)	1	A
tetrataenite	FeNi	1	
awaruite	Ni_3Fe	1	
graphite	C (hexagonal)	2	
diamond	C (cubic)	5	
lonsdaleite*	C (hexagonal)	5	
copper	Cu	4	B
Sulfides			
troilite	FeS (hexagonal)	1	
mackinawite	FeS (tetragonal)	5	
sphalerite	(Zn,Fe)S	4	
alabandite	MnS	4	
pentlandite	$(Fe,Ni)_9S_8$	5	
chalcopyrite	$CuFeS_2$	3	
brezinaite*	Cr_3S_4	5	
daubréelite*	$FeCr_2S_4$	2	
djerfisherite	$K_3CuFe_{12}S_{14}S$	4	
Carbides, nitrides, phosphides			
cohenite	$(Fe,Ni)_3C$	2	
haxonite*	$(Fe,Ni)_{23}C_6$	3	
unnamed iron carbide*	$Fe_{2.5}C$	5	
carlsbergite*	CrN	3	
roaldite*	Fe_4N	4	
schreibersite*	$(Fe,Ni)_3P$	2	
Oxides			
chromite	$FeCr_2O_4$	3	C
silica	SiO_2	4	D
Phosphates			
sarcopside	$(Fe,Mn)_3(PO_4)_3$	4	
graftonite	$(Fe,Mn)_3(PO_4)_3$	4	
beusite	$Fe_3Mn_3(PO_4)_4$	5	E
buchwaldite*	$NaCaPO_4$	4	
galileiite*	$Na(Fe,Mn)_4(PO_4)_3$	4	
brianite*	$Na_2CaMg(PO_4)_2$	5	F
panethite*	$Na_2(Mg,Fe)_2(PO_4)_2$	5	F
farringtonite*	$(Mg,Fe)_3(PO_4)_2$	5	F
johnsomervilleite*	$Na_2Ca(Fe,Mg,Mn)_7(PO_4)_8$	5	
maricite*	$NaFePO_4$	5	

Column 3: Frequency of occurrence (see text for further explanation); 1 - ubiquitous, 2 - very common, 3 - common minor mineral, 4 - rare, 5 - only found in one or a few meteorites, * - not know as terrestrial minerals.
Column 4: notes; A - Taenite is apparently not a single phase (see text). Additional types of metal, such as ε-iron, can be produced by shock, B - The presence of small amounts of Cu-sulfides is suspected, but has never been unambiguously confirmed, C - Chromite associated with silicate inclusions contains Mg, Al, etc., but chromite associated with metal is usually close to pure $FeCr_2O_4$ in composition, D - Both tridymite and cristobalite have been found in iron meteorites, and other silica polymorphs may be present, E - Structurally continuous with graftonite; unlike all terrestrial beusite, the meteoritic variety is Ca-free, F - Brianite, panethite, and farringtonite may be part of a separate oxide/silicate lithology in the few meteorites where they have been found.

Most of the minerals listed in Table 2 have been discussed in greater detail by Buchwald (1977), but more have been discovered since then, for example roaldite, Fe_4N, (Nielsen and Buchwald 1981) and galileiite, $Na(Fe,Mn)_4(PO_4)_3$ (Olsen and Steele 1997). Other compounds known or suspected to be present are as yet insufficiently characterized to be either identified as a known mineral or described as a new one. Some phosphates, like brianite, panethite, and farringtonite, are probably more closely related to silicate inclusions, but are included in Table 2 because of their ambiguous status.

Several minerals in Table 2 are only known from meteorites, some others have been discovered in meteorites first, and only later found at a terrestrial location. Meteoritic minerals that have no naturally occurring terrestrial counterpart are identified with an asterisk in Table 2. Some of these are common in industrial products. For example, the mineral cohenite, Fe_3C, is a common inclusion in steel where it is known as cementite.

Column 3 of Table 2 denotes the frequency of occurrence by assigning minerals to five categories in order of decreasing abundance. By definition, all metal-rich meteorites contain one or more of the iron-nickel phases. A few other minerals, such as troilite and schreibersite, are also present in nearly all samples, and are designated "ubiquitous." A 2 denotes those minerals that are so common that they can usually be found in most large specimens. Rare minerals are designated 3 to 5 according to the following criteria: minerals that are present in many meteorites, but usually only in very small amounts, are assigned to category 3. An example is carlsbergite, CrN, which occurs in many members of several groups of irons, but in very small amounts (Buchwald and Scott 1971). Minerals that occur in only one or a few meteorites are assigned to categories 4 and 5. For minerals in category 5 there are usually theoretical reasons, in addition to observation, to assume that the mineral is confined to unusual specimens, such as in the case of brezinaite, Cr_3S_4, which occurs only in the highly reduced Tucson iron (Bunch and Fuchs 1969, Nehru et al. 1982). On the other hand, a mineral such as buchwaldite (Olsen et al. 1977), although rare, may well be present in many more samples than observed so far, and is therefore assigned to category 4.

Classification and chemical groups

Whereas the subdivision into hexahedrites, octahedrites, and ataxites is purely descriptive, a genetically more significant taxonomy is based on the trace element content of the metal phase. In a series of papers (Wasson 1967, 1969, 1970; Wasson and Kimberlin 1967, Wasson and Schaudy 1971, Schaudy et al. 1972, Scott et al. 1973, Scott and Wasson 1976, Kracher et al. 1980, Malvin et al. 1984, Wasson et al. 1989, 1998a,b) data on Ni, Ga, Ge, and Ir have been published on practically all known metal-rich meteorites, and several more elements have been determined in most others. When all likely pairings of samples are taken into account, the number of independent iron meteorites that had been analyzed as of 1990 was about 605 (Wasson 1990).

On plots of log(E) vs. log(Ni), where E denotes some well determined trace element, about 85% of iron meteorites are seen to fall into one of 13 clusters or chemical groups. With two exceptions these groups fall within restricted areas on a log(Ge) vs. log(Ni) plot (Fig. 3a), whereas on log(Ir) vs. log(Ni) plots (Fig. 3b) the same samples form narrow, elongated fields spanning a considerable range in Ir contents. It is customary to refer to these clusters as groups if they contain at least five members. Samples that fall outside defined chemical groups are called ungrouped (or sometimes anomalous) iron meteorites, and some of these form grouplets of two to four related individuals (Scott 1979a).

The fields outlined in Figure 3 are not equally populated, which is indicated by shading the more densely populated areas. For example, the shaded part of the IAB field

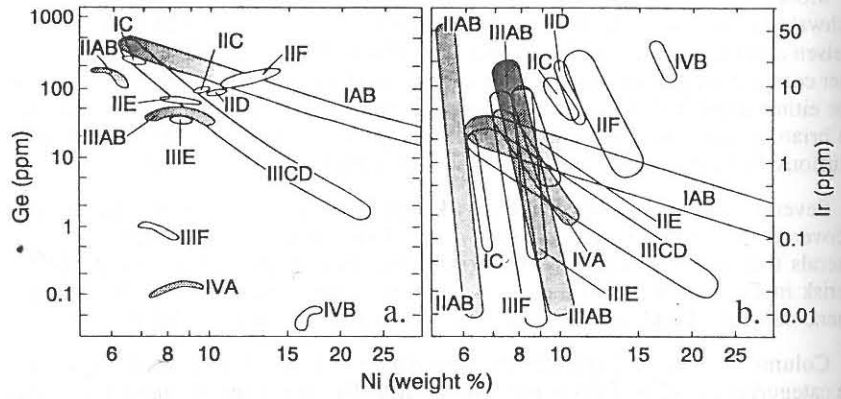

Figure 3. Plots of (a) Ge vs. Ni and (b) Ir vs. Ni showing the fields for the 13 iron meteorite groups. Germanium is one of the elements originally used to classify irons into groups I through IV based on decreasing Ge and Ga content. Note that most iron meteorite groups have limited ranges in Ge and Ni content; groups IAB and IIICD are unusual on this plot. The Ir content of most iron meteorite groups varies enormously from low to high Ni members, due to its strong fractionation between solid and liquid metal. This results in the observed steep trends on this plot for these so-called magmatic iron meteorite groups. Again, IAB and IIICD irons show an unusual distribution on this plot.

contains about 100 meteorites, whereas only 3 samples fall in the region ≥25% Ni. Likewise, in groups IIAB, IIIAB and IVA, the low-Ni, high-Ir regions contain more members than the opposite end of the outlines. The shaded areas in Figure 3 account for about half of all known iron meteorites.

The taxonomic significance of Ga and Ge derives from the fact that they are the most volatile siderophile elements (Wasson and Wai 1976, Wai and Wasson 1979), and in analogy to the situation in chondrites, more volatile elements tend to be more strongly fractionated between different groups (Wai and Wasson 1977). Thus both Ga and Ge show a narrow range within groups of similar iron meteorites, but large differences between different groups.

Early determinations of these elements (Lovering et al. 1957) resolved only four groups, designated by Roman numerals I through IV in order of decreasing content of Ga and Ge. Letters were added later, as in IVA and IVB, to distinguish additional groups. Not all of these groups proved to be independent, however, leading to the current nomenclature, in which some groups have a combination of two letters after their Roman numeral. For example, as more samples were analyzed, the hiatus between IIIA and IIIB was filled in, and the entire group is now designated IIIAB. On the other hand, no genetic relationship exists between groups IVA and IVB. A more detailed explanation of this nomenclature, together with a compilation of Ni, Ga, Ge, and Ir data, can be found in Wasson (1974).

Average compositions of the chemical groups calculated by Willis (1980) are given in Table 3. For elements like Ga, which do not show a large range within a given group, determining the average group content is fairly straightforward. However, in the case of an element like Ir, the "average" is model-dependent. As explained in more detail in the "Origin" section below, the modification of the Willis (1980) averages listed in Table 3 refer to models of the parent material from which the meteorites formed, rather than the average of actually analyzed samples.

Table 3. Average compositions of iron meteorite chemical groups.

Group	structure*	Ni wt%	Ga µg/g	Ge µg/g	Ir µg/g	C µg/g	P mg/g	S wt%	Cr µg/g	Co mg/g	Cu µg/g	Mo µg/g	W µg/g	Pd µg/g	Au µg/g	As µg/g	Sb ng/g	Group
IAB	see note 1	6.4	96	400	2.7	-	2.1	-	16	4.6	132	8.2	1.6	3.5	1.5	11	270	IAB
IC	var.	7.1	51.7	230	0.38	-	4.3	-	70	4.6	160	7.7	1.3	3.5	1.14	11	98	IC
IIAB	H (IIA)	6.15	58.3	173	10	2000[a]	6	0.20[a]	38	5.3	129	6.9	2.1	2.6	1.1	9.9	201	IIAB
	Ogg (IIB)	6.1[a]	-	64[b]	11a	-	20[a]	17.0[b]	-	-	-	-	-	-	1.0[a]	-	-	IIAB
		5.1[b]	-	-	1.3b	-	10[b]	-	-	-	-	-	-	-	-	-	-	IIAB
IIC	Opl	10.8	37.3	94.6	6.4	-	5.3	-	87	6.5	260	8.4	-	6	1.1	8.2	150	IIC
IID	Om	11.2	76.2	87	9.9	-	9.8	-	31	4.7	280	9.4	2.4	5.3	1.1	10	220	IID
IIE	anom.	9.13	24.4	68.3	4.1	-	-	-	-	4.7	416	6.8	0.78	5.3	1.6	16	300	IIE
IIF	var.	12.9	9.8	140	6.2	-	2.6	-	-	7.0	300	-	1	-	1.5	16	250	IIF
IIIAB	Om	8.49	19.7	38.9	4.1	140[a]	5.6	1.4[a,d]	40	5.0	160	7.2	1	3.5	1.2	10.5	265	IIIAB
		8.25[a]	18.5[c]	40[a]	5.0[a]	-	9.3[a]	5.0[b]	-	-	160	-	-	-	1.1[a]	-	-	IIIAB
		7.6[b]	-	35[b]	3.5[c]	-	-	6.0[c]	-	-	160	-	-	-	0.7[b]	-	-	IIIAB
		8.2[c]	-	36.25[c]	-	-	-	-	-	-	160	-	-	-	1.05[c]	-	-	IIIAB
IIICD	see note 2	-	-	-	-	-	-	-	-	-	-	-	-	-	-	-	-	IIICD
IIIE	Og	8.49	17.6	35.6	4.1	-	5.6	-	40	5.0	160	7.2	1	3.5	1.2	10.5	265	IIIE
IIIF	var.	7.95	6.82	0.91	3.2	-	2.2	-	210	3.6	170	7.2	1.2	4.4	0.91	11	86	IIIF
IVA	Of	8.0	2.15	0.124	1.9	200[a]	0.88	0.8[a]	140	4.0	150	5.9	0.6	4.6	1.5	7.6	9	IVA
		8.4[a]	-	0.12[a]	2.0[a]	-	3.3[a]	1.0[b]	-	-	-	-	-	-	1.6[b]	-	-	IVA
		-	-	0.15[b]	1.8[b]	-	2.4[b]	-	-	-	-	-	-	-	-	-	-	IVA
IVB	D	17.1	0.221	0.0526	22	40[a]	1	0.03[a]	87.7	7.4	12	27	3	12	0.15	1.1	1.5	IVB
		17.0[b]	-	0.053[a]	20[a]	-	3.0[a]	0[b]	-	-	-	-	-	-	-	-	-	IVB
		-	-	-	-	-	5.7[b]	-	-	-	-	-	-	-	-	-	-	IVB

*The structural classification for typical group members. Larger groups often contain a few members with anomalous (reheated, brecciated, etc.) structures. No "typical" group structure exists for groups IC, IIE, IIF, and IIIF. **Note 1:** Structures in groups IAB and IIICD vary, in part because of the large spread in Ni values. Most low-Ni IAB members are Og, but group also includes finer structures and brecciated, silicate-rich members. **Note 2:** Because of the uncertainty of separating group IIICD from IAB, and reclassifications proposed after Willis (1980), no average composition is available for this group. The structure of IIICD members ranges from Om to D, depending on Ni content.

Data are from Willis (1980) except as noted:
[a]"Final" compositions from Table 5, Willis and Goldstein (1982:A444)
[b]Values of C_0 from Table 3, Jones and Drake (1983:1206)
[c]Model #6I from Table 4, Haack and Scott (1993)
[d]Esbensen et al. (1982)

The largest chemical group, IIIAB, comprises about one third of all known iron meteorites. On log(E) vs. log(Ni) plots, some groups (IIAB, IIC, IID, and IVA) occupy fields of similar shape, although in different regions of the plot. As Scott (1972) has demonstrated, the behavior of these groups is consistent with fractional crystallization from a melt, and these groups are therefore called "magmatic iron meteorite groups."

Groups IAB and IIICD, which account for about 20% of all iron meteorites, as well as the small group IIE, exhibit a different behavior from the magmatic groups. For example, their Ni and Ge contents span a larger range, and their Ir contents a smaller range than those of the other groups. They also tend to be rich in inclusions, and some members contain abundant silicates or, in some cases, phosphates. Their formation mechanism was clearly different from that of the magmatic iron meteorite groups, but the nature of this process remains poorly understood. Kracher (1982) proposed formation of group IAB by cotectic crystallization of metal and sulfide, but Wasson et al. (1980) suggested that the non-magmatic groups originated in small impact melt pools.

Cooling rates

Two factors control the lamella width of the Widmanstätten pattern in octahedrites: the average Ni content of the metal and the cooling rate. The higher the Ni content, the lower the temperature at which the α phase begins to precipitate; the faster the cooling, the less time the α lamellae have to grow. Therefore higher Ni content and faster cooling lead to finer patterns. The growth process can be simulated by computer models of Ni diffusion during nucleation and growth of kamacite in the original taenite crystals. Wood (1964) and Goldstein and Ogilvie (1965) showed that cooling rates can be determined by comparing the computer models to actually observed textures and compositions. The calibration of these models requires accurately determined diffusion coefficients, which are sensitive to minor element content, and accurate phase diagrams. The original cooling rate estimates, which were generally in the range of 1-10°C/Ma, had to be revised upward by about a factor of 5 (Saikumar and Goldstein 1988) when the improved diffusion data of Dean and Goldstein (1986) became available.

Cooling rates determined from diffusion-controlled Ni concentration profiles resulting from phase transformations in the metal phase are collectively known as metallographic cooling rates. In the case of octahedrites and many stony-irons, these are generally derived from analyzing the Ni distribution in the Widmanstätten pattern. Quantification can be based on matching the M-shaped Ni profiles in taenite lamellae, or measuring width versus central Ni content of taenite regions. The two methods give similar results, but a third method, suggested by Narayan and Goldstein (1985) turned out to be invalid (Saikumar and Goldstein 1988). In irons that contain chondritic silicates it is possible to determine cooling rates from both the Widmanstätten patterns and isolated metal grains in the silicates. The two are generally in agreement (Herpfer et al. 1994). The most reliable cooling rate determinations for the major iron meteorite groups have been compiled in Table 4.

In the last decade, cooling rate determinations have undergone a number of refinements to take into account the presence of minor phases and elements, impingement of growing kamacite plates (Saikumar and Goldstein 1988), undercooling of kamacite nucleation, and local variations in Ni content (Rasmussen 1981, 1982). Nonetheless it is still uncertain whether kamacite requires the prior formation of phosphides to nucleate without undercooling (Saikumar and Goldstein 1988) or not (Rasmussen et al. 1995). Although most iron meteorites have a sufficiently high bulk P content for schreibersite to nucleate before kamacite, this is not the case for low-Ni members of group IVA. This is the same group that shows a significant and systematic difference in calculated cooling rates between its low-Ni and high-Ni members.

Table 4. Metallographic cooling rates of selected iron and stony iron meteorite groups.

meteorite group	cooling rate (°C/Ma)	ref.	parent body radius (km)
IAB	25	(a)	33
	310	(b)	10
IC	highly variable	(c)	
IIAB	0.8-3	(e)	165-90
	6-12	(d)	65-47
IID	5	(a)	70
IIIAB	3-75	(d)	90-20
	7.5-15	(a)	58-42
IIICD	10	(a)	51
	200	(b)	13
IVA	11-500	(d)	49-8
	40-325	(a)	27-10
IVB	30-260	(d)	30-11
	4300	(b)	3
pallasites	2.5-4	(a)	97-78
mesosiderites	0.5	(a)	206

References: (a) Yang et al (1997a), based on Goldstein (1969) as modified by Saikumar and Goldstein (1988), (b) Rasmussen (1989), (c) Scott (1977a), (d) Haack et al. (1990), (e) Randich and Goldstein (1978).

See text for method of calculation for parent body radius.

Since conventional metallographic cooling rates are based on the kamacite-taenite exsolution, both phases have to be present for a quantitative determination. Almost all meteorites contain sufficient kamacite to determine cooling rates by this method, even the members of group IVB, whose Ni content reaches 18% (Rasmussen et al. 1984). However, in hexahedrites no taenite is present. To circumvent this limitation, Randich and Goldstein (1978) developed a method to determine cooling rates from the growth of schreibersite. The metal-phosphide cooling rates of 0.8-3°C/Ma for group IIA are in agreement, within accepted error, with the kamacite-taenite cooling rates of 4-12°C/Ma for group IIB, which, based on chemical evidence, originated from the same parent melt. Cooling rates derived from two different reactions are thus in approximate agreement, and also consistent with an origin of group IIAB from a single melt reservoir.

A similar situation exists in group IIIAB, but in group IVA, which also shows a distinctly magmatic signature in terms of chemistry, cooling rates vary widely. In addition, four silicate-bearing irons, Bishop Canyon, Gibeon, Saõ João Nepomuceno and Steinbach, are members of this group. These unusual features led Scott et al. (1996) and Haack et al. (1996) to postulate that the IVA parent body was fragmented while it was still hot, and cooled as a "rubble pile" rather than a body with a continuous core. A similar history has been proposed by Scott (1977a) for group IC, whose members, although chemically similar, show widely differing metallographic structures.

In principle, burial depths, and hence parent body sizes, can be inferred from metallographic cooling rates, but the calculations depend on the knowledge of the thermal properties of material of which we have no samples, viz., mantle and regolith of the iron meteorite parent bodies. Haack et al. (1990) have shown that the thickness of the regolith layer is a critical parameter, and since the accumulation of regolith and megaregolith is a stochastic process, there are fundamental limitations to such calculations. Considering these uncertainties, the complex formula relating cooling rate, thermal properties, and parent body radius can be simplified to give an estimate of parent body size:

$$R = g \times 149 \times CR^{-0.465}$$

where R is the parent body radius in km, g is a factor that is equal to 1 for a chondritic parent body, and the cooling rate CR is given in °C/Ma. Parent body radii based on this

formula are shown in Table 4.

Ages

Most commonly used radionuclide clocks are all based on lithophile elements, such as K, Rb, Sm, Th and U, and are not applicable to iron meteorites. In fact, a considerable fraction of the light lithophile elements present in iron meteorites is due to cosmic-ray spallation rather than inherited from the parent body (Voshage 1967, Imamura et al. 1980, Honda 1988, Xue et al. 1995). However, the high content of noble metals, combined with their strong fractionation within groups, makes it feasible to use the β decay of ^{187}Re to ^{187}Os as a chronometer for iron meteorites. The half-life of ^{187}Re, which is about an order of magnitude longer than the age of the solar system, is not known accurately enough to make an absolute comparison with Rb-Sr or Sm-Nd ages of stony meteorites. Taking the value of 42.3±1.3 Ga (Lindner et al. 1989), Morgan et al. (1992, 1995) found that the ages of IIAB and IIIAB irons are identical (4.583 Ga), and indistinguishable from the age of chondrites, although high-Ni IIBs show some slight disturbance. The uncertainty in the half life places the lower limit of their age at 4.46 Ga. Shen et al. (1996) determined Re-Os isotopic systematics for a number of IAB, IIAB, IIIAB, IVA and IVB irons. Their data for IIAB irons yielded an age within uncertainty identical to that determined by Morgan et al. (1995). Further, Shen et al. (1996) determined an isochron age for IVA irons, which was 60±45 Ma older than that for IIAB irons. Horan et al. (1998) determined Re-Os isochron ages for groups IAB-IIICD, IIAB, IIIAB, IVA and IVB. They found that the IAB-IIICD, IIAB, IIIAB and IVB irons have the same age within uncertainties, although the IIIAB irons could be slightly older. Excluding the IVA irons, the ages obtained by Horan et al. (1998) and Shen et al. (1996) are identical within uncertainty, after recalculation to a common ^{187}Re half-life. Horan et al. (1998) found the IVA irons to be significantly younger than the other meteorite groups by about 80 Ma, in contrast to the conclusion of Shen et al. (1996).

Chronological information can also be derived from extinct radionuclide systems, if isotopic anomalies due to early radioactivity are preserved. Extinct radionuclides of potential significance for iron meteorite genesis are ^{107}Pd ($t_{1/2}$ 6.5 Ma), ^{182}Hf ($t_{1/2}$ 9±2 Ma) and ^{205}Pb ($t_{1/2}$ 14 Ma). Evidence for live ^{107}Pd in the form of radiogenic silver (^{107}Ag*) has been found in iron meteorites of the magmatic groups IIAB, IIIAB, IVA, and IVB (Chen and Wasserburg 1990), as well as some ungrouped irons. The IVA irons have a higher ^{107}Ag*/^{108}Pd ratio than other iron meteorite groups, indicating that the IVA irons are older. This agrees with the Re-Os results of Shen et al. (1996) but disagrees with those of Horan et al. (1998). The failure to find ^{107}Ag* in members of groups IAB and IIICD may be due to the larger Ag content of these samples, and hence a higher detection limit, and not necessarily a later formation age.

The preservation of ^{107}Ag* argues that fractional crystallization took place within a few million years of parent body accretion. Reconciling the rapid heat loss implied by this scenario with slow metallographic cooling rates probably requires more sophisticated models of parent body evolution than are currently available. Perhaps most small asteroids acquired the kind of insulating regolith envisioned by Haack et al. (1990) only after their interiors had solidified, but before they cooled through the temperature range at which metallographic cooling rates became established.

Refractory lithophile ^{182}Hf decays to refractory siderophile ^{182}W, and thus can be used to constrain the timing of metal-silicate separation (core formation) in differentiated bodies. Horan et al. (1998) have determined the W isotopic composition for the meteorites they studied by Re-Os chronometry. They found that all the iron meteorite groups have the same W isotopic composition within uncertainty, indicating that metal-silicate separation occurred on all these parent bodies within a limited time span (<5 Ma). Further, Horan et al. (1998) concluded that for all iron meteorite groups excluding the IIIAB irons, the time of crystallization as determined by Re-Os was measurably later than the time of metal-silicate separation as given by the W isotope systematics, suggesting that core crystallization may have been a protracted process.

A third kind of isotopic measurement that has attained particular importance for iron meteorites is the determination of cosmic-ray exposure ages. High energy cosmic-rays cause spallation in their targets, producing elements with characteristic isotopic signatures that are usually very different from average solar system isotope ratios. Cosmic-rays have a limited penetration depth. For the vast majority of matter in an asteroid, spallation only occurs after the material from which meteorites are formed has been fragmented to meter size or less. Exposure ages thus measure the time a meteorite has spent in space in essentially the same shape in which it fell.

In stony meteorites measurable spallation effects are usually limited to noble gases, but in iron meteorites with their high abundance of heavy target nuclei and low abundance of lithophile elements, it is possible to use the very precise ^{41}K/^{40}K method (Voshage 1967). Cosmic-ray exposure ages of iron meteorites are typically in the range of 200 to 1000 Ma, some 5 to 50 times longer than typical for stony meteorites. Tight clusters in exposure ages for groups IIIAB and IVA suggest discrete breakup events for their parent bodies 650±75 and 420±70 Ma ago, respectively (Voshage and Feldmann 1979). No other clusters have been observed. The highest ^{41}K/^{40}K exposure age measured for an iron meteorite is 2.3 Ga, or half the age of the solar system, for the ungrouped Deep Springs iron.

Exposure ages based on ^{26}Al/^{21}Ne ratios are systematically lower than ^{41}K/^{40}K ages (Aylmer et al. 1988). The two ages can be reconciled if it is assumed that the cosmic-ray flux increased by some 35% over the last 10^7 years, although the more mundane explanation of an error in spallation cross sections cannot yet be ruled out.

Origin of magmatic iron meteorite groups

Chemical evidence indicates that magmatic iron meteorite groups formed by fractional crystallization. The most plausible asteroidal setting for such a process would be the core of a differentiated asteroid. This would imply that each group comes from a separate asteroid, and that core compositions varied considerably between different parent bodies.

The partition coefficient of an element, E, is defined as $k_E = C_s/C_l$, where C_s is the concentration of E in the solid, and C_l is the concentration of E in the liquid. If the partition coefficient of an element is constant throughout the crystallization process, successive fractions of crystallizing solid follow the Scheil (or Rayleigh) equation,

$$C_s = k \times C_0 \times (1-g)^{k-1}$$

where C_0 is the concentration in the liquid before crystallization started, and g is the fraction that has already solidified. Mutually consistent partition coefficients can be derived from the fact that, given two elements A and B, the track of successive fractions of crystallizing solid on a plot of log(A) vs. log(B) is a straight line with slope $(k_A-1)/(k_B-1)$. This techniques was used by Scott (1972) to estimate partition coefficients for a number of elements based on log(E) vs. log(Ni) plots for magmatic iron meteorite groups.

In practice, the condition of constant partition coefficients is rarely fulfilled, particularly because k_E for most elements depends strongly on the concentration of non-

metals (S, P, and C) in the parent melt (Willis and Goldstein 1982, Jones and Drake 1983, Malvin et al. 1986). Since the non-metals largely remain in the residual liquid, their influence on k_E becomes more pronounced as solidification progresses. Refined models have been proposed to take non-ideal behavior into account, such as trapping of small amounts of liquid (Scott 1979b), solid state diffusion (Narayan and Goldstein 1982), partition coefficients that change during crystallization (Sellamuthu and Goldstein 1985, Jones 1994), and liquid immiscibility (Ulff-Møller 1998).

For the largest meteorite groups, which are probably fairly representative samples of their asteroidal precursors, average group compositions can be estimated (Willis 1980). The average group composition, however, is not identical to the composition of the parent melt, since the last amount of residual material, which contains most of the non-metals, is apparently missing (Kracher and Wasson 1982). Average compositions based on actual samples as well as a fractional crystallization model with constant k_E values have been calculated by Willis (1980), and are given in Table 3.

Since P has a small but finite partition coefficient, plots of log(P) vs. log(Ni) can be used to infer initial P contents. Sulfur is almost entirely excluded from the crystallizing solid, and the S content of the parent melt can only be estimated indirectly. For example, the partitioning of Ge is very sensitive to the S content of the melt, $k_{Ge}<1$ for melts low in S, and >1 for S-rich melts. Phosphorous has a similar effect. The change in slope on log(Ge) vs. log(Ni) plots of group IIIAB (Fig. 3) can thus be modeled with a melt containing 4 to 5% S at the beginning of crystallization, even though there are no samples of the S-rich material in our meteorite collections.

Models that take the influence of S on trace element partitioning into account (Jones and Drake 1983, Malvin et al. 1986) have led to some revisions in the original group composition estimates of Willis (1980). It should be pointed out, however, that these revised figures, denoted with superscripted letters in Table 3, are intended to represent the parent melt from which meteorites crystallized. For example, the average Ni content of group IIAB is estimated to be 6.1%. Element distribution patterns suggest an initial S content of the IIAB parent melt of 17% (Jones and Drake 1983). Since S is effectively excluded from the crystallizing solid, this model leads to an original Ni content of 6.1×(1/1.17)=5.1%. Both values are given in Table 3.

The largest discrepancies between the Willis (1980) values and the model melt compositions of Willis and Goldstein (1982) and Jones and Drake (1983) are for elements whose partition coefficients are highly sensitive to S content. This explains the large differences in Ge and Ir estimates for group IIAB. Since Ir concentrations in this group span five orders of magnitude, the average group value is poorly constrained by actual measurements. Meteorite collections are not unbiased samples of an entire core, and considering the large spread in values, even a very small bias can seriously affect the calculation of a meaningful average. An argument in favor of the lower Ir estimate is that it corresponds to an Ir/Ni ratio that is within a factor 2 of the chondritic value, in accordance with other roughly chondritic element/Ni ratios in groups IIAB.

Jones and Malvin (1990) presented a semi-empirical interaction model for the influence of non-metals on siderophile partitioning in the Fe-Ni-S-P system. The partition coefficients for siderophile element E are calculated from two parameters α and β_E, and the mole fraction X of the non-metal according to:

$$\log(k_E) = \log(k_E^*) + \beta_E \times \log(1-n\alpha X)$$

where k_E^* is the partition coefficient in the pure Fe-Ni-E system, and α and n depend only on the non-metal (n = 2, α = 1.09 for S; n = 4, α = 1.36 for P). The values of β_E depend on both E and the non-metal, and range from +0.5 (Cr, S) to -2.6 (Ir, S). Based on this model, Jones (1994) gave formulas for calculating slopes on $\log(E_1)$ vs. $\log(E_2)$ diagrams even if they are non-linear.

Little work has been done on the effect of C at low pressures, which also has a significant influence on trace element partitioning. Following Willis and Goldstein (1982), the C content of the original melt is assumed to be relatively small, and Jones and Malvin (1990) have confined their discussion to S and P.

The large sulfide nodules present in some magmatic iron meteorites are thought to be derived from trapped melt. If the amount of trapped melt could be determined, the modal sulfide content would allow an independent estimate of melt composition. Unfortunately there is no way to estimate the amount of trapped melt without resorting to parameters like partition coefficients, which themselves depend on S content. Esbensen et al. (1982) have tried to model melt trapping in members of the Cape York shower, which apparently represent mixtures of solid and trapped liquid in varying proportions. Estimating solid:liquid ratios between 93:7 to 36:64 in different samples on the basis of trace elements, they arrived at an S content of 2%. Taking into account the amount of solid that had already crystallized before the Cape York specimens formed, the calculated S content of the original liquid was 1.4% by weight.

Haack and Scott (1993) contend the assumptions of Esbensen et al. (1982) in calculating the solid:liquid ratios were oversimplified, and estimate an initial S content for the IIIAB parent melt of about 6%, close to the 5% calculated by Jones and Drake (1983). Recently, Ulff-Møller (1998) has estimated the S content of the IIIAB iron parent melt at 10.8 wt % by using the Ir-Au distribution of high-Ir IIIAB irons. The partition coefficient of Ir is highly sensitive and that of Au less sensitive to the S content of the melt (Jones and Malvin 1990).

To account for the low abundance of S estimated for iron meteorite parent melts, Keil and Wilson (1993) suggest that parent bodies lost considerable amounts of S into space by explosive volcanism during incipient differentiation. Eutectic Fe-S liquid is probably finely dispersed along grain boundaries and in the network of early silicate melt (Kracher 1985). A small amount of volatiles can cause liquid to be erupted, and lost into space due to the low gravity on small asteroids (Wilson and Keil 1991).

Anomalous iron meteorites

About 15% of all known iron meteorites do not belong to one of the defined chemical groups (Wasson 1990). Some ungrouped irons have unique features, others are in many respects similar to group members, except that their trace element contents do not fall near any clusters on log(E) vs. log(Ni) diagrams. Most iron meteorites with extreme compositions are ungrouped, although the most Ni-rich meteorite known, Oktibbeha County, appears to be related to group IAB (Kracher and Willis 1981). Among compositionally unique samples, Butler has a Ge concentration almost four times higher than any other iron meteorite, and is enriched in some other trace elements as well. A few ungrouped irons contain Si dissolved in the metallic phase, a feature characteristic of metal in enstatite chondrites. Tucson not only contains reduced Si, but highly reduced silicates and the sulfide brezinaite, but no troilite. The ungrouped meteorites Soroti and LEW 86211 contain more troilite than Fe,Ni by volume.

Most of the remaining ungrouped iron meteorites, however, are not so unusual, and it is likely that they are simply fragments of poorly sampled parent bodies (Scott 1979a). If each ungrouped individual or grouplet represents a separate parent body, then iron meteorites have sampled between 30 and 50 asteroids (Scott 1979a, Wasson 1990). In a

few cases relationships to existing groups may have been overlooked, but even so it is obvious that iron meteorites sample many more differentiated parent bodies than the known classes of achondrites.

This is not unexpected. The most abundant types of iron meteorites are clearly related to stony meteorites: group IIIAB and main group pallasites to the howardite-eucrite-diogenite (HED) association, and the most common silicate inclusions, in group IAB as well as in group IIE, show affinities to winonaites and H chondrites, respectively. But the number of ungrouped iron meteorites alone (88 according to Wasson 1990) is greater than the number of all achondrite types, and the chances that a poorly sampled body is represented among them is correspondingly greater.

Some of the diversity of iron meteorites can be explained simply by the fact that they are easier to find than stony meteorites, and because of their greater number the probability of collecting rare types is higher. But even more important is the very long space lifetime of iron meteorites, as indicated by their long cosmic-ray exposure ages. When asteroids are broken up, the resulting meteorite-sized fragments have to undergo perturbations that bring them into earth-crossing orbits before they can be captured by earth. The longer the space lifetime of an object, the greater the probability of such a perturbation. Some of these perturbations are due to actual collisions, which may fragment a stony meteorite, but not an iron.

Most meteorites that arrive at earth come from particular locations in the asteroid belt where perturbations into earth-crossing orbits are likely. One such location is the 3:1 period resonance with Jupiter at 2.501 AU (Wasson 1990). The most common meteorite groups are probably fragments of asteroids that were at one time close to this location, or a similarly unstable one.

When objects some small distance away from the resonance are broken up by collisions, some fragments change their orbits to move closer to the resonance, increasing their probability of becoming earth-crossers. In general, the magnitude of change in orbital parameters depends on ejection velocity, which is in turn inversely correlated with mass. In other words, the debris close to the resonance can be expected to consist of a range of fragments, the larger ones predominantly from objects close to the resonance, the smaller ones sampling a more diverse population. This hypothesis is also consistent with the finding that ungrouped meteorites are more abundant among Antarctic meteorites than in Museum collections of iron meteorites. The Antarctic set is less biased toward larger sizes than collections elsewhere on earth that depend on chance discoveries. This is the explanation given by Wasson (1990) for the high abundance of ungrouped iron meteorites among the Antarctic collection.

The large number of iron meteorite parent bodies is also consistent with the observation that most asteroids in the inner asteroid belt are differentiated (Gaffey 1990). This indicates that the number of potential parent bodies for differentiated meteorites is relatively large. The reason why achondrites apparently sample only a small number of bodies is not a scarcity of differentiated asteroids, but rather the relatively short space lifetime of stony meteorites, which allows only samples from very few locations to reach earth as recoverable objects. This constraint is much relaxed for irons, hence a broader range of parent bodies is sampled by metallic meteorites.

SILICATE-BEARING IAB AND IIICD IRONS AND STONY WINONAITES

Of the 13 major iron meteorite groups, only the IAB and IIICD groups have broad ranges in Ni and some trace elements (e.g. Ga, Ge). These ranges are unlike those in the

other 11 groups and difficult to explain by simple fractional crystallization of a metallic core. In addition, many members of these groups contain silicate inclusions, which are abundant in the IAB irons but are also found in a few IIICD irons. These silicate inclusions are roughly chondritic in mineralogy and chemical composition, but the textures are achondritic, exhibiting recrystallized textures. Silicate inclusions in IAB irons are linked through oxygen-isotopic (Clayton and Mayeda 1996) and mineral compositions to the stony winonaites and may be related to IIICD irons. Recently, comprehensive studies have been conducted of the winonaites (Kimura et al. 1992, Yugami et al. 1996, Benedix et al. 1998a), silicate inclusions in IAB irons (Yugami et al. 1997, Benedix et al. 1998b), silicate inclusions in IIICD irons (McCoy et al. 1993) and metal in the IAB and IIICD irons (Choi et al. 1995). The apparently contradictory features of these meteorites have led to a range of models to explain their formation, from those invoking impact melting (Choi et al. 1995) to those which suggest asteroid-wide partial melting (Kracher 1982, 1985). Yugami et al. (1997) suggested that partial melting and melt migration as a result of impact heating can produce the diversity of meteorite types observed on this parent body. Benedix et al. (1998b) proposed a model in which a partially-melted parent body is catastrophically disrupted and reassembled to explain the origins of these meteorites.

Table 5. Silicate-bearing IAB and IIICD irons, and winonaites.

Silicate-bearing IAB irons	Caddo County, Campo del Cielo, Canyon Diablo, EET 83333, EET 87505, EET 87504, EET 84300, EET 87506, Four Corners, Jenny's Creek, Kendall County, Landes, Leeds, Linwood, Lueders, Mertzon, Mundrabilla, Ocotillo, Odessa, Persimmon Creek, Pine River, Pitts, San Cristobal, Tacubaya, TIL 91725, Toluca, Udei Station, Woodbine, Youndegin, Zagora
Silicate-bearing IIICD irons	Maltahöhe, Carlton, Dayton
Winonaites	Winona, Mt. Morris (Wis.), Pontlyfni, Tierra Blanca, QUE 94535, Yamato 74025, Yamato 75261, Yamato 75300, Yamato 75305, Yamato 8005

Classification, petrology and mineralogy

Silicate-bearing IAB and IIICD iron meteorites and winonaites are listed in Table 5. As a group, the silicate-bearing IAB iron meteorites exhibit a number of common properties. The metallic textures of the IAB irons have been described in detail by several authors (e.g. Buchwald 1975). Overall, the silicate-bearing IAB iron meteorites span the range of structural classification from hexahedrites (e.g. Kendall County with 5.5% Ni) through fine octahedrites and coarsest octahedrites to ataxites (e.g. San Cristobal with 24.9% Ni). Silicate inclusions contain variable amounts of low-Ca pyroxene, olivine, plagioclase, calcic pyroxene, troilite, graphite, phosphates and Fe,Ni metal, and minor amounts of daubreelite and chromite. The abundance of silicates varies dramatically between different IAB irons, as well as between different sections of the same iron (Table 6). Plagioclase generally comprises ~10% of the total silicates present (Table 6), similar to the abundance found in ordinary chondrites (Van Schmus and Ribbe 1968, McSween et al. 1991). Overall, mafic mineral compositions are quite reduced (Table 7), with olivine compositions ranging from Fa_1 (Pine River) to Fa_8 (Udei Station) and low-Ca pyroxenes ranging from $Fs_{1.0}$ (Kendall County) to $Fs_{8.7}$ (Udei Station) (Bunch et al.

1970). Average anorthite contents of plagioclases are relatively narrow in range, from $An_{11.0}$ in Persimmon Creek to $An_{21.5}$ in Pine River, and calcic pyroxene is diopside varying from $Fs_{2.4}Wo_{44.7}$ in Mundrabilla to $Fs_{3.9}Wo_{43.9}$ in Persimmon Creek (Ramdohr et al. 1975, Bunch et al. 1970).

Table 6. Modal compositions (vol %) of silicate-bearing IAB and IIICD irons and winonaites. Data from McCoy et al. (1993) and Benedix et al. (1997a,b).

meteorite	section number	mafics*	plag	troilite	metal	W.P.	chr	daub	schreib	graph	Cohen
Troilite-rich IAB irons											
Mundrabilla	USNM 5914-1†	48.5	14.9	30.5	0.12	0.69	-	1.6	-	3.7	-
Persimmon Creek	USNM 2990	23.4	2.0	22.1	43.7	6.8	-	-	0.67	1.4	-
Pitts	USNM 1378	21.3	1.9	51.7	11.5	10.6	-	-	0.15	2.8	-
Zagora	USNM 6392	22.2	4.4	2.8	65.7	2.8	-	-	0.58	1.6	-
IAB irons with non-chondritic, silicate inclusions											
Caddo County	UNM 937†	37.2	44.7	4.7	5.9	7.3	-	-	0.23	-	-
Ocotillo	UH 226										
IAB irons with rounded inclusions											
Toluca	M8.53	5.1	1.4	23.8	43.1	9.9	0.08	-	14.9	1.7	-
	M8.79	0.7	-	1.4	56.7	22.6	-	-	9.4	4.4	4.9
	M8.150-1	-	-	17.9	68.4	0.55	-	-	4.3	-	8.9
	M8.150-2	8.5	1.7	28.4	50.9	0.50	-	0.07	4.7	5.4	-
Jenny's Creek	M217	-	-	67.9	-	13.7	-	0.92	14.2	-	3.2
Odessa	UH 256	-	-	3.3	85.0	1.4	-	0.14	0.79	8.4	1.1
Youndegin	M173	0.03	0.03	17.8	61.8	4.6	-	0.47	1.5	1.3	12.5
IAB irons with angular silicate inclusions and related winonaites											
Campo del Cielo	USNM 5615-2†	60.8	5.8	0.98	-	0.75	-	-	-	31.7	-
	USNM 5615-4†	72.1	10.2	6.4	1.6	1.3	0.24	-	0.06	8.1	-
	USNM 5615-6	44.4	8.4	4.0	31.7	0.83	-	-	2.9	7.7	-
	USNM 5615-8	20.6	12.0	3.9	41.2	3.9	-	-	1.4	16.9	-
	USNM 5615-9†	63.5	18.2	5.2	1.4	1.2	-	-	-	10.5	-
Copiapo	USNM 3204-2	17.9	2.3	0.43	71.0	4.6	0.11	-	1.2	2.5	-
EET 83333		13.8	2.6	0.91	78.4	1.3	-	-	1.3	1.8	-
EET 84300		5.8	1.4	1.5	84.9	1.6	-	-	2.8	1.9	-
EET 87504	,5	11.2	2.8	11.5	59.8	12.6	-	-	0.87	1.4	-
EET 87506		9.1	1.8	10.5	69.9	5.4	-	-	2.9	0.42	-
Four Corners	USNM 728	20.2	5.9	3.5	59.1	4.9	-	-	3.1	3.3	-
Landes	UH 147	35.7	2.9	1.3	50.9	2.4	-	-	0.49	6.3	-
Lueders	UH 255	25.4	3.7	1.1	45.3	21.2	-	-	1.6	1.8	-
Linwood	USNM 1416	8.3	0.4	6.9	46.7	10.0	-	-	5.7	21.9	-
Pine River	USNM 1421	24.8	4.6	1.1	65.4	0.70	-	-	2.2	1.3	-
Udei Station	USNM 2169	43.9	1.7	8.9	38.6	1.3	0.44	0.10	0.49	4.5	-
Woodbine	USNM 2169	36.6	7.0	7.0	3.4	9.8	-	-	6.8	1.4	-
Pontlyfni	M6.2	57.9	9.5	18.2	9.5	3.1	0.06	0.67	1.04	-	-
	M6.3	53.2	8.7	19.9	12.3	4.6	-	0.80	0.20	-	-
Winona	UH 133	66.1	13.3	5.1	1.8	13.4	0.10	-	-	-	-
	UH 195	68.2	12.2	6.1	2.3	11.2	0.10	-	-	-	-
	USNM 854	64.7	14.0	6.3	2.2	12.4	0.10	-	-	-	-
Mt. Morris (Wis.)	UH 157	65.5	9.4	5.8	3.5	15.1	-	0.20	-	-	-
	USNM 1198-2	65.7	11.5	8.7	0.2	13.2	-	0.30	-	-	-
Y-75300	,51-3 (coarse)	57.8	13.3	15.2	0.4	12.7	-	0.70	-	-	-
	,51-3 (fine)	75.2	12.2	7.5	-	5.1	-	-	-	-	-
Y-74025	,52-1	71.5	12.7	9.1	1.5	4.9	-	0.30	-	-	-
Tierra Blanca	M-3,1	63.1	8.8	1.4	-	26.2	-	-	-	0.56	-
	M-3,2	61.6	6.3	0.17	0.1	31.8	0.09	-	-	-	-
Y-8005	,51-3	52.9	8.1	8.3	12.5	16.8	-	0.7	0.6	-	-
IAB irons with phosphate-rich inclusions											
San Cristobal	UCLA	16.9‡	2.9	2.6	74.7	1.1	-	-	1.6	0.16	0.08

* Mafic silicates were not distinguished and include olivine, orthopyroxene, and clinopyroxene

† Thin section samples of separated silicate inclusions without metallic host.

‡ Includes ~ 0.9 vol.% brianite.

- = not observed.

Table 7. Representative analyses of silicates from IAB irons demonstrating the range of compositions, from Bunch et al. (1970).

	Olivine			Orthopyroxene			Clinopyroxene		Plagioclase	
	Pine River	Toluca	Udei Station	Pine River	Toluca	Udei Station	Pine River	Udei Station	Persimmon Creek	Pine River
Chemical Composition (wt %)										
SiO_2	42.1	42.1	41.3	58.0	57.8	56.5	54.3	54.3	64.1	62.9
Al_2O_3	b.d.	b.d.	b.d.	0.51	0.17	0.85	0.96	1.72	21.6	23.0
TiO_2	b.d.	b.d.	b.d.	0.10	0.23	0.22	0.33	0.57	--	--
Cr_2O_3	b.d.	b.d.	0.09	0.19	0.06	0.37	0.38	1.16	--	--
FeO	1.17	4.5	7.5	2.55	4.5	5.6	1.00	1.84	0.68	0.29
MnO	0.17	0.24	0.41	0.30	0.22	0.45	0.18	0.28	--	--
MgO	57.0	53.4	51.0	38.4	35.6	34.7	19.4	18.6	--	--
CaO	b.d.	b.d.	b.d.	0.70	0.52	0.92	22.2	20.2	2.41	4.8
Na_2O	b.d.	b.d.	0.20	0.18	0.09	0.11	0.65	1.06	10.3	9.4
K_2O	b.d.	b.d.	b.d.	b.d.	b.d.	0.23	0.10	0.08	0.71	0.47
Total	100.44	100.24	100.50	100.93	99.19	99.95	99.50	99.81	99.80	100.86
Cation Formula (O=4 for olivine, 6 for pyroxene, 8 for plagioclase)										
Si	0.990	1.004	0.995	1.967	1.993	1.955	1.967	1.962	2.849	2.777
Al^{IV}	b.d.	b.d.	0.004	0.021	0.007	0.035	0.033	0.038	1.132	1.191
Al^{VI}				b.d.	b.d.	b.d.	0.008	0.035		
Ti	b.d.	b.d.	b.d.	0.003	0.006	0.006	0.009	0.016	--	--
Cr	b.d.	b.d.	0.002	0.005	0.002	0.010	0.011	0.033	--	--
Fe	0.022	0.090	0.150	0.072	0.130	0.162	0.030	0.056	0.025	0.011
Mn	0.002	0.005	0.009	0.009	0.006	0.013	0.006	0.009	--	--
Mg	1.997	1.898	1.833	1.921	1.831	1.790	1.048	1.002	--	--
Ca	b.d.	b.d.	b.d.	0.025	0.006	0.034	0.862	0.782	0.115	0.228
Na	b.d.	b.d.	0.008	0.012	0.006	0.015	0.046	0.074	0.888	0.807
K	b.d.	b.d.	b.d.	b.d.	b.d.	0.005	0.005	0.004	0.040	0.027
Total Cations	3.011	2.997	3.001	4.035	4.000	4.025	4.025	4.011	5.049	5.041
Molar Mineral End Members and mg# (100(MgO/(MgO+FeO)))*										
Wo	--	--	--	1.2	1.9	1.7	44.3	42.3	--	--
En	--	--	--	94.8	92.2	89.6	53.8	54.2	--	--
Fs	--	--	--	4.0	6.9	8.7	1.9	3.5	--	--
Or	--	--	--	--	--	--	--	--	3.9	2.5
Ab	--	--	--	--	--	--	--	--	85.1	76.0
An	--	--	--	--	--	--	--	--	11.0	21.5
mg#	98.9	95.5	92.4	96.4	93.4	91.7	97.2	94.7	--	--

Despite these gross similarities, extraordinary heterogeneity is found between individual samples and sometimes between different sections of the same sample. Bunch et al. (1970) developed a dual classification scheme (Odessa and Copiapo types) based on modes, mineralogies, mineral compositions, textures, and shapes of the inclusions. With more recent work, a five-fold classification scheme is needed. The five types are: (1) sulfide-rich IAB irons; (2) IAB irons with non-chondritic silicate inclusions; (3) IAB irons with rounded inclusions (Odessa type of Bunch et al. 1970); (4) IAB irons with angular silicate inclusions (Copiapo type of Bunch et al. 1970); and (5) IAB irons with phosphate-rich inclusions. We discuss one or two meteorites that illustrate the characteristics of each of these groups.

Sulfide-rich IAB irons. Several of the IAB irons have unusually high troilite contents, found as irregular masses (Pitts, Persimmon Creek), veins (Zagora) or large grains. The type member is Mundrabilla (Fig. 4). With 7.47 wt % Ni in the metallic host, Mundrabilla plots in the low-Ni cluster of IAB-IIICD irons on plots of Ni vs. Ir, Ga, and

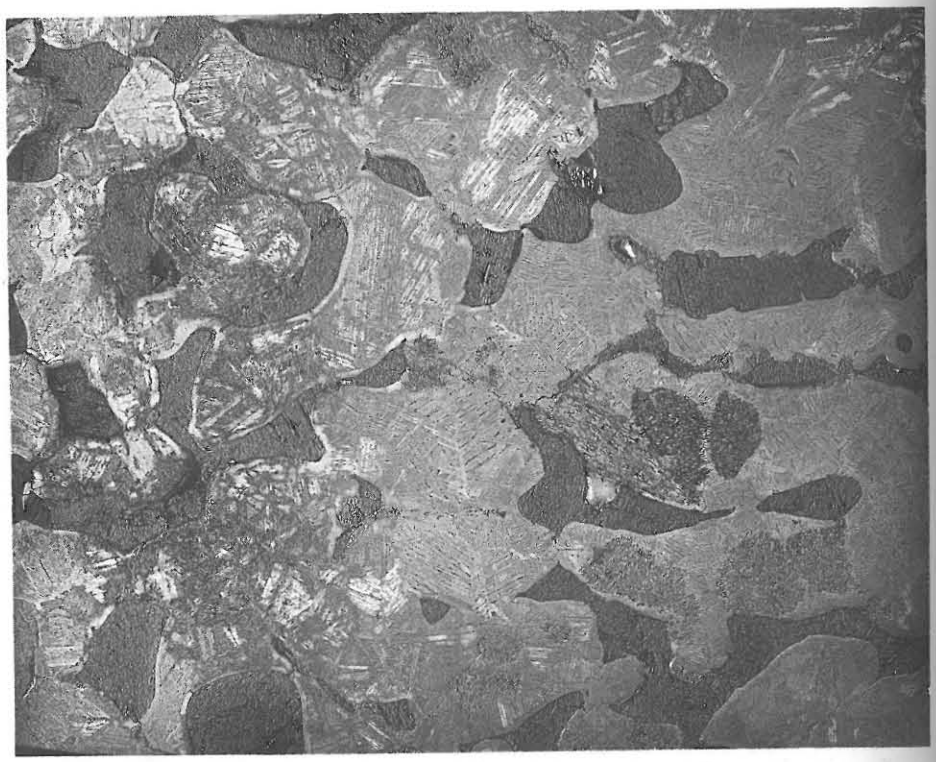

Figure 4. Photograph of the Mundrabilla iron meteorite showing metal-troilite intergrowths. White areas are Fe,Ni metal and gray areas are troilite. A cooling rate of ~5°C per annum during solidification is inferred from the weak dendritic texture. Field of view is 16 cm in maximum dimension.

Ge (Choi et al. 1995). Troilite comprises 25 to 35 vol % (Buchwald 1975) of Mundrabilla and occurs as mm-sized veins or lenses generally found along parent taenite grain boundaries (Buchwald 1975). Scott (1982) noted that the weak dendritic texture of the metal grains is a characteristic quench texture of metal-sulfide melts. In addition to abundant troilite, graphite, and minor amounts of schreibersite, these meteorites also contain silicate inclusions. Mundrabilla contains rare angular silicate inclusions, ranging in size from a few mm to a few cm, which are texturally similar to Winona (Benedix et al. 1998a) and silicates in Lueders (McCoy et al. 1996a).

IAB irons with non-chondritic silicate inclusions. IAB irons with non-chondritic silicates inclusions include Caddo County (basaltic inclusions) and Ocotillo (troctolitic inclusions). Coarse-grained, olivine-rich inclusions in some winonaites (e.g. Winona, Mt. Morris (Wis.)) also fit into this type. Caddo County, the type meteorite, is quite complicated in hand sample. Silicate inclusions are up to 7 cm in maximum dimension, but are truncated by the edge of the meteorite. Silicates comprise ~35 vol % (Fig. 5) of the slice. Metal occurs as the metallic host into which the clasts are embedded, as large grains within the silicate inclusions, and as veins which are clearly produced by post-solidification shock. In the hand sample, silicate grain sizes are observed to be highly variable and this is consistent with our thin section observations. Many inclusions, or parts of inclusions, consist of silicates with roughly chondritic modal proportions, but equigranular, recrystallized textures (Palme et al. 1991, Takeda et al. 1997a). These types

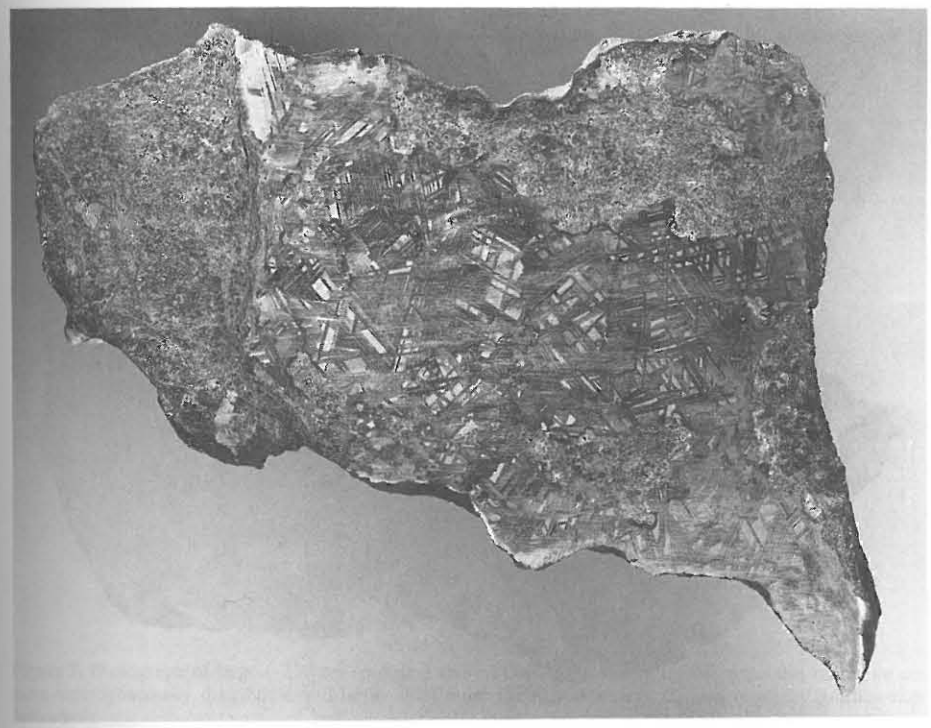

Figure 5. Photograph of Caddo County. Slab is 16.5 cm in maximum dimension. (Courtesy of the Smithsonian Institution).

of inclusions will be discussed in the section on IAB irons with angular silicate clasts. Rare inclusions of basaltic composition are also found in Caddo County. These are composed of major calcic pyroxene and sodic plagioclase and minor amounts of low-Ca pyroxene, olivine, troilite, and metal. Modal analyses by Takeda et al. (1993, 1994a), Yugami et al. (1997) and Benedix et al. (1998b; Table 6) indicate that these inclusions are broadly basaltic in composition, containing 45 to 55 vol % plagioclase, although texturally they are coarse-grained gabbros. Mafic silicates are relatively reduced (olivine, $Fa_{3.3}$; low-Ca pyroxene, $Fs_{6.5}$; calcic pyroxene, $Fs_{2.5}$), and plagioclase is $Ab_{75}An_{21}Or_3$ (Benedix et al. 1998b, Takeda et al. 1993, 1997a).

IAB irons with rounded inclusions. Several IAB irons contain inclusions which are typically rounded or ovoid and contain variable amounts of silicates, graphite and troilite, the latter two often being the dominant or sole constituents. These include Odessa, Toluca (Fig. 6) (and the paired Tacubaya), Canyon Diablo, Jenny's Creek and Youndegin. These meteorites have a relatively narrow range of Ni contents from 6.80 to 7.86 wt % Ni, within the low-Ni cluster of IAB irons. Bunch et al. (1970) referred to these as Odessa-types, while Benedix et al. (1998b) chose Toluca to represent this type, since a large number of specimens were readily available for study, allowing investigation of inter-inclusion heterogeneity.

Inclusions in Toluca consist of a core of either silicates or, more often, troilite surrounded by a sequence of swathing minerals such as graphite, schreibersite, and cohenite, although not all of these minerals are present in the sequence all of the time.

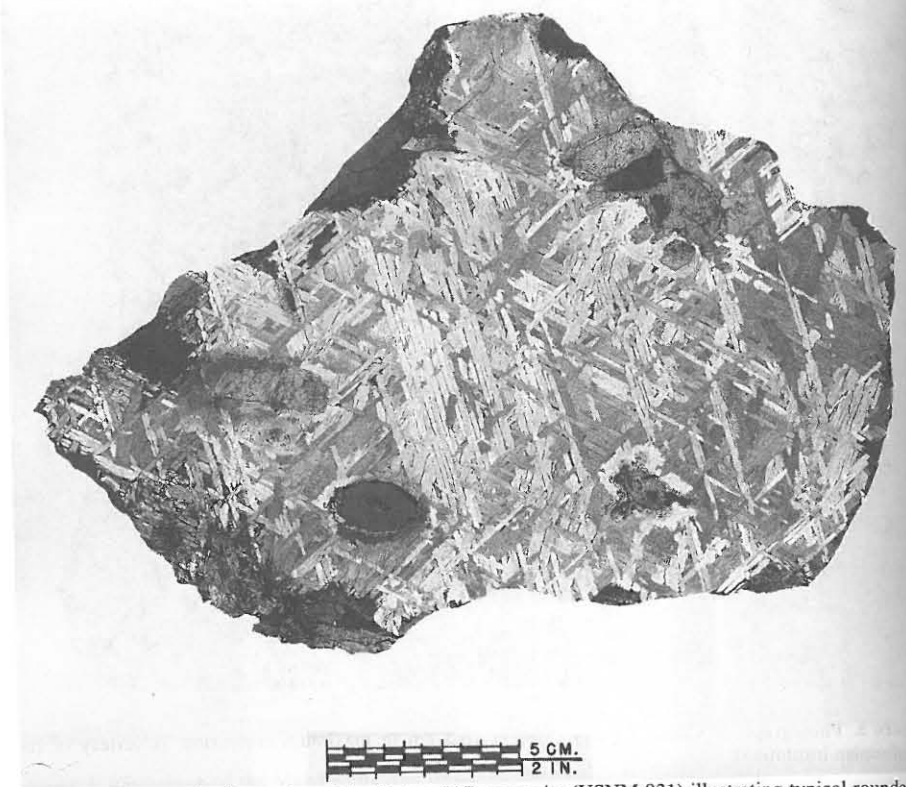

Figure 6. Photograph of a portion of the Toluca IAB meteorite (USNM 931) illustrating typical rounded to amoeboid graphite and/or troilite-bearing inclusions, sometimes containing angular silicate inclusions. (Courtesy of the Smithsonian Institution).

Inclusions which contain troilite and silicates are typically ovoid, while the graphite-troilite-rich inclusions tended to be rounded. The silicate inclusions, when present, are generally surrounded by cm-sized troilite areas. In this type, silicates do not appear to occur without either troilite or graphite-troilite surrounding them. Marshall and Keil (1965) and Buchwald (1975) reported similar inclusion properties for Odessa and Canyon Diablo, respectively. Mineral compositions of the rare silicates found in this type are reduced (Fa_{3-6}) and similar to those of other silicate inclusions in IAB irons.

A feature that seems to be common among the IAB irons is the heterogeneous distribution, morphology and mineralogy of the inclusions within a single meteorite. Silicate-bearing inclusions in Toluca are heterogeneously distributed and range in shape from nearly round to elongate and amoeboid (Benedix et al. 1998b). Modes of four Toluca inclusions (Table 6) showed ranges in abundance of mafic silicates (0-8.5 vol %), plagioclase (0-1.7 vol %), metal (43.1-68.4 vol %), troilite (1.4-28.4 vol %), schreibersite (4.3-14.9 vol %), cohenite (0-8.9 vol %) and graphite (0-5.4 vol %). This heterogeneity significantly complicates our ability to obtain representative samples.

IAB irons with angular silicate inclusions and winonaites. This type is characterized by the angular shapes of the inclusions and includes most of the IAB irons that Bunch et al. (1970) referred to as Copiapo type. Typical examples are Campo del

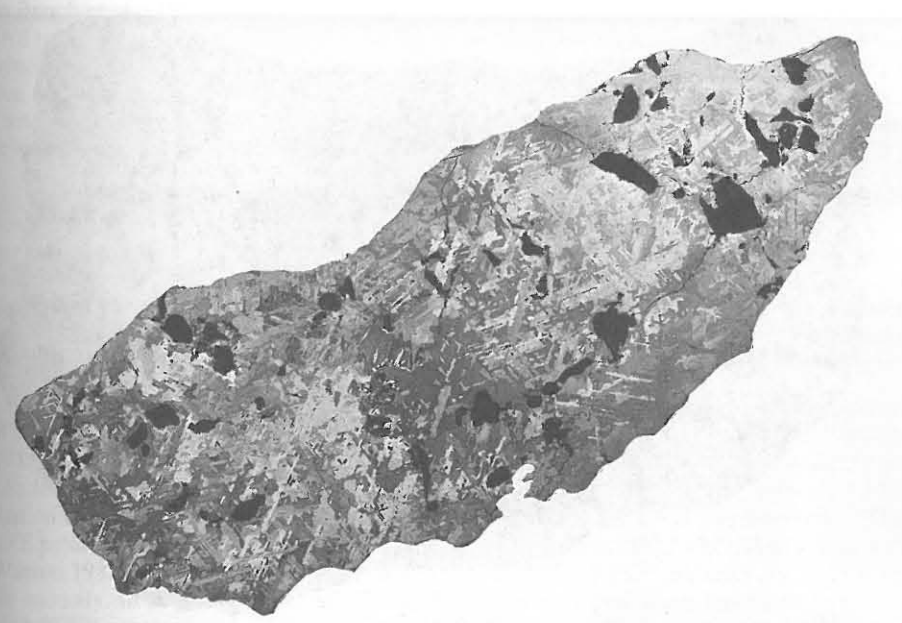

Figure 7. Photograph of large (~130 cm) polished slab of Campo del Cielo. Inclusions in this meteorite are more heterogeneously distributed and larger than those found in Lueders. (Courtesy of the Smithsonian Institution).

Cielo (Wlotzka and Jarosewich 1977, Bild 1977; Fig. 7) and Lueders (McCoy et al. 1996a; Fig. 8). The majority of IAB irons containing silicate inclusions fall into this category. Examples are Pitts, Persimmon Creek, and Zagora. The Ni contents of the members of this type span a wide range (6.58-13.78 wt %), extending beyond the low-Ni cluster of IAB irons. Of the inclusion types found in IAB irons, these angular inclusions most closely resemble the stony winonaites in texture, mineralogy, and mineral composition (Benedix et al. 1998a).

The members of this type are the most silicate-rich of the IAB iron meteorites, although silicate abundances are quite variable even in this group. The large El Taco mass of Campo del Cielo contains a few vol % of angular silicate inclusions, while other IAB irons such as Lueders, Landes, and Woodbine contain upwards of 40 vol % silicate inclusions (e.g. McCoy et al. 1996a). The inclusions are composed mainly of silicates of three basic morphologies: (1) fine-grained, recrystallized "chondritic" silicates (usually the more angular types); (2) medium-grained silicates; and (3) coarse-grained monomineralic crystals usually rounded and found individually in the metallic matrix, as first noted by Bunch et al. (1972). While some IAB irons of this type contain silicate inclusions which are apparently unrelated to each other (Campo del Cielo, Fig. 7), others (e.g. Lueders, Fig. 8) contain adjacent silicate inclusions which appear to have been invaded by molten metal. Adjacent silicate inclusions in these IAB irons, while slightly rotated, are obviously fragments of the same, larger parental inclusion. This relationship is not unlike that expected of a wall-rock invaded by melt from a dike.

The abundance of plagioclase relative to total silicate abundances is quite variable in these inclusions. Most of the inclusions have chondritic abundances of plagioclase

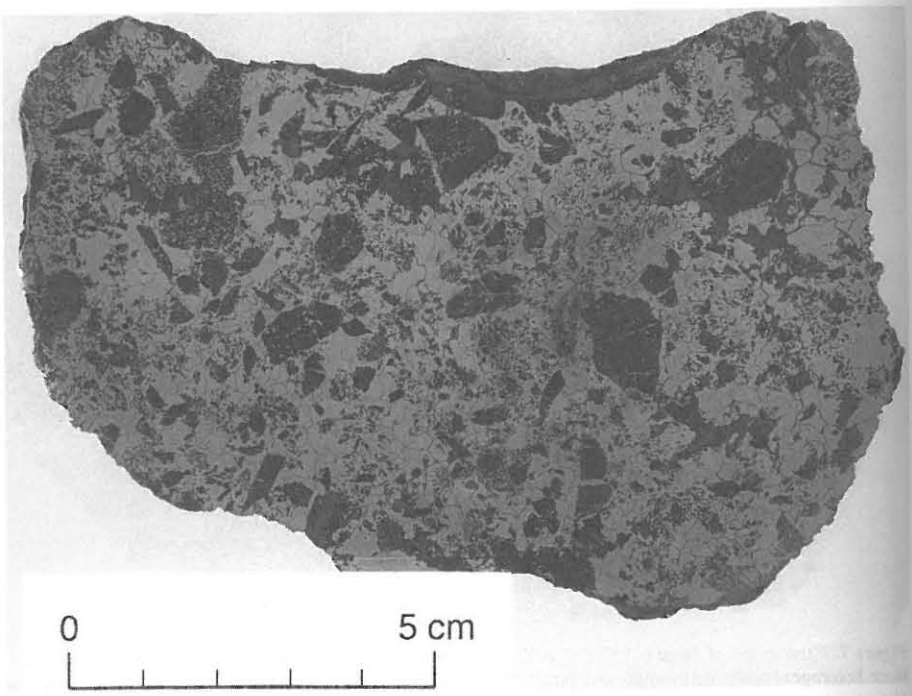

Figure 8. Photograph of polished slice of the Lueders IAB iron illustrating abundant angular silicate inclusions embedded in a metallic matrix.

(~10 vol %; Van Schmus and Ribbe 1968, McSween et al. 1991), although some exhibit enrichments (e.g. Campo del Cielo, Four Corners) or depletions (e.g. Udei Station) relative to chondrite modes. Given the small size and large grain size of some of these inclusions, at least part of this heterogeneity may be due to unrepresentative sampling, while others are clearly indicative of partial melting and melt migration. The depletion of plagioclase in Udei Station is quite striking, where areas up to 5 mm across are virtually devoid of plagioclase. In contrast, some inclusions in Campo del Cielo exhibit evidence for migration of melts in the form of veins of coarse-grained plagioclase and pyroxene with accompanying graphite, as first noted by Wlotzka and Jarosewich (1977).

The stony winonaites are most similar to these angular silicate inclusions. Indeed, they are so similar that Bevan and Grady (1988) have suggested that at least one, the Mount Morris (Wisconsin) winonaite, may be a separated silicate inclusion from the Pine River IAB iron. Some differences do exist (Benedix et al. 1998a); rare relict chondrules are found in Pontlyfni and, possibly, Mt. Morris (Wis.) (Benedix et al. 1998b), but these are apparently absent from silicate-bearing IAB irons. Both Winona and Mt. Morris (Wis.) contain mm-sized, coarse-grained areas which are dominated by olivine, in sharp contrast to the orthopyroxene-rich host. Finally, Tierra Blanca contains poikilitic calcic pyroxenes which reach 9 mm in maximum dimension (King et al. 1981). Neither of these textures is found in IAB silicates.

This group contains minerals with the most and least reduced compositions, which are found in Pine River ($Fa_{1.0}$), Kendall County ($Fs_{1.0}Wo_{0.8}$) and Udei Station ($Fa_{8.0}$; $Fs_{8.7}Wo_{1.7}$). Interestingly, Kendall County is probably the most reduced of the IAB irons,

as Bunch et al. (1970) found no olivine grains they could analyze. Silicate inclusions in IAB irons generally have higher Fa and Fs values than the winonaites. However, as in the winonaites, Fa values are typically lower than Fs values in the IAB inclusions, indicating that reduction may have occurred. (The Fa content of olivine will be greater than the Fs content of orthopyroxene at equilibrium.) Supporting evidence for reduction comes from reverse zoning profiles in olivines in Campo del Cielo (Wlotzka and Jarosewich 1977).

Most of the existing bulk inclusion major and trace element compositions for IAB irons have been measured in this silicate-rich type (Table 8). Bulk major element compositions suggest that IAB silicate inclusions are similar to those of chondrites. Measured Si/Mg ratios for Landes (Kracher 1974), Woodbine (Jarosewich 1967), and Campo del Cielo (Wlotzka and Jarosewich 1977) are roughly similar to chondritic values as noted by Kracher (1974). Bild (1977) also found abundances of lithophile elements roughly similar to chondrites.

Bulk inclusion trace element analyses have been performed for Copiapo, Landes, Woodbine, Campo del Cielo (Bild 1977) and Udei Station (Kallemeyn and Wasson 1985). Measured rare earth element (REE) patterns and abundances for Copiapo and Landes are essentially chondritic. In contrast, Woodbine, Campo del Cielo and Udei Station exhibit fractionated patterns which can be roughly grouped into two types. The REE patterns measured in Campo del Cielo and Udei Station (Bild 1977, Kallemeyn and Wasson 1985) are negatively-bowed (V-shaped) with low REE^{3+} contents and a positive Eu anomaly. In contrast, Woodbine (Bild 1977) exhibits a positively-bowed pattern with high REE^{3+} contents and a negative Eu anomaly. Interestingly, the same two fractionated patterns have been widely observed in the winonaites (Benedix et al. 1998a and references therein). Kallemeyn and Wasson (1985) attribute these patterns to unrepresentative sampling of phosphates, which exhibit a pattern similar to that in Woodbine. Phosphates are concentrated near the edges of the inclusions in these meteorites and are often difficult to sample. While unrepresentative sampling may be important, Bild (1977) notes this range of patterns is consistent with heterogeneous distribution of plagioclase, diopside and phosphates, all of which occur in a low temperature melt and for which there is ample petrologic evidence of melt migration (Wlotzka and Jarosewich 1977, Benedix et al. 1998b).

IAB irons with phosphate-rich inclusions. Phosphates occur in many of the IAB irons as part of the rim sequence at the boundary between silicate inclusions and metal. However, a small number of IAB and IIICD irons are included in this type because they contain more abundant phosphates scattered throughout the silicate inclusions. In addition, these phosphates are often evolved Mg, Na-bearing phosphates (brianite, panethite, chladniite), rather than the more common Ca-bearing phosphates (whitlockite, apatite). Among the IAB irons, San Cristobal (24.97 wt % Ni; Choi et al. 1995) is the only member of this type (Scott and Bild 1974). We discuss here the IIICD irons Carlton (13.28 wt % Ni) and Dayton (17.03 wt % Ni), which contain abundant phosphates (McCoy et al. 1993), because of the possible relationship between IAB and IIICD irons (Kracher 1982, Choi et. al. 1995). These irons are all very high in Ni. Fuchs (1969) reported brianite in the low-Ni IAB Youndegin (6.80 wt % Ni), although compositional data were not given.

Silicate inclusions in San Cristobal examined by Benedix et al. (1998b) are subangular and incompletely rimmed by schreibersite. Veins of troilite and Fe,Ni metal cross-cut the inclusions. The silicates are equigranular and appear to be recrystallized. Silicates comprise ~20% of the sample and plagioclase comprises ~15% of the silicates. Minor graphite rims the inclusion and cohenite is observed within the metallic host. Brianite, first identified in San Cristobal by Scott and Bild (1974), is scattered

Table 8. Selected bulk chemical analyses of silicate-bearing IAB irons and winonaites.

	(1)	(2)	(2)	(3)			(4)	(5)	(6)	(6)	(7)	(8)	(9)
SiO_2	8.55	37.82	45.86	40.52	53.78	Na	mg/g	3.72	6.60	9.1	7.04	8.14	9.20	8.71
TiO_2	0.02	0.13	0.12	0.13	0.20	Mg	mg/g	146	181	158	208	169	149	163
Al_2O_3	0.53	1.36	3.41	1.64	4.13	Al	mg/g	7.0	12.3	14.2	12.4	13.2	14.0	14.2
Cr_2O_3	0.03	0.10	0.33	0.30	0.30	K	µg/g	337	627	750	606	733	--	--
FeO	0.49	3.95	4.94	3.33	3.17	Ca	mg/g	8.2	7.6	5.4	6.8	18	16	18
MnO	0.03	0.35	0.32	0.31	0.39	Sc	µg/g	8.10	10.4	5.8	8.3	12.3	12.1	11.8
MgO	5.19	28.63	28.27	31.94	31.58	V	µg/g	55	59	31	38	61	56	22
CaO	0.34	1.09	1.09	2.48	4.64	Cr	mg/g	1.95	2.68	2.55	1.46	2.09	1.86	0.95
Na_2O	0.29	0.52	1.23	0.47	1.74	Mn	mg/g	2.07	2.36	2.33	2.76	2.08	2.10	1.30
K_2O	0.02	0.04	0.11	0.06	0.07	Fe	mg/g	198	122	128	34.1	160	232	187
P_2O_5	--	0.39	0.26	0.03	n.d.	Co	µg/g	761	132	355	50.8	550	795	665
H_2O^+	--	1.13	0.85	0.76	n.d.	Ni	mg/g	12.1	3.3	4.23	0.73	12.9	13.0	18.7
H_2O^-	--	0.07	0.17	0.12	n.d.	Zn	µg/g	131	259	200	182	291	200	170
Fe (metal)	73.06	1.75	0.80	0.25	n.d.	Ga	µg/g	10.9	6.1	6.58	3.94	14.9	24.8	_7.84
Ni	9.08	0.18	0.27	0.10	n.d.	Ge	µg/g	37.5	5.6	30.7	3.46	32.2	90.7	15.7
Co	0.15	0.02	0.02	b.d.	n.d.	As	µg/g	2.57	0.45	n.d.	n.d.	n.d.	n.d.	n.d.
FeS	1.65	0.33	7.29	1.32	n.d.	Se	µg/g	11.2	15.9	n.d.	n.d.	n.d.	n.d.	n.d.
C	0.21	23.00	5.35	16.41	n.d.	Br	µg/g	0.27	0.56	n.d.	n.d.	n.d.	n.d.	n.d.
P	0.47	--	--	--	n.d.	Cd	ng/g	19	32	n.d.	n.d.	n.d.	n.d.	n.d.
						Sb	ng/g	121	47	n.d.	n.d.	n.d.	n.d.	n.d.
Total	100.11	100.86	100.69	100.17	100.00	La	ng/g	190	132	70	58	250	180	550
						Sm	ng/g	90	70	18	49	260	270	550
						Eu	ng/g	48	71	88	97	95	120	120
						Yb	ng/g	157	137	130	170	300	280	410
						Lu	ng/g	24	21	17	32	49	38	45
						Re	ng/g	99	4	n.d.	n.d.	n.d.	n.d.	n.d.
						Os	ng/g	1220	65	n.d.	n.d.	n.d.	n.d.	n.d.
						Ir	ng/g	1150	59	340	15.7	460	870	240
						Au	ng/g	265	44	86	12.9	185	310	210

(1) Woodbine whole rock, Jarosewich (1967), (2) Separated silicate inclusions from the El Taco mass of Campo del Cielo, Wlotzka and Jarosewich (1977), (3) Landes, Kracher (1974), (4) Tierra Blanca, Kallemeyn and Wasson (1985), (5) Udei Station, Kallemeyn and Wasson (1985), (6) Campo del Cielo silicate inclusions, Bild (1977), (7) Copiapo, Bild (1977), (8) Landes, Bild (1977), (9) Woodbine, Bild (1977)

throughout the silicates, but tends to be in contact with metal, either as veins within the silicates or at the edges of the inclusion.

McCoy et al. (1993) described inclusions in the Carlton and Dayton IIICD irons. These inclusions were extremely enriched in phosphates, in some cases comprising up to 70 vol % of the inclusion and forming the host into which the silicates were embedded. Chlorapatite is the dominant phosphate in Carlton, while Dayton contains abundant whitlockite, brianite and panethite. Silicates in these IIICD inclusions extend to more FeO-rich compositions than in IAB irons ($Fs_{11.6}$ in Dayton) and pyroxene compositions correlate with Ni concentration of the metallic host. In addition, plagioclase compositions are consistently less calcic in IIICD silicate-bearing inclusions ($An_{1.1\text{-}4.9}$) than in IAB inclusions ($An_{9.2\text{-}21.5}$).

Cooling rates

Cooling rates can constrain the physical setting of IAB irons during their solidification and subsolidus cooling. Scott (1982) argued that, in some cases, the cooling rate at the temperature of crystallization of an iron can be determined. If the parent taenite crystals have a dendritic texture, the distance between the dendrite limbs is proportional to the cooling rate at the time of solidification. The only IAB iron to which this method can be readily applied is Mundrabilla, which exhibits a weak dendritic pattern of the parent taenite crystals within the Fe,Ni-FeS intergrowth. Scott (1982) derived a cooling rate of ~5°C per annum, implying relatively rapid cooling at temperatures near the liquidus of Mundrabilla, about 1390°C as estimated using the Fe-S binary phase diagram from Ehlers (1972) and a S concentration of ~8 wt % given by Buchwald (1975). Using conventional methods of determining cooling rates, several authors (e.g. Herpfer et al. 1994, Yang et al. 1997a, Meibom, pers. comm. 1997) have found cooling rates of tens of °C/Ma for a number of IAB irons, implying a slow cooling environment at the time these irons cooled through ~500°C (see Table 4).

Table 9. Ages of silicate inclusions in IAB irons.

meteorite	K-^{40}Ar Ga (1)	^{39}Ar-^{40}Ar Ga (2)	I-Xe ΔMa* (3)	^{147}Sm-^{143}Nd Ga (4)
Caddo County				4.53 ± 0.02
Copiapo		4.45 ± 0.03	+1.36 ± 0.66	
Four Corners	4.49 ± 0.1			
Landes		4.43 ± 0.03	+2.61 ± 0.62	
Mundrabilla		4.52 ± 0.03	-0.68 ± 0.59	
Pitts		4.49 ± 0.03		
		4.52 ± 0.03		
Toluca	4.51 ± 0.1			
Woodbine		4.52 ± 0.03	-3.38 ± 0.30	

Sources: (1) Bogard et al. (1967); (2) Niemeyer (1979b); (3) Niemeyer (1979a), uncertain ages for Pitts silicates omitted; (4) Stewart et al. (1996). Ages from (1) and (2) corrected for new monitor age or decay constant by Herpfer et al. (1994).

*Age is in Ma relative to the Bjurböle chondrite with positive age indicating formation after Bjurböle.

Ages

Most ages for IAB irons are those of the silicate inclusions (Table 9), since it is these inclusions which can be readily dated by a number of isotopic systems (e.g. I-Xe, K-Ar, ^{39}Ar-^{40}Ar, ^{147}Sm-^{143}Nd). More recently, isotopic systems for direct dating of the metallic

host have been developed (e.g. Re-Os), although the interpretation of internal isochrons (e.g. metal-schreibersite pairs, Shen et al. 1996) is not straightforward and may reflect a lengthy period of slow cooling. Absolute ages for the silicate inclusions range from 4.43 Ga to 4.53 Ga. The oldest age, measured in Caddo County, comes from the ^{147}Sm-^{143}Nd chronometer (Stewart et al. 1996), which closes at a relatively high temperature. Supporting evidence for early formation comes from I-Xe closure intervals relative to Bjurböle of -3.38 to +2.61 Ma (Niemeyer 1979a). Ages of 4.43 to 4.52 Ga are derived from the K-Ar and ^{39}Ar-^{40}Ar systems (Bogard et al. 1967, Niemeyer 1979b), which close at lower temperatures. These ages support the idea that partial melting, crystallization and metal-silicate mixing occurred very early in the history of the solar system, as suggested by a number of these authors.

Formation of the IAB and IIICD irons, and winonaites

In this section, we explore whether IAB and IIICD irons and the stony winonaites originate from a common parent body and, thus, reveal different aspects of the history of a common parent body. We then briefly review models for the origin of these meteorites.

A common parent body for IAB irons, IIICD irons and winonaites? It seems almost certain that the stony winonaites sample the same parent body as the IAB iron meteorites. Identical oxygen-isotopic compositions (Clayton and Mayeda 1996; and see Fig. 1) suggest a common oxygen-isotopic reservoir and, possibly, a common parent body. Mineralogies and mineral compositions are overlapping between winonaites and IAB silicate inclusions, particularly the angular silicate inclusions described above. In addition, textures are nearly identical between these two groups. While there are some differences (e.g. a number of silicate inclusion types are found in IAB irons which are not sampled as winonaites and vice versa), these differences probably result from unrepresentative sampling of these two populations, rather than real differences. Cosmic-ray exposure ages, which are commonly used to indicate sampling of meteorites by a common cratering event on a single parent body, are of little use given the considerable scatter in these ages in winonaites (Benedix et al. 1998a) and IAB irons (Voshage 1967).

It seems less clear whether IAB and IIICD irons sample a common parent body. Certainly, some features would seem to support a common parent body. Oxygen-isotopic compositions of silicate inclusions in IIICD irons (Clayton and Mayeda 1996) are essentially indistinguishable from those of the IAB irons and winonaites, again suggesting a common oxygen-isotopic reservoir, if not a common parent body. In addition, inclusions broadly similar in mineralogy to those in IIICD irons can be found among the IAB irons (McCoy et al. 1993, Yugami et al. 1997, Benedix et al. 1998b). However, important differences do exist. Most prominent among these are the differing trends on log-log plots of Ni vs. Ga, Ge and Ir for the metal phase, particularly at high Ni contents (see Fig. 3). Kracher (1982) suggested that these different trends could represent complementary fractional crystallization/partial melting trends on a common parent body. Choi et al (1995) suggested that no compositional hiatus exists between IAB and IIICD irons and, thus, they should be treated as a single group originating from a common parent body. While no hiatus exists at low Ni (<7.2 wt % Ni, Choi et al. 1995), at high Ni the groups are clearly distinguished, a surprising result if these indeed sample a common fractional crystallization/partial melting sequence. Differences exist within the silicate inclusions as well. Pyroxene compositions in IIICD silicate inclusions are correlated with Ni content in the host metal, a trend unlike that from IAB irons, and extend to higher Fs contents than do IAB irons (McCoy et al. 1993). In addition, plagioclase compositions are consistently more albitic than those in IAB irons (McCoy et al. 1993). In summary, the possibility that IAB and IIICD irons sample a common parent body cannot be excluded, but such a conclusion is probably premature. Further discovery of silicate-bearing IIICD irons may resolve this issue. It is also clear that even if IIICD irons sample a different parent body, they likely underwent many of the same processes as the IAB irons and winonaites.

Models for the formation of IAB irons and winonaites. While few theories have been postulated for the formation of the winonaites, several have been suggested for the IAB (and IIICD) irons. Wasson (1972) argued that elemental trends in the IAB irons were due to condensation of the metal directly from the nebula, giving rise to the term "non-magmatic." The major flaw of this hypothesis is that if the variation in elemental abundances is due to nebular processes, comparable ranges in the metal compositions should be found in chondritic material, but are not (Wasson et al. 1980). Another problem with this hypothesis is difficulty of forming parent taenite crystals tens of cms in size by condensation (Wasson et al. 1980).

Wasson et al. (1980) and Choi et al. (1995) have more recently championed a model which suggests IAB irons formed in localized impact melt pools within the chondritic megaregolith of an asteroid. These authors argue that impacts would selectively melt low-temperature fractions (Fe,Ni-FeS eutectic), which would migrate to form pools. Impacts occurred over a range of time and temperatures, producing the correlated variations between Ni and Ga, Ge and Ir. In an extreme view, each IAB iron represents an individual melt pool. While the pools would cool relatively quickly, trapping the unmelted, angular silicate inclusions, Choi et al. (1995) argued that both limited fractional crystallization and magma mixing would occur, producing both the high-Ni IAB irons and the scatter in Ga, Ge and Ir observed at high-Ni concentrations. Impact melting does provide a ready mechanism for mixing silicates and metal, but impact is probably incapable of producing copious quantities of Fe,Ni-FeS-rich melts by selective melting of these phases. Keil et al. (1997) summarize experimental and observational evidence that selective melting by impact occurs only locally and produces an extremely low percentage of melt. Any melt that is produced in this way quenches rapidly, making migration of these selective melts into larger pools difficult, if not impossible.

Several authors have proposed an alternative model in which IAB and IIICD irons formed as a result of partial melting and core formation (Kelly and Larimer 1977, Kracher 1982, 1985, McCoy et al. 1993). Kelly and Larimer (1977) argued that the composition of the metal was consistent with fractional melting of a single composition which was isolated from later melted material so that it would not reequilibrate. Wasson et al. (1980) marshaled several arguments against this model, the most compelling of which were the apparent contradictions between predicted and measured siderophile element partition coefficients and the unreasonably high temperatures required to form the last fractional melts. Kracher (1982, 1985) revived the partial melting model by suggesting that migration of the Fe,Ni-FeS eutectic melt could form a S-rich core at low temperatures. Thus, crystallization of both metal and sulfide determined the siderophile element trends observed. Choi et al. (1995) argued that crystallization of such a magma cannot produce the observed distribution of Ni concentrations. In fact, the system is probably far more complicated than envisioned by Kracher (1982, 1985), including large amounts of carbon and phosphorus, in addition to sulfur. Both McCoy et al. (1993) and Choi et al. (1995) pointed out that the partition coefficients of siderophile elements within such a complicated system remain essentially unknown. Finally, McCoy et al. (1993) argued that correlated trends between the properties of IIICD silicate-bearing inclusions (e.g. mineral compositions, modal mineralogies) and the Ni concentration of the metallic host are best explained by reaction between these two during a prolonged period of fractional crystallization of a common metallic magma. A serious flaw in these models is the inability to explain the mixing and retention of unmelted silicate clasts within the

metallic core. This is particularly problematic in an asteroidal core, which crystallizes from the outside, thus armoring the inner core (Choi et al. 1995). Kracher (1982, 1985) argued that silicates may have been spalled into the core from the core-mantle boundary by impact-generated tectonic activity, although retention of the silicates remains problematic.

Takeda et al. (1994a) argued that IAB irons formed by partial melting and melt migration with heating by both ^{26}Al and impacts. Benedix et al. (1998b) extended this model. These authors argued against impact as a heat source for partial melting. Peak temperatures were insufficient to completely differentiate the body, although limited partial melting did occur. After the peak temperature was reached and cooling and crystallization had begun, a catastrophic impact occurred. The impact caused extensive mixing of metallic and silicate material of this body. Differing silicate lithologies were mixed to form winonaites and IAB irons were produced by co-mingling of silicate clasts and molten metal. After the impact, crystallization (creating high-Ni IAB irons), metamorphism and cooling occurred. Ages of 4.43 Ga to 4.53 Ga imply that this entire process occurred very early in the history of the solar system.

SILICATE-BEARING IIE IRONS

Despite including only eight silicate-bearing members, the IIE irons contain an enormous diversity of silicate inclusion types, ranging from silicate clasts with obvious chondrules, to elongate blebs of quenched basaltic melts. The existence of this stunning diversity within a single group has led to a range of models for the origin of IIE irons. Like the IAB irons discussed above, these models center on impact-generated melting and mixing (Wasson and Wang 1986, Olsen et al. 1994) and indigenous partial melting (McCoy 1995). IIE irons are also quite interesting because they are the only group of silicate-bearing irons for which young ages have been measured, thus lending additional support for the idea that impact played some role in the formation of these meteorites. In this section, we review the petrology and chronology of the silicate-bearing IIE irons and briefly discuss models for their origin.

Petrology and mineralogy

We divide the silicate-bearing IIE irons into five groups which adequately describe the range of inclusion types. Modal analyses and representative silicate compositions are gicen in Tables 10 and 11, respectively.

Netschaëvo. The host metal in Netschaëvo contains 8.6 wt % Ni, midway within the range for all IIE irons of 7.51 to 9.5 wt % Ni (Wasson and Wang 1986). Unfortunately, Netschaëvo was forged shortly after its recovery and this heating has altered much of its extraterrestrial record, although the exact extent of this alteration remains unknown. Netschaëvo is unique among silicate-bearing iron meteorites in containing angular clasts (Fig. 9) which are chondritic in the strictest sense. Bunch et al. (1970), Olsen and Jarosewich (1971), and Bild and Wasson (1977) noted that recrystallized chondrules typical of those found in type 6 ordinary chondrites are present within Netschaëvo. Mineralogically, these clasts are essentially identical to chondrites, containing olivine, orthopyroxene, sodic plagioclase and phosphates. Modally, Netschaëvo is richer in orthopyroxene and phosphates than typically found in ordinary chondrites (Table 10). Compositions of olivine ($Fa_{14.1}$) and orthopyroxene ($Fs_{13.6}$) are more reduced than found in H chondrites (Table 11) and the approximately equal Fa and Fs values suggest that reduction has played a role in the formation of these clasts. Rubin (1990) reported a metallographic cooling rate of ~3°C/Ma for metal within a silicate clast in Netschaëvo.

Table 10. Modal compositions (vol %) of silicate inclusions in IIE irons, excluding Fe,Ni metal and FeS.

	Colomera (1)	Elga (1)	Kodai-kanal (1)	Miles (2)*	Miles (2)**	Netsch-aëvo (3)	Techado (4)	Watson (5)	Weekeroo Station (1)
olivine	0	0	0	tr	0.6	26	81***	56	0
orthopyroxene	2-4	2-4	2-4	17.1	-	52		22	24
clinopyroxene	21-28	21-28	21-28	33.6	-	5	0	5	16
plag-trid-glass	67	68	73	49.3	91.1	14	19	15	59
phosphate	0.4-2	0.4-2	0.4-2	-	6.4	2	nd	1	0.4-2
yagiite	~3	-	-	-	-	-	-	-	-

*Average gabbroic inclusion
**Cryptocrystalline inclusion, also 0.6 vol% rutile and 0.3 vol% sodalite
***Includes both olivine and orthopyroxene
Sources of data: (1) Prinz et al. (1983b); (2) Ikeda and Prinz (1996); (3) Olsen and Jarosewich (1971); (4) McCoy, unpublished; (5) Olsen et al. (1994), the mode has been converted to vol% from the published wt % data.

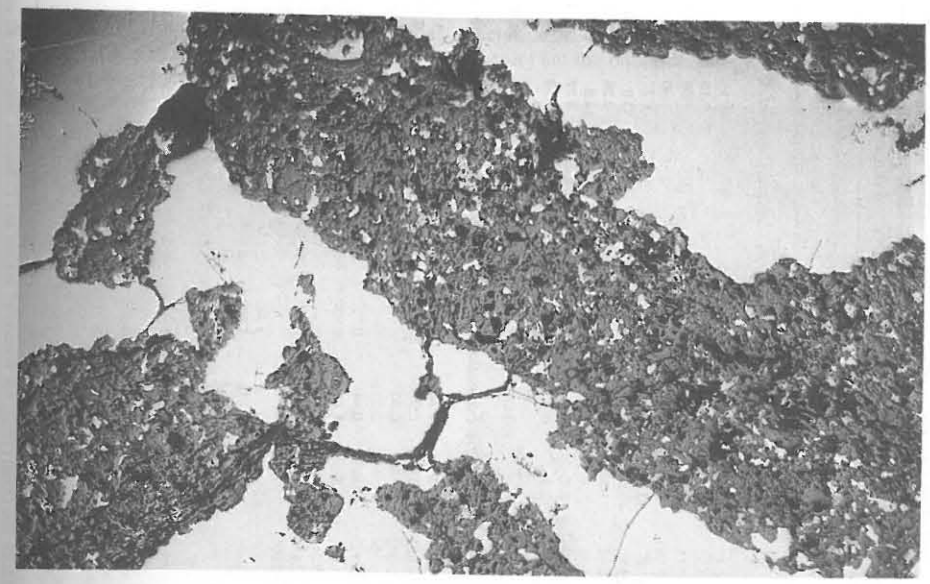

Figure 9. Photograph of angular, chondritic silicate inclusions in Netschaëvo. Field of view is 13 mm wide.

Techado. Techado contains 8.88 wt % Ni in its metallic host and, thus, also lies in the mid range of Ni concentrations for IIE irons. Casanova et al. (1995) described a single silicate inclusion ~1.5 cm in length from Techado. Like the inclusions in Netschaëvo, this inclusion is roughly chondritic in bulk composition, consisting of olivine, orthopyroxene, plagioclase, Fe,Ni metal and troilite. Although Casanova et al. (1995) suggested that the inclusion was unmelted, it has an unusual elongated shape (Fig. 10) that suggests that it might have been heated to temperatures sufficient to cause it to soften and become stretched. Unlike Netschaëvo, no relict chondrules were observed within the inclusion. Mineral compositions for olivine ($Fa_{16.4}$) and orthopyroxene

Table 11. Representative silicate compositions from IIE iron meteorites.

	OLIVINE		ORTHOPYROXENE				CLINOPYROXENE					PLAGIOCLASE						
	Netschaëvo	Watson	Netschaëvo	Watson	Weekeroo Station	Colomera	Netschaëvo	Watson	Weekeroo Station	Colomera		Netschaëvo	Watson		Weekeroo Station		Colormera	
Chemical Composition (wt %)																		
SiO_2	40.0	39.3	56.3	56.4	55.1	55.2	55.3	54.2	52.7	52.1	51.0	65.5	67.1	67.1	67.9	67.4	67.1	65.3
Al_2O_3	b.d.	b.d.	0.22	0.51	0.30	0.06	0.70	0.74	0.96	1.18	4.1	20.8	19.0	18.3	19.6	18.9	19.9	18.4
Cr_2O_3	b.d.	0.06	0.24	0.71	0.25	0.24	n.d.	1.57	0.90	1.08	0.83	n.d.	b.d.	b.d.	n.d.	n.d.	n.d.	n.d.
TiO_2	b.d.	b.d.	0.22	0.16	0.30	1.33	n.d.	0.34	0.52	1.00	2.41	n.d.	b.d.	b.d.	n.d.	n.d.	n.d.	n.d.
FeO	13.5	18.7	9.1	11.2	13.7	14.8	3.5	5.58	11.7	8.2	4.6	0.40	0.61	0.29	0.27	0.23	0.17	0.17
MgO	46.0	40.4	31.8	28.6	28.5	27.1	17.0	16.4	15.7	15.6	14.6	n.d.	b.d.	b.d.	n.d.	n.d.	n.d.	n.d.
MnO	0.35	0.45	0.39	0.46	1.35	0.11	n.d.	0.30	0.75	0.38	0.39	n.d.	b.d.	b.d.	n.d.	n.d.	n.d.	n.d.
CaO	b.d.	0.04	0.75	1.88	1.47	1.07	21.9	19.1	17.2	19.3	21.0	2.96	0.43	0.28	2.33	1.91	0.36	0.05
Na_2O	b.d.	b.d.	0.06	0.09	b.d.	0.11	n.d.	0.84	b.d.	0.77	0.98	9.7	10.1	6.20	9.5	7.6	11.7	1.00
K_2O	n.d.	b.d.	b.d.	b.d.	b.d.	b.d.	n.d.	b.d.	b.d.	0.09	0.05	0.76	0.84	6.83	0.86	4.9	115	14.7
Total	99.85	98.95	99.08	100.01	100.97	100.02	98.40	99.07	99.43	99.70	99.96	100.12			100.46	100.94	100.38	99.62
Atomic Formula (O = 4 for olivine, 6 for pyroxene, 8 for plagioclase)																		
Si	0.999	1.014	1.988	1.999	1.963	1.984	2.028	1.998	1.972	1.941	1.874	2.892	2.997	3.024	2.970	2.983	2.948	3.010
Al	-	-	0.008	0.021	0.012	0.003	0.030	0.032	0.042	0.054	0.176	1.083	1.000	0.972	1.010	0.994	1.031	0.997
Cr	-	0.001	0.008	0.020	0.009	0.007	-	0.046	0.027	0.037	0.026	-	-	-	-	-	-	-
Ti	-	-	0.006	0.004	0.008	0.036	-	0.009	0.015	0.024	0.066	-	-	-	-	-	-	-
Fe	0.282	0.404	0.269	0.332	0.408	0.445	0.107	0.172	0.335	0.255	0.141	0.016	0.023	0.011	0.010	0.005	0.006	0.005
Mg	1.712	1.555	1.674	1.511	1.519	1.452	0.930	0.901	0.876	0.866	0.799	-	-	-	-	-	-	-
Mn	0.007	0.010	0.013	0.014	0.041	0.003	-	0.009	0.024	0.011	0.013	-	-	-	-	-	-	-
Ca	-	0.001	0.028	0.071	0.056	0.041	0.861	0.755	0.690	0.770	0.825	0.141	0.021	0.014	0.109	0.090	0.017	0.003
Na	-	-	0.004	0.006	-	0.008	-	0.060	-	0.054	0.070	0.828	0.875	0.542	0.806	0.648	0.997	0.089
K	-	-	-	-	-	-	-	-	-	0.004	-	0.043	0.048	0.393	0.048	0.276	0.065	0.864
Total Cations	2.991	2.985	3.998	3.979	4.016	3.979	3.849	3.983	3.981	4.016	3.990	5.003	4.964	4.956	4.953	4.996	5.064	4.968
Molar Mineral End Members and mg# (100(MgO/(MgO+FeO)))*																		
Fs	-	-	13.6	17.3	23.0	5.6	5.6	9.4	17.6	13.5	8.0	-	-	-	-	-	-	-
Wo	-	-	1.4	3.7	2.1	45.4	45.4	41.3	36.3	40.7	46.7	-	-	-	-	-	-	-
En	-	-	85.0	78.9	74.9	49.0	49.0	49.3	46.1	45.8	45.3	-	-	-	-	-	-	-
Ab	-	-	-	-	-	-	-	-	-	-	-	81.8	92.7	57.2	83.7	63.9	92.5	9.3
An	-	-	-	-	-	-	-	-	-	-	-	13.9	2.2	1.4	11.3	8.9	1.6	0.3
Or	-	-	-	-	-	-	-	-	-	-	-	4.3	5.1	41.4	5.0	27.2	5.9	90.4
mg#	85.9	79.4	86.2	82.0	78.8	76.5	89.6	84.0	70.5	77.2	85.0	-	-	-	-	-	-	-

Data from Olsen et al. (1994) for Watson; Bunch and Olsen (1968) for Weekeroo Station and Colomera feldspars; all others from Bunch et al. (1970)

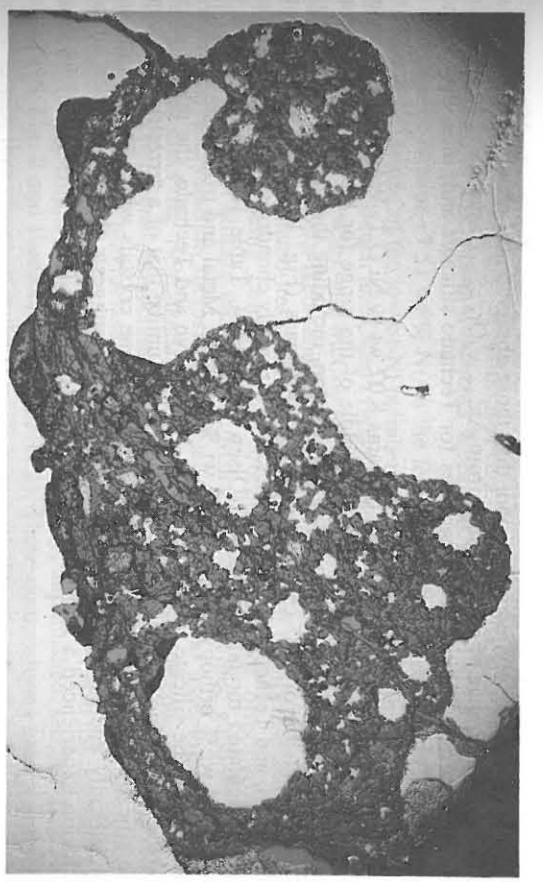

Figure 10. Photograph of elongate, curved silicate inclusion in Techado. The shape of this inclusions implies that it was heated to the point where it was ductile, but the bulk mineralogy is undifferentiated. Field of view is 13 mm wide.

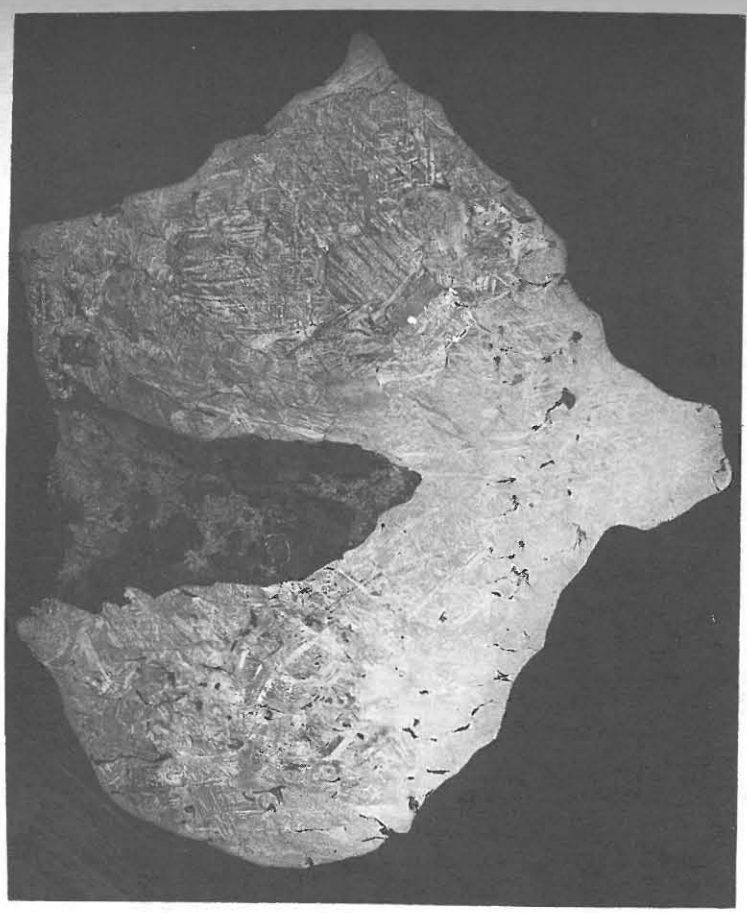

Figure 11. Photograph of a slab containing the large silicate inclusion in Watson. This inclusion is chondritic in silicate mineralogy, but essentially lacks metal and troilite. The silicate inclusion is ~10 cm in maximum dimension. (Photograph courtesy of the Smithsonian Institution).

($Fs_{15.3}Wo_{1.6}$) are slightly more FeO-poor than those observed in H chondrites. Plagioclase exhibits a small range of compositions from $An_{14.9\text{-}15.4}Or_{5.6\text{-}6.3}$. Casanova et al. (1995) did not report complete microprobe analyses for Techado silicates and, thus, they are not included in Table 11.

Watson. The Watson meteorite contains 8.07 wt % Ni (J.T. Wasson, pers. comm. 1995) within its metallic host, near the middle of the range for IIE irons. Olsen et al. (1994) reported a comprehensive study of Watson, including the discovery of a single silicate inclusion of ~30 cm^3 within the 93 kg mass (Fig. 11). Like inclusions in Netschaëvo and Techado, the Watson inclusion is roughly chondritic in bulk composition and a calculated modal mineralogy (Olsen et al. 1994, Table 10) contains 57 wt % olivine, 23 wt % orthopyroxene and 12 wt % feldspar. Metal and troilite are essentially absent from the silicate inclusion. Unlike Netschaëvo and Techado, the texture of the Watson silicate inclusion is decidedly igneous, not unlike that of a terrestrial peridotite. The silicate inclusion is dominated by orthopyroxene crystals which reach 1 mm and poikilitically enclose olivine crystals. This texture suggests that the Watson silicate inclusion experienced a high degree of melting. Mineral compositions (olivine $Fa_{20.6}$,

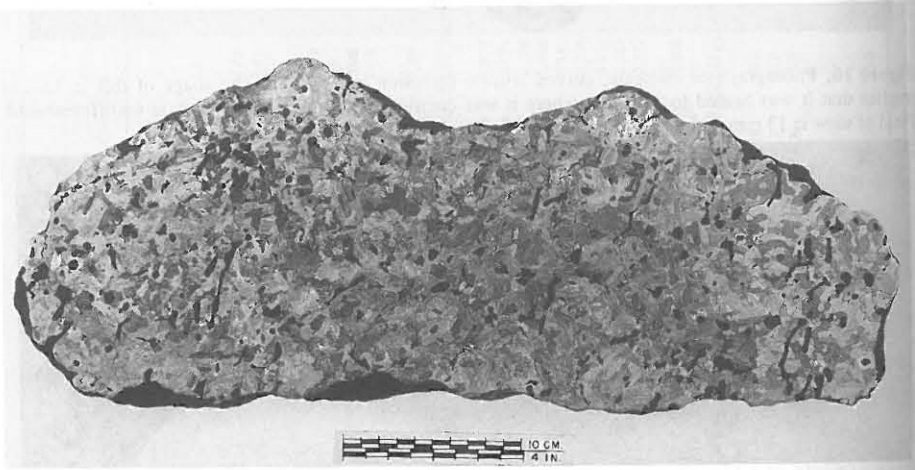

Figure 12. Photograph of a slab of Weekeroo Station exhibiting globular, silicate inclusions typical of Weekeroo Station, Miles, Colomera, Kodaikanal and Elga. Silicate inclusions are composed of plagioclase, orthopyroxene and clinopyroxene in a ratio of ~2:1:1. (Photograph courtesy of the Smithsonian Institution).

orthopyroxene $Fs_{17.6}Wo_{3.8}$) are within the range for H chondrites. Plagioclase is composed of an albitic host with K feldspar exsolution (antiperthite). Olsen et al. (1994) noted that shock-melted pockets are found in the metallic host and McCoy (1995) found shearing and shock deformation within the silicate inclusions, all of which indicate that Watson experienced a relatively severe post-formational shock event.

Weekeroo Station and Miles. The remaining silicate-bearing IIE irons (Weekeroo Station, Miles, Colomera, Kodaikanal and Elga) all contain what Prinz et al. (1983b) aptly described as globular silicate inclusions. Macroscopically, there is little to distinguish the silicate inclusions between these five meteorites and Figure 12 illustrates silicate inclusions in Weekeroo Station. Modal analyses (Table 10), however, indicate that Weekeroo Station and Miles mostly contain inclusions composed of orthopyroxene,

clinopyroxene and plagioclase, while inclusions in Colomera, Kodaikanal and Elga consist almost exclusively of clinopyroxene and plagioclase with only minor orthopyroxene. For this reason, we discuss Weekeroo Station and Miles first.

Weekeroo Station (7.51 wt % Ni) is the lowest-Ni member of group IIE and Miles (7.96 wt % Ni) is one of the lowest-Ni members. Silicate inclusions in Weekeroo Station have been studied by Bunch and Olsen (1968), Bunch et al. (1970), Olsen and Jarosewich (1970), Prinz et al. (1983b), and McCoy (1995), and Miles silicate inclusions have been studied by McCoy (1995), Ikeda and Prinz (1996), Ikeda et al. (1997) and Ebihara et al. (1997). Both of these meteorites contain subequal amounts of plagioclase and pyroxene, with the pyroxene being comprised of subequal amounts of orthopyroxene and clinopyroxene. Most silicate inclusions in Miles are coarse-grained gabbros, but fine-grained, cryptocrystalline inclusions with a variey of mineral assemblages are also present (Ikeda and Prinz 1996, Ikeda et al. 1997). Weekeroo Station contains a mixture of coarse-grained pyroxene-plagioclase inclusions and inclusions with coarse pyroxene and radiating fine-grained plagioclase-tridymite mixtures. Bunch et al. (1970) reported a composition of Fs_{22} for orthopyroxene in Weekeroo Station. Miles also has a small range of orthopyroxene compositions from $Fs_{19.9\text{-}23.2}$ (McCoy, unpublished, see also Ikeda and Prinz 1996, Fig. 2 and Ikeda et al. 1997, Fig. 2). These compositions are considerably more FeO-rich than observed in the two IIE irons with "primitive" silicates, Netschaëvo and Techado. As is the case in most of the globular silicates, both plagioclase feldspar and potassium feldspar are present in both Weekeroo Station and Miles (Table 10). Pyroxene and plagioclase in Miles and Weekeroo Station exhibit shock deformation features indicative of mild shock.

Colomera, Kodaikanal and Elga. The other subgroup of globular silicate inclusions are those in Colomera (7.86 wt % Ni), Kodaikanal (8.71 wt % Ni) and Elga (8.25 wt % Ni). Prinz et al. (1980) examined silicate inclusions in all three meteorites, while Bunch and Olsen (1968) and McCoy (1995) examined Colomera and Kodaikanal. Elga was extensively studied by Osadchii et al. (1981), Bence and Burnett (1969) studied Kodaikanal, and Wasserburg et al. (1968) studied Colomera. Silicate inclusions in these meteorites are dominated by glass of plagioclase-tridymite composition and clinopyroxene in a ratio of ~2:1. Wasserburg et al. (1968) identified one sanidine crystal of 11 cm in length. Minor orthopyroxene, olivine, and phosphate are also found. Yagiite, $(K,Na)_2(Mg,Al)_5(Si,Al)_{12}O_{30}$, comprises ~3% of the silicate inclusions in Colomera (Table 10). Texturally, silicate inclusions in these meteorites are similar to, but more diverse, than those in Weekeroo Station and Miles. Buchwald (1975) and McCoy (1995) noted that in addition to the coarse-grained inclusions and those with radiating, fine-grained intergrowths of plagioclase and tridymite, glassy inclusions are also present and that these inclusions occur well beneath the heat-altered zone formed during atmospheric entry of the meteorite. McCoy (1995) observed coarse-grained and glassy silicate inclusions occurring within a few mm of one another. Mineral compositions within this group are somewhat more diverse, ranging from $Fa_{15\text{-}16}$ in Elga (Osadchii et al. 1981) and Fa_{23} in Colomera (Bunch et al. 1970). Clinopyroxene exhibits a range of compositions within both Colomera and Kodaikanal (Table 11; Bunch et al. 1970) and both plagioclase and potassium feldspar are present in these meteorites (Table 10).

Composition

Few analyses of silicate inclusions from IIE irons have been done. Bulk major element analysis of a composite of 12 Weekeroo Station inclusions was presented by Olsen and Jarosewich (1970), major and trace element data were given by Olsen et al. (1994) for an inclusion from Watson, and major and trace element data were given for 6 gabbroic and 3 cryptocrystalline inclusions from Miles by Ebihara et al. (1997). The

composite of Weekeroo Station inclusions is unlike any chondrite in composition, although it is similar to bulk chondritic composition minus 50% olivine (Olsen and Jarosewich 1970). The Watson inclusion has a bulk composition like that of an H chondrite, minus most of the metal and troilite (Olsen et al. 1994). The Miles inclusions show fractionated lithophile element abundances, with the cryptocrystalline clasts showing the most extreme fractionations (Ebihara et al. 1997). The plagiophile elements Na, Al and K are enriched, as are the incompatible elements Ti and Hf, while Mg is depleted relative to H chondrites. The REE abundances are generally elevated over CI values, although some of the cryptocrystalline clasts have LREE depletions. These clasts clearly are not chondritic in composition, but neither are they what one might expect for a partial melt of a chondritic source (Ebihara et al. 1997).

Chronology

A particularly intriguing feature of the silicate-bearing IIE irons is the broad range of ages measured for different meteorites (Table 12). IIE irons can be divided into an "old" subgroup consisting of Techado, Miles, Weekeroo Station and Colomera and a "young" subgroup which includes Netschaëvo, Watson and Kodaikanal. Ages for a single meteorite from a variety of radiometric techniques generally agree with these broad groupings, although the spread in ages for Weekeroo Station ranges by as much as 200 Ma (Table 12). In addition to the ages given in Table 12, Burnett and Wasserburg (1967a) argued that the relatively low initial $^{87}Sr/^{86}Sr$ ratio of Kodaikanal for the very high Rb/Sr requires a late Rb/Sr fractionation, rather than simple metamorphic equilibration.

Table 12. Measured ages for silicate inclusions in IIE iron meteorites.

	^{39}Ar-^{40}Ar Ga	K-Ar Ga	Rb-Sr Ga	I-Xe ΔMa	Pb-Pb Ga
Colomera		4.24	4.51		
Kodaikanal		3.5±0.1	3.7±0.1		3.676±0.003
Miles	4.41±0.01				
Netschaëvo	3.75±0.03				
Techado	4.48±0.03				
Watson	3.656±0.005	~3.5			
Weekeroo Station	4.49±0.03		4.28, 4.39±0.07	+10 Ma	

Sources of ages: ^{39}Ar-^{40}Ar - Miles, Techado, Watson (Garrison and Bogard, 1995), Netschaëvo, Weekeroo Station (Niemeyer, 1980) (using corrected age for the St. Severin monitor); K-Ar - Colomera (D.D. Bogard, unpublished data), Kodaikanal (Bogard et al., 1969), Watson (Olsen et al., 1994); Rb-Sr - Colomera (Sanz et al., 1970), Kodaikanal (Burnett and Wasserburg, 1967b), Weekeroo Station (Burnett and Wasserburg, 1967b; Evensen et al., 1979) (all recalculated using $\lambda = 1.420 \times 10^{-11}$); I-Xe - (Niemeyer, 1980) (age in Ma relative to the Bjurböle chondrite, positive age indicates formation after Bjurböle); Pb-Pb - (Göpel et al., 1985).

Origin

A detailed discussion of the origin of IIE irons is beyond the scope of this review. Many of the arguments concerning a near-surface impact melt origin vs. a deep-seated indigenous origin are similar to those of other silicate-bearing irons. In particular, the siderophile element trends are difficult to explain by fractional crystallization of a largely metallic core and a core setting provides no ready mechanism for mixing silicates into the molten metal (Wasson et al. 1980). In support of a core origin is the difficulty of

producing metallic metal melts from localized impact melt events and the slow metallographic cooling rates which appear to require deep burial (McCoy 1995). However, some features of silicate-bearing IIE irons are unique and it is these features which are worthy of further consideration.

Diversity of silicate inclusions types. Silicate inclusions in IIE irons are the most diverse in all silicate-bearing irons. These inclusion types can be arranged from most "primitive" to most "differentiated." Such a sequence would include five types: (1) Chondritic silicate inclusions in Netschaëvo, which are true chondritic clasts within a metallic matrix, (2) Partially melted, but undifferentiated clasts found in Techado, exhibiting evidence of partial melting in the overall outline of the inclusion, but maintaining an approximately chondritic mineralogy, (3) Totally melted inclusions which have lost metal and troilite, of the type observed in Watson, (4) Plagioclase–orthopyroxene–clinopyroxene "basaltic" partial melts of the type found in Weekeroo Station and Miles, which contain mineral abundances expected of a simple partial melt from a chondritic source, and (5) Plagioclase-clinopyroxene partial melts, such as those in Colomera, Kodaikanal, and Elga, which appear to be more differentiated than those in Weekeroo Station and Miles. There appears to be no correlation between the degree of evolution of the silicate inclusions and the Ni concentration in the host metal, which increases during fractional crystallization. Thus, the evolution of the silicates and metal does not appear to have progressed systematically. There are no clasts whose mineralogy would indicate that they are residues from partial melting of chondritic material.

Precursor chondritic material. A number of authors have argued that IIE irons represent impact melting at the surface of the H chondrite parent body. Olsen et al. (1994) pointed out the numerous similarities between H chondrites and Watson, including silicate mineral and bulk composition, oxygen-isotopic composition, and cosmic-ray exposure ages. Casanova et al. (1995) echoed this sentiment in their examination of a silicate inclusion in Techado. Clayton and Mayeda (1996) pointed out the similarities in oxygen-isotopic composition between H chondrites and IIE irons. The question of the link between IIE irons and H chondrites cannot be easily resolved, but IIE irons and H chondrites may not be as similar as previously suggested. In particular, oxygen-isotopic compositions differ between the two groups, $\Delta^{17}O = 0.73\pm0.09$ for H chondrites and 0.59 ± 0.05 for IIE irons, although there is some overlap. In addition, "primitive" IIE irons whose mineral compositions are unchanged by igneous processes are FeO-poor compared to H chondrites. However, the Sr isotopic results of Kodaikanal argue for late Rb/Sr fractionation (Burnett and Wasserbuerg 1967a), which could be due to shock melting and redistribution. The role of reduction in the formation of Netschaëvo and Techado is not fully established. These observations suggest that it is premature to declare a definitive link between IIE irons and H chondrites.

Age interpretation. Probably the most intriguing question in the genesis of IIE irons is the interpretation of the "young" ages for some silicate-bearing members. If these young ages record the formation of these rocks, this would provide definitive evidence for an impact-melt origin, since any indigenous heat source would have dissipated by 3.8 Ga in an asteroidal-size body.

We argue that the young ages do not represent the formation of these rocks, although some late melting and differentiation may have occurred. There is no correlation between the degree of differentiation experienced by the silicate inclusions and their ages. Thus, one cannot argue for a progression of increasing silicate differentiation with time. An alternative to the young formation scenario is that the ages were reset by shock events. Clearly, there is abundant evidence for post-formational shock in the form of deformation features within the silicate minerals. The real question is whether melting may have

occurred at 3.8 Ga related to these shock events. We find the most compelling evidence for this in the form of the diversity of inclusion textures present within a single silicate-bearing IIE iron. Colomera contains coarse-grained igneous inclusions, fine-grained inclusions with radiating plagioclase-tridymite intergrowths, and glassy inclusions. This diversity clearly did not result from a single cooling event. Instead, we suggest that shock waves were focused into the inclusions, a feature commonly seen in the metallic hosts of some IIE irons (e.g. Watson; Olsen et al 1994). Intense, localized shock melting occurred within these inclusions and rapid cooling followed. Thus, silicate inclusions in some IIE irons record both early, slow cooling and later, rapid cooling following an intense shock event. An interesting consequence of this diversity is that different inclusions may have had dramatically different histories and yield different ages. Petrographic characterization of age-dated inclusions may prove absolutely essential in interpreting IIE iron ages and origins.

PALLASITES

Pallasites are stony irons composed of roughly equal amounts of silicate, dominated by olivine, and metal plus troilite. There are currently three separate pallasite types; the main-group pallasites, the Eagle Station grouplet, and the pyroxene-pallasite grouplet. The Eagle Station and pyroxene-pallasite grouplets contain 3 and 2 members, respectively, while the main-group contains approximately 41 members. Uncertainties in pairings makes precise census of main-group pallasites difficult. The three pallasite groups are distinguished from each other by differences in silicate mineralogy and composition, metal composition and O-isotopic composition. Figure 13 shows the O-isotopic compositions of the different pallasite groups, the most diagnostic characteristic, compared to meteorite groups in nearby O-isotope space. Note that the main-group pallasites are in the oxygen-isotope cluster occupied by IIIAB irons, mesosiderites, howardites, eucrites, diogenites, angrites and brachinites (Figs. 1d, 13).

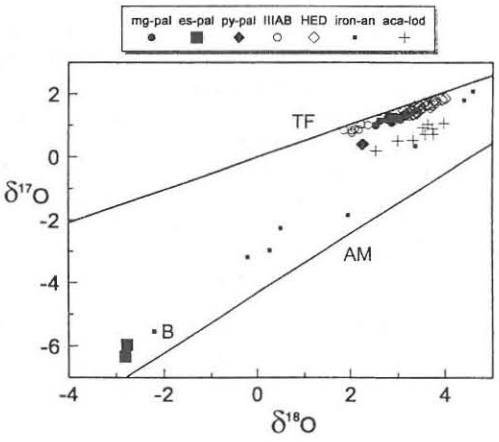

Figure 13. Oxygen-isotopic compositions of pallasites compared to other achondrites. Main-group pallasites (mg-pal) have O-isotopic compositions within the same O-isotope group as oxide phases in IIIAB irons, howardites, eucrites and diogenites (HED) and mesosiderites and angrites, which are not shown for clarity. The pyroxene-pallasites (py-pal) stand alone in O-isotope space, although an acapulcoite and a lodranite (aca-lod) plot nearby. The Eagle Station pallasites (es-pal) occupy a distinct region near the Allende mixing line (AM), and near silicates from the anomalous iron (iron-an) Bocaiuva (B). All data from Clayton and Mayeda (1996).

Individual olivine grains in pallasites can be on the order of a cm in size, and clusters of grains can be several cm in size (e.g. see Ulff-Møller et al. 1998). Olivine can be heterogeneously distributed. An extreme example is Brenham. Different specimens of Brenham can contain large regions of metal devoid of olivine with a few patches of typical pallasite material here and there (Fig. 14). This makes determination of modes

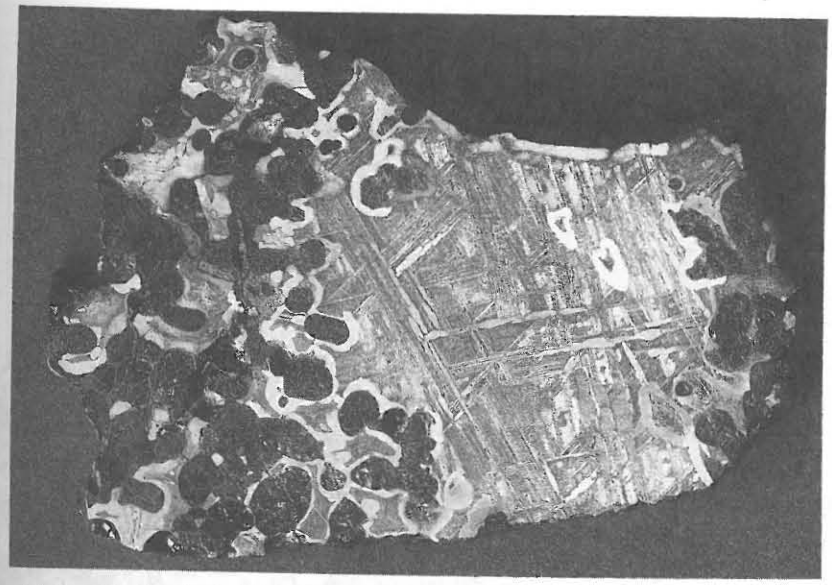

Figure 14. A polished and etched slab of the Brenham main-group pallasite display the very heterogeneous nature of some specimens of this pallasite. The specimen is 13 cm in maximum dimension. (Courtesy of the Smithsonian Institution).

difficult and fraught with uncertainties. The most reliable modal data obtained from polished slabs show that olivine varies from about 35-85 vol %, with chromite and phosphates generally <1 vol % each (Buseck 1977, Ulff-Møller et al. 1998). The olivine/metal weight ratio of pallasites ranges from 0.3-2.5. The macroscopic olivine-metal textures are also variable, with olivine grains varying from highly angular, fragmental shapes (Fig. 15) to well rounded grains (Fig. 16) (Buseck 1977, Scott 1977d). On a microscopic scale, even the most angular grains show evidence of rounding of the corners (Scott 1977d).

Main-group pallasites

The main-group pallasite silicates are composed dominantly of olivine, with minor amounts of low-Ca pyroxene, chromite and several different phosphates. Most main-group pallasites contain olivine of ~$Fo_{88\pm1}$ composition, but a few have anomalously ferroan olivines, down to Fo_{82} for Phillips County and Springwater (Fig. 17). Representative olivine compositions are given in Table 13. Few modern analyses of pallasite olivines are available in the literature, and most available data are from the partial analyses of Buseck and Goldstein (1969). Modern analyses for olivines from a few pallasite can be found in Davis and Olsen (1991), Mittlefehldt (1980), Righter et al. (1990) and Yanai and Kojima (1995). In addition to normal olivines, some pallasites also contain a minor amount of phosphoran olivine with 4 to 5 wt % P_2O_5 (Table 13) in zones continuous with normal olivine (Buseck 1977).

Main-group pallasite olivines contain very low concentrations of the trace transition elements (Table 14). The Sc contents vary from 0.5 to 2.4 μg/g, Cr from 160 to 600 μg/g, Mn from 1.5 to 3.2 mg/g and Zn from 5 to 8 μg/g (Davis 1977, Mittlefehldt 1980, and unpublished). The siderophile elements Co and Ni are generally at low concentrations. Nearly all modern Co analyses and most Ni analyses have been done by a bulk technique (INAA—Davis 1977, Mittlefehldt 1980 and unpublished), so contamination from the

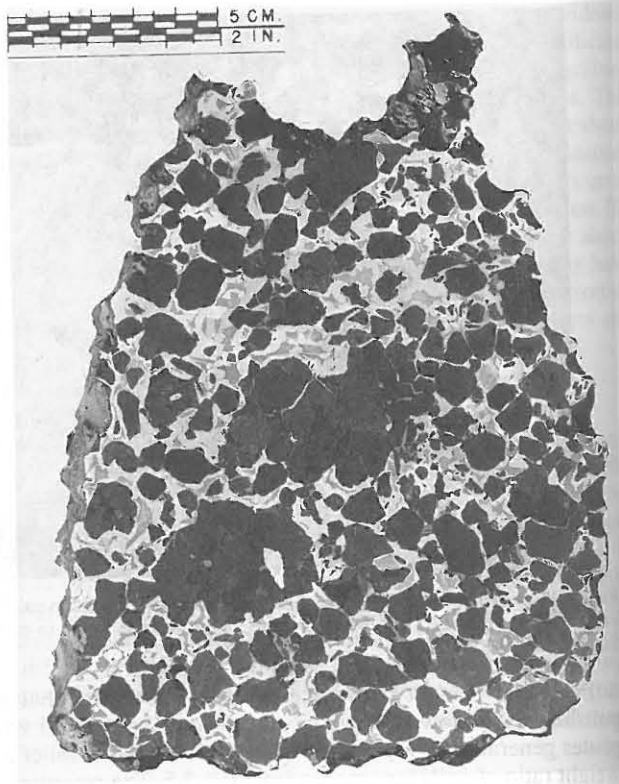

Figure 15. A polished and etched slab of the Salta main-group pallasite showing roughly cm-sized angular-subangular olivines dispersed in metal, and two larger olivine masses, one of which is veined by metal as though it was in the process of breaking up when the metal crystallized. (Photo courtesy of the Smithsonian Institution).

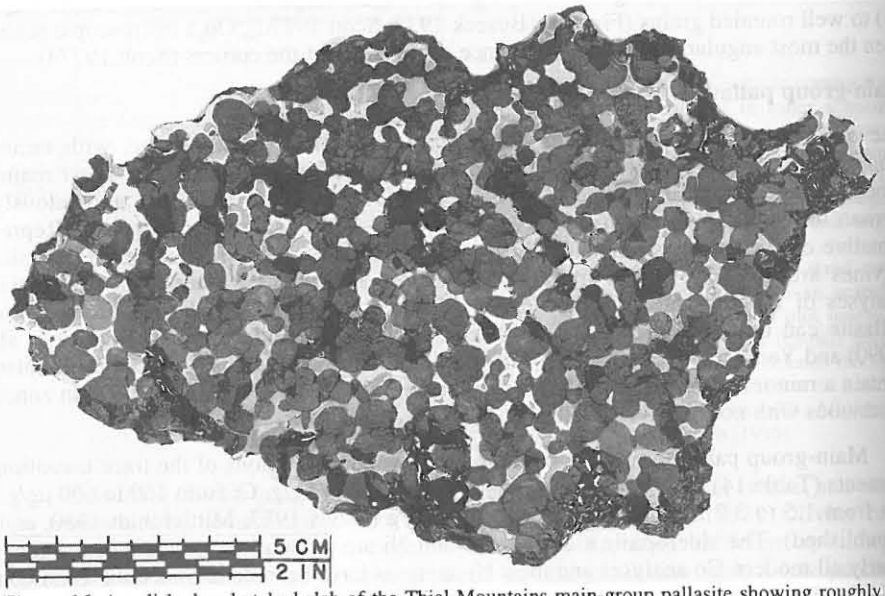

Figure 16. A polished and etched slab of the Thiel Mountains main-group pallasite showing roughly cm-sized, well rounded olivines dispersed in metal. (Photograph courtesy of the Smithsonian Institution).

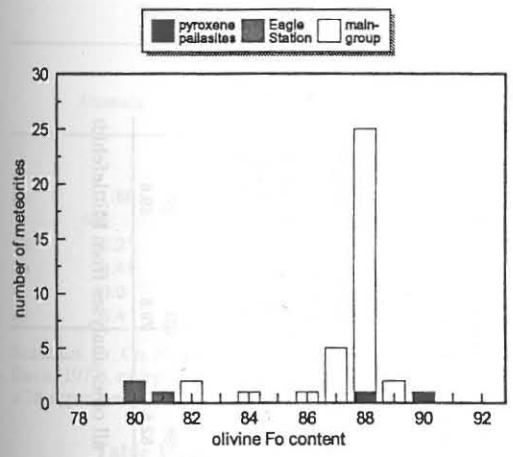

Figure 17. Histogram of Fo contents of pallasite olivines. Main-group pallasites have a narrow range in olivine compositions, except for three ferroan outliers. Data are from Boesenberg et al. (1995), Buseck (1977), Buseck and Goldstein (1969), Mittlefehldt (unpublished), Yanai and Kojima (1995).

metal phase is a worry. Main-group pallasite metal contains 660 to 900 times the Co and 4200 to 6400 times the Ni measured in most olivines. For a few pallasites, analyses of Ni in olivine have been done by ion microprobe (Reed et al. 1979) and these data agree well with the INAA bulk data (Mittlefehldt, unpublished), except that the latter are systematically lower than the ion probe data. Nickel in pallasite olivines shows a depletion in rims compared to cores, and in small compared to large grains (Reed et al. 1979). The systematically lower Ni content in the bulk analyses compared to the olivine core analyses reported by (Reed et al. 1979) are therefore understandable. The bulk analyses yield means of 7.4 μg/g Co and 18 μg/g Ni for main-group pallasite olivines.

Major and minor element contents are zoned in main-group pallasite olivines. Zhou and Steele (1993) showed that the count rates from electron microprobe analyses for Al, Cr and Ca decreased toward the rims of Springwater olivines, while that for Mn increased. Zhou and Steele (1993) did not report concentration profiles, only "normalized counts", but they estimated concentrations: Mn—2.75 mg/g; Cr—140 μg/g; Al—10 μg/g; Ca—64 μg/g. Presumably, these are for homogeneous cores. Miyamoto and Takeda (1994) similarly showed decreasing concentrations of CaO and Cr_2O_3, and Fa content for Esquel olivines toward the rim. The ion probe results of Hsu et al. (1997) also show that Cr decreases and Mn increases from the center to the rim for Brenham olivines.

Pyroxene occurs as a trace component in at least some main-group pallasites (Buseck 1977). The grains are typically only a few microns in size, and occur in symplectic intergrowths on the margins of olivine grains with one or more of the phases troilite, chromite, kamacite and phosphate. There are few analyses of pallasite pyroxenes; representative data are given in Table 15. The most remarkable feature of these pyroxenes is their very low Ca contents; 0.02 to 0.28 wt % CaO (Buseck 1977).

The phosphate mineralogy of main-group pallasites is complex. At least three phosphates are known to be native to the pallasites, farringtonite, stanfieldite and whitlockite, and a suite of poorly characterized phosphates believed to be terrestrial alteration produces are also present (Buseck and Holdsworth 1977). Representative farringtonite, stanfieldite and whitlockite analyses are given in Table 16. Phosphates must be the major repository for large ion lithophile elements in pallasites. The Springwater pallasite is an anomalous main-group pallasite based on olivine composition (Table 13), and the greater abundance of phosphates it contains (Buseck 1977). Ion probe analyses of all three phosphates from Springwater (Davis and Olsen 1991) show that farringtonite

Table 13. Compositions of olivine grains from representative pallasites.

	Brahin	Giroux	main-group Krasno-jarsk	Mount Vernon	Rawlinna	Spring-water	Spring-water	Eagle Station grouplet Eagle Station	pyroxene-pallasite grouplet Y-8451
Chemical Composition (wt %)									
SiO_2	36.5	40.8	40.0	40.4	35.9	39.0	35.5	38.7	40.2
FeO	13.7	10.7	11.8	12.8	14.3	17.2	16.2	19.0	10.2
MgO	43.2	48.9	48.0	47.5	44.8	43.9	43.0	42.2	49.1
MnO	0.30	0.25	0.19	0.29	0.26	0.33	0.45	0.18	0.37
Cr_2O_3	nd	0.052	0.041	0.049	nd	0.021	nd	0.031	0.08
CaO	nd	0.017	0.011	0.014	nd	0.004	nd	0.070	0.05
P_2O_5	3.82	nd	nd	nd	4.91	nd	4.14	nd	nd
Total	93.70	100.719	100.042	101.053	95.26	100.455	95.15	100.181	100.00
Cation Formula Based on 4 Oxygens (Ideal Olivine = 3 Cations per 4 Oxygens)									
Si	0.9289	0.9968	0.9899	0.9938	0.8912	0.9866	0.9000	0.9895	0.9891
Fe	0.2916	0.2186	0.2442	0.2633	0.2969	0.3639	0.3435	0.4063	0.2099
Mg	1.6384	1.7806	1.7704	1.7413	1.6574	1.6551	1.6247	1.6080	1.8005
Mn	0.0065	0.0052	0.0040	0.0060	0.0055	0.0071	0.0097	0.0039	0.0077
Cr	0.0000	0.0010	0.0008	0.0010	0.0000	0.0004	0.0000	0.0006	0.0016
Ca	0.0000	0.0004	0.0003	0.0004	0.0000	0.0001	0.0000	0.0019	0.0013
P	0.0823	0.0000	0.0000	0.0000	0.1032	0.0000	0.0889	0.0000	0.0000
Total Cations	2.8654	3.0026	3.0096	3.0058	2.8510	3.0132	2.8779	3.0102	3.0101
*Cation Ratios Fe/Mn and mg# (100*Mg/(Mg+Fe))*									
Fe/Mn	45	42	61	44	54	51	36	104	27
mg#	84.9	89.1	87.9	86.9	84.8	82.0	82.5	79.8	89.6

Phosphoran olivine analyses from Buseck (1977), Y-8451 from Yanai and Kojima (1995), all other analyses from Mittlefehldt (unpublished). nd = not determined.

Table 14. Trace element contents of olivine from representative pallasites.

	main-group						Eagle Station grouplet	
	Ahumada	Giroux	Glorieta Mountain	Krasno-jarsk	Mount Vernon	Spring-water	Cold Bay	Eagle Station
Trace element contents in µg/g except Mn in mg/g								
Sc	1.86	1.09	2.29	1.23	1.65	0.54	2.55	2.66
Cr	595	312	280	228	306	169	289	404
Mn	2.2*	2.14	2.04	1.68	2.76	3.18	1.4*	1.34
Co	9.41	6.40	8.19	7.03	7.22	8.84	19.3	26.0
Ni	40.0	18.3	20.8	14.5	19.6	20.4	75.5	45.1
Zn	6.4	7.0	5.9	7.9	5.9	7.7	1.4	<2.4

Scandium, Cr, Co, Ni and Zn determined by INAA by Mittlefehldt (unpublished); Mn determined by INAA by Davis (1977), except * by electron microprobe analysis by Mittlefehldt (unpublished). Zinc in Eagle Station is a 2σ upper limit.

Table 15. Compositions of pyroxene grains from representative pallasites.

	main-group			pyroxene-pallasite grouplet Y-8451		
	Ahumada	Glorieta Mountain	Spring-water	(1)	(2)	(3)
Chemical Composition (wt %)						
SiO_2	58.4	58.4	57.8	57.0	57.2	54.9
Al_2O_3	nd	nd	nd	0.13	0.26	0.29
TiO_2	nd	nd	nd	0.03	0.04	0.06
Cr_2O_3	nd	nd	nd	0.62	0.70	1.24
FeO	7.44	7.89	11.4	6.02	6.20	3.06
MnO	0.28	0.32	0.34	0.35	0.41	0.24
MgO	34.2	34.2	32.1	35.6	34.3	18.3
CaO	0.20	0.18	0.04	0.34	1.06	21.5
Na_2O	nd	nd	nd	0.04	0.05	0.63
Total	100.52	100.99	101.68	100.13	100.22	100.22
Cation Formula Based on 6 Oxygens (Ideal Pyroxene = 4 Cations per 6 Oxygens)						
Si	2.0087	2.0042	2.0011	1.9678	1.9771	1.9896
^{IV}Al	0.0000	0.0000	0.0000	0.0053	0.0106	0.0104
Total tet*	2.0087	2.0042	2.0011	1.9731	1.9877	2.0000
Ti	0.0000	0.0000	0.0000	0.0008	0.0010	0.0016
^{VI}Al	0.0000	0.0000	0.0000	0.0000	0.0000	0.0020
Cr	0.0000	0.0000	0.0000	0.0169	0.0191	0.0355
Fe	0.2140	0.2265	0.3301	0.1738	0.1792	0.0927
Mn	0.0082	0.0093	0.0100	0.0102	0.0120	0.0074
Mg	1.7531	1.7492	1.6563	1.8316	1.7669	0.9884
Ca	0.0074	0.0066	0.0015	0.0126	0.0393	0.8349
Na	0.0000	0.0000	0.0000	0.0027	0.0034	0.0443
Total Cations	3.9914	3.9958	3.9990	4.0217	4.0086	4.0068
*Cation Ratios Ca:Mg:Fe, Fe/Mn and mg# (100*Mg/(Mg+Fe))*						
Ca	0.4	0.3	0.1	0.6	2	43.6
Mg	88.8	88.2	83.3	90.8	89	51.6
Fe	10.8	11.4	16.6	8.6	9	4.8
Fe/Mn	26	24	33	17	15	13
mg#	89.1	88.5	83.4	91.3	90.8	91.4

Ahumada, Glorieta Mountain and Springwater analyses by Buseck (1977); Y-8451 analyses by Yanai and Kojima (1995). Y-8451 pyroxenes analyses are; (1) polysynthetically twinned coarse orthopyroxene, (2) non-polysynthetically twinned orthopyroxene inclusion in olivine, (3) clinopyroxene inclusion in orthopyroxene. nd = not determined.

Table 16. Compositions of phosphates from representative pallasites.

	WHITLOCKITE					STANFIELDITE				FARRINGTONITE	
	Ahumada	Ollague	Rawlinna	Spring-water	Cold Bay	Eagle Station	Ollague	Rawlinna	Spring-water	Eagle Station	Rawlinna	Spring-water
Chemical Composition (wt %)												
CaO	48.2	49.0	43.8	47.30	45.4	48.15	26.4	24.4	25.58	25.61	0.07	0.077
P_2O_5	46.0	46.5	42.8	46.92	43.5	47.27	48.6	46.0	49.34	50.28	52.2	53.46
FeO	1.69	0.28	5.19	0.913	2.11	0.608	2.60	6.02	4.43	4.73	5.67	4.09
MgO	3.91	3.82	4.48	3.61	6.43	3.59	21.50	21.8	20.86	20.88	40.5	42.84
MnO	nd	0.10	nd	0.027	nd	0.025	0.41	0.32	0.488	0.301	0.14	0.225
Na_2O	0.20	0.90	2.96	2.50	1.08	1.55	nd	nd	nd	nd	nd	nd
K_2O	nd	0.06	0.11	0.070	nd	0.002	nd	nd	0.001	0.003	nd	0.002
SiO_2	0.21	0.10	0.88	0.026	1.94	0.022	nd	1.29	0.030	0.026	0.05	0.022
TiO_2	na	na	na	na	na	na	na	na	na	na	na	na
Al_2O_3	na	na	na	0.003	na	0.002	na	na	0.002	0.002	na	0.003
Cr_2O_3	na	na	na	0.011	na	0.006	na	na	0.023	0.006	na	0.012
Total	100.2[1]	100.7[6]	100.2[2]	101.3[8]	100.4[6]	101.22[5]	99.5[1]	99.8[3]	100.75[4]	101.83[8]	98.6[3]	100.73[1]
Cation Formula Based on 8 Oxygens												
Ca	2.6578	2.6614	2.5214	2.5671	2.5070	2.6027	1.3837	1.3167	1.3416	1.3280	0.0035	0.0037
P	2.0043	1.9958	1.9469	2.0122	1.8981	2.0191	2.0128	1.9614	2.0448	2.0602	2.0660	2.0419
Fe	0.0727	0.0119	0.2332	0.0387	0.0909	0.0257	0.1064	0.2535	0.1813	0.1914	0.2217	0.1543
Mg	0.2999	0.2886	0.3587	0.2725	0.4938	0.2699	1.5673	1.6362	1.5217	1.5059	2.8214	2.8801
Mn	0.0000	0.0043	0.0000	0.0012	0.0000	0.0011	0.0170	0.0137	0.0202	0.0123	0.0055	0.0086
Na	0.0200	0.0885	0.3084	0.2455	0.1079	0.1516	0.0000	0.0000	0.0000	0.0000	0.0000	0.0000
K	0.0000	0.0039	0.0075	0.0045	0.0000	0.0001	0.0000	0.0000	0.0001	0.0002	0.0000	0.0001
Si	0.0108	0.0051	0.0473	0.0013	0.1000	0.0011	0.0000	0.0650	0.0015	0.0013	0.0023	0.0010
Ti	0.0000	0.0000	0.0000	0.0000	0.0000	0.0000	0.0000	0.0000	0.0000	0.0000	0.0000	0.0000
Al	0.0000	0.0000	0.0000	0.0002	0.0000	0.0001	0.0000	0.0000	0.0001	0.0001	0.0000	0.0002
Cr	0.0000	0.0000	0.0000	0.0004	0.0000	0.0002	0.0000	0.0000	0.0009	0.0002	0.0000	0.0004
Total Cations	5.0655	5.0595	5.4234	5.1436	5.1977	5.0716	5.0872	5.2465	5.1122	5.0996	5.1204	5.0903
*Cation Ratios Fe/Mn and mg# (100*Mg/(Mg+Fe))*												
Fe/Mn	-	2.8	-	33	-	24	6.3	19	9.0	16	40	18
mg#	80.5	96.0	60.6	87.6	84.4	91.3	93.6	86.6	89.4	88.7	92.7	94.9

Springwater and Eagle Station data from Davis and Olsen (1991), remainder from Buseck and Holdsworth (1977).

Table 17. Analyses of chromite grains from representative pallasites.

	Glorieta Mountain	Brahin	Mount Vernon	Phillips County	Eagle Station
Chemical Composition (wt %)					
TiO_2	0.32	0.23	0.27	0.16	nd
Al_2O_3	6.9	1.66	7.8	1.45	7.0
Cr_2O_3	62.1	69.1	61.3	68.5	62.1
V_2O_3	0.67	0.53	0.59	0.57	0.48
FeO	22.0	23.3	23.1	25.1	25.5
MgO	6.9	5.4	6.2	4.4	4.4
MnO	0.77	0.67	0.75	0.75	0.29
Total	99.66	100.89	100.01	100.93	99.77
Cation Formula Based on 4 Oxygens (Ideal Spinel = 3 Cations per 4 Oxygens)					
Ti	0.0083	0.0061	0.0070	0.0043	0.0000
Al	0.2793	0.0687	0.3149	0.0605	0.2877
Cr	1.6862	1.9175	1.6598	1.9186	1.7118
V	0.0185	0.0149	0.0162	0.0162	0.0134
Fe	0.6319	0.6839	0.6616	0.7436	0.7435
Mg	0.3532	0.2824	0.3164	0.2323	0.2286
Mn	0.0224	0.0199	0.0218	0.0225	0.0086
Total Cations	2.9998	2.9934	2.9977	2.9980	2.9936
*Cation Ratios Fe/Mn, mg# (100*Mg/(Mg+Fe)) and 100*Cr/(Cr+Al)*					
Fe/Mn	28	34	30	33	87
mg#	35.9	29.2	32.4	23.8	23.5
Cr/(Cr+Al)	85.8	96.5	84.1	96.9	85.6

All data taken from Bunch and Keil (1971).

contains very low abundances of the rare earth elements (REE) compared to either stanfieldite or whitlockite, while whitlockite is enriched in REE compared to stanfieldite from ~4 times for La to ~20 times for Lu.

Chromites are present in most, if not all, main-group pallasites; representative compositional data are given in Table 17. Pallasite chromites are fairly uniform in composition, except that Cr_2O_3 and Al_2O_3 vary and are anticorrelated; Cr_2O_3 from 69.1 to 60.5 wt %, Al_2O_3 from 1.66 to 9.1 wt %, maintaining a relatively constant (Cr+Al)/O atom ratio of ~0.5 (Bunch and Keil 1971).

Troilite and schreibersite are minor minerals in main-group pallasites. Troilite varies from ~0.1 to 7.3 vol %, and schreibersite varies from 0.3 to 2.8 vol % (Buseck 1977).

Eagle Station grouplet

In these pallasites, olivine is the dominant silicate phase, making up 75 to 80 vol % of the two meteorites measured by Buseck (1977). Minor clinopyroxene and orthopyroxene are reported in Eagle Station (Davis and Olsen 1991). Chromite has been reported by Bunch and Keil (1971) in Eagle Station, and whitlockite and stanfieldite, but not farringtonite, have been reported in the Eagle Station pallasites (Davis and Olsen 1991, Buseck and Holdsworth 1977).

The olivines in the Eagle Station grouplet are more ferroan than the main-group pallasites, have higher CaO contents, and slightly lower MnO contents leading to much

higher FeO/MnO ratios (Table 13, Fig. 18). The trace transition elements in Eagle Station pallasites are also distinct. Their olivines contain higher Sc, Co and Ni than main-group pallasite olivines, but lower Zn contents (Table 14).

Only partial analyses of pyroxene are available. Davis and Olsen (1991) gave representative compositions of orthopyroxene (Wo_1Fs_{17}, 0.11 wt % Al_2O_3) and clinopyroxene ($Wo_{45}Fs_7$, 0.20 wt % Al_2O_3) in Eagle Station.

The major element compositions of stanfieldite and whitlockite in Eagle Station pallasites are very similar to those in the ferroan main-group pallasite, Springwater. The most noticeable difference is that whitlockite in the latter is richer in Na_2O than in the Eagle Station pallasites (Buseck and Holdsworth 1977, Davis and Olsen 1991; see Table 16). The REE in Eagle Station stanfieldite and whitlockite are LREE-depleted, a pattern quite distinct from that seen in Springwater phosphates (Davis and Olsen 1991).

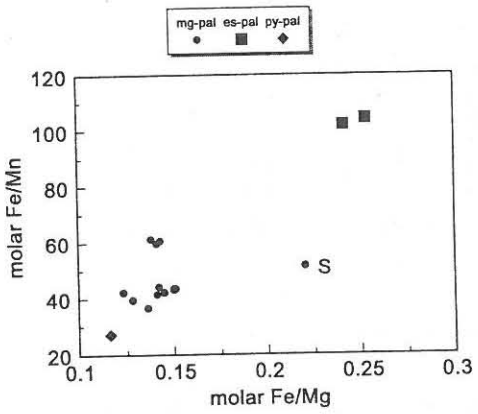

Figure 18. Molar Fe/Mn vs. Fe/Mg for pallasite olivines. The three pallasite types have distinct Fe/Mn ratios, but Fe/Mg ratios for the main-group and pyroxene-pallasites overlap (see Fig. 17). The three main-group pallasites with high Fe/Mn are Brenham, Krasnojarsk and Thiel Mountains. Springwater (S) is an anomalously ferroan main-group pallasite. All data from Mittlefehldt (unpublished).

Chromite in Eagle Station was analyzed by Bunch and Keil (1971). Eagle Station chromite grains are more ferroan when compared to the main-group pallasite chromites, except for those in Phillips County (Table 17), which also has anomalously ferroan olivines for a main-group pallasite (Buseck and Goldstein 1969).

Pyroxene-pallasite grouplet

The pyroxene-pallasite grouplet, consisting of Vermillion and Yamato 8451, has only recently been defined (Boesenberg et al. 1995) and very little data on them are yet in the literature. Hiroi et al. (1993) and Yanai and Kojima (1995a) gave brief descriptions of the first known member, Y-8451. Based on two modal analyses, this pallasite consists of about 55 to 63 vol % olivine, 30 to 43 vol % metal, 1 to 3 vol % pyroxene, 1 vol % troilite, plus minor whitlockite. Chromite was not mentioned. Olivine and pyroxene occur as 1 to 6 mm-sized rounded grains enclosed in a metal-troilite matrix. The occurrence of mm-sized pyroxenes distinguishes this pallasite from other types (compare with pyroxene textural descriptions for main-group and Eagle Station grouplet pallasites in Buseck 1977, Davis and Olsen 1991). The large pyroxenes poikilitically contain small olivine grains, and vice versa. Yanai and Kojima (1995a) list three distinct pyroxenes, polysynthetically twinned orthopyroxenes, which occur as large, rounded grains, non-polysynthetically twinned orthopyroxenes, which occur as inclusions in olivine, as aggregates, and as rims on polysynthetically twinned orthopyroxenes, and small clinopyroxenes. Hiroi et al. (1993) found only two distinct pyroxenes, orthopyroxene

with ~2 mol % wollastonite and protopyroxene (inverted protoenstatite) with ~0.6 mol %. They also found that metal-olivine boundaries have slight dislocations.

Vermillion contains much less olivine, ~14 vol % (Boesenberg et al. 1995), than any other pallasite. The olivines occur as rounded to subrounded grains up to 1.5 cm in size in cm-sized bands interspersed with metal in bands of similar width. This texture is unique among pallisites. Minor amounts of orthopyroxene (~0.7 vol %), chromite (~0.2 vol %) and whitlockite (~0.07 vol %) are also present. The orthopyroxene occurs both along the rims of smaller olivine grains, and as large (mm-size) inclusions in olivine.

Pyroxene-pallasite olivines overlap the magnesian end of the range of main-group pallasites (Table 13, Fig. 17). Pyroxene-pallasite olivines have distinctly higher MnO contents, resulting in significantly lower FeO/MnO ratios than in the main-group pallasites (Table 13, Fig. 18).

There are three distinct pyroxene composition groups in Y-8451 that correlate with textures (Yanai and Kojima 1995a); the large, polysynthetically twinned orthopyroxenes have very low CaO contents, the non-polysynthetically twinned orthopyroxenes have intermediate CaO contents, and the clinopyroxenes are calcic (Table 15). The polysynthetically twinned orthopyroxenes also tend to be more magnesian than the non-polysynthetically twinned orthopyroxenes (Yanai and Kojima 1995a). Based on CaO content, the polysynthetically twinned orthopyroxene of Yanai and Kojima (1995a) appears to be equivalent to the protopyroxene of Hiroi et al. (1993). Boesenberg et al. (1995) described a similar range in orthopyroxene wollastonite contents for Vermillion, but do not give information of possible correlations between texture and composition.

Whitlockite in Vermillion and Y-8451 have LREE-depleted REE patterns similar to those determined for Eagle Station, but at higher concentrations (Boesenberg et al. 1995, Davis and Olsen 1991).

Metal phase

The metal phase of main-group pallasites is generally low in refractory siderophile elements such as Ir and high in Ni and moderately volatile siderophile elements such as As and Au (Fig. 19). Main-group pallasite metal is close in composition to Ni-rich IIIAB irons, but has slightly higher incompatible/compatible siderophile element ratios (e.g. Au/Ir) than IIIAB irons with similar Ir contents (Scott 1977b). There is also considerable scatter in main-group pallasite metal composition, particularly in the contents of compatible siderophile elements like Ir (Fig. 19a). The metal phase of Eagle Station grouplet pallasites is distinct in composition, having higher Ni and Ir, and lower moderately volatile siderophile element contents (Scott 1977b). Eagle Station grouplet metal is close in composition to IIF irons (Kracher et al. 1980). The two pyroxene-pallasites have widely different metal compositions (Wasson et al. 1998a,b). Y-8451 has Ni and Ir contents like those of the Eagle Station grouplet, but a Au content more like those of high Ni main-group pallasites, while Vermillion has Ni, Ir and Au contents similar to low Ni, high Ir main-group pallasites (Fig. 19). However, Vermillion has very different contents of moderately volatile siderophile elements (e.g. Ga, Ge) than any main-group pallasite (Wasson et al. 1998b). Wasson (pers. comm.) believes the metals in the two pyroxene-pallasites are too different in composition to support assignment to a single grouplet.

Ages

Very little is known of the formation ages of pallasites; older K-Ar ages are probably unreliable indicators of formation times. Recently, Mn-Cr dating has been done on

several main-group pallasites (Hsu et al. 1997, Hutcheon and Olsen 1991, Shukolyukov and Lugmair 1997) and the Eagle Station pallasite (Birck and Allègre 1988). The data indicate that ^{53}Mn ($t_{1/2}$—3.7 Ma) was present at the time the pallasites were formed, and thus they formed very early in the history of the solar system. By tying the Mn-Cr data on the Omolon main-group pallasite to the Mn-Cr and Pb-Pb data on the LEW 86010 angrite, Shukolyukov and Lugmair (1997) determined an absolute age of 4.558±0.001 Ga for closure of the Mn-Cr system in Omolon. Eagle Station had a distinctly lower $^{53}Mn/^{55}Mn$ ratio at isotopic closure than did the main-group pallasites so far studied, suggesting Eagle Station reached closure ~10 to 15 Ma later (Hsu et al. 1997).

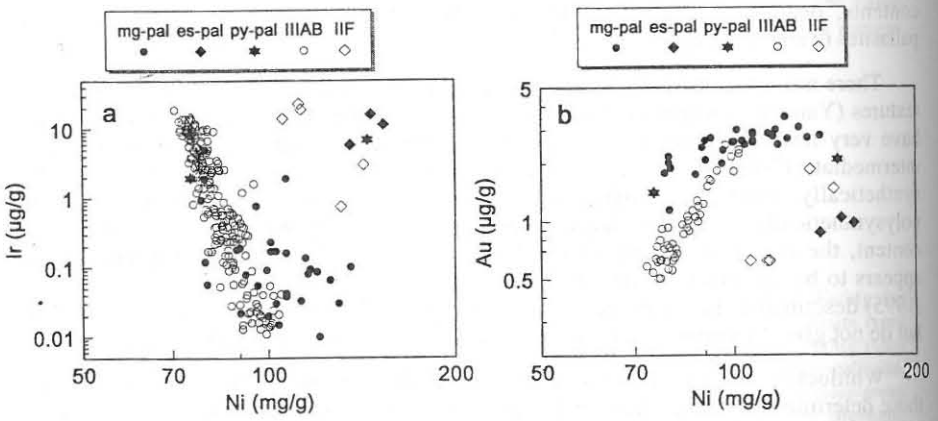

Figure 19. Diagrams of (a) Ir vs. Ni and (b) Au vs. Ni for metal from main-group pallasites, Eagle Station and pyroxene-pallasite grouplets compared to IIF and IIIAB irons. Main-group pallasites show wide ranges in Ir-Ni and Au-Ni, indicating that their metal is not simply quenched residual metallic melt. The high-Ni pyroxene-pallasite is Y-8451. Data are from Davis (1977), Esbensen et al. (1982), Malvin et al. (1984), Scott (1977), Scott and Wasson (1976), Ulff-Møller et al. (1998), Wasson (1974), Wasson et al. (1989, 1998a,b).

Cooling rates

Buseck and Goldstein (1969) determined cooling rates from the metal phase of pallasites. Because of changes in values of Ni diffusion parameters (Dean and Goldstein 1986), the cooling rate values given by Buseck and Goldstein (1969) need to be increased 5-fold (Saikumar and Goldstein 1988). This leads to cooling rates of 2.5-7.5°C/Ma for main-group pallasites. Cooling rates for three main-group pallasites determined by a different method agree with these values (Yang et al. 1997a, see Table 4). These cooling rates are lower than those of most irons (Table 4). Phosphorous is a moderately volatile element, and the formation of the Widmanstätten structure used in cooling rate determinations is strongly influenced by P content (Dean and Goldstein 1986). Because main-group pallasites contain higher moderately volatile siderophile element abundances than do Eagle Station grouplet pallasites (Scott 1977b), there could be a systematic difference in metallographic cooling rates calculated for the two types. Taken at face value, however, the cooling rate for Eagle Station, 10°C/Ma, is similar to those of main-group pallasites.

Miyamoto and Takeda (1994) have presented cooling rates based on fitting Fe-Mg and Ca zoning profiles in olivine for a main-group and a pyroxene-pallasite. The calculated cooling rates are very high, on the order of 10^6 times the metallographic

cooling rates. It is difficult to evaluate the veracity of these cooling rates from the abstract, but the cooling rate based on Fe-Mg zoning is highly model dependent as it is a strong function of the assumed initial temperature.

Pallasite formation

The customary hypothesis for pallasite formation is that they were formed at the core-mantle boundary of their parent body. Metal will sink to form the core of a differentiated rocky body, while dunite is a plausible lowermost mantle material, either as partial melting residue or as cumulate from a crystallizing ultramafic melt. There are two possible problems with the simple core-mantle boundary model, both long discussed in the literature: (1) pallasites seem too abundant in the meteorite collection considering the small volume a core-mantle boundary will occupy in an asteroid, and (2) the large density difference between solid olivine and metal liquid will result in rapid separation of the two even in the low gravity field of asteroids. In spite of these problems, the core-mantle boundary origin still seems most plausible.

Main-group pallasite metal is close to IIIAB metal in composition (Fig. 19). Scott (1977c) showed that the mean composition of main-group pallasite metal is very similar to the composition of a model residual liquid after about 82% crystallization of a metallic melt like that parental to IIIAB irons. He suggested that main-group pallasites and IIIAB irons formed on the same parent body. This is compatible with a core-mantle boundary model for pallasite formation, assuming the core crystallized from the center out. However, Haack and Scott (1993) suggested that IIIAB irons were formed by inward dendritic growth from the core-mantle boundary. In order to explain the apparent close relationship between main-group pallasite metal and IIIAB irons, they suggested that some of the residual metallic melt was forced up to the core-mantle boundary by an unspecified process. The composition of metal in main-group pallasites is quite variable compared to Ni-rich IIIAB irons, which suggests the pallasite metal cannot be simply quenched residual melt. Ulff-Møller et al. (1997) suggest the wide range in Ir contents in main-group pallasite metal is caused by variable mixing of residual melt with earlier metal crystals at the time of metal-olivine mixing. As noted by Ulff-Moller et al. (1998), main-group pallasites have lower S contents than expected for trapped metallic melts. They thus concluded that the injected residual melt underwent a period of equilibrium crystallization, and that the last dregs of S-rich melt escaped the pallasite region.

The relationship between IIF irons and the metal phase of Eagle Station grouplet pallasites is not as close as that between IIIAB irons and the main-group. Kracher et al. (1980) suggested that IIF irons and Eagle Station grouplet pallasites were formed on similar parent bodies. The metal phase of the Bocaiuva silicate-bearing iron (discussed later) is also similar to IIF irons and the Eagle Station grouplet, and the oxygen-isotopic composition of Bocaiuva silicates is similar to those of the Eagle Station grouplet (Malvin et al. 1985, and see Fig 1a). All of these meteorites likely are from similar parent bodies formed in the same region of the solar system (Malvin et al. 1985).

Scott (1977d) addressed the problem of how the metal-silicate texture was formed through detailed study of the macrotextures of pallasite slabs. He found that pallasites display a range of textures, from those containing highly angular olivine grains with large olivine masses several cm in size, some of which are veined with metal, to pallasites with rounded olivines dispersed in the metal. The large olivine masses preserve textural evidence indicating that they were in the process of breaking up into smaller, angular olivine grains when the process was frozen by crystallization of the metal. Scott (1977d) favored a model in which solid olivine layers were invaded, broken up and dispersed by molten metal near its freezing point. Crystallization of the metal prevented density

separation of the metal and olivine. Ullf-Møller et al. (1997) state that the most plausible mechanism to produce the textures seen in olivine masses by Scott (1977d) and by themselves in the Esquel main-group pallasite is by high pressure injection of metal, possibly by impact. Pallasites with rounded olivines were formed in a similar way, but annealing of the mixture with subsequent rounding of initially angular olivines occurred. Ohtani (1983) used thermodynamic, kinetic and physical models to constrain the time and temperature of formation of the olivine-metal textures. He suggested that the rounded olivine textures were formed at temperatures above the metal-troilite solidus, and that the time scale must have been <5 Ka or olivine and metal would have segregated. Pallasites with angular olivine were annealed at lower temperatures. In contrast, Buseck (1977) considered the rounded olivines to represent the primary shapes, while angular olivines were secondary. He suggested that pallasites are exotic cumulates; olivine and chromite grains represent cumulus minerals, while the metal is an intercumulus phase.

Davis and Olsen (1991) argued that the REE contents of pallasite phosphates are not compatible with simple models forming the silicates of all pallasites as either residual mantle or early cumulates during differentiation of their parent bodies. Many main-group and Eagle Station grouplet pallasites have REE patterns consistent with phosphate formation through redox reactions between the metal and olivine in which metallic P is oxidized. The REE in the phosphates are inherited from the olivine and show LREE depleted patterns consistent with either residual or cumulate dunites, and therefore core-mantle boundary models (Davis and Olsen 1991). However, the Springwater and Santa Rosalia main-group pallasites contain phosphates far too rich in REE for this scenario. Davis and Olsen (1991) suggested that the phosphates in these pallasites are consistent with crystallization at a late stage from a chondritic melt, and therefore indicate that some pallasites may have originated nearer the parent body surface. Note that both Santa Rosalia and Springwater yield cooling rates at the low end of the main-group pallasite range (Buseck and Goldstien, 1969), which may be inconsistent with the formation scenario inferred by Davis and Olsen(1991). Buseck and Holdsworth (1977) described textural evidence which they believed indicated that some phosphates crystallized from a residual melt. They did not specify which meteorites contained these textures, so one cannot correlate anomalous REE patterns with phosphate texture.

Minor and trace elements, and fayalite content show zoning profiles from core to rim in pallasite olivines. This, plus rounding of olivines suggestive of subsolidus annealing indicate that small scale element migration was occurring in pallasites at the time they cooled below the blocking temperature for these processes. The decreasing Fa and Ni contents at the rims, plus evidence for formation of at least some phosphates by oxidation of metallic P, suggest that redox reactions between metal and silicate were responsible for some element migration. However, the cause of zoning in Cr and Al remain obscure, and there is no consensus on the origin of all the phosphates and the pyroxenes.

Main-group pallasites appear to be closely related to the howardite, eucrite and diogenite (HED) meteorites. Oxygen-isotopic compositions show that all these meteorite types came from the same O-isotope reservoir (Clayton and Mayeda 1996, see Fig. 1d). Extreme differentiation can in principle produce olivines as magnesian as those in main-group pallasites and basalts as ferroan as basaltic eucrites on a single parent body (Mittlefehldt 1980). Hence, it is possible that all of these meteorite types, plus the IIIAB irons, represent fragments of a single parent asteroid. This will be discussed in more detail in the section on HED meteorites.

Clearly, time is ripe for renewed detailed studies of the pallasites. Recent ion microprobe studies of phosphate compositions, electron microprobe studies of zoning profiles, renewed attempts to date pallasite formation, and the characterization of new

pallasite types all suggest that pallasite studies are being reinvigorated after their heyday in the mid-seventies.

SILICATE-BEARING IVA IRONS

The IVA iron meteorite group contains only four known silicate-bearing members. Unlike the other silicate-bearing iron groups discussed earlier in this chapter, silicates in IVA irons are distinctly non-chondritic in their mineralogy. Two of the IVA irons, Steinbach and São João Nepomuceno, contain abundant rounded pyroxene-tridymite inclusions (Reid et al. 1974, Bild 1976, Prinz et al. 1984, Ulff-Møller et al. 1995, Scott et al. 1996, Haack et al. 1996a). The IVA irons Bishop Canyon and Gibeon contain rare SiO_2 grains up to several cm in length (Schaudy et al. 1972, Buchwald 1975, Ulff-Møller et al. 1995, Scott et al. 1996, Marvin et al. 1997). Their linkage to IVA irons is confirmed by concentrations of Ni, Ga, Ge and Ir similar to those in IVA irons without silicates (Scott et al. 1996). Until recently, there existed a relative scarcity of basic data about the silicates in these meteorites. Their small number and unusual mineralogy make the origin of these meteorites probably the most enigmatic of all silicate-bearing irons.

Petrology and mineralogy

Pyroxene-tridymite-rich IVA irons. The pyroxene-tridymite-bearing IVA irons Steinbach and São João Nepomuceno have been widely studied. Figure 20a illustrates the main mass of Steinbach (from Scott et al. 1996). Metal and troilite occupy 29 vol % of this mass as irregularly shaped grains and two small, metal-rich areas are present. In this metal (Fig. 20b), metal grains that appear distinct actually have the same orientation of their Widmanstätten pattern over areas as large as 10 cm (McCall 1973), indicating that they were originally composed of single γ-Fe,Ni crystals of this size. Silicates comprise 19 vol % of São João Nepomuceno (Scott et al. 1996) but are heterogeneously distributed. Silicates are partly concentrated on grain boundaries of parent taenite crystals which reach 4 by 8 cm and silicate-free regions reach 10 by 20 cm. In areas where silicates are concentrated, the texture very closely resembles that of Steinbach.

Silicates in Steinbach and São João Nepomuceno are orthobronzite, clinobronzite and tridymite (Reid et al. 1974, Dollase 1967, Ulff-Møller et al. 1995, Scott et al. 1996). Modal data from Ulff-Møller et al. (1995) and Scott et al. (1996) show that Steinbach is composed of orthobronzite (37.3, 38.0 vol %, respectively), clinobronzite (4.5, 1.6), tridymite (20.2, 20.8), metal (32.4, 32.2), troilite (5.7, 6.6) and traces of chromite. The agreement between these values suggests that Steinbach is quite homogeneous on the scale of ~10 cm^2, although Scott et al. (1996) documented considerable heterogeneity in modes and pyroxene/tridymite ratios between individual polished thin sections. A smaller area of São João Nepomuceno (~3.5 cm^2) contains orthobronzite (37.8), clinobronzite (0.1), tridymite (5.1), metal and its weathering products (52.4), troilite (4.6) and traces of chromite (Scott et al. 1996). Compared to Steinbach, São João Nepomuceno is poorer in tridymite and clinobronzite.

A mixture of pyroxene and SiO_2 fills the spaces between the metallic host in both Steinbach and São João Nepomuceno. Silicate grain sizes are typically 1 to 5 mm (Ulff-Møller et al. 1995, Scott et al. 1996). Metal-silicate and silicate-silicate grain boundaries are typically complex. In many cases, metal adjacent to silicates forms cusps at triple junctions. Many adjacent pyroxene grains are irregular, indicative of silicate co-crystallization (Scott et al. 1996).

A remarkable feature of both Steinbach and São João Nepomuceno is the occurrence of twinned clinobronzite within orthobronzite. The clinobronzite islands are either totally enclosed in orthobronzite (Ulff-Møller et al. 1995, Scott et al. 1996) or occur at

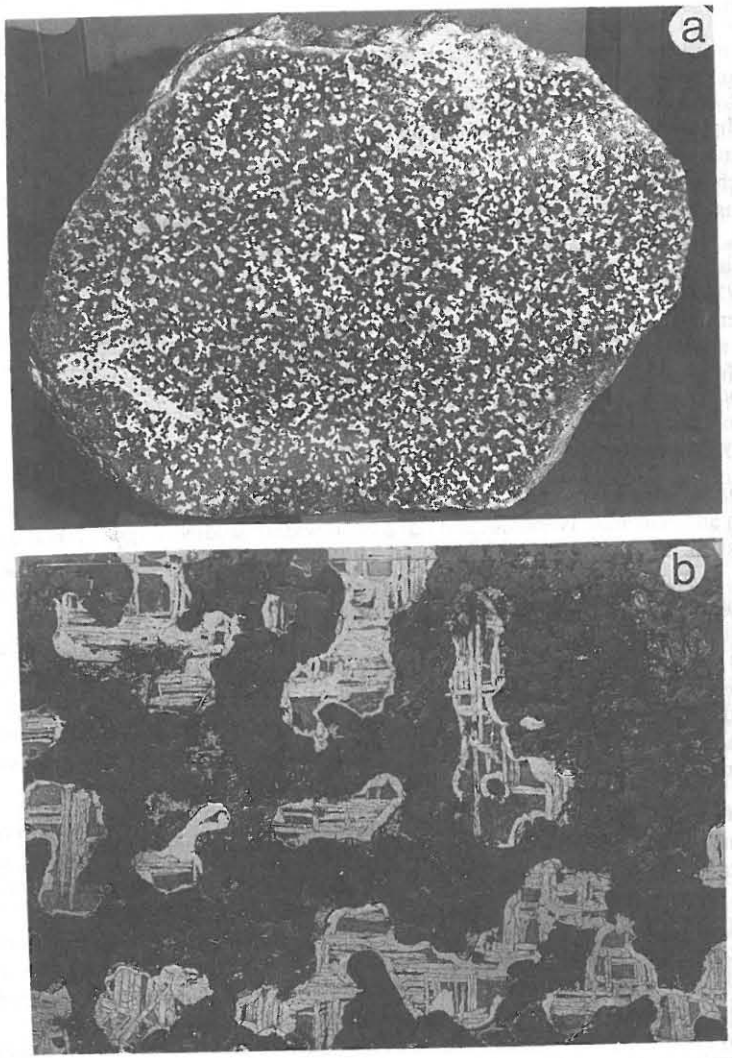

Figure 20. Photographs of the Steinbach silicate-bearing IVA iron. (a) A polished slice showing white metallic Fe,Ni and troilite in a dark silicate matrix. Longest dimension is 51 cm. (b) Part of an etched slice showing fine, oriented kamacite lamellae in metallic Fe,Ni. The continuity of the Widmanstätten pattern across the field shows that the grains are connected and once formed a single large skeletal taenite crystal. Width is 3.4 cm.

pyroxene-SiO_2 grain boundaries (Scott et al. 1996), but are not observed bordering metal. Reid et al. (1974) studied the pyroxenes by x-ray diffraction methods and Haack et al. (1996a) reported on a transmission electron microscope study of a pyroxene grain in Steinbach. These pyroxene grains contained a continuum of microstructures ranging from ordered clinobronzite to a highly striated microstructure consisting of a disordered intergrowth of clinopyroxene and orthopyroxene. Orthopyroxene lamellae are typically <10 unit cells in thickness, while clinopyroxene lamellae extend up to 50 unit cells in

thickness. As noted earlier, São João Nepomuceno also contains a similar, but less abundant, clinobronzite, but this has not been examined by TEM.

Steinbach orthobronzite ($Fs_{15.0}$) is more FeO-rich than clinobronzite ($Fs_{14.5}$) (Reid et al. 1974, Scott et al. 1996). A similar relationship is seen in São João Nepomuceno (orthobronzite, $Fs_{14.2}$; clinobronzite, $Fs_{13.6}$), although São João Nepomuceno is slightly poorer in FeO than Steinbach (Scott et al. 1996). Ulff-Møller et al. (1995) also observed Ca-Cr-rich regions in orthobronzite and documented zoning within Steinbach pyroxenes and tridymite. Steinbach tridymite has been studied in detail by a number of authors (e.g. Tagai et al. 1977). Rare Al-rich regions may perhaps be related to contamination with Al polishing compound.

SiO_2-bearing IVA irons. Bishop Canyon and Gibeon contain large, but very rare, grains of SiO_2. Bishop Canyon contains two adjoining plate-like SiO_2 grains, probably tridymite (Buchwald 1975, Scott et al. 1996). Troilite with exsolved daubreelite occurs around the grains.

Silica grains from the widely-distributed Gibeon meteorite have been more widely-studied (Schaudy et al. 1972, Ulff-Møller et al. 1995, Scott et al. 1996, Marvin et al. 1997). Ulff-Møller et al. (1995) and Scott et al. (1996) studied the same sample, which contained a single crystal measuring 21 by 1 mm. This grain had been fractured into three pieces prior to complete solidification of the metallic host. Marvin et al. (1997) studied slices through a very large SiO_2 grain. The length of the original grain may have been up to 10 cm. These authors confirmed by x-ray diffraction studies and characteristic fluorescence that the grain was dominantly composed of tridymite. However, cracked areas 3-4 mm across in the center of the tridymite were quartz.

Ulff-Møller et al. (1995) and Scott et al. (1996) observed zoning in Gibeon tridymite, with FeO increasing from the core to the rim of the grain and Al_2O_3 decreasing.

Origin

The origin of the IVA irons remains enigmatic. Any favored interpretation depends critically on whether the origin of silicates in Steinbach and São João Nepomuceno are linked to that of the large SiO_2 grains in Bishop Canyon and Gibeon, or whether these two occurrences formed through independent processes. Certainly, recovery of more silicate-bearing IVA irons would substantially improve our understanding of their origin.

Prinz et al. (1984) suggested that silicates in pyroxene-tridymite-rich IVA irons formed by remelting of igneous cumulates. Several problems exist with this scenario. Prinz et al. (1984) suggested that the pyroxene/tridymite ratios are appropriate for eutectic mixtures, but new modal data of Ulff-Møller et al. (1995) and Scott et al. (1996) suggest that this is not the case. Cumulate remelting would also produce a melt with more Ca than Al and a strongly steepened REE pattern, neither of which is observed in Steinbach or São João Nepomuceno (Ulff-Møller et al. 1995).

A second model proposed by Prinz et al. (1984) and expanded upon by Scott et al. (1996) suggests oxidation of Si from metal and reaction with an olivine-bearing pallasite to produce pyroxene and tridymite observed in IVA irons. The gross texture of Steinbach is strikingly similar to some pallasites (e.g. Brenham; Nininger 1952). Oxidation of Si from metal could also form the silica observed in Bishop Canyon and Gibeon and may have formed silica in IIIAB irons (Kracher et al. 1977). Indeed, a pyroxene-bearing pallasite precursor (e.g. Yamato 8451, Yanai and Kojima 1995a) could provide a source of minor and trace elements observed in pyroxene of Steinbach and São João

Nepomuceno. A problem with this scenario is envisioning the presence of significant Si dissolved in metal, which requires very reducing conditions, and yet having relatively oxidized pyroxene is these meteorites (Fs_{14-15}).

Ulff-Møller et al. (1995) proposed that the silicates were derived by direct melting of a chondritic precursor with subsequent reduction. In this model, low degrees of partial melting would occur, with subsequent melt removal and reduction. Through this reduction, the Fe/Mn ratio of the melt was lowered and the SiO_2 content of the residual magma was increased. This process would occur most efficiently within the molten core of the asteroid, where sufficient reducing agents (e.g. P) exist. Ulff-Møller et al. (1995) argued that this reduction could have forced the melt to crystallize only tridymite.

It is unclear how the silicates were mixed with the metal in IVA irons. The oxidation of a pallasite-like precursor provides a ready explanation for mixing. Mechanisms which call for mixing of silicate melt into the molten core are more controversial. Ulff-Møller et al. (1995) proposed that large, metallic dendrites which formed at the core-mantle boundary could founder into the molten core, carrying pieces of the adhering mantle and, thus, explaining the mixing. Alternatively, a crystallizing core would undergo significant shrinkage and this might lead to injection of overlying, molten silicates into the cracks produced. Scott et al. (1996) criticized these passive mechanisms and suggested instead that silicate-bearing IVA irons formed during catastrophic breakup and reassembly of the IVA parent body, an idea explored in greater detail by Haack et al. (1996a). Evidence for such a process may be found in the complex cooling history required to explain the features of these meteorites. The orthobronzite-clinobronzite intergrowths clearly require very rapid cooling (Reid et al. 1974, Haack et al. 1996a) at high temperature, while the existence of the Widmanstätten pattern in these meteorites requires slow cooling at low temperature.

BRACHINITES

Brachina was originally thought to be a second chassignite (Johnson et al. 1977, Floran et al. 1978a, Ryder 1982), but was shown on the basis of chemistry, oxygen-isotopic and noble gas composition, and age to be unique (Nehru et al. 1983, Clayton and Mayeda 1983, Crozaz and Pellas 1983, Ott et al. 1983). Four other meteorites are now classified as brachinites: ALH 84025, Eagles Nest, Nova 003 (probably paired with Reid 013) and Hughes 026 (Table 18). Divnoe has been considered to be a brachinite on the basis of oxygen-isotopes (Clayton and Mayeda 1996), but is petrologically unique (Petaev et al. 1994). LEW 88763 has also been thought to be brachinite (AMN 14-2; Nehru et al. 1992, Kring and Boynton 1992), but its oxygen isotpoic composition is distinct from brachinites and falls near the trend defined by acapulcoites and lodranites (Fig. 1c), and is now considered to be unique (Swindle et al. 1998).

Petrography and mineral chemistry

Brachinites are dunitic wehrlites, consisting dominantly of olivine; reports for individual brachinites range from 79-93%, but Nehru et al. (1992) cite 74 to 98% for the group. They contain augite (4 to 15%), chromite (0.5 to 2%), Fe-sulfides (3 to 7%), minor phosphates, and minor Fe-Ni metal. Brachina contains 9.9% plagioclase, Nova 003 and Hughes 026 have <0.1%, and ALH 84025 and Eagles Nest have no plagioclase. Brachina, Nova 003 and Hughes 026 contain traces of orthopyroxene.

Brachina has an equigranular texture (subhedral to anhedral grains with 120° triple junctions) with average grain size 0.1 to 0.3 mm (Fig. 21a). Hughes 026 is also equigranular, with average grain size 0.65 mm. ALH 84025 is coarser-grained, with olivine

Table 18. Petrographic data for brachinites.

	olivine Fo (modal %)	clinopyroxene Wo/En (modal %)	orthopyroxene Wo/En (modal %)	plagioclase An/Ab (modal %)	Fe sulfide Ni wt % (modal %)	Texture	Ref.	Notes
Brachina	68-70 (80.4%)	38.7/48.4 (5.5%)	(trace)	22/76 (9.9%)	0.6-3.6 (2.9%)	equigranular (0.1-0.3 mm)	1	
ALH 84025	67-68 (79-90.2%)	44/46 (4.2-15%)	(none)	(none)	0.8-2.0 (3-4%)	prismatic-subhedral (up to 2.7 mm); equigranular	2-4	texture and grain size vary between thin sections
Nova 003	68.5	45/44	2.4/72.1	33.3			5	formerly named Window Butte
Reid 013	66.1	45.5/43.6	1.7/71.3	31.5/68.1			5	probably paired with Nova 003 (M. Prinz, pers. comm.)
Eagles Nest	68 (81%)	45/45 (6%)	(none)	(none)	(7%)	subequant, triple junctions (up to 1.5 mm)	6-8	
Hughes 026	65 (92.7%) (3.6%)	46-47/43-44	3/69 (1.6%)	32 (<0.1%)	(1.20%)	equigranular (0.65 mm)	9,10	previously, informally called Australia I

References: 1. Nehru et al. (1983); 2. Prinz et al. (1986a); 3. Warren and Kallemeyn (1989a); 4. AMN 8-2; 5. Wlotzka (1993); 6. Kring et al. (1991); 7. Kring and Boynton (1992); 8. Swindle et al. (1997); 9. M. Prinz (pers. comm.); 10. Nehru et al. (1996).

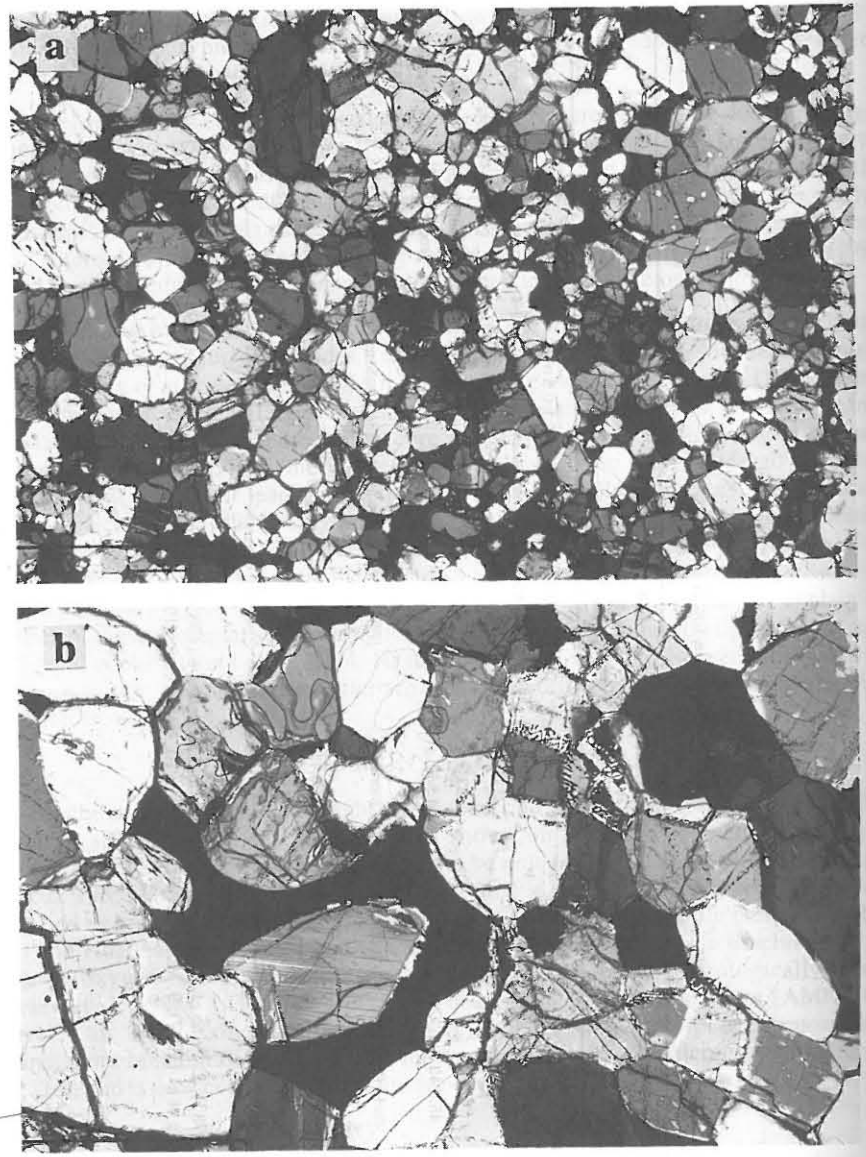

Figure 21. Photomicrographs of brachinites in transmitted light with partially crossed nicols. Scale bars are 0.2 mm and fields of view are ~2.9 × 1.7 mm. (a) Brachina. Equigranular texture of olivine, augite and plagioclase, with minor chromite and Fe,Ni metal and sulfides. (b) ALH 84025,7. Olivine and augite in equigranular texture. Interstitial troilite (black) left of center surrounds augite with fine twin lamellae.

up to 1.8 mm and augite up to 2.7 mm. Warren and Kallemeyn (1989a) observed that in two thin sections of ALH 84025 olivine is prismatic, with an aspect ratio of ~3:1, and shows a possible preferred orientation (Fig. 21b). However, Prinz et al. (1986a) reported an equigranular texture in two other thin sections; whereas yet another thin section is described as being polygonal-granular (AMN 8-2). Eagles Nest is also coarser-grained than Brachina. It contains olivine up to 1.5 mm, with subequant grain shapes and 120° triple junctions (Kring et al. 1991). In all brachinites augite, chromite, and plagioclase appear to be interstitial to olivine. Sulfide is anhedral and interstitial, or occurs as veins with minor Fe-Ni metal cross-cutting the silicates and chromite. Brachina has 20-25 μm, rounded melt inclusions in olivine, similar to those in Chassigny (Floran et al. 1978a, Nehru et al. 1983). The inclusion-bearing olivine grains tend to be euhedral to subhedral (Floran et al. 1978a). Olivine in Eagles Nest has inclusions of chromite, apatite and troilite, but no melt inclusions (Swindle et al. 1998).

Olivine is homogeneous within each brachinite, and ranges from Fo_{65-70} among the brachinites. Augite is more magnesian: mg# = 79 to 82. In olivine MnO ranges from ~0.3 to 0.6%, Cr_2O_3 ranges from 0.01 to 0.08%, CaO ranges from 0.05 to 0.27% (Kring et al. 1991, Warren and Kallemeyn 1989a, Johnson et al. 1977, Nehru et al. 1983), and NiO is detectable—up to 0.05% (Nehru et al. 1992). In augite MnO ranges from 0.15 to 0.32%, Cr_2O_3 from 0.68 to 1.04%, Na_2O from 0.39 to 0.61%, TiO_2 from 0.1 to 0.4%, and Al_2O_3 from 0.55 to 0.98% (Kring et al. 1991, Warren and Kallemeyn 1989a, Johnson et al. 1977, Nehru et al. 1983).

Chromite has molar Cr/(Cr+Al) ratios of 0.81 to 0.83 in Brachina, ALH 84025, and Eagles Nest and 0.73 in Hughes 026, with mg# of 19 to 26 (Johnson et al. 1977, Warren and Kallemeyn 1989a, Nehru et al. 1983, Swindle et al. 1998, Nehru et al. 1996). Prinz et al. (1986a) reported that only minor Fe_2O_3 was required by stoichiometry for chromite in Brachina and Eagles Nest, but recalculation of published analyses does not confirm this. The TiO_2 contents of chromite range from 1.4% in Eagles Nest and ALH 84025 (Swindle et al. 1998, Warren and Kallemeyn 1989a) to ~2.9% in Brachina (Nehru et al. 1983).

The sulfide in brachinites is mainly Ni-rich (0.5 to 3%) troilite (Nehru et al. 1992), but pentlandite has also been observed in Brachina (Nehru et al. 1983). Metal contains 19 to 55% Ni (Nehru et al. 1992).

Chlorapatite is the dominant phosphate in brachinites (Nehru et al. 1992), but whitlockite also occurs in Hughes 026 (Nehru et al. 1996). Eagles Nest contains an Fe-phosphate, tentatively identified as being either ludlamite, vivianite or beraunite, but this is believed to be a terrestrial weathering product of apatite (Swindle et al. 1998).

Composition

Lithophile elements. Lithophile elements in Brachina are close to chondritic in abundance and are relatively unfractionated (Table 19, Fig. 22). Eagles Nest is slightly depleted in Al, Ca, K, Rb and more so in Na (0.07 × CI), and ALH 84025 is depleted in Al and Na (0.1 × CI), consistent with the lack of plagioclase in these two brachinites.

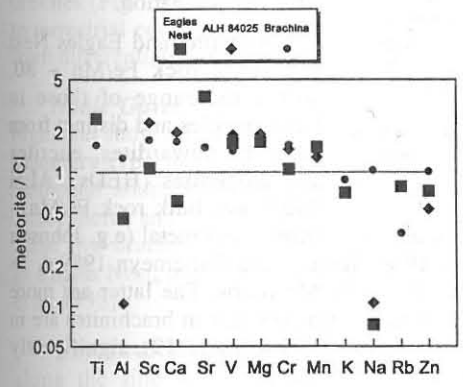

Figure 22. CI-normalized lithophile element abundances in brachinites. Data from Johnson et al. (1977), Nehru et al. (1983), Swindle et al. (1998), Warren and Kallemeyn (1989a).

Table 19. Bulk compositions of brachinites.

		ALH 84025 (1)	Brachina (2)	Eagles Nest* (3)
Na	mg/g	0.51	5.10	0.351
Mg	mg/g	184	162	161
Al	mg/g	0.90	11.0	3.91
Si	mg/g	170	178	
P	mg/g		1.2	
S	mg/g		15.2	
K	µg/g	_40	700	400
Ca	mg/g	18	15.5	5.5
Sc	µg/g	13.6	8.2	6.19
Ti	mg/g	_1.6	0.72	1.1
V	µg/g	108	77	94
Cr	mg/g	3.94	4.15	2.80
Mn	mg/g	2.53	2.6	3.04
Fe	mg/g	250	206	245
Co	µg/g	365	232	201
Ni	mg/g	5.10	3.09	2.20
Zn	µg/g	164	313	223
Ga	µg/g	2.1	7.6	1.5
As	µg/g	0.55	0.18	3.72
Se	µg/g	12.4	3.5	3.71
Br	µg/g	0.33	0.49	2.95
Rb	µg/g		2.0	1.8
Sr	µg/g		15	29.4
Zr	µg/g		2.7	8.4
Sb	ng/g	56		95
Cs	ng/g		200	104
Ba	µg/g		12	208
La	µg/g	0.065	0.665	2.66
Ce	µg/g		1.6	2.00
Nd	µg/g		0.86	2.51
Sm	µg/g	0.034	0.235	0.527
Eu	µg/g	0.033	0.08	0.131
Tb	µg/g		0.05	0.071
Yb	µg/g	0.098	0.21	0.186
Lu	µg/g	0.016	0.07	0.0255
Ir	ng/g	123	111	98
Au	ng/g	61	15	25.3
Th	ng/g		130	173

(1) whole rock, Warren and Kallemeyn (1989a); (2) average whole rock, Johnson et al. (1977), except Zn, Ga, As, Se and Br, Nehru et al. (1983); average whole rock, Swindle et al. (1998).

*Contamination and weathering have affected the composition of Eagles Nest. Data should be treated with caution (see Swindle et al. 1998).

Brachina has a nearly flat REE pattern, at ~1 × CI abundances (Fig. 23). ALH 84025 is LREE-depleted, with La = 0.28 × CI, consistent with its depletion in lithophile incompatible major elements. Eagles Nest, which is also depleted in lithophile incompatible major elements, is LREE-enriched, with La ~ 11 × CI, and shows a significant negative Ce anomaly. These features are most likely due to contamination by terrestrial REE (Swindle et al. 1998).

Incompatible lithophile element depletion in various meteorites can be gauged on a plot of CI-normalized Na/Sc vs. Sm/Sc ratios (Fig. 24). During melting or crystallization in ultramafic/mafic systems, Na and Sm will be more incompatible than Sc, and Na/Sc and Sm/Sc ratios will be low in partial melt residues or ultramafic cumulates. On this plot Brachina appears to be only slightly depleted and in this regard resembles acapulcoites and winonaites, while ALH 84025 is more depleted than most lodranites, and as depleted as some ureilites. Eagles Nest is not shown because of likely terrestrial REE contamination.

Brachina and Eagles Nest have bulk rock Fe/Mn ~ 80, within the range of those in lunar samples and distinct from those in howardites, eucrites and diogenites (HEDs). ALH 84025 has bulk rock Fe/Mn ~ 100. However, brachinites contain a few percent Ni-rich troilite and metal (e.g. Johnson et al. 1977, Nehru et al. 1992, Swindle et al. 1998, Warren and Kallemeyn 1989a), so bulk rock Fe/Mn ratios are higher than bulk silicate Fe/Mn ratios. The latter are more directly comparable to lunar or eucritic data. Measured Ga/Al ratios in brachinites are in the range 2×10^{-3} for Brachina to 7×10^{-4} for ALH 84025 (Table 19), significantly higher than those of eucrites which are on the order of 2×10^{-6}.

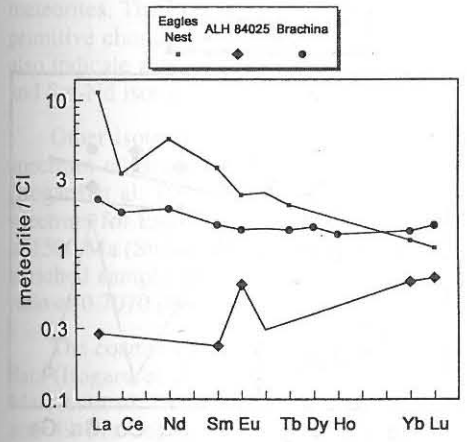

Figure 23. CI-normalized REE abundances in brachinites. Data from Johnson et al. (1977), Nehru et al. (1983), Swindle et al. (1998), Warren and Kallemeyn (1989a).

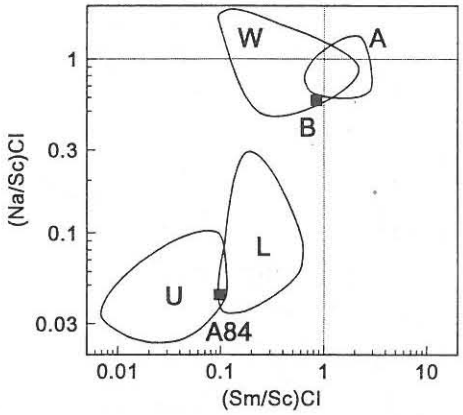

Figure 24. CI-normalized Na/Sc vs. Sm/Sc ratios for Brachina (B) and ALH 84025 (A84), compared to fields for acapulcoites (A), lodranites (L), ureilites (U) and winonaites-IAB silicates (W). Brachinite data are from Johnson et al. (1977), Nehru et al. (1983), Warren and Kallemeyn (1989a). Other data are from numerous sources.

Siderophile Elements. Siderophile element abundances in brachinites (Table 19) are near-chondritic (~0.1-1 × CI), similar to ureilites, but show a different pattern from ureilites (Fig. 25). Tungsten is enriched in Eagles Nest at ~4.6 × CI, but this may be due to terrestrial contamination. These abundances are much higher than in groups of rocks from differentiated bodies such as the Earth, Moon and Mars.

Noble Gases. Abundances of trapped noble gases in Brachina and ALH 84025 are high, and show a fractionated, or planetary-type pattern, similar to ureilites (Fig. 26). (A planetary-type noble gas pattern is one of increasing abundance, relative to solar elemental abundances, with increasing mass. This pattern is found for the terrestrial atmosphere, and in most chondrites.) Interelement ratios of Kr/Ar/Xe are similar in these two brachinites, and distinct from those in Chassigny (Ott et al. 1985a, 1987). In Eagles Nest, trapped noble gases are dominated by terrestrial contamination (Swindle et al. 1998).

Oxygen-isotopes. On an oxygen-isotope plot, the five brachinites and Divnoe plot along the line with slope ~1/2 defined by HED meteorites (Fig. 1c,d) and are

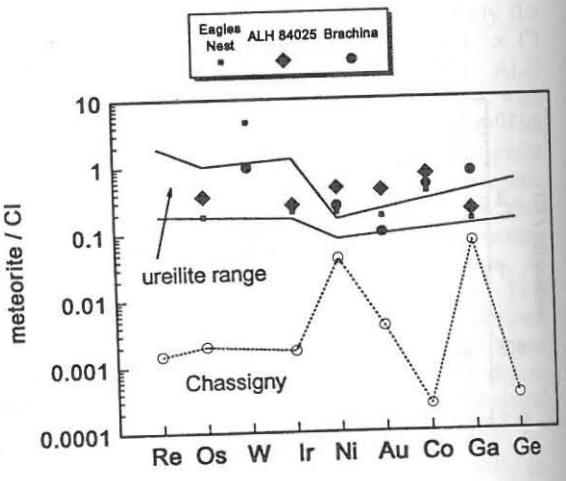

Figure 25. CI-normalized siderophile element abundances in brachinites, compared to the range in ureilites, and to Chassigny. Brachinite data are from Johnson et al. (1977), Nehru et al. (1983), Swindle et al. (1998) and Warren and Kallemeyn (1989a). Ureilite data are from numerous sources. Data for Chassigny from Treiman et al. (1986), Burghle et al. (1983), Warren (1987).

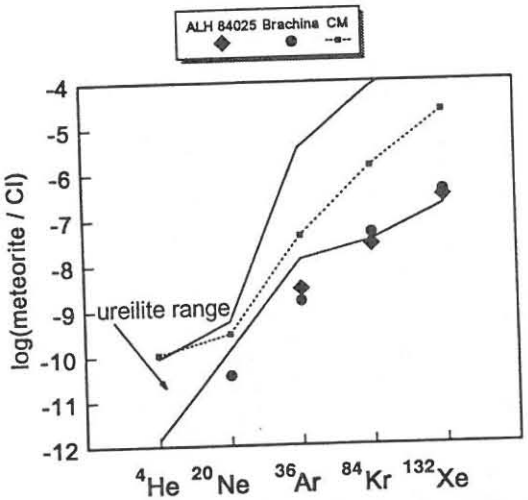

Figure 26. Noble gas abundances in Brachina (Bogard et al. 1983; Ott et al. 1983; Ott et al. 1985—1600° extraction) and ALH 84025 (Ott et al. 1987—1800° extraction) relative to cosmic abundances and compared to ureilites (for sources of ureilite data see Fig. 38). A typical CM chondrite (Haripura) as a representative planetary-type pattern is shown for reference (Mazor et al. 1970).

indistinguishable from the HED trend: $\Delta^{17}O$ = -0.26±0.08 for brachinites and -0.25±0.08 for HEDs (Clayton and Mayeda 1996).

Chronology

Chronological studies indicate that brachinites are extremely old. Brachina contains excess ^{53}Cr correlated with the Mn/Cr ratio (Wadhwa et al. 1998), which indicates that the short-lived radionuclide ^{53}Mn ($t_{1/2}$ ~ 3.7 Ma) was present at the time of last Cr isotopic equilibration. Combining the calculated $^{53}Mn/^{55}Mn$ ratio of Brachina with that ratio for the angrite LEW 86010 and its Pb-Pb age, yields an estimated formation age of 4.5637±0.0009 Ga for Brachina (Wadhwa et al. 1998).

In addition, Brachina, ALH 84025 and Eagles Nest all contain excess ^{129}Xe from in-situ decay of ^{129}I (Bogard et al. 1983, Ott et al. 1987, Swindle et al. 1993, 1998). In Brachina, a $^{128}Xe/^{129}Xe$ correlation indicates that retention of Xe began not later than ~4.4 Ga, and probably by 4.5 Ga ago (Bogard et al. 1983). In Eagles Nest, however, the

lack of an I-Xe correlation indicates a disturbance resembling that in highly-shocked meteorites. The data indicate only that Eagles Nest began retaining Xe within ~50 Ma of primitive chondrites (Swindle et al. 1998). Fission track excesses due to decay of ^{244}Pu also indicate a formation age for Brachina of close to 4.5 Ga (Crozaz and Pellas 1983), and Sm-Nd isotopic data give a model age of 4.61 Ga (Bogard et al. 1983).

Other isotopic systems in brachinites indicate younger disturbances. The ^{39}Ar-^{40}Ar spectrum of Brachina shows a maximum age of 4.3 Ga and an average age of 4.1 Ga (Bogard et al. 1983), and its U-Th-He age is 400 Ma (Ott et al. 1985a). The ^{39}Ar-^{40}Ar spectrum for Eagles Nest yields a minimum age of 955 Ma and a maximum age of 1300 to 1500 Ma (Swindle et al. 1993). Rb-Sr isotopic data for a whole rock and a plagioclase-enriched sample of Brachina yield an apparent age of 2.5 Ga, with an initial $^{87}Sr/^{86}Sr$ ratio of 0.7070 (Bogard et al. 1983).

The cosmic-ray exposure age of Brachina is 2.0-3.5 Ma based on ^{3}He, ^{21}Ne and ^{38}Ar data (Bogard et al. 1983, Ott et al. 1983). ALH 84025 has a ^{21}Ne exposure age of 10.1 Ma (Ott et al. 1987), while for Eagles Nest the exposure ages are 44 Ma based on ^{21}Ne, and 49 Ma based on ^{38}Ar (Swindle et al. 1998). The $^{22}Ne/^{21}Ne$ ratios indicate that Brachina experienced very low shielding exposure (corresponding to ~3 cm depth), while Eagles Nest experienced higher shielding (Swindle et al. 1998).

Discussion

Nehru et al. (1983, 1992, 1996) consider brachinites to be a primitive achondrite group. Primitive achondrites are meteorites whose bulk compositions are approximately chondritic, but whose textures are igneous or metamorphic. The primitive achondrites are generally thought to be ultrametamorphosed chondrites or residues of very low degrees of partial melting on small parent bodies. Winonaites, silicates from IAB and IIICD irons, acapulcoites, lodranites, and recently even ureilites (Clayton and Mayeda 1996) have been considered to be primitive achondrites.

The near-chondritic abundances of lithophile elements, siderophile elements, and noble gases in Brachina support the interpretation that it has been only slightly modified by igneous processes, if at all. ALH 84025 also has siderophile elements and noble gases in near-chondritic abundances, but it is depleted in Al and Na, and has a fractionated REE pattern. Brachinites do not have a strictly chondritic mineralogy; their pyroxene is dominantly clinopyroxene rather than orthopyroxene, and only Brachina has a near-chondritic plagioclase content.

Nehru et al. (1992, 1996) suggest that brachinites evolved from CI-like material that was oxidized during planetary heating, converting orthopyroxene to olivine via the reaction $MgSiO_3 + Fe + 1/2O_2 \rightarrow (Mg,Fe)_2SiO_4$ (McSween and Labotka 1993). Partial melting occurred in some places, removing a basaltic component which is unsampled. Extensive thermal metamorphism produced equilibrated mineral compositions and textures. Equilibration temperatures calculated for brachinites range from 825° to 1070°C (orthopyroxene-clinopyroxene), 965° to 1246°C (Ca distribution between olivine and clinopyroxene), or 800° to 1080°C (olivine-chromite), supporting a high-temperature history (Nehru et al. 1996).

In contrast, Warren and Kallemeyn (1989a) have suggested that ALH 84025 is an olivine heteradcumulate, and that Brachina is an olivine orthocumulate. They point out that the coarse size, prismatic habit, and apparent preferred orientation of silicate grains in most of ALH 84025 are typical of cumulate rather than metamorphic rocks, and resemble similar features that have been argued to be the result of cumulus processes in ureilites (Berkley et al. 1980). In this model, the simple mineralogy, LREE-depletion, and

low Al content of ALH 84025 indicate that it contains very little trapped liquid, while the presence of plagioclase, higher REE contents, and high Al content of Brachina indicate a far higher trapped liquid component. A cumulate model for Brachina was also discussed by Johnson et al. (1977) and Floran et al. (1978a).

A third model that has been discussed for Brachina is that it is an igneous rock that crystallized from a melt of its own composition (Johnson et al. 1977, Floran et al. 1978a). As a variant on this theme, Ryder (1982) modeled Brachina as an impact melt, but this model was largely contrived to accommodate Brachina and Chassigny on the same parent body.

There are enough petrologic and geochemical differences among the different brachinites to suggest that they may not have all formed by the same process. The question of whether brachinites are primitive achondrites, in the sense defined above, or are igneous cumulates, is one that applies to lodranites and ureilites as well. Trends in mineralogy, lithophile incompatible element abundances, and oxygen-isotopic systematics do not, however, show a coherent transition from the most chondritic to the least chondritic of the groups that have been considered to be primitive achondrites (Goodrich 1997c). Basaltic complements to brachinites are missing in the meteorite record, and this is also true for lodranites and ureilites. Whether the vagaries of meteorite delivery simply never sent them earthward, or whether they never existed remains unknown.

ACAPULCOITES AND LODRANITES

Acapulcoites and lodranites have evolved from being one or two "oddities" to a substantial group of meteorites that promise to greatly increase our understanding of partial melting and melt migration on asteroids early in the history of the solar system. This stems largely from the dramatic increase in the number of acapulcoites and lodranites recognized in our meteorite collections. We now recognize 9 acapulcoites which sample 5 distinct fall events and 14 lodranites representing 12 distinct fall events. The unique meteorite LEW 86220 is clearly related to this group, but is neither an acapulcoite or lodranite. With this increased sample suite, a number of recent, comprehensive studies have examined, and in some cases identified, this growing number of group members. Broader reviews of this group have been published by Nagahara (1992), Takeda et al. (1994a), Mittlefehldt et al. (1996) and McCoy et al. (1996b, 1997a,b).

Mineralogy and petrology

Acapulcoites and lodranites are composed of orthopyroxene, olivine, chromian diopside, sodic plagioclase, Fe,Ni metal, schreibersite, troilite, whitlockite, chlorapatite, chromite and graphite, a mineral assemblage broadly similar to that found in ordinary chondrites. However, mineral compositions, mineral abundances and textures of acapulcoites and lodranites differ from ordinary chondrites and, to a certain extent, from each other.

The distinction between acapulcoites and lodranites is not clear cut and disagreement exists as to the definitions and memberships of these groups. Acapulco is a fine-grained meteorite with approximately chondritic abundances of olivine, pyroxene, plagioclase, metal and troilite, while Lodran is a coarse-grained meteorite which is depleted in troilite and plagioclase. Comparison to these type meteorites suffices for classification of most of the members of this clan. However, meteorites like EET 84302 are problematic in being coarser-grained and depleted in troilite but not plagioclase. Most authors consider this

meteorite intermediate between acapulcoites and lodranites (e.g. Takeda et al. 1994a, Mittlefehldt et al. 1996, McCoy et al. 1997a,b).

Modally, acapulcoites are similar to chondrites. In acapulcoites, orthopyroxene is more abundant than olivine (Yugami et al. 1997), as one might expect for chondritic silicates with relatively Mg-rich mafic mineral compositions. Plagioclase and troilite appear to occur in approximately the same abundances observed in ordinary chondrites (~10 wt % plagioclase and 5 to 6 wt % troilite), despite uncertainties due to sampling heterogeneity and weathering. In contrast, lodranites are sometimes enriched in olivines and often depleted in plagioclase and/or troilite relative to chondrites (McCoy et al. 1997b, Yugami et al. 1997). It should be emphasized that some lodranites contain relatively abundant plagioclase, but lack troilite, while others lack plagioclase but contain moderate abundances of troilite. In addition, plagioclase can be heterogeneously distributed, such as in EET 84302 (Takeda et al. 1994a).

Texturally, acapulcoites and lodranites are fine- to medium-grained equigranular rocks (Fig. 27a,c,e). Recrystallization is evident from abundant 120° triple junctions (Palme et al. 1981). Rare relict chondrules have been reported in the acapulcoites Monument Draw (McCoy et al. 1996b), Yamato 74063 (Yanai and Kojima 1991), and ALHA77081 (Schultz et al. 1982). In each case, only one or two relict chondrules have been observed. McCoy et al. (1996b) demonstrated that acapulcoites are significantly finer-grained (150 to 230 μm) than lodranites (540 to 700 μm), while EET 84302 is intermediate in grain size (340 μm). Both acapulcoites and lodranites generally exhibit only very minor shock effects (S1-S2), although a small number of lodranites (e.g. MAC 88177, Y-8307) are more heavily shocked, exhibiting shock melt veins which cross-cut the specimens. Substantial debate exists about the genesis of 1- to 5-μm blebs of Fe,Ni-FeS found in the cores of mafic silicates. Some authors (e.g. Takeda et al. 1994a) argue that these blebs decorate pre-existing planar fractures formed during an earlier shock event and that were subsequently annealed. Other authors (e.g. Schultz et al. 1982) suggest that these were trapped during chondrule formation and mark the outlines of relict chondrules. Zipfel et al. (1995) suggest that these were trapped during a period of extensive melting of acapulcoites. Acapulcoites and lodranites also exhibit a wide range of veins. Most acapulcoites contain mm-sized Fe,Ni-FeS veins which cross-cut all silicate phases. Monument Draw is unique in containing a cm-sized metal vein (Fig. 27b) with adjacent troilite-enriched areas. Acapulco and Monument Draw both contain phosphate veins hundreds of microns in length. Lodranites often exhibit plagioclase grains pinching between and partially enclosing mafic silicates (Fig. 27d).

Acapulcoites and lodranites have Mg-rich mafic silicate compositions compared to ordinary chondrites. Mafic silicate compositions of acapulcoites range from $Fa_{4.2\text{-}11.9}$ and $Fs_{6.5\text{-}12.6}$. In each case, the Fa content of olivine is approximately equal to or slightly less than the Fs content of orthopyroxene. McCoy et al. (1996b) reviewed evidence for zoning in mafic silicates in acapulcoites. Yugami et al. (1993) found orthopyroxene grains depleted in FeO in the rims relative to the core in low-FeO acapulcoite ALHA81187, although this feature is not observed in other acapulcoites. Lodranites exhibit similar ranges in composition of olivine ($Fa_{3.1\text{-}13.3}$) and orthopyroxene ($Fs_{3.7\text{-}13.8}$). Representative analyses that span this range are given in Table 20. Reverse zoning with rims lower in FeO than cores is common in both olivine and orthopyroxene of lodranites (McCoy et al. 1997a and references therein). Zoning is particularly prominent in olivines in high-FeO lodranites and in orthopyroxenes in lodranites in which the average Fs content of orthopyroxene is greater than the average Fa content of olivine. Chromian diopside exhibits a smaller range in FeO concentrations ($Fs_{4.3\text{-}5.2}$) and contains 0.74 to 1.74 wt % Cr_2O_3. Plagioclase compositions range from $An_{12.3\text{-}30.9}$ (McCoy et al. 1997a and

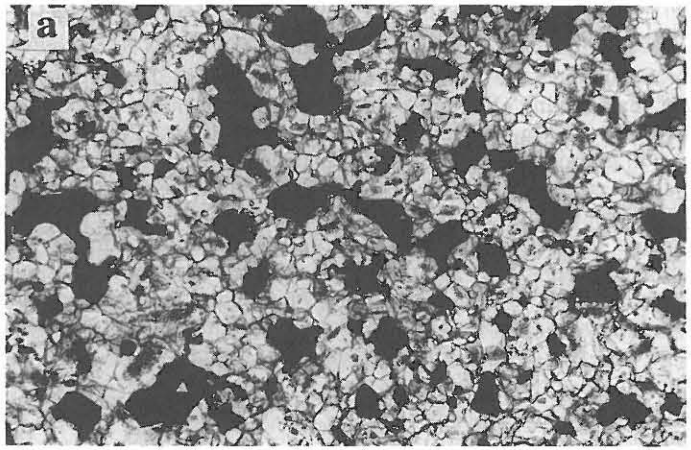

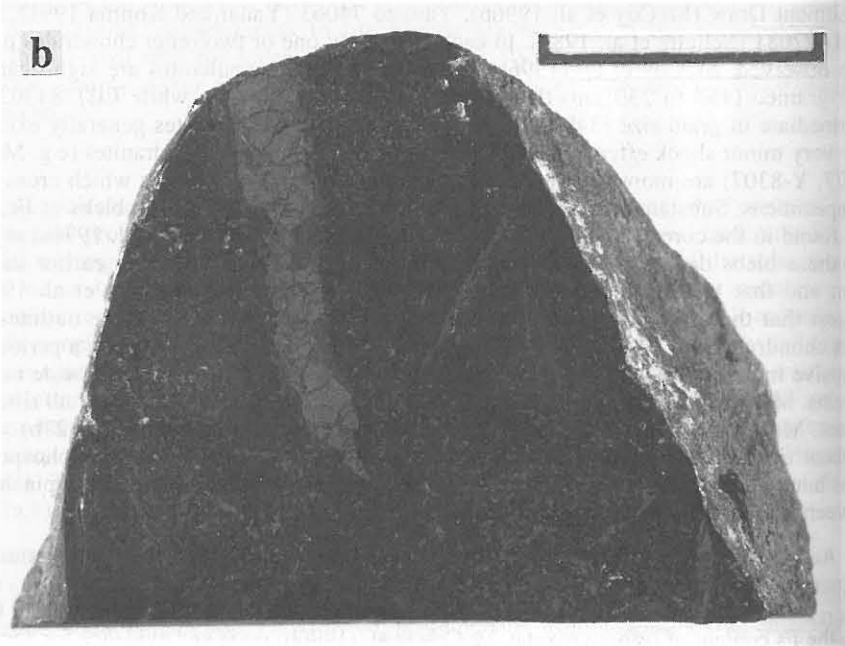

Figure 27. Photographs of acapulcoites and lodranites. (a) Photomicrograph of Acapulco showing its fine-grained, equigranular texture. Field of view is 5.2 mm. (b) Hand sample of Monument Draw with cm-sized metal veins. *On the following page:* (c) Photomicrograph of EET 84302, which exhibits a medium-grained, equigranular texture. Field of view is 5.2 mm. (d) Photomicrograph of Yamato 8002 with interstitial plagioclase, suggestive of melt migration. Field of view is 1.3 mm. (e) Photomicrograph of Lodran, which is coarse-grained and depleted in metal and troilite. Field of view is 5.2 mm.

references therein). Calculated two-pyroxene equilibration temperatures exhibit a substantial range from ~1000° to 1200°C.

One meteorite within the acapulcoite-lodranite clan is so unusual in both its texture and modal mineralogy as to deserve special attention. LEW 86220 (Fig. 27f) is linked to the other acapulcoites and lodranites through both its oxygen-isotopic and mineral

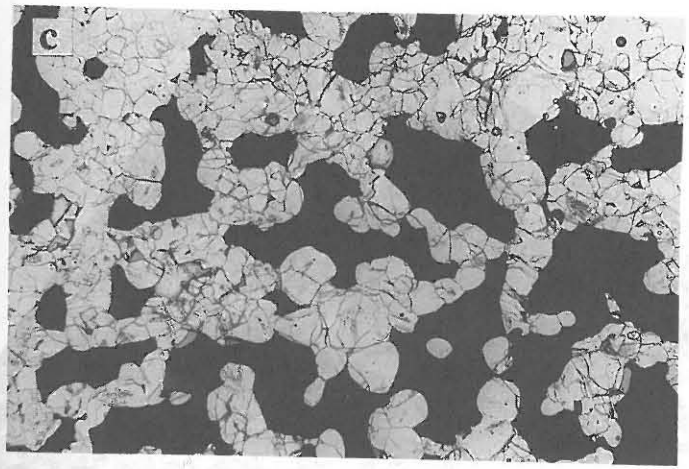

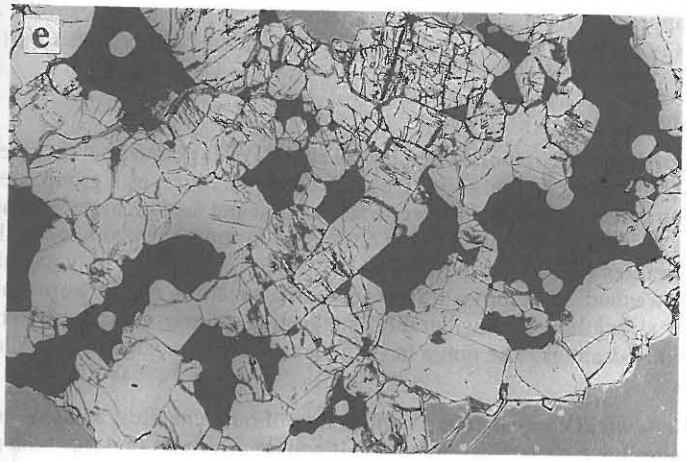

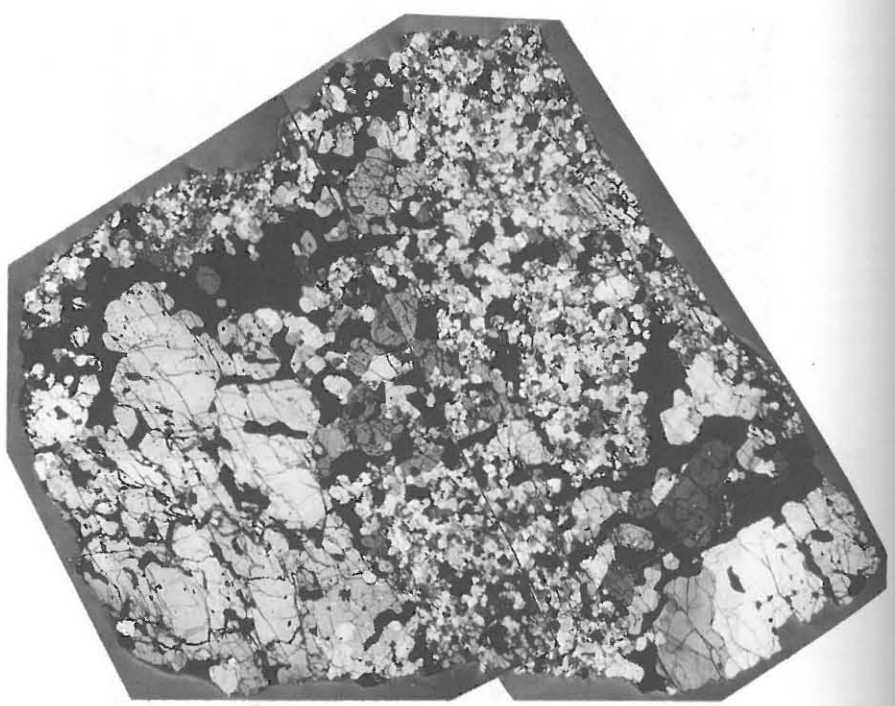

Figure 27 (cont'd). Photographs of acapulcoites and lodranites. (f) Photomosaic in crossed polars of an entire thin section of LEW 86220. Coarse-grained gabbroic, and Fe,Ni–FeS melts have intruded an acapulcoite host. Maximum dimension of specimen is 12 mm.

compositions (Clayton and Mayeda 1996, McCoy et al. 1997b). The meteorite consists of two different lithologies, one of acapulcoite modal mineralogy and grain size, the other of Fe,Ni metal, troilite and plagioclase-augite (basaltic-gabbroic) mineralogy and a very coarse grain size (plagioclase grains reach 9 mm in maximum dimension). These two lithologies do not occur as clasts, as in meteoritic breccias, but rather the coarse-grained lithology appears to have intruded into the acapulcoite lithology. A similar dichotomy of lithologies is found in silicate inclusions in the Caddo County IAB iron (Takeda et al. 1997a).

Composition

Oxygen-isotopic composition. Clayton et al. (1992) pointed out that the variability in oxygen-isotopic compositions of acapulcoites and lodranites, as a group, are beyond what could be attributed to mass-dependent fractionation and analytical uncertainty. Fayalite in olivine vs. $\Delta^{17}O$ (Fig. 28) are weakly correlated in lodranites, similar to the correlation found in ureilites (Clayton and Mayeda 1988). However, when only samples which had been acid-washed to remove terrestrial contamination (rust) were considered, the correlation strengthened considerably, suggesting primary nebular heterogeneity was preserved in lodranites. The range in both parameters is much smaller in lodranites than in ureilites.

Bulk chemical composition. A wide array of bulk chemical analyses of acapulcoites and lodranites have been published in the literature. Table 21 presents bulk major element

Table 20. Representative mineral compositions for acapulcoites and lodranites.

	OLIVINE					ORTHOPYROXENE					CLINOPYROXENE					PLAGIOCLASE		
	ALH A81187 (1)	Monument Draw (1)	Gibson (2)	EET 84302 (2)	LEW 88280 (2)	ALH A81187 (1)	Monument Draw (1)	Gibson (2)	EET 84302 (2)	LEW 88280 (2)	ALH A81187 (1)	Monument Draw (1)	Gibson (2)	EET 84302 (3)	LEW 88280 (2)	ALH A81187 (3)	Gibson (2)	EET 84302 (3)
Chemical Composition (wt %)																		
SiO_2	41.5	42.1	42.0	40.4	39.8	58.0	58.3	57.9	57.2	55.6	54.4	54.5	53.6	54.0	52.1	63.5	64.3	62.4
Al_2O_3	n.d.	n.d.	b.d.	n.d.	b.d.	n.d.	0.28	0.42	n.d.	0.46	n.d.	0.75	1.00	1.18	1.07	23.1	22.6	23.9
Cr_2O_3	n.d.	n.d.	0.07	n.d.	b.d.	n.d.	0.25	0.47	n.d.	0.50	n.d.	1.18	1.74	1.56	1.60	n.d.	n.d.	n.d.
TiO_2	n.d.	n.d.	b.d.	n.d.	b.d.	n.d.	0.20	0.16	n.d.	0.12	n.d.	0.53	0.41	0.56	0.31	n.d.	n.d.	n.d.
FeO	4.27	9.45	3.10	8.17	12.2	4.79	6.92	3.86	5.67	7.88	2.06	2.63	2.62	2.15	2.98	0.16	0.28	0.13
MgO	54.2	47.1	54.8	50.2	46.3	34.8	32.0	34.4	34.5	32.9	19.0	16.8	17.4	18.0	17.7	0.03	b.d.	0.01
MnO	0.67	0.52	0.39	0.62	0.48	0.83	0.55	0.51	0.73	0.54	0.53	0.31	0.30	0.31	0.34	n.d.	n.d.	n.d.
CaO	b.d.	b.d.	b.d.	b.d.	b.d.	1.73	0.84	1.09	0.96	1.32	20.7	21.7	21.5	21.2	22.0	3.89	3.87	4.86
Na_2O	n.d.	n.d.	n.d.	n.d.	n.d.	n.d.	b.d.	b.d.	n.d.	b.d.	n.d.	0.74	0.65	0.70	0.71	9.27	9.27	8.71
K_2O	n.d.	n.d.	n.d.	n.d.	n.d.	n.d.	n.d.	n.d.	n.d.	n.d.	n.d.	n.d.	n.d.	n.d.	n.d.	0.29	0.66	0.30
Total	100.64	99.17	100.36	99.39	98.78	100.15	99.34	98.81	99.06	99.32	96.69	99.15	99.22	99.66	98.81	100.24	100.98	100.31
Atomic Formula (O = 4 for olivine, 6 for pyroxene, 8 for plagioclase)																		
Si	0.988	1.035	0.996	0.991	1.000	1.995	2.027	2.003	1.993	1.959	2.021	1.994	1.965	1.963	1.931	2.801	2.821	2.758
Al	--	--	--	--	--	--	0.011	0.017	--	0.019	--	0.032	0.043	0.051	0.047	1.201	1.169	1.245
Cr	--	--	0.001	--	--	--	0.007	0.013	--	0.014	--	0.034	0.050	0.045	0.047	--	--	--
Ti	--	--	--	--	--	--	0.005	0.004	--	0.003	--	0.015	0.011	0.015	0.009	--	--	--
Fe	0.085	0.194	0.061	0.168	0.256	0.138	0.201	0.112	0.165	0.232	0.064	0.080	0.080	0.065	0.092	0.006	0.010	0.005
Mg	1.924	1.726	1.937	1.836	1.734	1.764	1.659	1.774	1.792	1.728	1.052	0.916	0.951	0.975	0.978	0.002	--	0.001
Mn	0.014	0.011	0.008	0.013	0.010	0.024	0.016	0.015	0.022	0.016	0.017	0.010	0.009	0.010	0.011	--	--	--
Ca	--	--	--	--	--	0.064	0.031	0.040	0.036	0.050	0.824	0.851	0.844	0.826	0.874	0.184	0.182	0.230
Na	--	--	--	--	--	--	--	--	--	--	--	0.052	0.046	0.049	0.051	0.793	0.789	0.746
K	--	--	--	--	--	--	--	--	--	--	--	--	--	--	--	0.016	0.037	0.017
Total Cations	3.012	2.965	3.003	3.009	3.000	4.005	3.958	3.978	4.007	4.021	3.977	3.984	4.000	3.999	4.039	5.003	5.007	5.002
Molar Mineral End Members and mg# (100(MgO/(MgO+FeO)))*																		
Wo	--	--	--	--	--	3.2	1.7	2.1	1.8	2.5	42.5	46.1	45.0	44.2	44.9	--	--	--
En	--	--	--	--	--	89.9	87.7	92.1	89.9	86.0	54.2	49.6	50.7	52.3	50.3	--	--	--
Fs	--	--	--	--	--	6.9	10.6	5.8	8.3	11.6	3.3	4.4	4.3	3.5	4.8	--	--	--
Ab	--	--	--	--	--	--	--	--	--	--	--		--		--	79.8	78.3	75.1
An	--	--	--	--	--	--	--	--	--	--	--		--		--	18.5	18.1	23.2
Or	--	--	--	--	--	--	--	--	--	--	--		--		--	1.6	3.7	1.7
mg#	95.8	89.9	96.9	91.6	87.1	92.8	89.2	94.1	91.6	88.2	94.3	91.9	92.2	93.7	91.4	--	--	--

Data sources: (1) McCoy et al. (1996), (2)McCoy et al. (1997a), (3) Mittlefehldt et al. (1996).

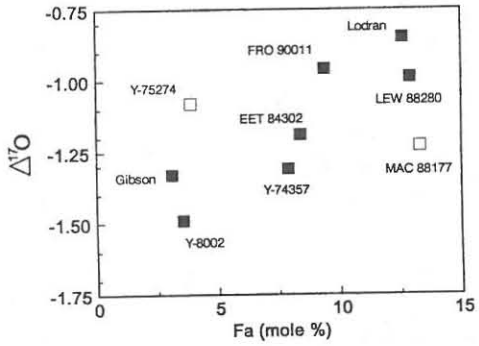

Figure 28. $\Delta^{17}O$ vs. Fa in olivine for lodranites. Non-Antarctic and acid-washed Antarctic lodranites are plotted as solid squares; non-acid-washed lodranites as open squares. The positive correlation for the former suggests nebular heterogeneity within the chondritic precursor to the lodranites.

Table 21. Bulk major element analyses (in wt %) of acapulcoites and lodranites.

	Acapulco (1)	ALHA 77081 (2)	Y-74063 (1)	Y-74357 (1)	Y-75274 (3)	Y-791493 (3)
SiO_2	37.8	40.9	39.0	37.7	24.1	34.9
TiO_2	0.07		0.08	0.09	0.02	0.05
Al_2O_3	2.06	2.27	2.96	0.20	0.18	0.90
Cr_2O_3	0.45	0.72	0.34	0.96	0.12	0.81
FeO	5.69	4.98	9.69	4.00	2.36	6.12
MnO	0.39	0.39	0.19	0.37	0.21	0.42
MgO	26.8	26.0	27.0	27.0	27.0	29.5
CaO	1.94	0.83	2.68	3.65	0.45	1.54
Na_2O	0.86	1.01	0.83	0.10	0.14	0.21
K_2O	0.06	0.08	0.07	0.02		
P_2O_5	0.37		0.46	0.26	0.27	0.49
Fe_2O_3	1.82		0.91	7.55	2.82	6.02
FeS	5.79	8.10	9.31	1.85	1.14	2.10
Fe	14.5	14.6	4.89	15.2	39.4	14.3
Ni	1.31	1.60	0.98	0.98	1.84	1.13
Co	0.11	0.08	0.03	0.08	0.14	0.07
sum	99.98	101.53	99.41	99.90	100.16	98.57

Data sources: (1) Yanai and Kojima (1991), (2) Nagahara and Ozawa (1986), (3) Haramura et al. (1983)

analyses, while Table 22 presents minor and trace elements. A complete discussion of this data is beyond the scope of this paper and the reader is referred to the original publications. However, it is clear that bulk chemical data can shed substantial light upon the processes which have effected these rocks. As noted by Mittlefehldt et al. (1996), a plot of Se/Co vs. Na/Sc (Fig. 29) is a proxy for tracking the abundances of the host minerals in which these elements are sighted. Thus, Se/Co is equivalent to troilite/metal, while Na/Sc equates to plagioclase/pyroxene. During partial melting, removal of the Fe,Ni-FeS eutectic should cause a large decrease in the Se/Co ratio. Continued partial melting at higher temperature to produce a basaltic melt, which is highly enriched in plagioclase, will cause a decrease in Na/Sc ratio. Thus, schematically, a meteorite should follow the track of decreasing Se/Co followed by a decrease in Na/Sc shown in Fig. 29. Note that many meteorites do not fall along this idealized path.

Table 22. Average bulk minor and trace element compositions of acapulcoites and lodranites.

		ACAPULCOITES							TRANSITIONAL	LODRANITES			
		Acapulco (1)	ALH 78230 (2)	ALHA 77081 (3)	ALHA 81187 (4)	ALHA 81261 (5)	Monument Draw (6)	Y-74063 (7)	EET 84302 (4)	FRO 90011 (6)	LEW 88280 (4)	Lodran (8)	MAC 88177 (5)
Na	mg/g	6.51	7.53	7.29	5.54	6.92	7.08	7.07	4.74	0.77	0.58	0.32	0.31
K	µg/g	510	540	660		620	390			70		14	6
Sc	µg/g	8.11	10.5	9.91	8.99	8.56	9.05	10.0	6.19	5.71	8.01	6.20	8.88
V	µg/g	83		93		92	96	91		82		72	80
Cr	mg/g	6.02	5.00	6.80	4.14	5.54	2.46	2.69	12.4	5.21	6.02	3.90	3.69
Mn	mg/g	3.07		2.91		2.70	2.60	2.64		2.90		2.60	3.19
Co	mg/g	0.88	0.77	0.77	0.73	0.76	0.70	0.46	1.76	0.71	0.47	1.23	0.17
Ni	mg/g	16.6	14.8	13.9	10.5	14.2	17.9	11.9	26.4	12.6	12.2	22.5	4.2
Zn	µg/g	220		280	150	240	100	90		130	170		60
Ga	µg/g	8.9		10.8		9.3	6.9			8.8			3.1
As	µg/g	2.2	1.8	2.1	1.8	2.3	2.7	1.7	4.5	2.3	1.8		0.5
Se	µg/g	9.0		9.4	2.6	8.6	11.5	22.5		5.0	9.2		4.8
Sb	ng/g	90		60	80	80					70		20
La	µg/g	0.70	0.27	0.26	0.27	0.35	0.32	0.28	0.05	0.06	0.09	0.02	0.15
Sm	µg/g	0.25	0.21	0.19	0.19	0.22	0.19	0.19	0.04	0.05	0.08	0.03	0.09
Eu	µg/g	0.11	0.08	0.09	0.09	0.09	0.09	0.10	0.01	0.01	0.01		0.06
Tb	µg/g	0.05		0.06	0.06				0.04	0.02	0.03	0.02	
Dy	µg/g		0.39			0.46	0.57	0.45		0.32	0.29		0.33
Yb	µg/g	0.23	0.27	0.28	0.24	0.25	0.20	0.23	0.12	0.14	0.21	0.13	0.21
Lu	µg/g	0.030	0.041	0.050	0.040	0.040	0.043	0.040	0.020	0.030	0.030	0.020	0.040
Hf	µg/g	0.13		0.17	0.20	0.22	0.24						0.08
Os	ng/g	960		950		690	220		1570				460
Ir	ng/g	870		780	810	600	310	2600	860	60	120	25	570
Au	ng/g	210		190	200	190	180	510	240	260	200	46	170

(1) average of analyses by Kallemeyn and Wasson (1985), Palme et al. (1981), Zipfel et al. (1995); (2) analysis by Fukuoka and Kimura (1990); (3) average of analyses by Kallemeyn and Wasson (1985), Schultz et al. (1982); (4) average of analyses by Mittlefehldt et al. (1996); (5) average of analyses by Mittlefehldt et al. (1996), Zipfel and Palme (1993); (6) analysis by Zipfel and Palme (1993); (7) average of analyses by Kimura et al. (1992); (8) average of analyses by Fukuoka et al. (1978).

Chronology

A variety of chronometers which close at relatively high temperature have been applied to Acapulco. Prinzhofer et al. (1992) reported a Sm-Nd isochron age of 4.60±0.03 Ga. This age is slightly older than the generally accepted age of the solar system (4.56 Ga) and has been questioned by a number of researchers (e.g. McCoy et al. 1996b). Göpel et al. (1992) reported a precise Pb-Pb isochron age of 4.557±0.002 Ga for U-enriched phosphates from Acapulco and the ^{129}I-^{129}Xe formation interval between Bjürbole and Acapulco is only 8 Ma (Nichols et al. 1994). Pellas et al. (1997) have shown that phosphates in Acapulco contained ^{244}Pu ($t_{1/2}$ 81.8 Ma) when they cooled through the fission track retention temperature, about 350-390 K. Thus, Acapulco must have formed only very shortly after the solar system.

A wider number of both acapulcoites and lodranites have had ^{39}Ar-^{40}Ar ages determined. These include Acapulco (4.503±0.011, 4.514±0.005 Ga), Monument Draw (4.517±0.011 Ga), ALHA81187 (4.507±0.024 Ga), ALHA81261 (4.511±0.007 Ga), EET 84302 (4.519±0.017 Ga) and Gibson (4.49±0.01 Ga) (McCoy et al. 1996b, 1997a; Mittlefehldt et al. 1996, Pellas et al. 1997). These ^{39}Ar-^{40}Ar ages are all substantially younger than the Pb-Pb age or I-Xe formation interval, suggesting that they reflect a prolonged period of cooling from high temperature (McCoy et al. 1996b). Pellas et al. (1997) showed that Acapulco initially cooled rapidly (~100°C/Ma) from high temperature, but cooled slowly at low temperature (~2°C/Ma).

Cosmic-ray exposure ages are between ~5.5 to 7 Ma for all acapulcoites and most

lodranites examined to date (McCoy et al. 1996b, 1997a), possibly indicating sampling by a single impact event from a common parent body. This clumping between acapulcoites and lodranites strengthens arguments from similarities in oxygen-isotopic and mineral compositions and mineralogy, as well as the presence of transitional meteorites like EET 84302, that acapulcoites and lodranites are samples of a single parent body.

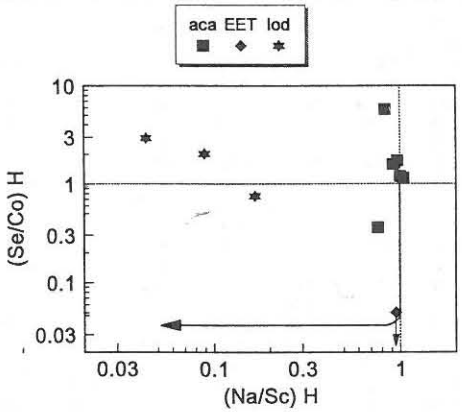

Figure 29. H-chondrite-normalized Se/Co vs. Na/Sc for acapulcoites (aca) and lodranites (lod).and the transitional meteorite EET 84302 (EET). See Mittlefehldt et al. (1996) for sources of data. These ratios serve as proxies for troilite/metal vs. plagioclase/pyroxene. Partial melting of a chondritic source should cause the residue to follow the arrowed line. High ratios for Se/Co in lodranites suggests that the Fe,Ni-FeS melts did not efficiently segregate from the residue when basaltic partial melts were removed, or that they were later re-introduced. The EET 84302 Se/Co ratio is an upper limit.

Discussion

Acapulcoites and lodranites formed from a chondritic precursor, based on the similarities in modal mineralogy between acapulcoites-lodranites and ordinary chondrites, the presence of rare relict chondrules in some acapulcoites, and the unfractionated bulk composition of acapulcoites (Fig. 29). This chondritic precursor was probably unlike known chondrites, differing in mineral, oxygen-isotopic and bulk compositions.

Acapulcoites and lodranites were extensively heated and experienced variable amounts of partial melting (Nagahara 1992, Takeda et al. 1994a, Mittlefehldt et al. 1996, McCoy et al. 1996b, 1997a,b). Disagreement exists over the extent of this partial melting in individual meteorites and in the efficiency with which melt migrated from their source regions. McCoy et al. (1996b, 1997a) argued that mm-sized Fe,Ni-FeS veins within acapulcoites represent melting of the Fe,Ni-FeS eutectic between ~950° and 1050°C. However, since these veins cross cut silicate phases, these authors argue that silicates must not have melted. Thus, acapulcoites experienced very low degrees of partial melting. Siderophile and chalcophile element evidence shows that these metallic-sulfide melts did not migrate out of many of the acapulcoites, although ALHA81187 lost and Y-74063 gained a small amount of these melts (Mittlefehldt et al. 1996). In contrast, lodranites exhibit depletions in troilite and plagioclase suggesting removal of the Fe,Ni-FeS and plagioclase-pyroxene partial melts and peak temperatures up to ~1250°C. In spite of the low modal troilite contents, some lodranites have Se/Co and Ir/Ni ratios indicating additions of a small amount of low temperature metallic-sulfide melt (Mittlefehldt et al. 1996). McCoy et al. (1997a) suggest that the coarser grain size of the lodranites reflects accelerated grain growth in the presence of a silicate melt.

Zipfel et al. (1995) hold a very different view of acapulcoite petrogenesis. These authors have suggested that Acapulco experienced extensive silicate partial melting and peak temperatures upwards of 1200°C. In part, these authors suggest that the inhomogeneous distribution of phosphates resulted from silicate melting. Mittlefehldt et al. (1996) have shown that acapulcoites have H chondritic ratios of Na/Sc, Sm/Sc and Eu/Yb, indicating that silicate partial melts, if they existed, did not migrate out of the acapulcoites. The presence of phosphate veins in some acapulcoites may suggest, instead, that phosphates are included in melting at the Fe,Ni-FeS eutectic (McCoy et al. 1996b), or that they participated in redox reactions with the metal at high temperatures (Mittlefehldt et al. 1996).

Takeda et al. (1994a) and Mittlefehldt et al. (1996) pointed out that while petrologic features might suggest partial melting of lodranites, melt migration was certainly complex. In particular, similar Se/Co ratios (Fig. 29) between acapulcoites and lodranites suggests that the Fe,Ni-FeS eutectic melt was not efficiently removed in at least some lodranites. Melt migration was addressed in considerable detail by McCoy et al. (1997b). In agreement with the work of Nagahara (1992) and Mittlefehldt et al. (1996), these authors argued that the migration of immiscible Fe,Ni-FeS and basaltic partial melts is complicated and could vary greatly depending on volatile contents, magma migration rates and conduit geometry. Indeed, Nagahara (1992) first pointed out that partial melts can migrate into, as well as out of, a source region, thus trapping migrating partial melts.

The migration of partial melts outside of the immediate source region was addressed by McCoy et al. (1997b), who argued that LEW 86220 sampled partial melts which migrated from a hotter lodranite source region and were trapped in a cooler acapulcoite host. At least some of these partial melts may have reached the surface where they may have been removed from the parent body by explosive volcanism (McCoy et al. 1997b). Recovery of an acapulcoite-lodranite regolith breccia would greatly elucidate whether basaltic partial melts formed thick deposits on the surface of the body.

Finally, all authors agree that these processes occurred very early in the history of the solar system, as reflected in the Pb-Pb, I-Xe and ^{244}Pu fission track retention ages. A substantial period of cooling or metamorphism (~50 Ma) occurred before Ar-Ar closure, leading to the younger ^{39}Ar-^{40}Ar ages, and another 100 Ma of cooling is required to explain the ^{244}Pu fission track ages. Finally, a small number of impacts, including one major impact at ~5.5 to 7 Ma, liberated most of the acapulcoites and lodranites from their common parent body.

UREILITES

Mineralogy, mineral chemistry and petrography

Olivine, pyroxene and chromite. Ureilites are essentially carbon-bearing ultramafic rocks. Their mineralogy is olivine + pyroxene, with <10% dark interstitial material, often referred to as matrix or vein material, consisting of varying amounts of carbon, metal, sulfides, and minor fine-grained silicates. None of the monomict ureilites contain plagioclase. The unusual ureilite LEW 88774 contains ~6% chromite. Modal pyroxene/(pyroxene+olivine) ratios range from 0 to ~0.9 (Table 23). In approximately 77% of the unpaired monomict ureilites, the sole pyroxene reported is pigeonite. In the remaining, a variety of pyroxene assemblages occur: pigeonite + augite, pigeonite + orthopyroxene, pigeonite + augite + orthopyroxene, orthopyroxene, and orthopyroxene + augite. The issue of the structural state of very low-Ca pyroxenes appears to be complex. For example, in LEW 88201, LEW 85440 and Y-791538, low-Ca pyroxene (~Wo_5) shows fine linear features under cross-polarized light (Takeda 1989, Takeda et al. 1992). Despite uniform composition, the Y-791538 pyroxene shows diffuse streaks in x-ray diffraction, which suggest that it was originally orthopyroxene but developed clinopyroxene lamellae during shock (Takeda 1989). In LEW 85440, TEM observations show an intimate alternation of ~10 nm-thick orthopyroxene and clinopyroxene lamellae

Table 23. Summary of petrographic information on ureilites. Ureilites are grouped by texture. Mineral compositions listed are for homogeneous cores.

	olivine Fo	pigeonite Wo/En	opx Wo/En	augite Wo/En	**py	texture	shock level	notes	references
Acfer 277	79	9.6/73			0.55, 0.33	typical	medium		1,2
ALH83014	82	8.0/77			0.13	typical	very low		AMN 8-1
ALHA77257	85	6.8/80			0.16	typical	low		13-15
ALHA78019	76	9.7/71			0.05	typical	very low		13-15
ALHA78262	78	8.4/72				typical	low		13-15
Asuka 87031	79	7.5/75			~0	typical	medium		3
Asuka 881931	76	8.8/73				typical	low-medium		3
EET 83225	87	10/78				typical	medium?		AMN 8-1
EET 87517	92	5.0/87			~0.5	typical	low		AMN 11-2
EET 90019	89	10/80				typical			AMN 15-1
FRO 90054	87		4.8/84	39/55	0.58,0.75	typical		1	22,23
GRA95205	79		4.0/77			typical			AMN 20-1
Hammadah al Hamra 126	79	8.4/74			0.3	typical	medium		4,35,36
*Havero	79	2.5/81			0.17	typical	high	2	5
Hughes 009	87		4.9/84	37/56	0.7	typical	medium		7,38
Jalanash	81	7.8/75			0.15	typical	medium		37
Kenna	79	9.8/72			0.25	typical	medium		5
*Lahrauli	79	7.7/74				typical	medium?		8,9
LEW 85328	80	9.0/74			0.33	typical	low		AMN 10-1
LEW85440	92		5.0/87	36/59	0.43,0.50	typical		3	24-26, AMN 13-2, AMN 13-3
LEW 88006	82	8.0/76				typical	low		AMN 13-2
LEW 88772	84	11/78				typical			AMN 16-1
*Novo Urei	79	10/72			0.31	typical	medium		5
Nullarbor 010	79	9.0/73	3.0/77		0.33	typical	very low	4	11
QUE 93336	77	10/72				typical	medium-high?	5	AMN 18-1
Roosevelt County 027	79	8.0/75			0.25	typical	low-medium		12
Y-74123	79	6.8/75			~0	typical			30-32
Y-74659	91	7.3/86	4.5/88		0.52	typical	low-medium		30,32,34
Y-790981	78	8.9/73			0.11	typical	medium	6	13,16,32
Y-791538	91	9.0/84	4.9/88		0.45	typical	low-medium		3,24,25
Y-791839	75	variable				typical			3
Y-82100	81	8.6/77			0.2	typical	low		3
Y-8448	78	variable				typical	low-medium		3

Table 23 (cont.). Summary of petrographic information on ureilites. Ureilites are grouped by texture. Mineral compositions listed are for homogeneous cores.

	olivine Fo	pigeonite Wo/En	opx Wo/En	augite Wo/En	**py	texture	shock level	notes	references
PCA 82506	78	6.0/76			0.48	typical/poikilitic	low		13,16
RKPA80239	83	6.7/78				typical/poikilitic	low		13,16
ALHA81101	79	8.1/78				mosaicized	high		16,17
Dar al Gani 084	79	5.0/81				mosaicized	high		4
*Dyalpur	84	11/76			0.41	mosaicized	high		5
FRO90036	80		3.0/81			mosaicized	high	13	1,22
Goalpara	79	4.4/76			0.33	mosaicized	high		5
LEW 86216	81		1.7/88		0.02	mosaicized	high		20
Y-74154	84	8.1/79				mosaicized	high	6	3
Dingo Pup Donga	84	5.0/81			~0.5	euhedral	medium		5
ALH 82106	95	4.9/90		37/60	0.35	bi-modal		7	13,18, AMN 9-3
EET 87511	85		4.5/82	36/55		bi-modal	low	8	20, AMN 11-2
Hammadah al Hamra 064	78		4.6/77	32/55	0.65	bi-modal	medium		4,37
META78008	77	16/66	4.5/76	32/55	0.05,0.37	bi-modal	medium		29
Y-74130	78	14/68	4.2/78	32/55	~0.5,~1	bi-modal			29,33
EET 83309	80-84	variable			0.27	polymict		9	19
EET 87720	79-87	8.0/83		35/52		polymict			21, AMN 12-3, AMN 13-1
Nilpena	80	9.0/75				polymict		10	10
North Haig	76-92	variable			0.26	polymict		11	5
Hajma	85	9.0/78				typical?	medium-high		6
LEW 87165	85	?Fs 13				?			AMN 12-1, AMN 13-1
LEW 88774	75		4.2/75	33/53	0.83-0.87	bi-modal?	medium?	12	27,28

*ureilite falls; **py = modal pyroxene/(pyroxene+olivine).

Notes: (1) paired with FRO93008; (2) pyroxene is clinobronzite; (3) paired with LEW 88201, LEW 882821 and LEW 88012; (4) paired with Nova 001; (5) paired with QUE 93341; (6) other highly variable pyroxene compositions are reported - these may be interstitial or shock melts; (7) paired with ALH 82130 and ALH 84136; (8) paired with EET 87523 and EET 87717; (9) compositions given are for monomict ureilitic clasts; (10) compositions given are for monomict ureilitic clasts; possibly paired with North Haig; (11) possibly paired with Nilpena; (12) contains ~6% chromite; (13) paired with FRO90168.

References: (1) Baba et al (1993); (2) Bland et al (1992); (3) Yanai and Kojima (1995b); (4) Weber and Bischoff (1996); (5) Berkley et al (1980); (6) Hutchison (1977); (7) Wlotzka (1994); (8) Malhotra (1962); (9) Bhandari et al (1981); (10) Jaques amd Fitzgerald (1982); (11) Treiman and Berkley (1994); (12) Goodrich et al (1987a); (13) Goodrich et al (1987b); (14) Goodrich and Berkley (1986); (15) Berkley and Jones (1982); (16) Berkley (1986); (17) Saito and Takeda (1990); (18) Berkley et al (1985); (19) Prinz et al. (1987); (20) Berkley (1990); (21) Warren and Kallemeyn (1991); (22) Folco (1992); (23) Fioretti and Molin (1996); (24) Takeda et al (1992); (25) Takeda (1989); (26) Takeda et al (1988b); (27) Warren and Kallemeyn (1994); (28) Prinz et al (1994); (29) Takeda et al (1989); (30) Takeda et al (1979a); (31) Takeda et al (1979b); (32) Takeda (1987); (33) Goodrich (1986b); (34) Takeda and Yanai (1978); (35) Sexton et al (1996); (36) Chikami et al. (1997b); (37) Weber and Bischoff (1998); Goodrich (1998)

with common (100) (Takeda et al. 1992). In Y-74130 and META78008, low-Ca pyroxene with $Wo_{\sim 4.5}$ appears to be a complex mixture of clino- and ortho-pyroxene sequences in x-ray diffraction (Takeda 1987, Takeda et al. 1989). It is possible that in all ureilites low-Ca pyroxene with $Wo_{<5}$ was originally protoenstatite.

The typical ureilite texture is characterized by large, anhedral olivine and pyroxene grains averaging ~1 mm in size, which meet in triple junctions and have curved intergranular boundaries (Fig. 30a). Olivine grains may contain small, rounded inclusions of pyroxene; pigeonite or orthopyroxene may contain similar inclusions of olivine and/or augite. This poikilitic texture is especially common in PCA 82506, RKPA80239, and LEW 85440. In some ureilites the olivine and pyroxene grains show a pronounced elongation, with aspect ratios up to ~6:1 (Fig. 30a). Fabric analysis (Berkley et al. 1976, 1980; Goodrich et al. 1987a) shows that this elongation reflects both a foliation defined by the {100} crystal face of olivine, and a lineation defined by the crystallographic [001] **c**-axis of olivine. Several ureilites display a mosaicized texture with much smaller grain size, which is probably a result of shock deformation and/or recrystallization. These ureilites appear to have originally had the typical ureilite texture, as evidenced by dark matrix material outlining relict grain boundaries of large, elongate grains, and a common preferred orientation of grains within relict domains (Neuvonen et al. 1972). Dingo Pup Donga has a unique texture of euhedral, non-interlocking grains, and size-sorted layers (Berkley et al. 1980).

Four ureilites have an unusual bimodal texture (Fig. 30b). They are characterized by extremely large crystals of low-Ca pyroxene up to at least 15 mm in size which poikilitically enclose domains that have the typical ureilite texture. In ALH 82130 these are pigeonite, while in META78008, Y-74130, and EET 87511 they are orthopyroxene. In ALH 82130 and EET 87511 the typical-textured domains are devoid of pyroxene; in Y-74130 and META78008 they consist of olivine + augite, the latter of which contains small, rounded, poikilitic inclusions of pigeonite. These ureilites are sufficiently heterogeneous and coarse-grained that some thin sections show only the large pyroxene crystals and some show only the typical-textured domains.

Pyroxene in most ureilites is characterized by a lack of exsolution features. However, in ALH 82130, augite occurs as irregular lamellae and blebs in large poikilitic pigeonite crystals. This texture may be the result of unmixing of an original pigeonite at the pigeonite eutectoid reaction line at ~1246°C (Takeda et al. 1986, Mori et al. 1986), although if this is the case the pigeonite should be orthopyroxene. X-ray diffraction of the ALH 82130 pigeonite shows a weak orthopyroxene-like stacking sequence, which may be a remnant of orthopyroxene that later reinverted to pigeonite (Takeda et al. 1989). In LEW 88774, large pyroxene crystals have exsolved to roughly equal proportions of orthopyroxene and augite, in coarse lamellae ~50 μm wide (Warren and Kallemeyn 1994, Chikami et al. 1997a). This meteorite may have a bimodal texture, but this is not yet clear.

Olivine and pyroxene core compositions within each ureilite are very homogeneous in terms of mg#. Forsterite contents range from ~74 to 95 (Table 23, Fig. 31). There are no significant gaps in this range, but there is a spike at $\sim Fo_{79}$. Coexisting pyroxenes span a similar range (Table 23, Fig. 32), and indicate olivine-pyroxene equilibrium. There is no correlation between mg# and modal pyroxene/(pyroxene+olivine), nor between mg# and pyroxene type (Fig. 32).

Ureilite olivines are characterized by high CaO (~0.30-0.45 wt %) and Cr_2O_3 (~0.56 to 0.85 %), and pigeonite also has high Cr_2O_3 (up to ~1.26 %). Representative analyses of olivine and pyroxene cores are given in Tables 24 and 25. Examination of olivine and

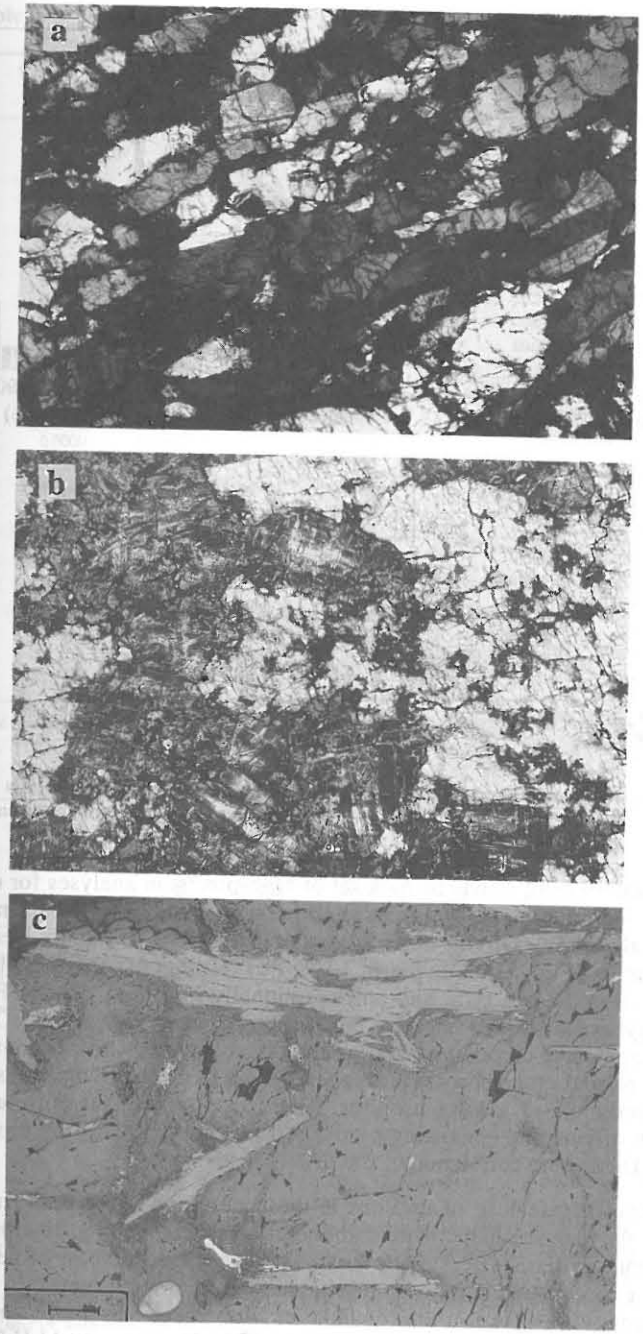

Figure 30. Photomicrographs of ureilites. (a) Kenna, showing typical ureilite texture and fabric. Field of view is 7 mm in width. (b) ALH 82130, illustrating bimodal texture of large low-Ca pyroxene crystal poikilitically enclosing areas that have the typical ureilite texture. Field of view is 5.8 mm in width. (c) Large euhedral graphite crystals in ALHA78019. Field of view is 1.5 mm in width.

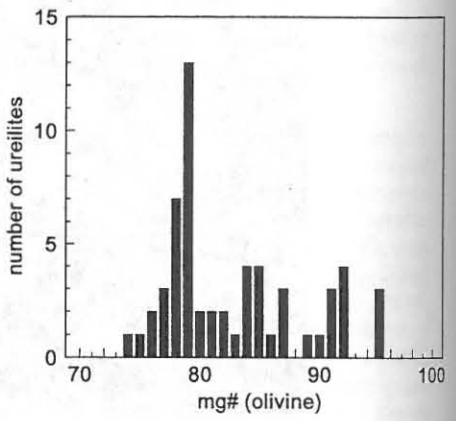

Figure 31. Histogram of mg# of olivine cores for monomict ureilites. Data from Table 23.

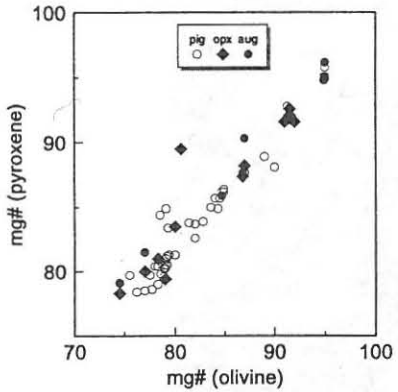

Figure 32. Correlation between mg# of olivine and pyroxene cores (pigeonite, orthopyroxene and augite) in monomict ureilites. Data from Table 23.

pyroxene minor element trends using a set of high-precision analyses for eight ureilites shows a very high degree of intragrain and intergrain homogeneity within each ureilite (Goodrich et al. 1987b). Olivine cores among ureilites have essentially identical Mg/Mn and Mg/Cr ratios (Fig. 33). Olivine in LEW 88774 plots off the Mg/Mn and Mg/Cr trends, with a low Fe/Mn ratio and an exceptionally high Fe/Cr ratio (Fig. 33). Both olivine and pyroxene show a negative correlation between FeO and MnO (Fig. 34), in contrast to the positive correlation with essentially constant FeO/MnO commonly shown by groups of related igneous rocks. Ratios of CaO/Al_2O_3 for olivine cores are high and vary by a factor of ~3 among ureilites. There is a significant correlation between CaO/Al_2O_3 in olivine and coexisting pyroxene cores, again indicating olivine-pyroxene equilibrium. There is no correlation of CaO/Al_2O_3 with mg#.

A characteristic feature of ureilites is the occurrence of reduced rims on olivine grains where they are in contact with carbonaceous matrix material or crosscut by veins of carbonaceous material (Berkley et al. 1980). These rims consist of nearly FeO-free olivine and/or enstatite, riddled with tiny inclusions of low-Ni metal. In most ureilites they are narrow (10-100 μm), and boundaries with cores are sharp; zonation can be detected only over ~30-40 μm (Miyamoto et al. 1985). However, in ALH 82130 and HH 126 the rims are considerably widened, to the point that the olivine grains have been almost completely reduced and only rare metal-free cores preserve the original composition (Berkley et al. 1985, Sexton et al. 1996). Pyroxene grains also sometimes

Table 24. Compositions of olivine grain cores from representative ureilites.

	Y-74659 (1)	ALHA77257 (1)	ALHA77257 (2)	Y-790981 (1)	Y-790981 (2)	Y-74130 (1)	ALHA78019 (1)	ALHA78019 (2)
Chemical Composition (wt %)								
SiO_2	40.3	39.3		38.2		37.6	37.5	
Al_2O_3	0.03	0.03	0.040	0.03	0.042	0.04	0.02	0.031
FeO	8.0	12.1	14.2	19.8	21.2	21.0	21.1	22.5
MgO	49.7	46.1	45.2	40.0	40.9	39.7	39.1	40.5
MnO	0.46	0.46	0.452	0.42	0.425	0.42	0.42	0.421
Cr_2O_3	0.58	0.72	0.743	0.55	0.606	0.39	0.72	0.698
CaO	0.30	0.34	0.340	0.28	0.326	0.24	0.41	0.453
Total	99.40	99.08		99.28		99.39	99.27	
Cation Formula Based on 4 Oxygens								
Si	0.9903	0.9883		0.9930		0.9830	0.9832	
Al	0.0009	0.0009		0.0009		0.0012	0.0006	
Fe	0.1650	0.2551		0.4304		0.4591	0.4627	
Mg	1.8201	1.7278		1.5496		1.5468	1.5278	
Mn	0.0096	0.0098		0.0092		0.0093	0.0093	
Cr	0.0113	0.0143		0.0113		0.0081	0.0149	
Ca	0.0079	0.0092		0.0078		0.0067	0.0115	
Total Cations	3.0051	3.0054		3.0022		3.0142	3.0100	
*Cation Ratios Fe/Mn and 100*Mg/(Mg+Fe) (mg#)*								
Fe/Mn	17	26	31	47	49	49	50	53
mg#	91.7	87.1	85.0	78.3	77.5	77.1	76.8	76.2

(1) Complete analyses by Takeda (1987); (2) Partial analyses by Goodrich et al. (1987b) are shown for comparison. These are high precision analyses for the minor elements.

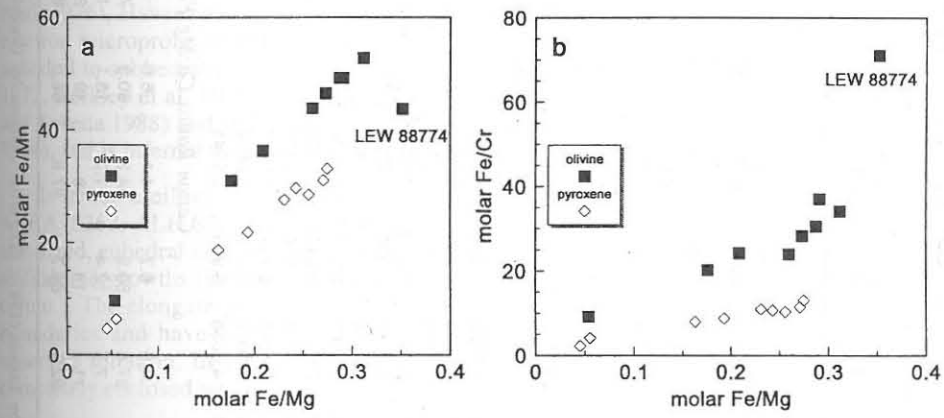

Figure 33. Correlations between (a) molar Fe/Mn and Fe/Mg ratios and (b) molar Fe/Cr and Fe/Mg ratios in olivine and pyroxene cores in 8 ureilites, indicating constant Mn/Mg and Cr/Mg ratios. Data from Goodrich et al. (1987b). The Fe/Mn-Fe/Mg trend has also been observed among other ureilites, based upon a less precise set of data (Mittlefehldt 1986). Olivine in LEW 88774 is off the trends shown by other ureilites. LEW 88774 data from M. Prinz (pers. comm.).

have reduced rims, consisting of enstatite with inclusions of low-Ni metal, but they are usually much narrower than the olivine reduction rims. In LEW 88774, chromite grains are also reduced along contacts with carbon, forming complex zones consisting mainly of

Table 25. Compositions of pyroxene grain cores from representative ureilites.

	Y-74659 (1)	Y-74659 (1)	ALHA77257 (1)	ALHA77257 (1)	ALHA77257 (2)	Y-790981 (1)	Y-790981 (1)	Y-790981 (2)	Y-74130 (1)	Y-74130 (1)	Y-74130 (1)	ALHA78019 (1)	ALHA78019 (2)
Chemical Composition (wt %)													
SiO_2	56.6	56.6	56.0	56.3		54.8	53.4		54.7	53.5	53.3	54.2	
Al_2O_3	0.48	0.51	0.61	0.66	0.65	1.13	0.54	1.39	1.92	1.96	2.82	0.53	0.54
TiO_2	0.10	0.11	0.06	0.09	0.081	0.06	0.30	0.093	0.13	0.14	0.25	0.05	0.042
Cr_2O_3	0.88	0.85	1.12	1.10	1.16	1.14	1.39	1.26	1.30	1.37	1.85	1.06	1.07
FeO	5.4	5.17	8.2	7.8	8.8	11.3	3.4	12.3	11.8	10.9	7.6	12.2	13.2
MnO	0.50	0.46	0.44	0.42	0.464	0.46	0.36	0.425	0.40	0.47	0.35	0.41	0.393
MgO	31.8	33.3	30.0	31.3	30.3	27.0	20.7	27.0	27.2	23.1	17.8	26.1	26.9
CaO	3.78	2.4	3.47	2.14	3.45	4.1	18.51	4.58	2.19	6.73	14.77	4.87	5.13
Na_2O	0.05	0.03	0.03	0.02	0.041	0.05	0.23	0.117	0.16	0.07	0.82	0.03	0.029
Total	99.54	99.41	99.90	99.78		100.11	98.79		99.79	98.25	99.55	99.48	
Cation Formula Based on 6 Oxygens													
Si	1.9787	1.9722	1.9746	1.9754		1.9615	1.9551		1.9563	1.9630	1.9505	1.9663	
^{IV}Al	0.0198	0.0209	0.0254	0.0246		0.0385	0.0233		0.0437	0.0370	0.0495	0.0227	
Total tet*	1.9985	1.9931	2.0000	2.0000		2.0000	1.9784		2.0000	2.0000	2.0000	1.9890	
Ti	0.0026	0.0029	0.0016	0.0024		0.0016	0.0083		0.0035	0.0039	0.0069	0.0014	
^{VI}Al	0.0000	0.0000	0.0000	0.0027		0.0092	0.0000		0.0372	0.0478	0.0721	0.0000	
Cr	0.0243	0.0234	0.0312	0.0305		0.0323	0.0402		0.0368	0.0397	0.0535	0.0304	
Fe	0.1564	0.1507	0.2409	0.2274		0.3395	0.1029		0.3526	0.3348	0.2320	0.3711	
Mn	0.0148	0.0136	0.0131	0.0125		0.0139	0.0112		0.0121	0.0146	0.0108	0.0126	
Mg	1.6568	1.7292	1.5765	1.6367		1.4403	1.1295		1.4497	1.2631	0.9713	1.4111	
Ca	0.1416	0.0889	0.1311	0.0805		0.1584	0.7262		0.0839	0.2646	0.5792	0.1893	
Na	0.0034	0.0020	0.0021	0.0014		0.0035	0.0163		0.0111	0.0050	0.0582	0.0021	
Total Cations	3.9984	4.0038	3.9965	3.9941		3.9987	4.0130		3.9869	3.9735	3.9840	4.0070	
*Cation Ratios Ca:Mg:Fe, Fe/Mn and 100*Mg/(Mg+Fe) (mg#)*													
Ca	7.2	4.5	6.7	4.1	6.6	8.2	37.1	8.9	4.4	14.2	32.5	9.6	9.7
Mg	84.8	87.8	80.9	84.2	80.3	74.3	57.7	72.6	76.9	67.8	54.5	71.6	70.8
Fe	8.0	7.7	12.4	11.7	13.1	17.5	5.3	18.6	18.7	18.0	13.0	18.8	19.5
Fe/Mn	11	11	18	18	19	24	9	29	29	23	21	29	33
mg#	91.4	92.0	86.7	87.8	86.0	80.9	91.7	79.6	80.4	79.0	80.7	79.2	78.4

(1) Complete analyses by Takeda (1987); (2) Partial analyses by Goodrich et al. (1987b) are shown for comparison. These are high precision analyses for the minor elements.

Figure 34. Negative correlation between MnO and FeO in olivine cores among ureilites. Data are from Goodrich et al. (1987b) (dots) and Takeda (1987) (circles). The data of Berkley and Jones (1982) (small squares) seem systematically high compared to other data for individual ureilites. The data of Berkley et al. (1980) are not shown because of problems with Mn standardization (Berkley, pers. comm.).

Cr-Fe-carbide, eskolaite (Cr_2O_3), and several other phases (Prinz et al. 1994, Warren and Kallemeyn 1994). Olivine rims show a negative correlation between FeO and MnO (Miyamoto et al. 1993), consistent with reduction. Chromite in LEW 88774 has 54 to 59% Cr_2O_3, 8 to 21% MgO, 14 to 19% Al_2O_3, 1 to 22% FeO and 0.6 to 2.8% TiO_2 (Warren and Kallemeyn 1994, Chikami et al. 1997a), and ranges from $FeCr_2O_4$-rich to $MgCr_2O_4$-rich to $MgAl_2O_4$-rich with increasing reduction (Prinz et al. 1994).

Carbon phases. The carbon-rich matrix of ureilites occurs mostly along silicate grain boundaries, but also intrudes the silicates along fractures and cleavage planes. In some ureilites, what appear to be isolated pockets of matrix are included in silicate grains, but these may be parts of veins intruding from grain boundaries in the unseen dimension. In rare cases matrix material surrounds poikilitic inclusions of olivine in low-Ca pyroxene.

Graphite is the most common polymorph of carbon in ureilites. Vdovykin (1970) found traces of chaoite and organic carbon compounds in Haverö, Novo Urei, Dyaplur and Goalpara. Diamond and lonsdaleite have been identified in Kenna (Gibson 1976, Berkley et al. 1976), Haverö and Goalpara (Marvin and Wood 1972) by electron diffraction and electron microprobe techniques. Diamond and lonsdaleite occur as small (<1 to 3 μm) anhedral to subhedral grains within a fine-grained matrix of graphite (Marvin and Wood 1972, Berkley et al. 1976). Diamond has also been identified in Dyalpur by TEM (Mori and Takeda 1988) and in Nilpena by x-ray diffraction of acid resistant residues (Ott et al. 1984), and is inferred to occur in other ureilites based upon the difficulty of cutting them.

In most ureilites the graphite is very fine-grained. However, in ALHA78019, ALHA78262, ALH 83014 and Nova 001 (paired with Nullarbor 010), it occurs as large, mm-sized, euhedral crystals (Fig. 30c), intergrown with metal, sulfide, or splotchy metal-sulfide intergrowths (Berkley and Jones 1982, Treiman and Berkley 1994, M. Prinz, pers. comm.). The elongate graphite blades commonly parallel the direction of silicate grain boundaries and have a strong tendency to align with their long axes parallel to the observed foliation. In places they intrude into silicate grains and, rarely, appear to be completely enclosed within silicate grains.

Carbon also occurs in the form of cohenite (Fe_3C) in metallic spherule inclusions in olivine and pigeonite in at least five ureilites (Goodrich and Berkley 1986). These spherules also contain C-bearing Fe-Ni metal, sulfide (predominantly troilite), and rare phosphorus-bearing minerals, and have textures typical of eutectic crystallization in the Fe-C system. Bulk compositions of the spherules range between 4 and 5 wt % C and 3 and 7 wt % Ni.

Metal, sulfides and phosphides. The composition of interstitial metal in ureilites is quite variable, both within individual specimens and among different ureilites. Nickel

contents range from 1 to 9%, Si contents range from undetectable to ~3%, and Cr contents range up to ~1.5%. High P contents (1%) have been reported in metal in FRO 90054 (Fioretti et al. 1996). Carbon contents of the metal are unknown, but must be very low. Schreibersite (Fe_3P) has been reported in FRO 90054 and several other ureilites. Sulfides are not abundant, and are also quite variable in composition. High Cr varieties with up to ~34% are common in the interstitial material of Kenna, and low-Cr (0.5 to 2.8%) varieties occur as μm-sized grains within the silicate grains (Berkley et al. 1976). Brezinaite (Cr_3S_4) occurs in LEW 88774 (Prinz et al. 1994).

Interstitial silicates. Fine-grained interstitial silicates are common in ureilites (Goodrich 1986a, Ogata et al. 1987, 1988, 1991; Saito and Takeda 1989, Tomeoka and Takeda 1989, Takeda et al. 1988b, Mori and Takeda 1983, Prinz et al. 1994). Interpretations of these materials vary and unfortunately so does the nomenclature used in their description. They occur along grain boundaries in narrow zones, generally 10 to 20 μm wide, but up to 70 μm in Y-74123, and as veins intruding into olivine and pyroxene from the grain boundaries. They are often difficult to distinguish optically because they resemble the reduced margins of olivine and pyroxene core crystals and may be masked by interstitial metal and carbon. An exception is in Roosevelt County (RC) 027, in which they are up to 200 μm wide and optically prominent (Goodrich et al. 1987a). In Y-790981 and LEW 85328 these materials occur as pockets within pigeonite (Saito and Takeda 1989, Ogata et al. 1987), making the pigeonite cloudy.

The interstitial silicates consist of euhedral to subhedral crystals of low-Ca pyroxene and augite, surrounded by Si-Al-alkali glass. Low-Ca pyroxene ranges from Wo_{1-14} and augite ranges from Wo_{26-43}. These pyroxenes have much higher mg# than core pyroxene (up to mg# 99) and lower Mn/Mg, Cr/Mg, Na/Mg, Ti/Mg and Al/Mg ratios (Goodrich et al. 1987b). Augite contains up to 13% Al_2O_3 and 0.3% Na_2O. Aluminian-titanian-diopside with 5.05% TiO_2 occurs in an Al-rich vein in Y-74130 (Tomeoka and Takeda 1989). In LEW 88774 the interstitial pyroxenes are Cr-rich, and intergrown with μm-sized chromite and corundum (Prinz et al. 1994). The glass in ureilites contains up to 21% Al_2O_3, 4.5% Na_2O and 4.5% K_2O (Goodrich 1986a). Tiny grains of SiO_2 are also observed in the glass. All phases are highly variable in composition.

Polymict ureilites. Four ureilites are polymict; North Haig, Nilpena, EET 83309 and EET 87720. They are fragmental breccias containing lithic clasts of typical monomict ureilite material plus a variety of other lithic clasts, set in a matrix of smaller mineral fragments, carbon, suessite (Fe_3Si), sulfides, minor chromite and minor apatite (Jaques and Fitzgerald 1982, Prinz et al. 1983a, 1986b, 1987, 1988a; Keil et al. 1982, Warren and Kallemeyn 1989b, 1991). Olivine grains in the ureilite clasts range from ~Fo_{76-84}. Other lithic clasts include a porphyritic enstatite clast resembling material from enstatite chondrites or aubrites, clasts resembling chondritic material, feldspathic melt rocks, and clasts of a distinct Ca-Al-Ti-rich assemblage that resembles angrites. The angrite-like clasts contain anorthitic plagioclase (An_{96-98}), aluminian-titanian-diopside with up to 8% Al_2O_3 and 2% TiO_2, and olivine (Fo_{49-70}) containing up to 1.7% CaO (Prinz et al. 1986b 1987). The feldspathic melt clasts contain feldspathic glass with fine crystallites of olivine and sometimes low-Ca pyroxene or phosphate. Some contain larger angular crystals of olivine, pyroxene, or phosphate. The composition of the glass ranges from ~An_{5-50}. Bulk compositions of the clasts are high in SiO_2 (up to ~61%), Al_2O_3 (up to ~21%), and alkalis (up to ~7% Na_2O, 0.8% K_2O). Nilpena contains clasts of carbonaceous chondrite matrix-like material. This material has close affinities to CI-matrix, containing saponitic smectite clays, serpentine, magnetite, pentlandite, pyrrhotite and ferrihydrite, and differs from CM-matrix (Brearley and Prinz 1992).

The mineral fragments in polymict ureilites are mostly olivine and pyroxene having compositions consistent with derivation from monomict ureilites. However, in EET 83309 olivine compositions span a greater range (Fo_{62-98}) than in monomict ureilites. Some olivine fragments have significantly lower Cr_2O_3 and CaO contents than olivine in monomict ureilites. Plagioclase, which does not occur in monomict ureilites, is common among the mineral fragments in polymict ureilites, and spans the entire range of An_{0-100}. Plagioclase in the range An_{30-80} contains no detectable K_2O (Prinz et al. 1987). Modally, polymict ureilites are quite similar to monomict ureilites, with the significant addition of 1-2% plagioclase. They have modal pyroxene/(pyroxene+olivine) ratios of ~0.25.

Shock state. Monomict ureilites are classified in Table 23 as being of very low, low, medium, or high shock level. Very-low shock ureilites contain large, euhedral graphite crystals. In low-shock ureilites the silicates show only minor fracturing, undulatory extinction and kink bands, primarily in olivine. Diamonds are believed to be absent and graphite can sometimes be distinguished as small, euhedral crystals. These features indicate shock pressures <20 GPa (Carter et al. 1968). Medium shock ureilites show a greater extent of fracturing, undulatory extinction, and kink banding. Sub-grain boundaries may be prominent in olivine, and pyroxene may be cloudy due to glassy inclusions. Diamonds and/or lonsdaleite are present. In high shock ureilites the olivine is completely shattered or mosaicized (Lipschutz 1964) and pyroxene is mottled by melt glass. Diamonds and/or lonsdaleite are present. Shock pressures of at least 100 GPa are indicated by these features (Carter et al. 1968). Some of the criteria used in this classification scheme are open to question, however.

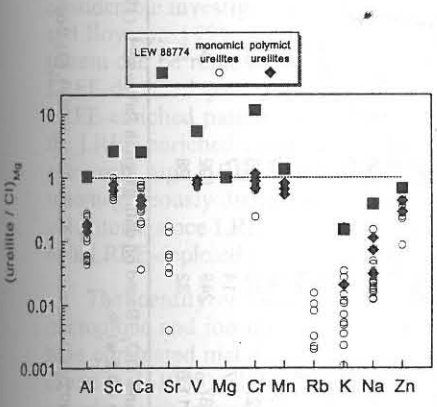

Figure 35. CI- and Mg-normalized lithophile element abundances in bulk monomict and polymict ureilites, and the unusual ureilite LEW 88774. Data plotted are averages of analyses from Bhandari et al. (1981), Binz et al. (1975), Boynton et al. (1976), Goodrich and Lugmair (1991, 1992, 1995), Goodrich et al. (1991, 1987a), Higuchi et al. (1976), Janssens et al. (1987), Jarosewich (1990), Jaques and Fitzgerald (1982), Kallemeyn and Warren (1994), Spitz and Boynton (1991), Takeda (1987), Wänke et al. (1972a), Warren, Kallemeyn (1989, 1992), Wasson et al. (1976), Wiik (1972), Yanai and Kojima (1995b). A few suspect values have not been plotted; Na and K values from Yanai and Kojima (1995b) and K from Wiik (1972). Data are plotted in order of increasing nebular volatility as estimated from calculated condensation temperatures compiled by Wasson (1985).

Chemistry

Lithophile elements. Lithophile element abundances in ureilites (Fig. 35, Table 26) reflect their ultramafic mineralogy. They are enriched in Sc, V, Mg, Cr and Mn, generally up to ~2.7 × CI. Chromite-rich LEW 88774 is unusually enriched in Sc, V and Cr (Table 26, Fig. 35). Calcium abundances are near-chondritic, varying mainly with pyroxene abundance and type. One analysis of Haverö (Wiik 1972) shows extremely low Ca (0.09 × CI) consistent with the upper limit reported by Wänke et al. (1972a), and LEW 88774 has exceptionally high Ca (3.7 × CI). Zinc is near-chondritic or slightly depleted. The plagiophile and incompatible elements Al, Sr, K, Na and Rb are moderately to strongly depleted (Fig. 35). Again, LEW 88774 is unusual, with high Al, K and Na (Table 26, Fig. 35). The polymict ureilite EET 83309 has higher abundances of Al, K and Na, and other polymict ureilites (EET 87720 and Nilpena) have abundances of these elements near the

Table 26. Select major*, minor and trace element contents of representative ureilites.

		ALH84136 *bi-modal* (1)	ALHA77257 *typical* (1)	ALHA81101 *mosaicized* (1)	EET 83309 *polymict* (2)	EET 87720 *polymict* (1)	Goalpara *mosaicized* (3)	Haverö** *typical* (4)	Kenna *typical* (3)	LEW 88774 *typical* (5)	Novo Urei *typical* (3)	PCA82506 *typical/poikilitic* (1)
Al_2O_3	wt %	0.23	0.25	0.16	0.70	0.57	0.21	0.21	0.23	2.46	0.35	0.11
Cr_2O_3	wt %	0.595	0.702	0.716	0.709	0.858	0.840	0.598	0.74	6.28	0.800	0.653
FeO	wt %	7.3	11.5	19.2	17.2	21.7	22.4	19.3	20.5	18.9	19.8	17.0
MnO	wt %	0.429	0.400	0.373	0.372	0.381	0.372	0.343	0.367	0.495	0.386	0.377
MgO	wt %	41.1	37.1	35.7	34.8	28.0	36.1	37.2	33.1	23.5	34.5	35
CaO	wt %	2.1	1.0	0.97	1.1	0.91	0.58	<0.14	1.3	4.67	1.1	0.52
Na_2O	wt %	0.0485	0.0247	0.0235	0.195	0.0485	0.018	0.033	0.033	0.364	0.047	0.0266
K	µg/g			8	238		42	35	1.3	121	17	
Sc	µg/g	10.7	7.7	7.2	7.8	8.9	6.3	4.9	8.5	21.5	8.1	5.8
V	µg/g	111	99	99	94	91	92		100	430	85	82
Co	µg/g	115	89	71	135	148	78	101	164	146	134	91
Ni	mg/g	1.55	0.89	0.82	1.67	2.23	0.85	0.92	1.18	1.69	1.30	0.82
Zn	µg/g	260	243	159	284	170		235		301		231
Ga	µg/g	2.6	1.84	1.44	3.0	2.8		1.13		28.7		1.8
As	ng/g	290	190	112	390	290				430		180
Se	µg/g	1.04		1.26	2.1	3				1.48		<0.9
La	ng/g	15	11	13	185	35	150	70	8.3	168	100	8.2
Sm	ng/g	25	2.8	2.6	62	12	6	14	1.6	146	12	<2
Eu	ng/g	4.5	<5	<6	30	<12	0.7	4.1	0.315	40	2.3	<2
Yb	ng/g	99	<40	27	76	25	24	25	39.5	380	45	27
Lu	ng/g	16	8.0	4.7	14	7		8.5	7.4	62		5.6
Ir	ng/g	149	184	37	249	102	80	240	560	480	440	198
Au	ng/g	32	20.0	11.6	32	28	19	24	40	34	70	17.5

* There are few modern analyses for SiO_2 and TiO_2. Based on data given in Jarosewich (1990), Takeda (1987) and Vdovykin (1970), SiO_2 contents are generally between 35-43 wt % and TiO_2 contents are <0.1 wt %.

** ureilite falls

References: (1) Warren and Kallemeyn (1992); (2) Warren and Kallemeyn (1989); (3) Boynton et al. (1976); (4) Wänke et al. (1972); (5) Kallemeyn and Warren (1994).

upper end of the ureilite ranges (Fig. 35). Y-74130 and Y-790981 have high Al and Na, probably due to a high augite content and a high content of Al-alkali-rich interstitial material, respectively.

The Ca/Al ratios of ureilites are superchondritic, ranging from ~2 to 14 × CI, with the exception of Y-74123, and the analysis of Haverö with low-Ca from Wiik (1972). Bulk ureilite compositions show a negative FeO-MnO correlation, similar to olivine and pyroxene (Fig. 33). The Mn/Mg ratios are nearly constant at 0.61±0.07 × CI, while Cr/Mg ratios are more variable: 0.79±0.17. (We suspect the unusually high Mn data of Spitz and Boynton (1991) are erroneous, and have not included them in this discussion.) Again, LEW 88774 is unusual, with Mn/Mg 1.3 × CI and Cr/Mg 11 × CI.

Rare earth elements. Rare earth element patterns have been determined for 28 ureilites. In general, REE abundances are low compared to other achondrites. This REE depletion is consistent with major incompatible element depletion. There is no correlation between degree of REE depletion and mg#. The classic CI-normalized REE pattern of ureilites is V-shaped at subchondritic values, with severe middle REE depletion (Fig. 36a). Europium ranges to as low as 0.005 × CI. Many ureilites, however, have LREE-depleted patterns, with La ranging from ~0.005-0.1 × CI, and negative Eu anomalies (Fig. 36b). LEW 88774 and FRO 90054 stand out with only slightly LREE-depleted patterns at near-chondritic values (Fig. 36b). For some ureilites, e.g. RC027 and Y-791538, one subsample may have a V-shaped REE pattern while another has a LREE-depleted pattern (compare Figs. 36a and 36b).

The nature and origin of the V-shaped REE patterns in ureilites has been a subject of considerable investigation and controversy. It has been shown (Boynton et al. 1976, Spitz and Boynton 1991, Goodrich and Lugmair 1995) that the LREE-enriched part of the pattern can be removed by leaching with weak acids, leaving a residue with a severely LREE-depleted pattern with a negative Eu anomaly, and yielding a leachate with a LREE-enriched pattern and positive Eu anomalies (Fig. 36d). It has been assumed that the LREE-enriched component is contained in an acid-soluble minor phase, which has extremely high LREE abundances. The LREE-enriched component also appears to be inhomogeneously distributed (Goodrich et al. 1987a, Goodrich et al. 1991), and it may be ubiquitous, since LREE-enriched leachates can be obtained even from samples that have bulk LREE-depleted patterns (Goodrich and Lugmair 1992).

The identity or host of the LREE-enriched component remains unknown. Electron microprobe and ion microprobe searches for LREE-enriched phases in interstitial areas have eliminated metal, sulfide, graphite, interstitial pyroxene and glass as LREE carriers (Spitz et al. 1988). However, ion microprobe analyses do show general LREE-enrichment in carbon-rich interstitial areas (Spitz et al. 1988, Guan and Crozaz 1995a). Some part of the LREE-enriched component is associated with olivine and is either on grain surfaces or internally equilibrated (Goodrich and Lugmair 1995). Guan and Crozaz (1995a) also observed LREE-enrichment in reduced rims on olivine grains in Novo Urei. The abundance of LREE-enriched component has been correlated only with the abundance of Sr and Ba (Goodrich and Lugmair 1995).

Polymict ureilites have higher REE concentration than most monomict ureilites and generally have distinct patterns (Fig. 36c). Ion microprobe analyses have shown that olivine and pyroxene fragments in EET 83309 have REE patterns typical of those in monomict ureilites (Guan and Crozaz 1995b). Feldspathic melt clasts in polymict ureilites have a variety of REE patterns unlike those of ureilites (Guan and Crozaz 1995b 1997). Aluminian-titanian-diopside in an angrite-like clast in North Haig has a REE pattern similar to that of aluminian-titanian-diopside in Angra dos Reis (Davis et al. 1988).

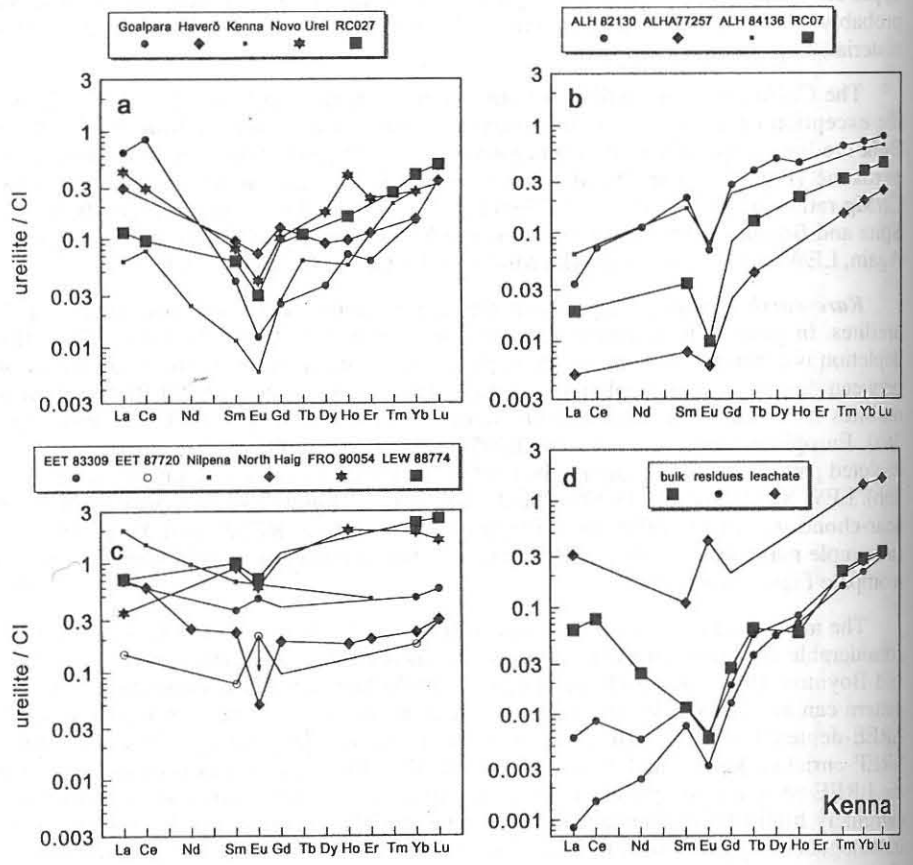

Figure 36. CI-normalized REE patterns for representative ureilites. (a) Many ureilites have V-shaped REE patterns. (b) Other ureilites have LREE-depleted patterns with negative Eu anomalies. Note that some ureilites (e.g. RC027) show V-shaped patterns in some subsamples and LREE-depleted patterns in other subsamples. (c) Polymict ureilites EET 83309, EET 87720, North Haig and Nilpena, unusual ureilite LEW 88774 and FRO 90054. Note that Eu in EET 87720 is an upper limit (arrow) and the positive Eu anomaly may not be real. (d) Leaching experiments, for example on Kenna, show that the LREE-enriched part of the V-shaped bulk ureilite REE pattern can be removed with weak acids. Leachates are LREE-enriched with positive Eu anomalies, and residues are extremely LREE-depleted with negative Eu anomalies. Data are from Boynton et al. (1976), Ebihara et al. (1990), Goodrich et al. (1987a), Jaques and Fitzgerald (1982), Spitz (1991, and pers. comm.), Spitz and Boynton (1991), Wänke et al. (1972a), Warren and Kallemeyn (1989, 1992).

Siderophile trace elements. Siderophile trace element data for bulk ureilites are summarized in **Figure** 37. Generally, abundances of the refractory siderophiles Re, Os, W and Ir are similar within each ureilite, and range from ~0.1-2 × CI among ureilites. Abundances of the more volatile siderophiles are generally lower, with Ni = 0.006 to 0.2 × CI, and tend to increase in the order Ni < Au < Co < Ga < Ge within each ureilite. EET 87511 has exceptionally low abundances of Ni, Au and Co, and an exceptionally steep Ni to Ge trend. LEW 88774 has very high Ga (2.8 × CI), considerably out of the range of other ureilites. Carbonaceous (metal-rich) vein separates from Kenna and Haverö show patterns similar to bulk ureilites, but at higher abundances (Fig. 37). There is no apparent correlation between siderophile element abundances and mg# among ureilites. Ureilite

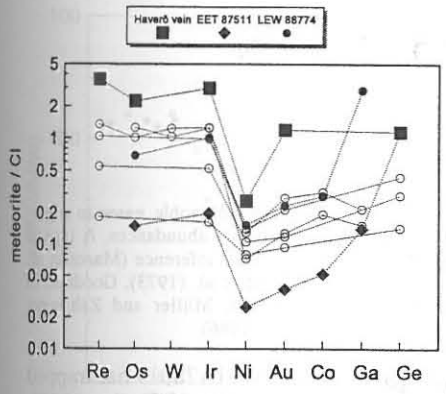

Figure 37. CI-normalized trace siderophile element abundances in representative ureilites (unlabeled). Bulk ureilites have higher abundances of the refractory elements Re, Os, W and Ir in approximately chondritic ratios, while abundances of the more volatile elements are lower and increase in the order Ni→Au→Co→Ga→Ge. Carbonaceous vein separates from Haverö show a similar pattern at higher abundances. LEW 88774 has exceptionally high Ga, while EET 87511 shows a highly fractionated pattern of volatile and moderately volatile siderophile elements. Data from Higuchi et al. (1976), Janssens et al. (1987), Kallemeyn and Warren (1994), Spitz and Boynton (1991), Warren and Kallemeyn (1992).

siderophile element abundances are considerably higher than those of ultramafic rocks from differentiated planets such as the Earth, Moon and Mars

There are good linear Re-Ir, Os-Ir, and to a lesser extent W-Ir correlations among bulk ureilites and carbonaceous vein separates, indicating that the refractory siderophiles are contained in a common component (e.g. see Goodrich 1992). The more volatile siderophiles also show linear correlations with Ir, suggesting that to a first approximation, ureilite siderophiles are a mixture of a refractory-rich and a refractory-poor component (Boynton et al. 1976, Higuchi et al. 1976, Janssens et al. 1987, Spitz and Boynton 1991). The refractory-rich component appears to be represented by the carbonaceous vein separates. Spitz (1992) observed two distinct Ga-Ir trends, suggesting distinct refractory-rich components for two groups of ureilites, but it seems likely this was spurious (Kallemeyn and Warren 1994). However, it has also been noted that ureilite siderophile element abundances are better correlated with solid metal/liquid metal partition coefficients than with volatility, suggesting that they are controlled by fractionation of metal in a magmatic system rather than mixing of two components (Goodrich et al. 1987a).

Carbon and nitrogen. Carbon contents measured for most ureilites range from ~2 to 6% (Bogard et al. 1973, Gibson 1976, Grady and Pillinger 1986, Grady et al. 1985a, Jarosewich 1990, McCall and Cleverly 1968, Wacker 1986, Wiik 1969, 1972). Measurements for individual ureilites are quite variable, as carbon is primarily contained in matrix material, which is inhomogeneously distributed. FRO 90054 has an unusually low carbon content of 0.24% (Grady and Pillinger 1993). There do not appear to be any correlations between carbon content and other geochemical or isotopic parameters. Nitrogen concentrations range from ~10 to 150 ppm (Grady et al. 1985a, Grady and Pillinger 1986, Murty 1994). The C/N ratios of ureilites are significantly lower than those in carbonaceous chondrites with similar C contents. Diamond is enriched in nitrogen; for example, diamond in Lahrauli contains 771 ppm N compared to 11.3 ppm for the whole rock (Murty 1994).

Noble gases. Ureilites contain trapped noble gases in chondritic abundances, with a fractionated or planetary type pattern as in CM chondrites (Fig. 38). Gas contents vary considerably, Xe contents vary by a factor of ~100 in bulk rocks, for example, but elemental and isotopic ratios are distinctive. Carbonaceous matrix material is enriched at least 600-fold in noble gases relative to the silicates, and the gases are largely contained in the carbon (Weber et al. 1971, 1976; Göbel et al. 1978). In diamond-bearing ureilites, diamond is the principal gas-carrier; graphite is virtually free of trapped gases (Weber et

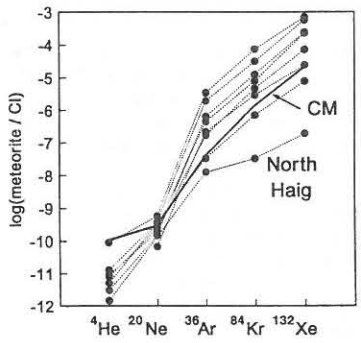

Figure 38. Elemental abundances of noble gases in representative ureilites relative to cosmic abundances. A typical CM (Haripura) pattern is shown for reference (Mazor et al. 1970). Ureilite data from Bogard et al. (1973), Goodrich et al. (1987b), Mazor et al. (1970), Müller and Zähringer (1969), Ott et al. (1993), Wacker (1986).

al. 1976, Göbel et al. 1978). However, the diamond-free ureilite ALHA78019 has trapped noble gas abundances comparable to those of diamond-bearing ureilites (Wacker 1986). In ALHA78019 the gases are contained in a fine-grained carbon whose structural state is unknown, while the coarse-grained graphite is gas-free. The fine-grained carbon has a near-chondritic Xe/C ratio.

Most of the ^{3}He in ureilites is cosmogenic in origin, while most of the ^{4}He appears to be trapped. The extremely low ^{4}He/^{3}He ratios are consistent with low U and Th contents. Ureilites have extremely low ^{40}Ar/^{36}Ar ratios, indicating very little radiogenic Ar and thus very early depletion of K. Neon in monomict ureilites appears to be a mixture of trapped and cosmogenic components. The composition of the trapped component has been estimated from Hajmah, which contains little cosmogenic Ne, and has been named Ne-U (Ott et al. 1985b). Solar wind implanted noble gases, notably Ne-B, are present in polymict ureilites (Ott et al. 1990, 1993), consistent with their being regolith breccias. Cosmic-ray exposure ages, based on ^{3}He and ^{21}Ne, range from 0.5 to 32 Ma for ten ureilites and show no apparent clustering (Bogard et al. 1973, Göbel et al. 1978, Goodrich et al. 1987a, Müller and Zähringer 1969, Ott et al. 1984, 1985b; Stauffer 1961, Weber et al. 1971).

Isotopic systematics

Oxygen-isotopes. On an oxygen-isotope plot, ureilites plot along the line with slope ~1 defined by C2-C3 matrix material and Allende CAIs (Fig. 1b), thought to be a nebular mixing line (Clayton et al. 1973, Clayton 1993). This pattern is unique among achondrites. Except for acapulcoites and lodranites, all other groups of achondrites and primitive achondrites plot along slope ~0.52 mass fractionation lines (e.g. see Fig. 1b,c). Ureilites show greater scatter about the CAI line than do the chondritic materials that define it, and it is possible to fit various slope ~0.52 lines to the data, possibly organizing some ureilites into groups related by mass-fractionation. Unique determination of such groups is difficult, and for those that have been postulated (Clayton and Mayeda 1988) there do not appear to be common petrographic features or chemical trends consistent with a fractionation relation.

There are no correlations between oxygen-isotopic composition and any petrographic or chemical parameters of ureilites except mg#. Ureilites show a good correlation (Fig. 39) between mg# (Fo in olivine) and Δ^{17}O. Such a correlation is shown by some chondritic materials (e.g. Rubin et al. 1990), but amongst achondrite groups is otherwise shown only by lodranites (Fig. 39; see also Fig. 28).

Sm-Nd. Ureilites fall into 3 Sm-Nd groups: (1) A Kenna group including whole rock samples and a pyroxene separate from Kenna, a whole rock sample of Novo Urei, and a

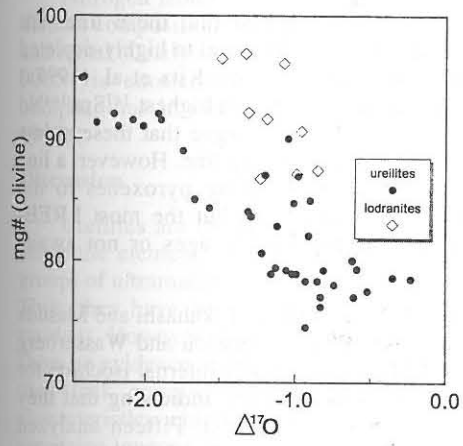

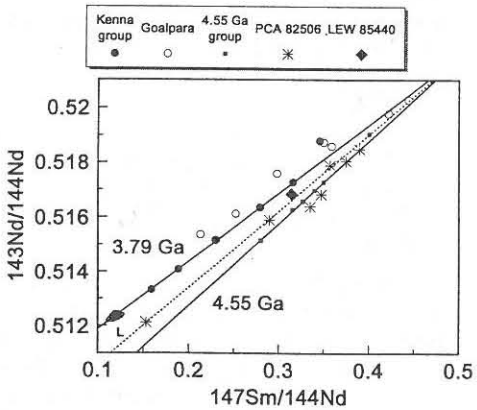

Figure 39 (left). Correlation between mg# of olivine and Δ^{17}O in ureilites. Data from Clayton and Mayeda (1996) and Table 23. Lodranites may show a similar correlation (see also Fig. 28). Data from McCoy et al. (1997a).

Figure 40 (right). Sm-Nd isotopic data for ureilites. Whole rock samples and a pyroxene separate from Kenna, and whole rock samples of Novo Urei and ALHA77257 define a line with a slope corresponding to an age of 3.79 Ga (Kenna group). Mineral separates and a whole rock sample of Goalpara are consistent with this line within error (analytical uncertainty not shown). Acid leachates of Kenna plot at the LREE-enriched end (low ^{147}Sm/^{144}Nd) of the line (field labeled L). Samples of ALH 82130, META78008 and some samples PCA 82506 are consistent with the 4.55 Ga chondritic evolution line (4.55 Ga group). One whole rock sample of PCA 82506, and a leachate and residue generated from it, define a line with a slope corresponding to an age of 4.23 Ga (dashed line). A whole rock sample of LEW 85440 is consistent with this line. Note that the 3.79 Ga and the 4.23 Ga lines intersect the chondritic evolution line at the same point (^{147}Sm/^{144}Nd ~ 0.51). Data from Goodrich and Lugmair (1991, 1992, 1995), Goodrich et al. (1991), Takahashi and Masuda (1990a), Torigoye-Kita et al. (1995a,b,c).

whole rock sample of ALHA77257. These define a ^{143}Nd/^{144}Nd-^{147}Sm/^{144}Nd line with a slope corresponding to an age of 3.79 Ga and an initial ^{143}Nd/^{144}Nd ratio of 0.50938. Mineral separates and a whole rock sample of Goalpara are consistent with this line (Fig. 40). Acid leachates of Kenna have ^{147}Sm/^{144}Nd and ^{143}Nd/^{144}Nd ratios very similar to those of the LREE-enriched whole rocks (Fig. 40), and are interpreted to represent the composition of the LREE-enriched component in Kenna (Goodrich and Lugmair 1995). (2) A 4.55 Ga group including some whole rock samples of PCA 82506, whole rock samples of ALH 82130 and META78008, and mineral fractions of META78008. These plot along the 4.55 Ga chondritic evolution (Fig. 40). (3) One whole rock sample of PCA 82506, and an acid leachate and residue generated from it, define a line with a slope corresponding to an age of 4.23 Ga. A whole rock sample of LEW 85440 is consistent with this line (Fig. 40). Both the 3.79 Ga line and the 4.23 Ga line intersect the chondritic evolution line at ^{147}Sm/^{144}Nd ~ 0.51. Interpretation of the significance of these data is controversial (Torigoye-Kita et al. 1995a,b; Goodrich et al. 1995), and clearly depends on understanding the LREE-enriched component in ureilites. Torigoye-Kita et al. (1995a,b) have argued that the 3.79 Ga line is a mixing line, and that the LREE-enriched component is a terrestrial contaminant, since its Sm-Nd isotopic composition is similar to that of average terrestrial crust. Soil from the site where Kenna was found has a similar, if not identical, composition (Goodrich and Lugmair 1995). However, Goodrich and Lugmair (1995) and Goodrich et al. (1995) argue that if the 3.79 Ga and 4.23 Ga lines are mixing lines, then samples devoid of LREE-enriched component, such as acid residues and leached mineral separates, should plot at the intersection of these lines with the

chondritic evolution line, at $^{147}Sm/^{144}Nd$ ~ 0.51. They suggest that these lines are isochrons and give the time of introduction of LREE-enriched material to highly-depleted ($^{147}Sm/^{144}Nd$ ~ 0.51) 4.55 Ga-old proto-ureilite material. Torigoye-Kita et al. (1995a) point out that two of their Goalpara pyroxene separates (those with highest $^{147}Sm/^{144}Nd$ in Fig. 40a) have error bars that overlap the 4.55 Ga line, and argue that these points represent the uncontaminated, 4.55 Ga-old end member of a mixing line. However, a line drawn from the 4.55 Ga line at the $^{147}Sm/^{144}Nd$ ratios of these pyroxenes to the composition of the LREE-enriched component, falls below all but the most LREE-enriched Kenna samples. Whether ureilites have young Sm-Nd ages or not awaits resolution.

Rb-Sr. Rubidium-Sr isotopic data for ureilites scatter widely. Takahashi and Masuda (1990a) report a BABI (basaltic achondrite best initial, Papanastassiou and Wasserburg 1969) whole rock model age of 4.55 Ga, and a 4.01±0.06 Ga Rb-Sr internal isochron for META78008. All other analyzed ureilites have older model ages, indicating that they have experienced open system behavior at some younger time(s). Fifteen analyzed samples of Kenna including whole rocks, leachates and residues show essentially identical $^{87}Sr/^{86}Sr$ ratios of ~0.70866 (Goodrich and Lugmair 1995). Strontium in soil from near the Kenna recovery site has a much higher $^{87}Sr/^{86}Sr$ ratio (0.7199), and so does not appear to be a contaminant.

U-Th-Pb. U-Th-Pb systematics have been investigated for META78008 and Goalpara (Torigoye-Kita et al. 1995a,c). Extensive leaching procedures were used to remove the effects of contamination. The Pb, Th and U abundances in the residues were extremely low—for example, up to ~8 ng/g Pb, 3.2 ng/g Th, and 0.9 ng/g U in META78008. The leachates were significantly enriched in Pb—up to 250 ng/g in META78008 and 1478 ng/g in Goalpara. On a $^{207}Pb/^{206}Pb$-$^{204}Pb/^{206}Pb$ diagram, the META78008 leachates plot along a mixing line between the Pb isotopic composition of Canyon Diablo troilite and modern terrestrial Pb, indicating terrestrial Pb contamination. The least-contaminated residues yield a Pb-Pb isochron age of 4.563±0.021 Ga. All of the Goalpara samples showed evidence of mixing with modern terrestrial Pb, and in some cases another Pb component, probably old terrestrial Pb. On a U-Pb concordia diagram, the META78008 residues plot along a line connecting modern terrestrial Pb with the concordia point of 4.562 Ga, and the Goalpara residues define a general trend that intersects concordia at ~4.5 Ga. This old age for Goalpara, and the observation that leachable fractions are contaminated with terrestrial Pb, led Torigoye-Kita et al. (1995a) to suggest that REE in the leachable fractions are also terrestrial, and therefore that the 3.79 Ga Sm-Nd line for Goalpara and Kenna (Fig. 40a) is a mixing line.

Ar-Ar. ^{39}Ar-^{40}Ar determinations have been made on bulk samples of Kenna, Novo Urei, PCA 82506, and Haverö (Bogard and Garrison 1994). Interpretation of the Ar release spectra is uncertain due to possible contamination effects, but the most recent times of Ar degassing can be inferred. These times are ~3.3 Ga for Haverö, ~3.3 to 3.7 Ga for Novo Urei, ~4.1 Ga for Kenna and 4.5 to 4.6 Ga for PCA 82506. It is possible that the younger degassing ages record the same events that affected Sm-Nd ages.

Carbon and nitrogen. Carbon isotopic compositions of ureilites are in the range $\delta^{13}C$ = -11 to 0‰ (Grady et al. 1985a,b; Grady and Pillinger 1987a), and some correlation with mg# has been suggested. Graphite and diamond appear to have the same isotopic composition, but a small fraction of the carbon, which combusts at high temperature, is ^{13}C-depleted. This may be from carbide. FRO 90054, which has an unusually low carbon content, also has an exotic carbon isotopic composition: $\delta^{13}C$ = -24.3‰ (Grady and Pillinger 1993).

Nitrogen isotopic compositions in ureilites are variable, and there is evidence for distinct compositions in carbon phases ($\delta^{15}N$ = -110 to 60‰), silicates ($\delta^{15}N$ = 0±20‰), and metal (Grady et al. 1985a, Grady and Pillinger 1986, Murty 1994). Nitrogen in FRO 90054 is exotic: $\delta^{15}N$ = +64‰ (Grady and Pillinger 1993). Nitrogen isotopic compositions in polymict ureilites range up to $\delta^{15}N$ = +527‰ (Grady and Pillinger 1987b).

Discussion

Ureilites are clearly achondritic, and in terms of their mineralogy, textures, bulk lithophile element ratios, and depletion of lithophile incompatible elements, resemble groups of ultramafic rocks from evolved parent bodies such as the Earth, Moon and Mars. Thus, they have been widely believed to be either igneous cumulates or partial melt residues. However, they differ from such groups in several important ways. First, they show no evidence of being related to one another by igneous fractionation processes, and they lack complementary rock types (i.e. ureilitic basalts). Second, they have characteristics which are typical of chondritic materials and difficult to reconcile with extensive igneous processing, namely their oxygen-isotopic characteris-tics, high trace siderophile element abundances, and the presence of planetary-type noble gases. Ureilites remain incompletely understood in the context of the distinction between primitive and differentiated solar system materials. Discussions of ureilite genesis usually tacitly assume that they originated on one parent body, but this may not be the case.

Igneous processes among ureilites. Ureilites lack plagioclase, have superchondritic Ca/Al ratios, and are depleted in incompatible lithophile elements. These features indicate a high degree of igneous processing. Ureilites also show a high degree of internal textural and chemical equilibration, both within and between olivine and pyroxene, which suggests slow cooling at high temperatures. Estimates of pyroxene equilibration temperatures range from ~1200° to 1280°C (Takeda 1987, Takeda et al. 1989, Chikami et al. 1997a). In partial melting models, at least 15% melting is required to eliminate plagioclase, while ~20 to 30% melting is required to produce the more extreme REE depletions and negative Eu anomalies of ureilites (Spitz and Goodrich 1987, Warren and Kallemeyn 1992, Goodrich 1997a), assuming a chondritic source. In cumulate models, much higher degrees of processing are required, because the superchondritic Ca/Al ratios of olivine in ureilites could only be produced if their parent magmas were derived from previously plagioclase-depleted sources (Goodrich et al. 1987a).

The question of whether ureilites are residues or cumulates is one of the classic problems of ureilite research. Berkley et al. (1976, 1980) and Berkley and Jones (1982) argued that they are cumulates largely on the basis of their textures and fabrics. The multi-stage history required by the cumulate model, however, predicts the existence of numerous complementary rock types, particularly various basalts. Scott et al. (1993) and Warren and Kallemeyn (1992) argued that the existence of a large number of ureilites, and no apparently related basaltic meteorites, indicates that ureilites comprise the major rock type on their parent body and are therefore residues. Although some textural features of ureilites remain difficult to explain in a pure residue model (Treiman and Berkley 1994), few workers now advocate a cumulate model for ureilites. Warren and Kallemeyn (1989b) proposed a hybrid paracumulate model, in which ureilites form as "mushy, cumulate-like partial melt residues."

Regardless of whether they are residues or cumulates, ureilites show no correlations of mg# with bulk composition, mineral minor element composition, pyroxene type, pyroxene/(pyroxene+olivine) ratio, or REE depletion. Such correlations would be expected if ureilites were related to one another either by progressive partial melting of

common source material, or by fractional crystallization of a common magma or similar magmas. Thus, ureilites do not seem to be a suite of related igneous rocks in the sense that other achondrite groups do.

This conclusion is consistent with the problem that large degrees of igneous processing and a high-temperature history are difficult to reconcile with the lack of oxygen-isotopic equilibration among ureilites (Clayton and Mayeda 1988). All other groups of achondrites and even most primitive achondrites show significant degrees of oxygen-isotopic equilibration (Fig. 39). Scott et al. (1993) suggested that individual ureilites formed in distinct zones that were sufficiently isolated from one another that they did not communicate isotopically. Warren and Kallemeyn (1992) also pointed out that kilometer-scale heterogeneities in oxygen-isotopic composition may have been preserved because oxygen diffusion is slow. However, the plausibility of deriving each (or at most a few) ureilite(s) from a distinct, kilometer-sized zone of a ureilite parent body (UPB), or a distinct UPB, decreases as the number of ureilites continues to grow. Alternatively, several models have suggested that the UPB accreted from material that was already depleted in the plagioclase component relative to chondrites (Takeda 1987, Kurat 1988). Such models require only a small degree of planetary igneous processing, which might not lead to oxygen-isotopic equilibration or readily distinguishable chemical trends. They also avoid the problem of locating the missing basaltic complements to ureilites, which in no way can be accounted for by the 1 to 2% plagioclase in polymict ureilites. Other suggestions for disposing of the basalts include blowing the crust off the UPB by volatile-enhanced, explosive volcanism (Warren and Kallemeyn 1992, Scott et al. 1993) or stripping it off via impacts.

Reduction among ureilites. The only apparent chemical trend observed among ureilites is the negative FeO-MnO (positive Fe/Mn-Fe/Mg with constant Mn/Mg) correlation shown by both bulk and mineral compositions (Figs. 33, 34), which indicates a relation by reduction, with no effects of fractional crystallization or partial melting (Mittlefehldt 1986, Goodrich et al. 1987b, Takeda 1987). Because ureilites contain carbon, it has been widely thought that carbon-silicate redox reactions must be responsible for this trend (Berkley and Jones 1982, Goodrich and Berkley 1986, Goodrich et al. 1987b, Walker and Grove 1993), particularly since there is also evidence in the form of reduced rims on primary minerals for a secondary, in-situ, carbon reduction event. Carbon redox reactions are strongly pressure dependent, and thus lead to estimates of the pressure range over which ureilites formed: experimental data indicate a pressure of ~2.5 MPa for the most magnesian ureilite and ~10 MPa for the most ferroan ureilite (Walker and Grove 1993).

However, several features of ureilites are inconsistent with a relation by progressive reduction of common material in a planetary setting: the lack of correlation between pyroxene/(pyroxene+olivine) and mg#; a lack of correlation between carbon content and mg#; and a lack of correlation between metal content or siderophile element abundances and mg#. Progressive reduction should lead to an increasing ratio of pyroxene/(pyroxene+olivine) through the reaction $(Mg,Fe)_2SiO_4 + C \rightarrow (Mg,Fe)SiO_3 + Fe + CO$ (McSween and Labotka 1993), decreasing carbon content through loss of CO, and increasing metal content, although metal may have segregated gravitationally. In addition, if reduction occurred in a magma or during partial melting, the Fe/Mn-Fe/Mg trend would show the effects of fractional crystallization or partial melting along with reduction, rather than pure reduction (Goodrich et al. 1987b).

The correlation between mg# and $\Delta^{17}O$ (Fig. 39) suggests that the reduction relation among ureilites may be a nebular, rather than planetary, feature. Some chondritic

materials which show mg#-$\Delta^{17}O$ correlations also show negative FeO-MnO correlations (Takeda 1987, Goodrich 1997b), and it has been shown that a nebular mg#-$\Delta^{17}O$ correlation could survive 15 to 30% silicate partial melting, assuming that each ureilite melted in isolation from the others and did not experience any further (planetary) reduction due to carbon (Goodrich 1997a).

This raises another classic problem of ureilite research—the question of whether their carbon is primary. The fine grain size of graphite in most ureilites, the presence of diamonds, the restriction of carbon to interstitial areas and veins, and its obvious reaction relation with primary minerals, led to the idea that the carbon was shock-injected into ureilites late in their history, probably by a carbonaceous chondrite-like impactor (Wasson et al. 1976, Boynton et al. 1976). However, the discovery of large euhedral graphite crystals in apparently unshocked ureilites, and of iron-carbon alloy spherule inclusions within primary minerals, showed that graphite was a primary igneous phase, which had been disrupted and converted to diamond in most ureilites by late shock events (Berkley and Jones 1982, Goodrich and Berkley 1986). In this case, the reduced rims on primary silicate grains could have formed when ureilites were excavated by impact and a sudden drop in pressure caused a drop in carbon-controlled f_{O_2}. Sudden excavation is consistent with the lack of exsolution in pyroxene in most ureilites, high Ca contents in olivine, and cooling rate determinations on reduced rims (Toyoda et al. 1986). Several authors have proposed catastrophic impact disruption models for the UPB (Takeda 1987, Warren and Kallemeyn 1992). Polymict ureilites may place constraints on such models (Guan and Crozaz 1995b, 1997).

If carbon was primary in ureilites, then planetary reduction, which would have disrupted a nebular mg#-$\Delta^{17}O$ correlation, can be avoided only if all ureilites formed at pressures sufficiently high to prevent carbon redox reactions, that is ~7.5-10 Mpa (Warren and Kallemeyn 1992, Walker and Grove 1993). This implies a parent body with a minimum radius of ~100 km, which is large by the standard of present day asteroids. This is considered by some authors to be a problem, although it is likely that the average size of the asteroids has decreased (see Warren and Kallemeyn 1992). An alternative explanation for the mg#-$\Delta^{17}O$ correlation is that the UPB accreted with a radial gradient in $\Delta^{17}O$, upon which was superimposed a radial gradient in mg# created by pressure-dependent carbon-silicate redox reactions (Walker and Grove 1993, J.H. Jones, pers. comm.).

The question of the role of carbon in ureilite petrogenesis is closely associated with the issue of their noble gas contents, because the gases are largely contained in the carbon. The presence of trapped noble gases in near-chondritic abundances is difficult to explain in a scenario involving large-scale igneous events, because gases would be expected to be lost from open magmatic systems at high temperatures. No other achondrite group, except the lodranites, contains trapped noble gases in such high abundances. However, if melting occurred in a closed system, that is, at sufficiently high pressures, the gases might be largely retained (Berkley and Jones 1982, Wacker 1986). Berkley and Jones (1982) calculated that 10 MPa pressure would permit noble gas retention, and Wacker (1986) argued that under these conditions noble gases would actually diffuse into the interior of carrier carbon grains from surface sites, hence becoming more tightly trapped. Again, this model implies a large parent body. Alternatively, if the carbon was a late addition, the primitive gases may have been introduced after the igneous events occurred and the problem of their retention is avoided.

The high siderophile element abundances of ureilites are also unusual compared to other achondrites and rocks from evolved parent bodies, and bear on the question of whether the apparent reduction relation among them was established by nebular or

planetary processes. If this relation was established in the nebula before accretion of the metal component, then there is no reason to expect a correlation between mg# and siderophile element abundances, as long as the degree of subsequent igneous processing was not high. If it was established by carbon reduction on the UPB, then ureilites should show either increasing metal content, if metal did not segregate or decreasing siderophile element abundances if metal did segregate, with increasing mg#. However, Goodrich et al. (1987b) proposed a complex magmatic model in which this is not the case. On the other hand, the siderophile element patterns shown by ureilites (Fig. 37) suggest the presence of two components, one refractory-rich and associated with metal-rich carbonaceous matrix material, and one refractory-poor (Boynton et al. 1976, Higuchi et al. 1976, Janssens et al. 1987, Spitz and Boynton 1991). This has led to the suggestion that the metal was a late addition, along with the carbon and noble gases (Wasson et al. 1976, Boynton et al. 1976), which again would be consistent with a lack of correlation of siderophile element abundances with mg#.

The relation of diamond to graphite remains unclear and this further complicates the picture. The idea that the diamonds were produced from original graphite by shock (Vdovykin 1970) is supported by the observation that apparently very low shock stage ureilites such as ALHA78019 do not appear to contain diamond (Wacker 1986). The high noble gas contents of diamonds relative to graphite can be explained because gas-free graphite has been shown to trap large amounts of noble gases upon shock transformation to diamond (Yajima and Matsuda 1989). The shock formation hypothesis for ureilitic diamond was originally taken as support for the carbon-gas-metal-injection hypothesis (Boynton et al. 1976, Wasson et al. 1976). However, studies of apparently low-shock ureilites have shown that there is no correlation of either noble gas abundance or carbon content with degree of shock. Matsuda et al. (1988, 1991) suggested that diamonds in ureilites were not produced by shock, but rather by chemical vapor deposition from an H_2-CH_4 gas onto refractory-rich early condensates in the solar nebula, thus explaining the association of refractory-rich siderophile elements with the carbonaceous vein material in ureilites. These authors found that fractionation of heavy noble gases during vapor deposition of diamond produced abundance patterns similar to those of ureilites. Conclusive evidence for diamonds in the very low shock stage (e.g. ALHA78019, Nullarbor 010) would support the vapor deposition hypothesis. If ureilitic diamonds did form by vapor deposition in the nebula, then at least part of their carbon may be primary.

How old are ureilites? Isotopic age data suggest that the ultramafic ureilite assemblage formed close to 4.55 Ga ago. Uranium-Th-Pb data clearly indicate ages of ~4.55 Ga for two ureilites, with no evidence for later disturbance aside from recent terrestrial Pb contamination (Torigoye-Kita et al. 1995a,c). Samarium-Nd data for several ureilites are also consistent with an ~4.55 Ga age, with no later disturbance (Fig. 40). These results may record the time of accretion of the UPB, consistent with the 4.56 Ga canonical age of meteorites. It is also possible that the ureilite assemblage was generated by planetary igneous processes within a few million years after accretion.

However, Sm-Nd data for several other ureilites (including one which has a 4.55 Ga U-Th-Pb age) suggest disturbances at 4.23 and 3.79 Ga, which are clearly associated with the poorly-understood LREE-enriched component in ureilites (Fig. 40). Whether this component is a terrestrial contaminant, in which case these young ages are meaningless, is controversial (Torigoye-Kita et al. 1995b, Goodrich et al. 1995). Because of the apparent pervasiveness of the LREE-enriched component in ureilites, and the importance that young Sm-Nd ages would have, this matter deserves further investigation. If it is shown that the LREE-enriched component is indigenous to ureilites and was introduced to the ultramafic assemblage at 3.79 and 4.23 Ga (Goodrich and Lugmair 1995), its

nature may still be uncertain. It might have been derived from a foreign impactor, or it might represent a crustal component of the UPB. It could, therefore, indicate either impact events or internal heating events. The latter possibility would require a large UPB, which would have implications for some of the issues discussed above.

Ureilite precursor material. Because ureilites have high carbon contents, and because their oxygen-isotopic compositions are similar to those of carbonaceous chondrites, it has been suggested that ureilite precursor material was similar to carbon+metal-bearing carbonaceous chondrites (Vdovykin 1970, Clayton et al. 1976a, Higuchi et al. 1976, Wasson et al. 1976). Tomeoka and Takeda (1989) and Takeda (1987) suggested that Ca-Al-rich interstitial materials in ureilites are remnants of CV-like parent material. In general, many models for ureilite petrogenesis have assumed carbonaceous chondrite-like precursor material. In detail, however, the data do not show a clear link to any carbonaceous chondrite group. Siderophile and volatile element abundance patterns in the carbonaceous vein material in ureilites are inconsistent with derivation from CI chondrites (Boynton et al. 1976, Binz et al. 1975), and carbon isotopic compositions of ureilites are quite distinct from those of carbonaceous chondrites (Grady et al. 1985a). Nevertheless, the observation that chondrules and chondrule rims in Allende show an mg#-$\Delta^{17}O$ correlation similar to ureilites (Rubin et al. 1990) suggests the possibility that ureilite precursor material resembled some components of carbonaceous chondrites. Whether ureilite precursor material ever had a chondritic-type plagioclase component is, as discussed above, uncertain. It seems likely that ureilite precursor material is not represented in terrestrial museums.

LEW 88774. Chromite-bearing LEW 88774 is an unusual ureilite. Compared to other monomict ureilites it is exceptionally enriched in Cr, Ca, Al, Sc, V, Na, Ga, and to a lesser extent K and REE (Table 26; Figs. 35, 36c, 37) and it plots off the Fe/Mn-Fe/Mg and Fe/Cr-Fe/Mg trends shown by other ureilites (Fig. 33). It has the lowest mg# ($Fo_{\sim 74.5}$) of any ureilite, which is consistent with the presence of chromite in indicating that it formed at higher f_{O_2} than other ureilites (Prinz et al. 1994). However, its Fe/Mn ratio is low (Fig. 33a) and indicates that it is not part of the same reduction sequence as other ureilites. It also has the highest pyroxene/(pyroxene+olivine) ratio (0.9) among ureilites, which is inconsistent with its fitting into a reduction sequence. If this rock is a cumulate, extensive fractional crystallization of chromite is required. If it is a residue, its starting material must have been Cr-enriched. Most of the enriched elements in LEW 88774 are refractory, and so its precursor material may have been a Cr-rich refractory chondritic component, similar to chromite-rich chondrules (Krot et al. 1993), although it is not clear that Ga enrichment can be explained this way (Kallemeyn and Warren 1994). LEW 88774 may provide clues to distinguishing nebular from planetary features in ureilites.

AUBRITES

Among all of the achondrites, aubrites may be the most fascinating from a mineralogical perspective. These meteorites formed under highly reducing conditions and, thus, contain a variety of minerals unknown from earth. Aubrites are brecciated pyroxenites that consist primarily of FeO-free enstatite. Keil (1989) summarized the membership of the aubrites at that time. Included were Aubres, Bishopville, Bustee, Cumberland Falls, Khor Temiki, Mayo Belwa, Norton County, Peña Blanca Spring, Pesyanoe, ALHA78113, 20 Allan Hills meteorites within the ALH 83009 pairing group, 9 Lewis Cliff meteorites within the LEW 87007 pairing group, and Yamato 793592. Eight of the 9 non-Antarctic meteorites were observed falls. Also related are the non-brecciated meteorites Shallowater and Mt. Egerton, both of which differ substantially from the remainder of the group and are discussed separately later. The Si-bearing iron

meteorite Horse Creek might be related to this clan. Aubrites are clearly related to enstatite chondrites, sharing similar mineralogy and mineral compositions (Keil 1968, Watters and Prinz 1979) and oxygen-isotopic compositions (Clayton et al. 1984), although the exact nature of this relationship is still controversial. In this section, we review the petrology and mineralogy of aubrites. We first focus on the silicate phases, which comprise the bulk of aubrites, and then turn our attention to the less abundant metallic phases, phosphides, nitrides and sulfides.

Table 27. Modal compositions of selected aubrites (Watters and Prinz, 1979).

	Bishopville	Cumberland Falls	Khor Temiki	Mayo Belwa	Norton County	Shallowater
enstatite	74.8	94.0	88.5	97.5	84.5	81.6
plagioclase	16.2	0.7	6.6	0.3	1.0	2.9
diopside	1.9	0.9	1.5	0.6	2.7	0.0
forsterite	6.7	1.5	3.6	1.6	10.0	4.7
kamacite	trace	0.7	0.1	trace	0.3	3.7
troilite	0.5	1.1	0.1	0.1	1.0	7.1

Mineralogy and petrology

Silicates. Enstatite, plagioclase, diopside, and forsterite are all found in aubrites. Bevan et al. (1977) reported rare fluor-amphibole in Mayo Belwa and Okada et al. (1988) reported silica in Norton County. Watters and Prinz (1979) reported the most comprehensive study of the mineralogy and mineral compositions of a suite of aubrites. Table 27 lists modal analyses for representative aubrites from this work.

Aubrites are dominated by pyroxenite clasts. Individual enstatite grains up to 10 cm in length have been reported from Peña Blanca Spring (Lonsdale 1947) and enstatite grains are commonly mm-sized in all aubrites. This extremely coarse grain size makes obtaining a representative sample for chemical analyses essentially impossible. The clasts exhibit igneous textures, with adjacent enstatite exhibiting irregular intergrown borders (Fig. 41) typical of co-crystallization (Okada et al. 1988). Post-crystallization shock has affected many of the enstatite grains, giving rise to a range of macroscopic appearances from white to colorless and transparent (Okada et al. 1988). Enstatite is essentially FeO-free (Table 28).

Diopside is also found in aubrites in abundances ranging from 0.2 to 8.1 vol % (Watters and Prinz 1979; Table 27). This diopside is essentially FeO-free and has $Wo_{40.1\text{-}46.1}$ (Table 28). Diopside occurs as both independent grains and as exsolution lamellae within enstatite (Reid and Cohen 1967, Watters and Prinz 1979, Okada et al. 1988). The abundance of diopside exsolution within the host grains ranges from ~9 to 25%, suggesting that the parent magma crystallized enstatite, pigeonite and diopside as distinct phases (Okada et al. 1988).

Plagioclase abundances are highly variable (0.3 to 16.2 vol %), although most aubrites are depleted in plagioclase relative to chondrites (~10 vol %, McSween et al. 1991). Plagioclase compositions range from $An_{1.8\text{-}8.2}$ (Table 28; Watters and Prinz 1979). Watters and Prinz (1979) observed one grain of $An_{23.8}$ in Khor Temiki, while other grains averaged $An_{2.0}$. Okada et al. (1988) reported a huge range of compositions from $An_{0\text{-}92.3}$, although these authors attributed much of this range to disequilibrium during rapid crystallization of impact-melt clasts within Norton County.

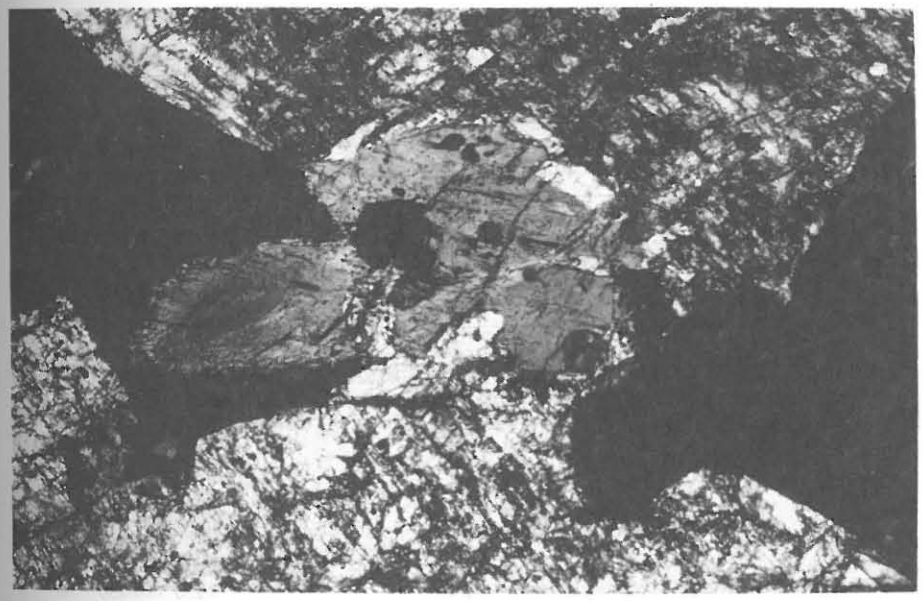

Figure 41. Photomicrograph in polarized light of Norton County illustrating the large enstatites which are mutually intergrown at their borders, suggesting co-crystallization. Field of view = 2.6 mm.

Forsterite shows a considerable range in abundance (0.3-10.0 vol %) and is essentially FeO-free (Table 28) (Watters and Prinz 1979). Grains up to 4 mm in size occur as distinct grains within the brecciated matrix and, less frequently, enclosed within enstatite grains.

Metal and associated phosphide and silicide. Metallic Fe,Ni is a minor but important constituent of most aubrites. It comprises from a trace to 0.7 vol % of aubrites (Watters and Prinz 1979), excluding the metal-rich Shallowater and Mt. Egerton. Aubritic metal is dominantly silicon-bearing kamacite with 3.7-6.8 wt % Ni and 0.12-2.44 wt % Si (Watters and Prinz 1979). Casanova et al. (1993a) observed a somewhat larger range in kamacite compositions, including the presence of Si-free kamacite in Norton County. Metal in aubrites occurs as inclusions in enstatite, interstitial grains up to several hundred μm in diameter, and cm-sized nodules. Okada et al. (1988) also observed rare taenite and tetrataenite within metal of Norton County. From the relationship between the composition and size of the taenite, these authors inferred a cooling rate of ≤1°C/Ma. A variety of phases occur intimately associated with aubritic metal and the metal itself is often associated with sulfides. Schreibersite is found associated with metal in most aubrites (Watters and Prinz 1979) and occasionally as isolated grains (Casanova et al. 1993a). Casanova et al. (1993a) observed the nickel silicide perryite ($(Ni,Fe)_5(Si,P)_2$) in the cm-sized metal nodules of Norton County and Mt. Egerton. Native copper has also been reported from aubrites (Ramdohr 1973).

Casanova et al. (1993a) analyzed the metal nodules from Norton County, ALH 84007, ALH 84008 and Mt. Egerton for the elements Cr, Co, Ni, Ga, As, W, Re, Ir and Au. With the exception of Cr, which behaves as a chalcophilic element at the oxygen fugacities experienced by aubrites, these elements were all present at approximately chondritic abundances. Casanova et al. (1993a) interpreted these results to indicate that

Table 28. Representative silicate compositions from aubrites (Watters and Prinz, 1979).

	enstatite		diopside		forsterite	plagioclase		
	Bustee	Norton County	Cumberland Falls	Bustee	Bustee	Khor Temiki	Khor Temiki	Norton County
Chemical Composition (wt %)								
SiO_2	59.4	59.1	54.4	54.6	42.8	67.6	61.9	65.3
Al_2O_3	0.09	0.07	0.70	0.39	b.d.	20.3	24.2	21.8
TiO_2	0.02	<0.02	0.19	0.28	<0.02	<0.02	0.03	0.03
Cr_2O_3	0.02	<0.02	0.04	0.02	n.d.	n.d.	n.d.	n.d.
FeO	0.05	0.07	0.12	<0.02	<0.02	<0.02	<0.02	0.02
MnO	0.11	<0.02	0.05	0.04	<0.02	n.d.	n.d.	n.d.
MgO	40.3	39.6	22.8	20.2	56.9	0.08	0.14	0.03
CaO	0.42	0.64	21.3	24.0	0.05	0.43	5.1	1.77
Na_2O	0.02	0.02	0.33	0.29	n.d.	11.2	9.0	10.7
K_2O	n.d.	n.d.	n.d.	n.d.	n.d.	0.64	0.23	0.53
Total	100.4	99.5	100.0	99.8	99.99	100.4	100.6	100.1
Cation Formula (O=4 for olivine, 6 for pyroxene, 8 for plagioclase)								
Si	1.983	1.991	1.947	1.968	1.004	2.956	2.733	2.873
Al	0.003	0.003	0.030	0.017	--	1.046	1.260	1.130
Ti	--	--	0.005	0.008	--	--	--	--
Cr	--	--	0.001	0.001	--	--	--	--
Fe	0.001	0.002	0.004	--	--	--	--	--
Mn	0.003	--	0.002	0.001	--	--	--	--
Mg	2.006	1.988	1.216	1.085	1.990	0.005	0.009	0.002
Ca	0.015	0.023	0.817	0.927	0.001	0.020	0.241	0.083
Na	0.001	0.001	0.022	0.020	--	0.950	0.771	0.913
K	--	--	--	--	--	0.036	0.013	0.030
Total	4.015	4.008	4.044	4.026	2.996	5.013	5.028	5.032
Molar Mineral End Members								
Wo	0.7	1.1	40.1	46.1	--	--	--	--
En	99.2	98.8	59.7	53.9	--	--	--	--
Fs	0.1	0.1	0.2	0.0	--	--	--	--
Or	--	--	--	--	--	3.6	1.3	2.9
Ab	--	--	--	--	--	94.4	75.2	89.0
An	--	--	--	--	--	2.0	23.5	8.1

these cm-sized nodules had not been part of a large central core that experienced fractional crystallization, but rather were metal particles which never segregated to the core.

The unusual Si-bearing iron meteorite Horse Creek is likely related to the aubrites. Horse Creek was described by Buchwald (1975), who also summarized the previous literature. This meteorite contains 6.3 wt % Ni and 2.3 wt. Si in the bulk. Horse Creek is composed of dominant kamacite with an exsolved Ni silicide along the (111) planes of the kamacite. Thus, the meteorite's structure is similar to a Widmanstätten structure, but with nickel silicide in place of kamacite and kamacite in place of taenite, although Horse Creek is a hexahedrite. The Ni silicide has been described by some workers as perryite similar to that found in enstatite chondrites and achondrites, although Buchwald (1975) questions whether these are a single phase or a range of compositions in a solid solution. Schreibersite is also found in Horse Creek. Horse Creek is clearly related to metal in aubrites and may also represent metal which never segregated to the core of the aubrite parent body (Casanova et al. 1993a).

Table 29. Representative sulfide analyses from aubrites.

	troilite		oldhamite		daubreelite	alabandite		caswell.	heideite	niningerite
	Pesyanoe	Bishopville	Khor Temiki	Pena Blanca Spring	Pesyanoe	Mayo Belwa	Norton County	Norton County	Bustee	Bustee
Chemical Compositions (wt %t)										
Ca	0.17	0.12	52.0	54.3	<0.02	0.72	0.29	b.d.	n.d.	0.45
Fe	62.5	57.1	<0.02	<0.02	17.8	23.5	17.1	b.d.	25.1	6.07
Ti	0.46	5.70	<0.02	0.12	0.17	0.16	<0.02	0.18	28.5	0.18
Mg	0.08	0.06	0.19	0.89	0.75	2.10	1.42	b.d.	<0.05	29.6
Mn	0.12	0.25	1.06	<0.02	1.27	33.7	42.9	0.08	0.02	12.8
Cr	0.21	0.52	<0.02	<0.02	33.9	1.50	0.13	37.4	2.9	0.13
Na	n.d.	n.d.	n.d.	n.d.	n.d.	n.d.	n.d.	15.7	n.d.	0.03
S	37.3	36.5	42.4	44.5	45.9	38.1	38.7	46.3	44.9	50.7
Total	100.84	100.25	95.65	99.81	99.79	99.78	100.54	99.66	101.42	99.96
Atomic Formula (S=4)										
Ca	0.015	0.011	3.924	3.904	--	0.060	0.024	--	--	0.028
Fe	3.847	3.592	--	--	0.890	1.416	1.015	--	1.284	0.275
Ti	0.033	0.418	--	0.007	0.010	0.011	--	0.010	1.699	0.009
Mg	0.011	0.009	0.024	0.106	0.086	0.291	0.194	--	--	3.080
Mn	0.008	0.016	0.058	--	0.065	2.065	2.588	0.004	0.001	0.589
Cr	0.014	0.035	--	--	1.821	0.097	0.008	1.992	0.159	0.006
Na	--	--	--	--	--	--	--	1.891	--	0.003
Total	3.928	4.081	4.006	4.017	2.872	3.94	3.829	3.897	3.143	3.991

Data for troilite, oldhamite, daubreelite and alabandite from Watters and Prinz (1979); caswellsilverite from Okada and Keil (1982); heideite from Keil and Brett (1974); and niningerite from McCoy (1996).

Sulfides. A remarkable feature of aubrites is the occurrence of elements which are normally lithophile under oxidizing conditions becoming chalcophile under such highly reducing conditions. This gives rise to the formation of a variety of cubic sulfides, including troilite, FeS; oldhamite, CaS; alabandite, (Mn,Fe)S; niningerite, (Mg,Mn,Fe)S; daubreelite, $FeCr_2S_4$; heideite, $(Fe,Cr)_{1+x}(Ti,Fe)_2S_4$; djerfisherite, $K_3(Na,Cu)(Fe,Ni)_{12}S_{14}$; and caswellsilverite, $NaCrS_2$ (Fuchs 1966, Watters and Prinz 1979, Okada and Keil 1982, McCoy 1998). Representative analyses of these phases in aubrites are given in Table 29.

Among these sulfides, that which has garnered the most attention is oldhamite (CaS). Oldhamite typically is a minor phase in aubrites, occurring as grains on the order of a hundred microns in size within the brecciated matrix (Floss and Crozaz 1993). Rare clasts of oldhamite-rich lithologies have, however, been identified in Norton County (Wheelock et al. 1994) and Bustee (Kurat et al. 1992, McCoy 1998). These clasts contain abundant oldhamite, ~30% in the Bustee clasts, with co-existing enstatite, diopside, plagioclase and/or forsterite. Oldhamite in these clasts can contain inclusions of alabandite, niningerite, troilite, daubreelite, caswellsilverite, metal, heideite, forsterite and osbornite (TiN). In the Bustee clast, the Ti-rich sulfides titanian troilite containing 17.2 to 25.2 wt % Ti, osbornite and heideite are all found within oldhamite.

Unlike most other meteorites, where silicates or phosphates act as the major REE carriers, oldhamite is the host in aubrites (Kurat et al. 1992, Floss et al. 1990, Lodders et al. 1993, Wheelock et al. 1994). Rare earth element abundances in oldhamite grains are typically 100 to 1000 times those found in CI chondrites. Further, Floss and Crozaz (1993) recognized 10 distinct REE patterns in their study of 109 oldhamite grains from the aubrites Mayo Belwa, Bustee and Bishopville. Some aubritic oldhamite grains exhibit REE abundances and patterns similar to unequilibrated enstatite chondrites (e.g. Floss

and Crozaz 1993; Crozaz and Lundberg 1995). Oldhamite also has an extraordinarily high melting temperature as a pure substance (2450-2525°C; Vogel and Heumann 1941; Chase et al. 1985).

A full discussion of the REE element abundances and patterns within aubrites is beyond the scope of this review. As stated earlier, representative bulk samples are virtually impossible to obtain, given the coarse grain size of the aubrites. Further, deriving petrogenetic information from such data requires extreme caution, since any "bulk" sample will consist of materials from a number of different lithologies. A small number of papers (e.g. Floss and Crozaz 1993, Lodders et al. 1993, Shimaoka et al. 1995) discuss mineral and bulk chemical data and interested readers should consult these references.

Unusual clasts and related meteorites. A variety of silicate-rich clasts and related meteorites are also found within aubrites and are briefly discussed here. With the exception of Shallowater and Mt. Egerton, all of the meteorites discussed here are either fragmental or regolith breccias (see Keil 1989 and references therein), consisting of a variety of rock clasts. Not surprisingly, impact-melt clasts are a fairly common component of aubrites. Several such clasts have been discussed by Okada et al. (1988). In the Cumberland Falls meteorite, clasts of chondritic material similar in composition to LL chondrites (Kallemeyn and Wasson 1985), but petrographically unique (Binns 1969), have been admixed during this surface residence. Since these lithologies do not speak directly to the origin or evolution of the aubrite parent body, they are not discussed further here.

The Shallowater aubrite has been recognized as unique since its original description by Foshag (1940). It is the only known unbrecciated aubrite. In addition, it contains significant quantities of both metal and troilite (Table 27). It is also the only aubrite to contain ordered orthopyroxene, rather than the disordered pyroxene common to other aubrites (Reid and Cohen 1967). Keil et al. (1989) noted that Shallowater consists of 80 vol % orthoenstatite crystals up to 4.5 cm in size which contain, as inclusions and in the interstices, xenoliths of an assemblage of twinned low-Ca clinoenstatite, forsterite, plagioclase, metallic Fe,Ni and troilite. These xenolithic phases can occur as polymineralic inclusions with all phases or as individual mineral grains and comprise ~20 vol % of the rock. The origin of Shallowater appears to be unrelated to that of the other aubrites. Keil et al. (1989) argue that Shallowater formed when a totally-molten enstatite-like asteroid was struck by an impactor of enstatite chondrite-like composition, but achondritic texture. The impactor was disrupted, forming the xenoliths, which were mixed into and quenched the enstatite-rich mantle of the molten target body. Thus, in this scenario Shallowater samples a separate parent body from the other aubrites with a dramatically different history. Several unanswered questions remain with this scenario, such as the lack of related lithologies which would have resulted from such an event.

Mt. Egerton is an unbrecciated meteorite composed of cm-sized enstatite crystals with about 21 wt % metallic Fe,Ni occurring in the interstices between the large enstatite laths. In addition to these phases, diopside, SiO_2, troilite, brezinaite and schreibersite are also found (Casanova et al. 1993b). Mineral and oxygen-isotopic compositions, as well as the unfractionated trace element composition of the metal, are all similar to other aubrites. In most respects, Mt. Egerton should be classified as an aubrite. It is, however, unusual in containing a far greater percentage of metal than other aubrites.

Fogel (1994, 1997) has found a small number of basaltic vitrophyre clasts within the Khor Temiki and LEW 87007 aubrites. The clasts are <1 cm in maximum dimension and consist of 60 to 90 vol % enstatite, minor diopside or olivine, troilite, metal and 10 to 40

vol % of glass which is highly enriched in Al_2O_3, Na_2O, K_2O and CaO relative to bulk aubrites or enstatite chondrites. In the case of the Khor Temiki vitrophyre, the glass also contains significant quantities of dissolved sulfur (0.82 wt %; Fogel 1994). It should be noted that not all dark clasts within aubrites are basaltic vitrophyres. Newsom et al. (1996) studied dark clasts in Khor Temiki and concluded that they are simply highly brecciated, containing a fine-grained matrix or enstatite with abundant inclusions.

Discussion

Although several authors have argued that aubrites formed by direct condensation from the solar nebula (Wasson and Wai 1970, Richter et al. 1979, Sears 1980), recent workers agree that the clasts within the breccias are of igneous parentage. Keil (1989) summarized the evidence for an igneous origin for aubrites, including textures of pyroxenitic clasts indicative of co-crystallization from a melt (Fig. 41), a range of clast types consistent with fractional crystallization (Okada et al. 1988), large crystal sizes inconsistent with condensation, and the presence of melt inclusions within enstatite grains (Fuchs 1974).

In a simplified model for the origin of aubrites (McCoy et al. 1997d), the direct precursor to the aubrites is an enstatite chondrite. Certainly, similarities in mineral and oxygen-isotopic compositions between enstatite chondrites and aubrites suggest some kind of link. Watters and Prinz (1979) argued that the precursor to aubrites may have been more similar to EL chondrites, while Fogel et al. (1988) favored an EH chondrite as the likely starting material. The enstatite chondrite is heated to the point of partial melting. The partial melts, both basaltic and Fe,Ni-FeS, are removed from the source region. The removal of these components is supported by the modal data of Watters and Prinz (1979) (Table 27) which demonstrate depletions relative to enstatite chondrites for most aubrites in plagioclase and for all aubrites in metal and troilite. Continued heating completely melts this ultramafic residual material, which subsequently crystallizes to form the coarse-grained, igneous aubrites. The pyroxene intergrowths typical of co-crystallization suggest that aubrites crystallized from a total or near-total melt, rather than being cumulates.

While this model may be broadly correct in concept, several questions and objections have arisen over the details of such a model. These questions include: (1) What happened to the basaltic partial melts? (2) Is aubritic oldhamite a nebular relict or an igneous crystallization product? (3) Can aubrites be derived by melting of known enstatite chondrites?

What happened to the basaltic partial melts? Differentiation of any likely chondritic precursor should produce a significant quantity of basaltic material. Despite this fact, brecciated aubrites contain a relative paucity of basaltic clasts. A number of theories have been proposed to explain the ultimate fate of these partial melts. As discussed earlier, Fogel (1994, 1997) has identified basaltic vitrophyres within aubrites which almost certainly sample these partial melts. Thus, partial melts are not completely absent from the aubrite parent body. However, it is clear that these rare basaltic clasts do not account for the abundant (10 to 20 vol %) basaltic material which would have been generated during partial melting of an enstatite chondrite-like source. One can, of course, speculate that we have an unrepresentative sample of the aubrite parent body, although the fact that aubritic regolith breccias do not contain abundant basaltic clasts suggests that such material does not occur as thick deposits on the surface of this body. Keil (1989) speculated that these materials could have been stripped from the parent body by impacts or, perhaps, the aubritic precursor was plagioclase-poor and abundant basalts were never formed. Wilson and Keil (1991) argued that basaltic material likely did exist and, owing

to the presence of volatiles, may have been erupted at velocities exceeding the escape velocity of the aubrite parent body and, thus, were lost as small pyroclasts into space early in the history of the solar system. Finally, it is worth noting that both modal analyses (Watters and Prinz 1979) and bulk chemical analyses (Lodders et al. 1993) demonstrate that some aubritic samples are enriched in plagioclase and it is possible that much of the basaltic material was locally redistributed. The absence of basaltic melts is also a problem for understanding the genesis of ureilites and lodranites.

Is aubritic oldhamite a nebular relict or an igneous crystallization product? Although general consensus exists that aubrites formed from a melt, some authors have suggested that many oldhamite grains are nebular relicts which survived igneous processing (Floss and Crozaz 1993, Kurat et al. 1992, Lodders 1996). In particular, these authors cite as support the similarities in REE patterns between oldhamite in aubrites and unequilibrated enstatite chondrites, the inability to produce these patterns through fractional crystallization, and the remarkably high melting temperature of pure oldhamite. In contrast, the large size of some aubritic oldhamite grains (which are difficult to reconcile with the small size of oldhamites found in enstatite chondrites if aubritic oldhamite is a relict) (Wheelock et al. 1994, McCoy 1998), the presence of oldhamite partially enclosing silicates (Wheelock et al. 1994), REE patterns in some oldhamite grains consistent with igneous fractionation (Floss and Crozaz 1993, Wheelock et al. 1994) and the occurrence of phases as inclusions within oldhamite which have condensation temperatures which are lower than oldhamite (Wheelock et al. 1994, McCoy 1998) all suggest that at least some oldhamite grains formed by igneous processes.

A recent focus of research on the origin of aubrites has been experimental studies which both examine REE partitioning between oldhamite and silicate melts and replicate partial melting of enstatite chondrites in an effort to examine questions of aubrite petrogenesis. Partitioning of REE between oldhamite and silicate melts has been examined by Jones and Boynton (1983), Lodders (1996) and Dickinson and McCoy (1997). Partition coefficients measured in these works are generally around unity, while apparent partition coefficients determined by ratioing REE elements in oldhamite to those in bulk aubrites are on the order of 100 to 1000 (Wheelock et al. 1994). Dickinson and McCoy (1997) demonstrated that the strongest control on REE partitioning is the composition of the crystallizing oldhamite. Calcium-poor oldhamite (63 to 79% CaS) produces a LREE-depleted, HREE-enriched pattern with a negative Eu anomaly. In contrast, Ca-rich oldhamite (88-89% CaS) produces a bowed pattern with a positive Eu anomaly. Temperature also strongly influences partitioning. Partition coefficients increase with decreasing temperature. Experiments run for 2 days at 1200°C and annealed at 800°C for 9 days exhibit larger partition coefficients for Eu and Gd than those which were not annealed.

Measured partition coefficients are clearly inconsistent with a simple igneous origin in which oldhamite is the first crystallizing phase and REE abundances are determined solely by high temperature partitioning between the oldhamite and bulk liquid. Partition coefficients near unity are consistent with the nebular model. Oldhamite REE patterns may have been established by a complex process of partial melting, melt removal, fractional crystallization with oldhamite of varying compositions crystallizing from isolated melt pools, subsolidus annealing and exsolution of Mg, Mn, Cr, and Fe-rich phases, producing a wide range of REE patterns.

More direct evidence for the history of aubritic oldhamite comes from the work of Dickinson and Lofgren (1992), Fogel et al. (1996) and McCoy et al. (1997c), in which

samples of the Indarch (EH4) chondrite were partially melted in the range of 1000° to 1500°C. Fogel et al. (1996) added synthetic CaS to their powdered Indarch to directly address the question of oldhamite melting. Each of these experiments produced melting of CaS at temperatures far below the melting temperature of the phase in isolation. McCoy et al. (1997c) found that at temperatures as low as 1200°C, no relict sulfides remained in the experimental charges and two sulfide melts, one Fe-rich and one Mg,Mn,Ca,Cr-rich, were found. Thus, it seems highly unlikely that oldhamite found within enstatite chondrites would survive as a relict phase within aubritic parent body. It is possible that oldhamite crystallizes from the Mg,Mn,Ca,Cr-rich sulfide melt or, as noted by Fogel et al. (1996), from the silicate melt, which contains weight-percent levels of dissolved S presumably combined with Ca or Mg. Thus, it appears likely that aubritic oldhamite is a product of igneous crystallization.

Can aubrites be derived by melting of known enstatite chondrites? Although aubrites clearly derived from a highly reduced precursor like enstatite chondrites, Keil (1989) presented several arguments that aubrites and enstatite chondrites formed on different parent bodies. These include the absence of enstatite chondrite clasts within aubritic breccias, the differences in cosmic-ray exposure and thus impact ejection ages, and the implausibility high thermal gradient necessary for a single enstatite chondrite-aubrite parent body. More relevant to this discussion, several differences exist between aubrites and known enstatite chondrites, e.g. Ti contents of troilite, (Keil 1989) and these features are not easily explained by igneous fractionation.

A unique oldhamite-pyroxene clast in Bustee contains the most Ti-rich troilite found in aubrites, as well as the Ti-rich phases osbornite and heideite. Thus, this occurrence may shed some light on the origin of the Ti enrichment in aubritic troilite relative to enstatite chondrite troilite. Previous workers have proposed that Ti could be enriched in aubritic troilite through immiscibility in the Fe-Ti-S system (Brett and Keil 1986), preferential fractionation of Ti-rich FeS (Fogel et al. 1988) or melting of osbornite (Casanova 1992). However, no immiscibility exists in the Fe-Ti-S system; temperature and density difference between Ti-rich and Ti-poor troilite are too small to produce fractionation; and the occurrence of Ti-rich troilite with osbornite in Bustee suggests that melting of osbornite is not producing the Ti-rich troilite. Instead, we suggest that co-crystallization with and/or exsolution from oldhamite provides such a mechanism. Indeed, oldhamite experiments by McCoy et al. (1997c) demonstrated immiscibility in the Fe-Ca-S system, in the form of one sulfide melt enriched in Fe and the other which contained all the Ca in the system. Oldhamite efficiently excludes Ti, which can be preferentially incorporated into troilite, thus providing a mechanism for enriching aubritic troilite in Ti and weakening arguments against a derivation of aubrites from known enstatite chondrites.

In addition, all of the Indarch melting experiments (Dickinson and Lofgren 1992, Fogel et al. 1996, McCoy et al. 1997c) demonstrated significant exchange of elements between different phases (e.g. Si between metal and silicate melt; S between sulfide and silicate melt). This movement of elements might produce compositions not readily predicted on the basis of equilibrium melting relations alone and could explain the origin of some features of aubrites not readily explicable by modeling of equilibrium or fractional partial melting.

HOWARDITES, EUCRITES AND DIOGENITES

The howardite, eucrite and diogenite (HED) meteorites make up the largest suite of crustal igneous rocks we have available from any solar system body other than the Earth

and Moon. These rocks include basalts, cumulate gabbros and orthopyroxenites, plus brecciated mixtures of the igneous lithologies. Together, they provide an unmatched look at differentiation processes that occurred on asteroidal-sized bodies early in the history of the solar system. The HED meteorites have O-isotopic compositions similar to those of the IIIAB irons, main-group pallasites, mesosiderites, angrites and brachinites (Fig. 1c,d), and thus may have been formed in the same region of the solar nebula.

Mineralogy and petrology

Diogenites. The diogenites are coarse-grained orthopyroxenites, typically containing from ~84 to ~100 vol % orthopyroxene (Bowman et al. 1997, Hewins, pers. comm.). Most of them have been brecciated, so the original grain size is not well known, but it must have been at least 5 cm based on the largest reported clasts (Mason 1963). The typical diogenite, for example Johnstown, is composed of orthopyroxene clasts in a fine-grained fragmental matrix of orthopyroxene. Four exceptional diogenites are GRO 95555, LEW 88679, Tatahouine and the Yamato Type A, or Y-74013-type, diogenites. The initial description of GRO 95555 (AMN 19-2) states that this diogenite has a polygonal-granular texture of anhedral orthopyroxene grains from <1 to 2.4 mm in size. The initial description of LEW 88679 (AMN 15-1) states that this diogenite does not have a cataclastic texture, but rather is composed of anhedral grains of pyroxene up to 6 mm in size. Tatahouine apparently broke up during or after atmospheric passage as it is composed of numerous coarse-grained orthopyroxene fragments of cm size, generally without fusion crust on them. Unlike pyroxenes in most diogenites, those in Tatahouine show patchy extinction under crossed polars. The Yamato Type A diogenites have a granoblastic texture composed of equant, rounded orthopyroxene grains a few tens of μm to mm size, containing inclusions dominantly of chromite and troilite.

Chromite and olivine are common minor minerals, each making up between ~0 to 5 vol % (Bowman et al. 1997, Hewins, pers. comm.). EETA79002 may be unusually olivine-rich (Sack et al. 1991, 1994a), but olivine is very heterogeneously distributed in this diogenite (e.g. Bowman et al. 1997), and a mean abundance is currently unknown. Chromite occurs as coarse, mm-sized equant grains as well as in smaller grains a few tens to hundreds of μm in size. The smaller chromite grains are often poikilitically enclosed in orthopyroxene. The coarser chromites are often found as separate euhedral grains or fragments in the matrix, but some are preserved in their original igneous contact with orthopyroxene. Olivine grains are commonly a few hundred μm in size, but they are usually crystal fragments in the matrix. Olivine has been found in Roda in its original textural context with orthopyroxene, where igneous grain borders between the minerals are preserved. A third minor mineral in typical diogenites is anorthitic plagioclase (~0-5 vol %; Bowman et al. 1997, Hewins, pers. comm.). This mineral has not been well described in the literature, but where the textural setting is mentioned, it has been reported only as crystal fragments in the diogenite matrix.

Accessory minerals in the typical diogenite include diopside (~0 to 2 vol %), troilite (~0-3 vol %), metal (<1 vol %), a silica phase (~0 to 2 vol %), and rare phosphates (modal data from Bowman et al. 1997 and Hewins, pers. comm.). Diopside occurs as exsolution lamellae in the orthopyroxene, with thicknesses of at most a few μm. Troilite is highly variable in abundance between different diogenites and within a given diogenite. In some, it is a trace phase usually of μm-sized grains enclosed in orthopyroxene, often forming inclusion "curtains" within the pyroxene (Mori and Takeda 1981a). In other diogenites, troilite occurs as larger equant grains or polycrystalline aggregates in the matrix. Like troilite, metal frequently occurs as μm-sized grains in inclusion "curtains" in orthopyroxene. A silica phase is sometimes associated with metal

and troilite in these inclusion "curtains" (Gooley and Moore 1976). A silica phase is also present as equant grains a few tens of μm in size in some diogenites, but the textural setting has not been well described. Phosphates are rare in diogenites, and not well described. In Roda, two rounded, 5-10 μm size light-rare-earth element-rich phosphates have been found enclosed in diopside exsolved from orthopyroxene (Mittlefehldt 1994).

The Yamato Type B, or Y-75032-type, diogenites are unusual. The many recovered specimens are undoubtedly all pieces of a single fall. These meteorites, described by Takeda et al, (1979a) and Takeda and Mori (1985) are brecciated rocks composed of subangular mineral and lithic clasts set in a black, glassy matrix containing fine-grained, clastic debris. The pyroxene in these meteorites is coarse-grained orthopyroxene and inverted pigeonite a few mm in size, which has exsolved augite lamellae and blebs. Enclosed in the rims of some pyroxene grains and interstitially at grain boundaries are irregular to triangular or lath-shaped plagioclase grains on the order of a few hundred μm in size. Plagioclase also is present as fragmental debris in the black glassy matrix. Chromite occurs as minute inclusions in the pyroxenes, and as clastic debris up to 300 μm in size in the black glassy matrix. Troilite has been reported in the black glassy matrix. Mittlefehldt and Lindstrom (1993) reported ilmenite and a silica polymorph in lithic clasts.

The compositions of pyroxenes in most diogenites are well known (Berkley and Boynton 1992, Fowler et al. 1994, Mittlefehldt 1994, Mittlefehldt and Lindstrom 1993, Sack et al. 1991, Takeda and Mori 1985, Takeda et al. 1979a, 1981). Table 30 gives representative pyroxene compositions for select diogenites, and Figure 42 shows a portion of the pyroxene quadrilateral displaying average orthopyroxene compositions for diogenites. Most diogenites contain orthopyroxene with a very uniform, common major

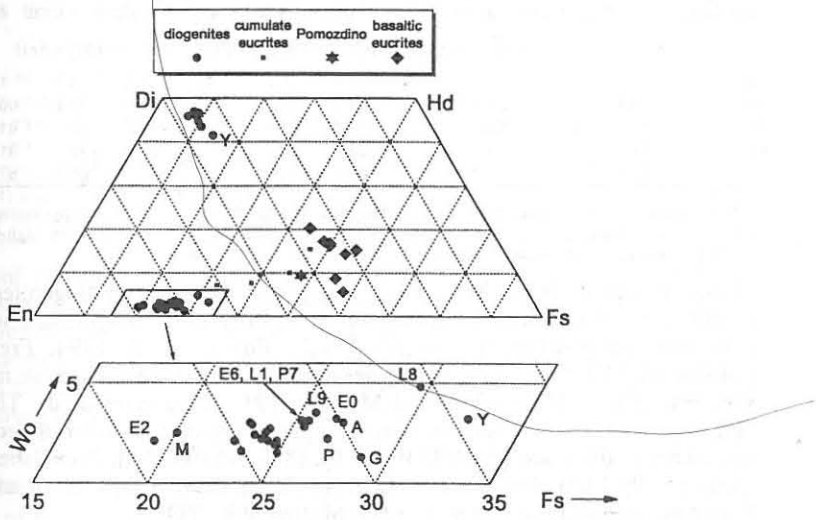

Figure 42. Pyroxene quadrilateral for HED pyroxenes, with detailed view of diogenite orthopyroxene compositions. Labeled diogenites are; E2 - most magnesian pyroxene in EETA79002, M - Manegaon, E6 - EET 83246, L1 - LAP 91900, P7 - PCA 91077, L9 - LEW 88679, P - Peckelsheim, E0 - EET 87530, A - ALH 85015, G - Garland, L8 - LEW 88008, Y - Yamato Type B diogenites. Diogenite data are from Fowler et al. (1994), Mittlefehldt (1994), Mittlefehldt and Lindstrom (1993), Mittlefehldt (unpublished). Bulk pigeonite compositions for cumulate eucrites, anomalous magnesian eucrite Pomozdino and representative basaltic eucrites are from the data in Table 30, plus Metzler et al. (1995). The dispersion of the basaltic eucrite data approximately parallel to lines of constant En content probably reflects the difficulty of determining bulk compositions in the exsolved pyroxenes.

Table 30. Compositions of pyroxene grains from representative diogenites and eucrites.

	EETA79002		PCA 91077	Johnstown		Peckelsheim	EET 87530	Garland	LEW 88008	Y-75032		
	(1)	(2)	(3)	(4)	(5)	(6)	(7)	(8)	(9)	(10)	(11)	(12)
Chemical Composition (wt %t)												
SiO_2	55.6	54.5	54.1	54.1	52.6	54.8	54.1	54.5	53.2	53.4	53.6	53.4
Al_2O_3	0.59	0.85	0.69	0.99	1.11	0.40	0.79	0.32	1.18	0.69	0.77	0.72
TiO_2	0.10	0.10	0.07	0.11	0.20	0.04	0.10	0.02	0.14	0.16	0.35	0.19
Cr_2O_3	0.44	0.60	0.58	0.66	0.55	0.34	0.48	0.39	0.74	0.24	0.45	0.31
FeO	12.7	15.1	16.0	15.4	5.65	17.3	17.4	18.6	19.1	20.3	6.87	20.0
MnO	0.43	0.50	0.56	0.50	0.24	0.59	0.60	0.69	0.67	0.65	0.27	0.66
MgO	29.4	27.5	25.2	26.5	16.0	25.7	25.6	25.4	23.7	23.8	16.4	22.5
CaO	1.10	1.16	1.37	1.24	23.3	1.10	1.60	0.63	2.40	0.67	21.3	2.19
Na_2O	nd	nd	0.02	nd	nd	0.01	nd	nd	nd	nd	bd	nd
Total	100.36	100.31	98.59	99.50	99.65	100.28	100.67	100.55	101.13	99.91	100.01	99.97
Cation Formula Based on 6 Oxygens												
Si	1.9752	1.9623	1.9900	1.9670	1.9499	1.9900	1.9644	1.9851	1.9462	1.9746	1.9747	1.9791
^{iv}Al	0.0247	0.0361	0.0100	0.0330	0.0485	0.0100	0.0338	0.0137	0.0509	0.0254	0.0253	0.0209
Total tet*	1.9999	1.9984	2.0000	2.0000	1.9984	2.0000	1.9982	1.9988	1.9971	2.0000	2.0000	2.0000
Ti	0.0027	0.0027	0.0019	0.0030	0.0056	0.0011	0.0027	0.0005	0.0039	0.0044	0.0097	0.0053
^{vi}Al	--	--	0.0199	0.0094	--	0.0071	--	--	--	0.0047	0.0081	0.0106
Cr	0.0124	0.0171	0.0169	0.0190	0.0161	0.0098	0.0138	0.0112	0.0214	0.0070	0.0131	0.0091
Fe	0.3773	0.4547	0.4922	0.4683	0.1752	0.5254	0.5284	0.5666	0.5844	0.6278	0.2117	0.6199
Mn	0.0129	0.0152	0.0174	0.0154	0.0075	0.0181	0.0185	0.0213	0.0208	0.0204	0.0084	0.0207
Mg	1.5565	1.4756	1.3815	1.4359	0.8839	1.3909	1.3853	1.3788	1.2922	1.3116	0.9005	1.2428
Ca	0.0419	0.0448	0.0540	0.0483	0.9255	0.0428	0.0623	0.0246	0.0941	0.0265	0.8408	0.0870
Na	--	--	0.0014	--	--	0.0007	--	--	--	--	--	--
Total Cations	4.0036	4.0085	3.9852	3.9993	4.0122	3.9959	4.0092	4.0018	4.0139	4.0024	3.9923	3.9954
*Cation Ratios Ca:Mg:Fe, Fe/Mn and mg# (100*Mg/(Mg+Fe))*												
Ca	2.1	2.3	2.8	2.5	46.6	2.2	3.2	1.2	4.8	1.3	43.1	4.5
Mg	78.8	74.7	71.7	73.5	44.5	71.0	70.1	70.0	65.6	66.7	46.1	63.7
Fe	19.1	23.0	25.5	24.0	8.8	26.8	26.7	28.8	29.7	31.9	10.8	31.8
Fe/Mn	29	30	28	30	23	29	29	27	28	31	25	30
mg#	80.5	76.4	73.7	75.4	83.5	72.6	72.4	70.9	68.9	67.6	81.0	66.7

(1, 2) average magnesian and typical pyroxenes, Mittlefehldt, unpublished; (3, 6) average pyroxene, Fowler et al. (1994); (4, 5, 7, 8, 9) average pyroxenes, Mittlefehldt (1994); (10, 11, 12) average low-Ca pyroxene, high-Ca pyroxene and bulk pigeonite, Takeda and Mori (1985). All meteorites are diogenites.

element composition of ~$Wo_{2\pm1}En_{74\pm2}Fs_{24\pm1}$ (Fig. 42). Several diogenites are exceptions to this general uniformity. Manegaon is slightly more magnesian, with an average pyroxene composition of $Wo_{2.8}En_{76.8}Fs_{20.4}$ (Fowler et al. 1994, Fredriksson 1982, Mittlefehldt 1994) and some pyroxenes in EETA79002 are even more magnesian, up to $Wo_{1.8}En_{79.9}Fs_{18.3}$ (Mittlefehldt and Meyers 1991, and unpublished). There are several diogenites that are more ferroan than the typical diogenite. In order of decreasing mg# (in parentheses), these are EET 83246 (73.6), EET 87530 (72.7), Peckelsheim (72.6), ALH 85015 (71.9), LEW 88679 (71.3), Garland (70.8), LEW 88008 (69.6) and Yamato Type B diogenites (66.4) (Fowler et al. 1994, Mittlefehldt 1994).

Excluding low-Ca clinopyroxenes formed by shock deformation of orthopyroxene (Mori and Takeda 1981a), clinopyroxenes in diogenites are the product of subsolidus exsolution from the orthopyroxene or low-Ca pigeonite (for Yamato Type B diogenites) grains. Few analyses of these clinopyroxenes are available in the literature. For typical diogenites, many of the clinopyroxenes are too narrow to analyze with the electron probe. Mori and Takeda (1981a) determined an average lamella width of 77 nm for Ibbenbüren and 6 nm for Johnstown. They identified these as augite. Larger clinopyroxene grains are

Table 30 (cont'd). Compositions of pyroxene grains from representative diogenites and eucrites.

	Binda			Moama			Serra de Magé			Moore County		
	(13)	(14)	(15)	(16)	(17)	(18)	(19)	(20)	(21)	(22)	(23)	(24)
Chemical Composition (wt %)												
SiO_2	53.4	53.0	53.3	51.6	51.7	51.5	52.3	52.7	52.4	51.5	52.1	51.6
Al_2O_3	0.51	0.85	0.55	0.39	0.62	0.47	0.34	0.69	0.40	0.24	0.78	0.30
TiO_2	0.22	0.37	0.24	0.28	0.40	0.29	0.24	0.37	0.26	0.31	0.67	0.35
Cr_2O_3	0.24	0.40	0.26	0.27	0.37	0.27	0.12	0.23	0.14	0.15	0.32	0.17
FeO	21.7	8.48	20.1	24.8	11.3	23.9	27.4	10.5	24.4	29.2	13.9	27.3
MnO	0.71	0.37	0.67	0.89	0.47	0.80	0.95	0.42	0.85	0.97	0.48	0.91
MgO	22.2	14.7	21.3	19.2	13.1	18.6	18.6	13.4	17.6	15.5	12.2	15.1
CaO	1.05	21.6	3.52	1.65	22.3	3.71	0.75	22.3	4.62	2.65	19.7	4.70
Na_2O	bd	0.06	0.01	bd	0.05	bd	0.02	0.07	nd	bd	0.07	0.01
Total	100.03	99.83	99.95	99.08	100.31	99.54	100.72	100.68	100.67	100.52	100.22	100.44
Cation Formula Based on 6 Oxygens												
Si	1.9866	1.9745	1.9846	1.9782	1.9528	1.9688	1.9865	1.9699	1.9852	1.9903	1.9740	1.9896
^{iv}Al	0.0134	0.0255	0.0154	0.0176	0.0276	0.0212	0.0135	0.0301	0.0148	0.0097	0.0260	0.0104
Total tet*	2.0000	2.0000	2.0000	1.9958	1.9804	1.9900	2.0000	2.0000	2.0000	2.0000	2.0000	2.0000
Ti	0.0062	0.0104	0.0067	0.0081	0.0114	0.0083	0.0069	0.0104	0.0074	0.0090	0.0191	0.0101
^{vi}Al	0.0090	0.0118	0.0087	--	--	--	0.0017	0.0003	0.0031	0.0012	0.0088	0.0032
Cr	0.0071	0.0118	0.0077	0.0082	0.0110	0.0082	0.0036	0.0068	0.0042	0.0046	0.0096	0.0052
Fe	0.6752	0.2642	0.6259	0.7951	0.3570	0.7641	0.8704	0.3282	0.7731	0.9438	0.4405	0.8803
Mn	0.0224	0.0117	0.0211	0.0289	0.0150	0.0259	0.0306	0.0133	0.0273	0.0318	0.0154	0.0297
Mg	1.2309	0.8162	1.1819	1.0970	0.7374	1.0597	1.0529	0.7465	0.9937	0.8928	0.6889	0.8677
Ca	0.0419	0.8623	0.1404	0.0678	0.9025	0.1520	0.0305	0.8931	0.1875	0.1097	0.7998	0.1942
Na	--	0.0043	0.0007	--	0.0037	--	0.0015	0.0051	--	--	0.0051	0.0007
Total Cations	3.9927	3.9927	3.9931	4.0009	4.0184	4.0082	3.9981	4.0037	3.9963	3.9929	3.9872	3.9911
*Cation Ratios Ca:Mg:Fe, Fe/Mn and mg# (100*Mg/(Mg+Fe))*												
Ca	2.1	44.4	7.2	3.5	45.2	7.7	1.6	45.4	9.6	5.6	41.5	10.0
Mg	63.2	42.0	60.7	56.0	36.9	53.6	53.9	37.9	50.8	45.9	35.7	44.7
Fe	34.7	13.6	32.1	40.6	17.9	38.7	44.5	16.7	39.6	48.5	22.8	45.3
Fe/Mn	30	23	30	28	24	29	28	25	28	30	29	30
mg#	64.6	75.5	65.4	58.0	67.4	58.1	54.7	69.5	56.2	48.6	61.0	49.6

(13, 14, 15, 22, 23, 24) average low-Ca pyroxene, high-Ca pyroxene and bulk pigeonite, Pun and Papike (1995); (16, 17, 18) average low-Ca pyroxene, high-Ca pyroxene and bulk pigeonite Lovering (1975); (19, 20, 21) average low-Ca pyroxene, high-Ca pyroxene and bulk pigeonite Harlow et al. (1979). All meteorites are cumulate eucrites.

present in both of the meteorites, and have been analyzed by electron microprobe by Floran et al. (1981) and Mittlefehldt (1994). The larger clinopyroxene grains in diogenites are compositionally diopside. The clinopyroxene grains in the Yamato Type B diogenites are augites based on both compositional and crystallographic criteria (Mittlefehldt and Lindstrom 1993, Takeda and Mori 1985, Takeda et al. 1979a). Table 30 gives representative clinopyroxene analyses from selected diogenites.

Although the major elements in diogenite orthopyroxene grains are very uniform, the minor incompatible elements show considerable variation. Mittlefehldt (1994) showed that the contents of Al_2O_3 and TiO_2, for average orthopyroxenes vary by factors of ~3 and 4, respectively, and are positively correlated. Fowler et al. (1994) further showed that the minor incompatible element contents for orthopyroxene from individual diogenites can also be highly variable, with Al contents varying by a factor of 2 in pyroxenes from ALH 85015, for example. The variation in incompatible elements is decoupled from mg#, and orthopyroxenes with similar mg# can have quite different TiO_2 and Al_2O_3 contents (Mittlefehldt 1994). The compatible minor element Cr varies as well by factors of 2 to 3 (Fowler et al. 1994, Mittlefehldt 1994). Berkley and Boynton (1992) found a weak

Table 30 (cont'd). Compositions of pyroxene grains from representative diogenites and eucrites.

	Y-791195			Pomozdino			Sioux County		Bouvante	Y-75011 ,84C		Y-793164
	(25)	(26)	(27)	(28)	(29)	(30)	(31)	(32)	(33)	(34)	(35)	(36)
Chemical Composition (wt %)												
SiO_2	49.9	51.1	50.3	50.6	51.4	50.7	49.1	50.7	49.8	53.4	47.4	48.5
Al_2O_3	0.27	0.68	0.33	0.29	0.87	0.47	0.23	0.47	0.15	0.84	0.96	0.59
TiO_2	0.16	0.40	0.23	0.30	0.65	0.36	0.25	0.32	0.13	0.10	0.82	0.33
Cr_2O_3	0.11	0.28	0.15	0.16	0.30	0.29	0.42	0.39	0.15	0.75	0.10	0.61
FeO	32.6	15.5	28.0	31.3	14.2	28.5	36.1	16.6	34.1	17.6	33.1	32.2
MnO	1.05	0.50	0.90	0.98	0.48	0.92	1.12	0.53	0.85	0.58	0.99	0.98
MgO	13.6	11.2	12.9	15.2	12.0	14.3	11.7	9.84	12.0	24.5	4.31	9.4
CaO	2.34	20.4	7.30	1.19	20.0	4.39	0.78	20.8	2.58	2.05	11.9	6.90
Na_2O	nd	nd	nd	0.04	0.10	0.05	nd	nd	nd	bd	0.03	nd
Total	100.03	100.06	100.11	100.06	100.00	99.98	99.70	99.65	99.76	99.82	99.61	99.51
Cation Formula Based on 6 Oxygens												
Si	1.9752	1.9620	1.9734	1.9801	1.9598	1.9780	1.9786	1.9695	1.9903	1.9627	1.9537	1.9606
^{iv}Al	0.0126	0.0308	0.0153	0.0134	0.0391	0.0216	0.0109	0.0215	0.0071	0.0364	0.0463	0.0281
Total tet*	1.9878	1.9928	1.9887	1.9935	1.9989	1.9996	1.9895	1.9910	1.9974	1.9991	2.0000	1.9887
Ti	0.0048	0.0116	0.0068	0.0088	0.0186	0.0106	0.0076	0.0093	0.0039	0.0028	0.0254	0.0100
^{vi}Al	--	--	--	--	--	--	--	--	--	--	0.0003	--
Cr	0.0034	0.0085	0.0047	0.0050	0.0090	0.0089	0.0134	0.0120	0.0047	0.0218	0.0033	0.0195
Fe	1.0792	0.4977	0.9187	1.0244	0.4528	0.9299	1.2166	0.5393	1.1398	0.5410	1.1410	1.0886
Mn	0.0352	0.0163	0.0299	0.0325	0.0155	0.0304	0.0382	0.0174	0.0288	0.0181	0.0346	0.0336
Mg	0.8023	0.6409	0.7543	0.8865	0.6819	0.8314	0.7027	0.5697	0.7148	1.3420	0.2647	0.5663
Ca	0.0992	0.8393	0.3069	0.0499	0.8171	0.1835	0.0337	0.8658	0.1105	0.0807	0.5255	0.2989
Na	--	--	--	0.0030	0.0074	0.0038	--	--	--	--	0.0024	--
Total Cations	4.0119	4.0071	4.0100	4.0036	4.0012	3.9981	4.0017	4.0045	3.9999	4.0055	3.9972	4.0056
*Cation Ratios Ca:Mg:Fe, Fe/Mn and mg# (100*Mg/(Mg+Fe))*												
Ca	5.0	42.4	15.5	2.5	41.9	9.4	1.7	43.8	5.6	4.1	27.2	15.3
Mg	40.5	32.4	38.1	45.2	34.9	42.8	36.0	28.8	36.4	68.3	13.7	29.0
Fe	54.5	25.2	46.4	52.2	23.2	47.8	62.3	27.3	58.0	27.5	59.1	55.7
Fe/Mn	31	31	31	32	29	31	32	31	40	30	33	32
mg#	42.6	56.3	45.1	46.4	60.1	47.2	36.6	51.4	38.5	71.3	18.8	34.2

(25, 26, 27) average low-Ca pyroxene, high-Ca pyroxene and bulk pigeonite, cumulate eucrite, Mittlefehldt and Lindstrom (1993); (28, 29, 30) average low-Ca pyroxene, high-Ca pyroxene and bulk pigeonite, anomalous, magnesian eucrite, Warren et al. (1990); (31, 32) average low-Ca pyroxene and high-Ca pyroxene, main-group eucrite, Mittlefehldt, unpublished; (33) average core, large pigeonite, Stannern-trend eucrite, Christophe Michel-Levy et al. (1987); (34, 35) core and rim pyroxene in least-metamorphosed basalt clast from polymict eucrite, Takeda et al. (1994c); (36) average bulk pigeonite, evolved, recrystalized basalt clast from polymict eucrite, Mittlefehldt and Lindstrom (1993).

positive correlation between orthopyroxene Cr_2O_3 content and mg# within individual diogenites.

There are relatively few analyses of diogenite olivine in the literature (Floran et al. 1981, Gooley 1972, Mittlefehldt 1994, Sack et al. 1991), and because many of them are either fragments in the matrix, or are of unknown textural context, it is difficult to know how they fit in diogenite petrogenesis. Representative olivine analyses are given in Table 31. Hewins (1981) found that orthopyroxene and olivine in 5 diogenites have an equilibrium distribution of Fe/Mn. Mittlefehldt (1994) presented data for olivine from Roda for grains in igneous contact with orthopyroxene, the only such case documented in the literature. The Fe/Mg data are compatible with subsolidus equilibration between olivine and orthopyroxene (Mittlefehldt 1994). Olivines in diogenites with the typical orthopyroxene composition are in the range Fo_{70-73} (Floran et al. 1981, Mittlefehldt 1994, Sack et al. 1991), whereas olivines from the slightly more ferroan diogenite Peckelsheim have an average composition of Fo_{65} (Gooley 1972), and those from the magnesian-

Table 31. Olivine analyses for representative diogenites, eucrites and howardites.

	Ellemeet (1)	Johnstown (2)	Peckelsheim (3)	Roda (4)	Y-793164 (5)	Washougal (6)	Y-7308 (7)	Y-82049 (8)	Y-82049 (9)	Yurtuk (10)
Chemical Composition (wt %)										
SiO_2	37.1	37.5	35.89	36.9	31.0	40.2	36.70	36.2	35.0	37.0
FeO	26.9	25.8	30.69	24.9	60.4	12.1	26.55	33.6	37.6	30.7
MgO	35.1	35.9	32.65	36.9	6.9	47.3	36.17	30.0	26.5	32.4
MnO	0.55	0.51	0.44	0.52	1.26	0.28	0.50	0.63	0.72	0.57
Cr_2O_3	0.03	0.03	nd	0.02	nd	0.10	bd	nd	nd	0.02
CaO	0.07	0.07	0.02	0.04	0.08	0.07	0.03	0.06	0.05	0.04
Total	99.75	99.81	99.69	99.3	99.60	100.05	99.95	100.49	99.87	100.73
Cation Formula Based on 4 Oxygens										
Si	0.9921	0.9959	0.9799	0.9832	1.0009	0.9960	0.9789	0.9931	0.9887	0.9966
Fe	0.6016	0.5730	0.7008	0.5549	1.6309	0.2507	0.5923	0.7709	0.8883	0.6915
Mg	1.3988	1.4208	1.3286	1.4653	0.3301	1.7466	1.4378	1.2265	1.1156	1.3006
Mn	0.0125	0.0115	0.0102	0.0117	0.0345	0.0059	0.0113	0.0146	0.0172	0.0130
Cr	0.0006	0.0006	--	0.0004	--	0.0020	--	--	--	0.0004
Ca	0.0020	0.0020	0.0006	0.0011	0.0028	0.0019	0.0009	0.0018	0.0015	0.0012
Total Cations	3.0076	3.0038	3.0201	3.0166	2.9992	3.0031	3.0212	3.0069	3.0113	3.0033
*Cation Ratios Fe/Mn and mg# (100*Mg/(Mg+Fe))*										
Fe/Mn	48	50	69	-	47	43	52	53	52	53
mg#	69.9	71.3	65.5	72.5	16.8	87.4	70.8	61.4	55.7	65.3

(1,4) Mittlefehldt (1994); (2) Floran et al. (1981); (3) Gooley (1972); (5, 8, 9) Mittlefehldt and Lindstrom (1993); (6,10) Desnoyers (1982); (7) Miyamoto et al. (1978).

pyroxene bearing diogenite EETA79002 have an average composition of Fo_{76} (Sack et al. 1991, 1994a, and Mittlefehldt, unpublished).

Chromite analyses for diogenites have been presented by Berkley and Boynton (1992), Floran et al. (1981), Fredriksson (1982), Gooley (1972), Mittlefehldt (1994), Mittlefehldt and Lindstrom (1993) and Sack et al. (1991), and ilmenite analyses for Yamato Type B diogenites have been given by Mittlefehldt and Lindstrom (1993). Representative chromite and ilmenite analyses are given in Table 32. Unlike the orthopyroxenes and olivines, chromites in diogenites are variable in mg#. Sack et al. (1991, 1994a) show a range in mg# for EETA79002 chromites from ~14 to 32. This is essentially the same as the range found for the averages of chromites from all diogenites. The range in Al_2O_3 contents of average chromites is considerable, from ~6.8 to 21.6 wt %, excluding small chromites (Mittlefehldt 1994). Within individual diogenites, chromite grains can also be variable in Al_2O_3 composition. Gooley reported a range in Al_2O_3 content in Roda chromites from 8.6 to 18.6 wt %, although most of the grains he analyzed contained between 8.6 and 10.2 wt %. Mittlefehldt (1994) and Mittlefehldt and Lindstrom (1993) showed that small grains were of different composition than large grains, but the differences were not systematic; small grains in Shalka had lower Al_2O_3 contents and lower mg# than large grains, the opposite was true for ALHA77256, while for Yamato Type A diogenites small chromites had higher Al_2O_3 and lower mg#.

Few analyses of plagioclase from diogenites are available. Analyses are given for Garland, Johnstown, Manegaon, Peckelsheim, Roda and Yamato Type B diogenites by Floran et al. (1981), Fredriksson (1982), Gooley (1972), Mittlefehldt (1978, 1994) and Mittlefehldt and Lindstrom (1993). Most plagioclase in diogenites lies in the range An_{82}-An_{96}, although plagioclase as sodic as An_{73-76} is present in Peckelsheim, LEW 88679 and Yamato Type B diogenites (Gooley 1972, Takeda and Mori 1985, Mittlefehldt, unpublished). Table 33 gives representative plagioclase analyses from selected diogenites.

Table 32. Compositions of chromite and ilmenite grains from representative diogenites and eucrites.

	Shalka	Johns-town	Mane-gaon	ALHA 77256	Y-75032		Moama	Serra de Magé		Moore County		Y-791195		Pomozdino		Peters-burg
	(1)	(2)	(3)	(4)	(5)	(6)	(7)	(8)	(9)	(10)	(11)	(12)	(13)	(14)	(15)	(16)
Chemical Composition (wt %)																
TiO_2	0.50	0.42	0.22	0.78	1.96	54.1	5.39	3.2	52.9	10.1	52.9	11.9	51.6	4.52	54.3	3.68
Al_2O_3	6.84	9.37	16.1	21.6	7.90	0.02	7.72	8.3	0.08	5.7	bd	5.02	0.03	7.30	0.07	14.5
Cr_2O_3	60.6	56.3	48.7	43.8	55.0	0.37	50.1	53.0	0.27	42.3	0.19	39.1	1.75	49.8	0.22	43.9
V_2O_3	0.96	0.35	0.40	0.40	0.59	bd	0.67	0.73	bd	0.81	bd	0.76	bd	0.68	0.23	nd
FeO	27.2	30.1	27.8	27.0	31.8	42.4	32.7	33.1	42.8	39.5	42.9	42.2	44.7	34.2	43.5	34.3
MgO	3.90	2.54	4.33	6.24	1.95	3.15	2.38	1.30	2.35	1.31	1.92	0.98	1.36	1.15	1.56	1.63
MnO	0.51	0.51	0.49	0.43	0.55	0.89	0.81	0.58	0.86	0.66	0.82	0.60	0.90	0.67	1.10	0.51
Total	100.51	99.59	98.04	100.25	99.75	100.93	99.77	100.21	99.26	100.38	98.73	100.56	100.34	98.32	100.98	98.52
Cation Formula Based on 4 Oxygens (Ideal Spinel = 3 Cations per 4 Oxygens, Ideal Ilmenite = 2 Cations per 3 Oxygens)																
Ti	0.0131	0.0111	0.0056	0.0189	0.0523	0.9943	0.1428	0.0849	1.3255	0.2714	1.0010	0.3216	0.9709	0.1231	1.3392	0.0723
Al	0.2808	0.3883	0.6479	0.8211	0.3301	0.0006	0.3205	0.3453	0.0031	0.2400	--	0.2126	0.0009	0.3116	0.0027	0.4467
Cr	1.6686	1.5649	1.3147	1.1168	1.5418	0.0071	1.3953	1.4790	0.0071	1.1949	0.0038	1.1108	0.0346	1.4257	0.0057	0.9072
V	0.0268	0.0099	0.0110	0.0103	0.0168	--	0.0189	0.0207	--	0.0232	--	0.0219	--	0.0197	0.0060	--
Fe	0.7922	0.8850	0.7938	0.7282	0.9429	0.8666	0.9633	0.9770	1.1926	1.1803	0.9028	1.2681	0.9353	1.0357	1.1931	0.7497
Mg	0.2024	0.1331	0.2203	0.2999	0.1030	0.1147	0.1249	0.0684	0.1167	0.0698	0.0720	0.0525	0.0507	0.0621	0.0762	0.0635
Mn	0.0150	0.0152	0.0142	0.0117	0.0165	0.0184	0.0242	0.0173	0.0243	0.0200	0.0175	0.0183	0.0191	0.0205	0.0306	0.0113
Total Cations	2.9989	3.0075	3.0075	3.0069	3.0034	2.0017	2.9899	2.9926	2.6693	2.9996	1.9971	3.0058	2.0115	2.9984	2.6535	2.2507
*Cation Ratios Fe/Mn, mg# (100*Mg/(Mg+Fe)) and cr# (100*Cr/(Cr+Al))*																
Fe/Mn	53	58	56	62	57	47	40	56	49	59	52	69	49	50	39	66
mg#	20.4	13.1	21.7	29.2	9.9	11.7	11.5	6.5	8.9	5.6	7.4	4.0	5.1	5.7	6.0	7.8
cr#	85.6	80.1	67.0	57.6	82.4	92.5	81.3	81.1	69.4	83.3	100.0	83.9	97.5	82.1	67.8	67.0

(1-4) average typical chromites, diogenites, Mittlefehldt (1994); (5, 6) average chromite and ilmenite, diogenite, Mittlefehldt (unpublished); (7) average chromite, cumulate eucrite, Lovering (1975); (8-11) average chromite and ilmenite, cumulate eucrite, Bunch and Keil (1971); (12,13) average chromite and ilmenite, cumulate eucrite, Mittlefehldt and Lindstrom (1993); (14, 15) average chromite and ilmenite, anomalous magnesian eucrite, Warren et al. (1990); (16) average chromite, magnesian basalt clast, polymict eucrite, Buchanan and Reid (1996).

Table 32 (cont'd). Compositions of chromite and ilmenite grains from representative diogenites and eucrites.

	Ibitira		Bouvante		Stannern	Sioux County		Y-82066	Millbillillie		Juvinas		Pasamonte		Y-75011,84C	Y-793164
	(17)	(18)	(19)	(20)	(21)	(22)	(23)	(24)	(25)	(26)	(27)	(28)	(29)	(30)	(31)	(32)
Chemical Composition (Weight Percent)																
TiO_2	23.8	53.2	4.20	53.2	52.9	3.4	52.9	52.0	2.37	52.5	5.0	52.5	1.38	52.5	53.2	51.5
Al_2O_3	3.01	nd	8.15	bd	0.08	7.2	0.03	0.01	8.09	0.06	7.9	0.06	17.7	0.11	0.06	0.01
Cr_2O_3	19.8	nd	51.7	0.12	0.05	51.6	0.06	0.08	52.6	0.03	50.6	0.05	44.4	0.10	0.03	0.06
V_2O_3	nd	nd	nd	nd	bd	0.93	bd	bd	nd	nd	0.77	bd	0.61	bd	bd	bd
FeO	50.6	43.1	34.5	44.8	44.7	35.5	45.0	45.5	33.4	44.3	35.5	44.7	34.5	44.6	44.5	45.7
MgO	1.39	1.58	0.52	0.54	0.49	0.28	0.61	0.78	0.36	0.63	0.24	0.85	0.74	0.46	0.53	0.50
MnO	0.71	0.36	0.57	1.02	0.87	0.62	0.87	0.94	0.58	0.96	0.63	0.87	0.46	0.85	1.14	0.90
Total	99.31	98.24	99.64	99.68	99.09	99.53	99.47	99.31	97.40	98.48	100.64	99.03	99.79	98.62	99.46	98.67
Cation Formula Based on 4 Oxygens (Ideal Spinel = 3 Cations per 4 Oxygens, Ideal Ilmenite = 2 Cations per 3 Oxygens)																
Ti	0.6233	1.4066	0.1078	1.2903	1.4105	0.0625	1.4013	1.3802	0.0594	1.4107	0.1262	1.4187	0.0346	1.4297	1.3121	1.3497
Al	0.1236	--	0.3280	--	0.0033	0.2074	0.0012	0.0004	0.3177	0.0025	0.3124	0.0025	0.6959	0.0047	0.0023	0.0004
Cr	0.5452	--	1.3957	0.0031	0.0014	0.9970	0.0017	0.0022	1.3856	0.0008	1.3422	0.0014	1.1710	0.0029	0.0008	0.0017
V	--	--	--	--	--	0.0182	--	--	--	--	0.0207	--	0.0163	--	--	--
Fe	1.4737	1.2672	0.9851	1.2083	1.3254	0.7256	1.3256	1.3430	0.9307	1.3237	0.9961	1.3433	0.9625	1.3506	1.2205	1.3319
Mg	0.0721	0.0828	0.0265	0.0260	0.0259	0.0102	0.0320	0.0410	0.0179	0.0335	0.0120	0.0455	0.0368	0.0248	0.0259	0.0260
Mn	0.0209	0.0107	0.0165	0.0279	0.0261	0.0128	0.0260	0.0281	0.0164	0.0291	0.0179	0.0265	0.0130	0.0261	0.0317	0.0266
Total Cations	2.8588	2.7673	2.8596	2.5556	2.7926	2.0337	2.7878	2.7949	2.7277	2.8003	2.8275	2.8379	2.9301	2.8388	2.5933	2.7363
*Cation Ratios Fe/Mn, mg# (100*Mg/(Mg+Fe)) and cr# (100*Cr/(Cr+Al))*																
Fe/Mn	70	118	60	43	51	57	51	48	57	46	56	51	74	52	39	50
mg#	4.7	6.1	2.6	2.1	1.9	1.4	2.4	3.0	1.9	2.5	1.2	3.3	3.7	1.8	2.1	1.9
cr#	81.5	--	81.0	100.0	29.5	82.8	57.3	84.3	81.3	25.1	81.1	35.9	62.7	37.9	25.1	80.1

(17, 18) individual chromite and ilmenite grains, basaltic eucrite, Steele and Smith (1976); (19,20) average chromite and ilmenite, Stannern-trend eucrite, Christophe Michel-Levy et al. (1987); (21) average ilmenite, Stannern-trend eucrite, Bunch and Keil (1971); (22, 23) average chromite and ilmenite, main-group eucrite, Bunch and Keil (1971); (24) aveargе ilmenite, main-group eucrite, Mittlefehldt and Lindstrom (1993); (25, 26) average chromite and ilmenite, main-group eucrite, Yamaguchi et al. (1994); (27-30) average chromite and ilmenite, main-group eucrites, Bunch and Keil (1971); (31) ilmenite, least-metamorphosed basalt clast, polymict eucrite, Takeda et al. (1994c); (32) average ilmenite, evolved basalt clast, polymict eucrite, Mittlefehldt and Lindstrom (1993).

Little is known of the composition of metal in diogenites. Gooley and Moore (1976) classified the metal as to textural setting depending on whether it occurred enclosed in orthopyroxene clasts or in the fragmental matrix. The mineralogy of the metal was not identified for 5 of the meteorites they studied, but for Ibbenbüren, Peckelsheim and Roda both kamacite and taenite occur. The metal in diogenites shows a wide range in Ni and Co contents, even within a single meteorite. For metal grains of unspecified mineralogy, median Ni contents range from ~0.07 wt % for that in the matrix of Shalka to 7.7 wt % for metal in the matrix of Ellemeet. Cobalt is variable too, from 0.11-1.7 wt % in these same grains, and the median Ni/Co ratio varies from 0.04-64.5. Roda contains some metal that is unusually rich in Co, with a median composition of 2.0 wt % Ni and 23.6 wt % Co. Kamacite varies in composition from 2.2-3.8 wt % Ni and from 0.5-7.6 wt % Co. Taenite varies in composition from 15.4-53.3 wt % Ni and from 1.1-2.7 wt % Co.

Cumulate eucrites. Cumulate eucrites are coarse-grained gabbros composed principally of low-Ca pyroxene and calcic plagioclase, with minor chromite and accessory silica polymorph, phosphate, ilmenite, metal, troilite (e.g. Delaney et al. 1984). Zircon has been listed for Serra de Magé, but the attribution is unclear (Gomes and Keil 1980, p. 77). Many cumulate eucrites are unbrecciated; ALH 85001, Binda, EET 87548 and Medanitos are exceptional in this. Binda, in fact, is a polymict breccia (Garcia and Prinz 1978) and some polymict eucrites contain abundant cumulate eucrite material (e.g. see Takeda 1991). The textures of unbrecciated cumulate eucrites are typically equigranular with subequal amounts of pyroxene and plagioclase grains 0.5-3 mm in diameter (Hess and Henderson 1949, Lovering 1975, Mittlefehldt and Lindstrom 1993). The cumulate eucrites have been subdivided into the feldspar- and orthopyroxene-cumulate eucrites based on modal abundances (Delaney et al. 1984).

The original igneous pyroxene of cumulate eudrites was pigeonite, which has subsequently undergone subsolidus exsolution of augite and, in some cases, inversion to orthopyroxene, with additional augite exsolution. Hess and Henderson (1949) determined that original pigeonite in Moore County had only partially inverted to orthopyroxene. They described four pyroxenes in Moore County; low-Ca pigeonite developed from the original igneous pigeonite by exsolution of coarse lamellae of augite, and hypersthene developed from the low-Ca pigeonite through inversion and exsolution of fine lamellae of salite. Mori and Takeda (1981b) found that the original pigeonite underwent a complex series of exsolution, decomposition and partial inversion to end as a mixture of seven pyroxene phases. Harlow et al. (1979) found that the original igneous pigeonite in Serra de Magé had inverted to hypersthene, with development of four types of augite exsolution during the subsolidus cooling history. Similarly, in Moama the original igneous pigeonite has exsolved augite and inverted to hypersthene (Lovering 1975, Takeda et al. 1976). Binda is the most magnesian of the cumulate eucrites, and the only one classified by Delaney et al. (1984) as an orthopyroxene-cumulate eucrite. Takeda et al. (1976) have shown that the original pyroxene in Binda was a low-Ca pigeonite that exsolved augite and inverted to hypersthene. Table 30 gives representative pyroxene analyses for selected cumulate eucrites, and estimated primary pigeonite compositions are plotted in Figure 42.

As is the case for all HED meteorites, plagioclase in cumulate eucrites is calcic, and is on average more calcic than that in basaltic eucrites. Basaltic eucrite plagioclase has compositions in the range of bytownite to anorthite, while in cumulate eucrites the plagioclase is anorthite, An_{91-95}. A-881394 contains unusually calcic plagioclase, An_{98} (Takeda et al. 1997b). The K_2O contents of cumulate eucrite plagioclases are very low, typically <0.1 wt %. Representative plagioclase analyses for selected cumulate eucrites are given in Table 33.

Table 33. Plagioclase analyses for representative diogenites, cumulate eucrites and basaltic eucrites.

	Johnstown (1)	LEW 88679 (2)	LEW 88679 (3)	Manegaon (4)	Peckelsheim (5)	Peckelsheim (6)	Roda (7)	Y-75032 (8)	Y-75032 (9)	Moama (10)	Serra de Magé (11)	Moore County (12)
Chemical Composition (wt %)												
SiO_2	46.7	46.0	50.5	45.5	46.0	50.8	46.2	45.7	48.4	45.0	44.8	45.3
Al_2O_3	33.8	34.9	31.9	34.4	35.1	32.3	35.3	35.5	34.0	35.8	35.0	35.5
FeO	0.29	0.23	0.21	0.11	0.73	0.86	0.05	0.50	0.14	0.09	0.12	0.12
MgO	0.46	0.04	0.09	0.10	-	-	0.05	-	-	0.08	bd	nd
CaO	16.9	18.1	15.0	18.0	17.9	14.6	18.0	17.9	16.9	19.3	19.5	18.5
Na_2O	1.39	1.08	2.44	1.51	1.07	2.89	1.35	0.97	1.76	0.63	0.54	0.93
K_2O	0.07	0.03	0.18	0.10	0.02	0.14	0.10	0.03	0.22	0.02	0.02	0.06
Total	99.61	100.38	100.32	99.72	100.88	101.64	101.05	100.60	101.42	100.85	99.98	100.41
Cation Formula Based on 8 Oxygens (Ideal Plagioclase = 5 Cations per 8 Oxygens)												
Si	2.1522	2.1099	2.2920	2.1055	2.1030	2.2833	2.1049	2.0925	2.1877	2.0607	2.0715	2.0800
ivAl	1.8361	1.8868	1.7066	1.8764	1.8936	1.7109	1.8957	1.9159	1.8115	1.9307	1.9076	1.9213
Total tet*	3.9883	3.9967	3.9986	3.9819	3.9966	3.9942	4.0006	4.0084	3.9992	3.9914	3.9791	4.0013
Fe	0.0112	0.0088	0.0080	0.0043	0.0279	0.0323	0.0019	0.0191	0.0053	0.0034	0.0046	0.0046
Mg	0.0316	0.0027	0.0061	0.0069	0.0000	0.0000	0.0034	0.0000	0.0000	0.0055	0.0000	0.0000
Ca	0.8345	0.8896	0.7295	0.8925	0.8778	0.7049	0.8787	0.8782	0.8185	0.9450	0.9661	0.9102
Na	0.1242	0.0961	0.2147	0.1355	0.0949	0.2518	0.1193	0.0861	0.1543	0.0559	0.0484	0.0828
K	0.0041	0.0018	0.0104	0.0059	0.0012	0.0080	0.0058	0.0018	0.0127	0.0012	0.0012	0.0035
Total Cations	4.9939	4.9957	4.9673	5.0270	4.9984	4.9912	5.0097	4.9936	4.9900	5.0024	4.9994	5.0024
*Cation Ratios 100*Mg/(Mg+Fe) (mg#) and Molecular Proportion of Orthoclase (Or), Albite (Ab), Anorthite (An)*												
mg#	73.9	23.7	43.3	61.8	-	-	64.1	-	-	61.3	-	-
Or	0.4	0.2	1.1	0.6	0.1	0.8	0.6	0.2	1.3	0.1	0.1	0.4
Ab	12.9	9.7	22.5	13.1	9.7	26.1	11.9	8.9	15.7	5.6	4.8	8.3
An	86.7	90.1	76.4	86.3	90.2	73.1	87.5	90.9	83.0	94.3	95.1	91.3

(1) Floran et al. (1981); (2, 3) Mittlefehldt, unpublished; (4) Fredriksson (1982); (5, 6) Gooley (1972); (7) Mittlefehldt (1994); (8, 9) Mittlefehldt, unpublished data used in Mittlefehldt and Lindstrom (1993); (10) Lovering (1975); (11) Gomes and Keil (198x); (12) Mittlefehldt, unpublished data used in Mittlefehldt (1990).

Table 33 (cont'd). Plagioclase analyses for representative diogenites, cumulate eucrites and basaltic eucrites.

	Y-791195	Bou-vante	Bou-vante	Ibitira	Juvinas	Pasa-monte	Peters-burg	Pomoz-dino	Y-82049	Y-82049	Y-793164	Y-793164
	(13)	(14)	(15)	(16)	(17)	(18)	(19)	(20)	(21)	(22)	(23)	(24)
Chemical Composition (wt %)												
SiO_2	45.8	45.9	50.4	44.8	45.9	46.6	48.0	46.8	44.565	49.215	45.328	52.195
Al_2O_3	35.8	34.2	31.8	35.9	33.2	33.0	34.0	33.0	35.992	32.736	34.165	31.09
FeO	0.25	0.21	0.22	0.21	1.20	0.90	0.12	0.40	0.12	0.389	1.407	0.19
MgO	nd	0.01	0.01	nd	0.30	bd	0.73	0.01	nd	nd	nd	nd
CaO	18.6	18.0	15.2	18.7	18.0	17.4	17.4	18.4	19.008	16.187	17.671	13.758
Na_2O	1.00	1.23	2.42	0.50	1.00	1.80	1.27	1.62	0.706	1.845	0.664	2.669
K_2O	0.07	0.08	0.49	0.08	bd	bd	0.09	0.15	0.049	0.22	0.112	0.479
Total	101.52	99.64	100.49	100.11	99.60	99.70	101.61	100.38	100.44	100.59	99.35	100.38
Cation Formula Based on 8 Oxygens (Ideal Plagioclase = 5 Cations per 8 Oxygens)												
Si	2.0812	2.1243	2.2884	2.0623	2.1323	2.1588	2.1666	2.1557	2.0496	2.2382	2.1097	2.3571
^{iv}Al	1.9175	1.8618	1.7016	1.9482	1.8179	1.8020	1.8089	1.7917	1.9511	1.7548	1.8743	1.6549
Total tet*	3.9987	3.9861	3.9900	4.0105	3.9502	3.9608	3.9755	3.9474	4.0007	3.9930	3.9840	4.0120
Fe	0.0095	0.0081	0.0084	0.0081	0.0466	0.0349	0.0045	0.0154	0.0046	0.0148	0.0548	0.0072
Mg	0.0000	0.0007	0.0007	0.0000	0.0208	0.0000	0.0491	0.0007	0.0000	0.0000	0.0000	0.0000
Ca	0.9057	0.8923	0.7410	0.9203	0.8960	0.8637	0.8416	0.9082	0.9367	0.7888	0.8813	0.6657
Na	0.0881	0.1103	0.2132	0.0446	0.0901	0.1617	0.1112	0.1447	0.0630	0.1627	0.0599	0.2337
K	0.0041	0.0047	0.0284	0.0047	0.0000	0.0000	0.0052	0.0088	0.0029	0.0128	0.0067	0.0276
Total Cations	5.0061	5.0022	4.9817	4.9882	5.0037	5.0211	4.9871	5.0252	5.0079	4.9721	4.9867	4.9462
*Cation Ratios 100*Mg/(Mg+Fe) (mg#) and Molecular Proportion of Orthoclase (Or), Albite (Ab), Anorthite (An)*												
mg#	-	7.8	7.5	-	30.8	-	91.6	4.3	-	-	-	-
Or	0.4	0.5	2.9	0.5	-	-	0.5	0.8	0.3	1.3	0.7	3.0
Ab	8.8	10.9	21.7	4.6	9.1	15.8	11.6	13.6	6.3	16.9	6.3	25.2
An	90.8	88.6	75.4	94.9	90.9	84.2	87.9	85.6	93.4	81.8	93.0	71.8

(13) Mittlefehldt, unpublished data used in Mittlefehldt and Lindstrom (1993); (14, 15) Christophe Michel-Levy et al. (1987); (16) Wilkening and Anders (1975); (17, 18) Metzler et al. (1995); (19) Buchanan and Reid (1996); (20) Warren et al. (1990); (21, 22, 23, 24) Mittlefehldt, unpublished data used in Mittlefehldt and Lindstrom (1993).

Chromite is an ubiquitous minor mineral in cumulate eucrites, while ilmenite has been reported from many of them. Delaney et al. (1984) found ilmenite in all the cumulate eucrites they studied except Moama. The textures of chromites in cumulate eucrites are not well described in the literature. Hostetler and Drake (1978) mention that chromite and ilmenite occur as "well developed crystals" in Moore County, while Lovering (1975) describes chromites in Moama as occurring as equidimensional grains and elongate grains intergrown with tridymite. Details of chromite compositional variation are not described in the literature, but this mineral is apparently variable in composition in individual meteorites. The mean composition of ten chromite grains reported by Bunch and Keil (1971) for Moore County is significantly different than the mean of five grains analyzed by Hostetler and Drake (1978). Hostetler and Drake (1978) did not find zoning for the major elements in chromite grains, however. Mittlefehldt and Lindstrom (1993) show that chromite grains in ferroan cumulate eucrite Y-791195 vary from 8.6 to 15.7 wt % in TiO_2 and from 44.6 to 32.4 wt % in Cr_2O_3. Ilmenite occurs as individual grains, and composite grains with chromite and as exsolution lamellae in chromite (Bunch and Keil 1971, Hostetler and Drake 1978, Mittlefehldt and Lindstrom 1993). Representative chromite and ilmenite analyses are given in Table 32.

The composition of metal in the cumulate eucrites Binda, Moama, Moore County and Serra de Magé has received only cursory study (Duke 1965, Lovering 1964, 1975). For the unbrecciated cumulate eucrites, the metal is poor in Ni, with ≤0.5 wt % Ni. Cobalt has been determined only for Moama among these meteorites, and it is similarly low: 0.23 wt % (Lovering 1975). For Binda, one grain contained 0.44 wt % Ni and 1.38 wt % Co, while five other grains ranged from 1.9-2.1 wt % Ni and had ~2.2 wt % Co (Lovering 1975). The textural setting of the metal analyzed in Binda was not given, so it is difficult to compare these with the analyses of unbrecciated cumulate eucrites.

Basaltic eucrites. This subsection includes discussion of unbrecciated and monomict basaltic eucrites, as well as clasts from polymict HED samples that are similar to the basaltic eucrites. Some unusual igneous clasts will be dealt with separately, below. Basaltic eucrites are pigeonite-plagioclase rocks with fine to medium grain size. Textures, where preserved, are generally subophitic to ophitic. One exceptional eucrite is ALHA81001, which has a fine-grained quench texture consisting of pyroxene microphenocrysts set in a groundmass of glass or cryptocrystalline material (AMN 6-1; Warren and Jerde 1987). Almost all basaltic eucrites are brecciated, resulting in a rock composed of mineral and lithic fragments set in a fine-grained, generally fragmental matrix. Some eucrites have been highly recrystallized, resulting in a granular texture such as in Ibitira (Steele and Smith 1976). Vesicles are rare in eucrites; Ibitira is a spectacular exception. Vesicles have also been reported from PCA 91007 (Warren et al. 1996).

Minor and accessory phases in basaltic eucrites include the silica polymorphs tridymite and quartz, chromite, ilmenite, metal, troilite, whitlockite, apatite, olivine and rare zircon. The minor and accessory phases are generally found interstitial to pyroxene and plagioclase. However, cloudy pyroxene grains contain inclusions of chromite, ilmenite, metal and/or troilite, while some plagioclase grains contain inclusions of phosphates.

The original igneous pyroxene in basaltic eucrites was pigeonite, which subsequently underwent subsolidus exsolution of augite. Inversion of pigeonite to orthopyroxene is uncommon. Some of the original igneous pyroxene in Sioux County was orthopyroxene (Takeda et al. 1978a). Takeda and Graham (1991) described the mineralogic characteristics of basaltic eucrite pyroxenes, and related them to a metamorphic sequence of types from 1 to 6. In the least metamorphosed, type 1, basaltic eucrites, augite exsolution lamellae in the pigeonite are <0.1 μm thick, the pyroxenes are

not cloudy, and the original igneous zoning is preserved. In the most metamorphosed, type 6, augite lamellae in pyroxenes are several μm thick, clouding of the pyroxenes is present, the pyroxenes are homogeneous in composition, and the pigeonite has partially inverted to orthopyroxene. Takeda and Graham (1991) used the amount of preservation of chemical zoning of the pyroxene as one of the criteria for classifying basaltic eucrites by metamorphic type. However, basaltic eucrites exhibit a range of grain sizes, and possibly not all had the same original igneous zoning.

Basaltic eucrites are ferroan, and their pyroxenes are iron-rich. Table 30 gives representative pyroxene analyses for selected basaltic eucrites, and estimated primary pigeonite compositions are shown in Figure 42. In the least metamorphosed basaltic eucrites, there are at least three types of zoning trends, as summarized by Takeda and Graham (1991). In one, the core of pyroxenes are magnesian pigeonites with low Ca contents. These are zoned through increasing Fe and Ca to ferroaugite or subcalcic ferroaugite compositions. Another type of zoning starts from low-Ca magnesium pigeonite cores, shows Fe/Mg zoning at roughly constant Ca content to low-Ca intermediate pigeonite compositions, and then is zoned through increasing Ca contents at roughly constant enstatite content to ferroaugite compositions. A third type of zoning is from relatively ferroan intermediate pigeonite compositions through increasing Ca contents at roughly constant enstatite content to ferroaugite compositions. In most cases, however, basaltic eucrite pyroxenes have undergone subsolidus Fe/Mg equilibration and augite exsolution, and are now composed of low-Ca, homogeneous intermediate or ferriferous pigeonite hosts containing lamellae of ferroaugite.

Plagioclase in basaltic eucrites is calcic, in the range of bytownite to anorthite (Table 33). Unlike cumulate eucrites, plagioclase compositions in individual basaltic eucrites can show considerable range in anorthite content. For example, Warren and Jerde (1987) reported that plagioclase in Nuevo Laredo spans the range ~An_{92-74}, which is most of the range observed for all basaltic eucrites. The K_2O contents are low, typically ≤0.2 to 0.3 wt %, although the more sodic plagioclase compositions can have K_2O contents of ~0.5 wt %.

Chromite and ilmenite (Table 32) are ubiquitous minor minerals in basaltic eucrites, but they have received little systematic study. Chromites in many basaltic eucrites have between ~3 to 6 wt % TiO_2 and ~7 to 9 wt % Al_2O_3 (Bunch and Keil 1971). Exceptionally titanian chromites are found in Ibitira, with ~15-24 wt % TiO_2, and these have low Al_2O_3 contents in the range ~3.0 to 5.5 wt % (Steele and Smith 1976). Chromites low in TiO_2 occur in Millbillillie (~2 wt % TiO_2; Yamaguchi et al. 1994) and Pasamonte (~1.4 wt %, Bunch and Keil 1971). The chromites in Millbillillie have Al_2O_3 contents within the typical range given above, while those in Pasamonte are unusually Al_2O_3-rich, 17.7 wt % (Bunch and Keil 1971). The titanian chromites in Ibitira appear to be clearly exceptional among basaltic eucrites, and the Al_2O_3-rich chromites from Pasamonte may also be unusual. The TiO_2-poor chromites in Millbillillie may simply represent the low TiO_2 end of the basaltic eucrite distribution.

Olivine in basaltic eucrites is rare, and is found in the more ferroan examples or in the mesostasis of the least-metamorphosed basaltic eucrites (e.g. Mittlefehldt and Lindstrom 1993, Takeda et al. 1994b). These olivines are very iron-rich (Table 31).

Partial cumulate eucrites. Some eucrites are partial cumulates, mixtures of cumulus crystals and a substantial amount of solidified melt. Warren et al. (1990) first suggested this based on their study of the unusual magnesian eucrite Pomozdino, and the following description is from this source. Pomozdino is a monomict breccia containing two types of mafic clasts in the comminuted matrix; coarser-grained ophitic-poikilophitic clasts and

fine-grained, anhedral-granular clasts. Pomozdino originally contained two distinct primary pyroxenes, one, $Wo_{9.4}En_{42.7}Fs_{47.9}$ (Table 30, Fig. 42), compositionally similar to the primary pigeonite of cumulate eucrite Moore County, and one exhibiting Ca zoning, $Wo_{19}En_{40}Fs_{41}$ to $Wo_{39}En_{34}Fs_{27}$, more like that seen in pyroxenes of the basaltic eucrites Bouvante and Stannern. Both of these pyroxene types are magnesian, with mg# of ~47 and ~52, respectively. Compare these with bulk pyroxenes from basaltic eucrites such as Bouvante which have mg# ~ 38 (Christophe Michel-Levy et al. 1987, see Table 30). Chromite and ilmenite in Pomozdino are similar to those in Moore County and more magnesian than those of basaltic eucrites (see Table 32). Plagioclase, however, is more sodic, An_{81-87}, than those found in cumulate eucrites, An_{91-98}. Warren et al. (1990) considered Pomozdino to be a mixture of between 20 to 40% cumulus minerals with melt. The polymict eucrite Petersburg also contains basaltic clasts more magnesian than typical basaltic eucrites (Buchanan and Reid 1996, Mittlefehldt 1979). Although these authors did not favor a partial cumulate model for the formation of the Petersburg clasts, the general petrologic and compositional similarities with Pomozdino suggest that this might be a plausible scenario. Warren et al (1996) have also identified Y-791195, Y-791186 and RKPA80224 as possible partial cumulates.

Howardites, polymict eucrites and polymict diogenites. Howardites have long been known to be polymict breccias (Wahl 1952). More recently, numerous polymict breccias with bulk compositions like those of eucrites have been recovered from Antarctica, leading to recognition of polymict eucrites as a distinct rock type (e.g. Miyamoto et al. 1978, Olsen et al. 1978, Takeda et al. 1978b). Diogenites with basaltic eucritic clasts are also known (Lomena et al. 1976), and it has thus become obvious that, in terms of major components, howardites are intermediate members of an essentially continuous sequence of polymict breccias, including polymict eucrites and polymict diogenites (Delaney et al. 1983), that extends from the monomict eucrites to the monomict diogenites. Most of the material in the polymict breccias is identical or very similar to the basaltic eucrites, cumulate eucrites or diogenites (e.g. Delaney et al. 1984, Duke and Silver 1967), and the description of this material will not be repeated. Here we will describe the general features of the matrix plus brecciated and melted clasts of the polymict breccias, concentrating on the howardites.

The polymict breccias are composed of diverse mineral and lithic clasts set in a fine-grained fragmental to glassy matrix. Howardites also commonly contain glassy spheres and irregularly shaped particles. Lithic clasts in the polymict breccias tend to receive the most detailed study, so descriptions of the matrix are typically cursory, if given at all. There is no good census of matrix types in the polymict breccias. Many polymict breccias have fragmental matrixes that have been little modified by metamorphism; the howardites Bholghati, Kapoeta and Frankfort are examples (Mason and Wiik 1966a,b; Reid et al. 1990). Some polymict breccias have metamorphosed matrixes; polymict eucrite Y-792769 has a fine-grained, sintered matrix (Takeda et al. 1994b). Glassy or glass-rich matrixes are also common, for example in the paired polymict eucrites LEW 85300, LEW 85302 and LEW 85303 (Kozul and Hewins 1988), the howardite Monticello (Olsen et al. 1987) and the polymict breccia (polymict diogenite?) Y-791073 (Takeda 1986).

The polymict breccias, especially the howardites and polymict eucrites, contain breccia clasts, melt rocks and glass particles of various types. Duke and Silver (1967) first recognized breccia clasts in howardites. Bunch (1975) divided the breccia clasts into three types, and he restricted his definition to polymict clasts. These clasts consist of angular mineral and lithic clasts in either a fine-grained fragmental matrix (crystalline matrix breccias), glassy or devitrified matrix (glassy matrix breccias), or troilite matrix

(sulfide matrix breccias). Labotka and Papike (1980) and Fuhrman and Papike (1981) also recognized sulfide matrix breccias as an important clast type, but lumped the crystalline and glassy matrix breccias, plus melt rocks, into their dark matrix breccia type. Melt rocks have a variety of textures. The matrix varies from glass to cryptocrystalline material to fine-grained quench-textured matrix; the melt rocks contain inclusions of rounded, partially melted minerals, subangular to rounded minerals, or euhedral plagioclase or pyroxene crystals (Bunch 1975, Delaney et al. 1984, Hewins and Klein 1978, Klein and Hewins 1979, Mittlefehldt and Lindstrom 1997, 1998). Glass particles vary from spherical to irregular in shape, from glass sensu stricto to devitrified glass; they may contain phenocrysts of olivine and/or low-Ca pyroxene (Bunch 1975, Hewins and Klein 1978, Labotka and Papike 1980, Mittlefehldt and Lindstrom 1998, Olsen et al. 1990).

Unusual igneous clasts. Most igneous clasts in polymict breccias are basically the same lithologies as occur as basaltic and cumulate eucrites and diogenites, and the descriptions of these meteorite types above serve to describe the clasts. There are some unusual clasts that deserve brief mention. Dymek et al. (1976) described a fine-grained porphyritic clast from the Kapoeta howardite composed of pyroxene microphenocrysts and a few chromite microphenocrysts in a holocrystalline, variolitic groundmass of acicular plagioclase and pyroxene. Mittlefehldt and Lindstrom (1997) described two similar clasts, a Kapoeta clast consisting of low-Ca pyroxene phenocrysts and microphenocrysts and ferroan olivine microphenocrysts in a cryptocrystalline granular textured groundmass, and a clast from the howardite EET 92014 consisting of skeletal pyroxene phenocrysts in a glassy groundmass containing microphenocrysts of pyroxene. The cores of the pyroxene phenocrysts in these clasts are magnesian, and can be more magnesian than core compositions of zoned basaltic eucrite pyroxenes (e.g. Mittlefehldt and Lindstrom 1997). Ikeda and Takeda (1985) briefly described magnesian olivine-orthopyroxene clasts in the Y-7308 howardite containing variable amounts of plagioclase, chromite and high-Ca clinopyroxene. Olivine is euhedral to anhedral and Fo_{65-73} in composition. Orthopyroxene is the major phase, and is similar in composition to pyroxenes in the ferroan diogenites; $Wo_{2-3}En_{67-72}Fs_{26-30}$. Ikeda and Takeda (1985) also describe unusually ferroan clasts composed of fayalitic olivine, Fo_{10-14}, hedenbergitic pyroxene, $Wo_{41}En_{16-19}Fs_{40-43}$, tridymite and plagioclase, An_{78-85}, with minor ilmenite, chromite, troilite, Fe-metal and whitlockite. Olivine is euhedral to subhedral a few tens of microns in size, and some is included within the larger pyroxene grains. Plagioclase and tridymite are several hundred microns in size.

Chondritic clasts. Chondritic clasts are a minor component of many HED meteorites, especially the polymict breccias. Zolensky et al. (1996) discussed the mineralogy and petrology of numerous chondritic clasts from HED meteorites and summarized previous work. They found that about 80% of the chondritic clasts are CM2 materials, while CR2 chondritic materials are less abundant. Some clasts appear to have CI chondrite parentage, but they have been heated, with consequent petrographic alteration (Buchanan et al. 1993). The polymict eucrite LEW 85300 contains a few chondritic clasts that are closest to CV3 chondrites in mineralogy and petrology, but have some unusual compositional characteristics (Zolensky et al. 1992).

Composition

The HED meteorites in general show limited ranges in major, minor and trace element composition within the different meteorite types. The polymict breccias, especially the howardites, are exceptional to this, and to a lesser extent, so are the cumulate eucrites. Bulk major and minor element compositions of selected HED meteorites are given in Table 34; trace element compositions are given in Table 35.

Table 34. Major element compositions of representative diogenite, eucrite and howardite whole rock samples.

	Johns-town (1)	Shalka (2)	Y-75032 (3)	Moama (4)	Serra de Magé (5)	Y-791195 (6)	Stannern (7)	Sioux County (8)	Juvinas (9)	Nuevo Laredo (10)	Y-74450 (11)	EETA 79004 (12)	Y-82049 (13)	Bholghati* (14)	Kapoeta (15)	Y-7308 (16)
Chemical Composition (wt %)																
SiO_2	52.5	51.6	52.9	48.6	48.5	49.3	49.7	49.2	49.2	49.5	48.3	49.6	49.6	49.0	50.3	50.8
TiO_2	0.10	0.062	0.26	0.22	0.13	0.25	0.980	0.58	0.63	0.83	0.90	0.63	0.41	0.54	0.30	0.23
Al_2O_3	1.5	0.60	3.4	13.7	14.8	13.3	12.3	13.1	13	12.2	11.4	11.5	8.3	8.38	8.3	4.27
Cr_2O_3	0.82	2.41	0.69	0.61	0.626	0.34	0.34	0.316	0.305	0.282	0.396	0.413	0.79	0.733	0.694	1.02
FeO	15.9	16.3	18.6	14.8	14.4	17.3	17.8	18.4	18.7	19.6	18.6	17.8	17.8	18.1	17.5	16.7
MnO	0.484	0.553	0.61	0.50	0.476	0.58	0.525	0.551	0.515	0.584	0.531	0.504	0.54	0.522	0.495	0.523
MgO	25.5	25.8	20.9	11.9	10.7	7.7	6.97	6.88	6.6	5.55	7.58	8.67	15.2	16.7	15.8	21.4
CaO	1.83	0.73	3.61	9.47	9.75	10.5	10.7	10.4	11	10.3	9.95	8.95	6.6	7.19	5.20	3.83
Na_2O	0.02	0.04	0.10	0.22	0.249	0.40	0.62	0.406	0.377	0.508	0.51	0.398	0.22	0.278	0.276	0.13
K_2O	0.0011	0.0016	0.007	0.01	0.012	0.03	0.066	0.033	0.027	0.050	0.054	0.072	0.020	0.025	0.022	0.008
P_2O_5	0.041	0.002	bd	nd	0.030	bd	0.102	nd	nd	nd	nd	0.050	0.04	nd	nd	nd
S	0.22	nd	nd	nd	0.150	nd	nd	0.066	nd	nd	0.236	0.261	nd	nd	nd	0.110
Total	98.92	98.10	101.08	100.03	99.82	99.70	100.10	99.93	100.35	99.40	98.46	98.85	99.52	101.47	98.89	99.02
*Cation Ratios Fe/Mn, mg# (100*Mg/(Mg+Fe))*																
Fe/Mn	32	29	30	29	30	29	33	33	36	33	35	35	33	34	35	32
mg#	74.1	73.8	66.7	58.9	57.0	44.2	41.1	40.0	38.6	33.5	42.1	46.5	60.3	62.2	61.7	69.5

(1, 11, 16) Wänke et al. (1977); (2) McCarthy et al. (1972); (3, 6, 13) Mittlefehldt and Lindstrom (1993), (4) Lovering (1975); (5, 8) Palme et al. (1978); (7) McCarthy et al. (1973); (9, 15) Wänke et al. (1972b); (10) Warren and Jerde (1987); (12) Palme et al. (1983); (14) Laul and Gosselin (1990).
*average matrix

Table 35. Trace element compositions of representative diogenite, eucrite and howardite whole rock samples.

		Johns-town (1)	Shalka (2)	Y-75032 (3)	Moama (4)	Serra de Magé (5)	Y-791195 (6)	Stannern (7)	Sioux County (8)	Juvinas (9)	Nuevo Laredo (10)	Y-74450 (11)	EETA 79004 (12)	Y-82049 (13)	Bhol-ghati* (14)	Kapoeta (15)	Y-7308 (16)
Sc	µg/g	15.8	9.9	21.1	23.4	22.1	30.4	30.6	31.4	28.5	33.3	30.0	28.4	22.9	22.8	20.7	18.1
V	µg/g	115	--	--	114	111	--	--	--	--	61	67.5	--	--	109	--	124
Co	µg/g	38.1	18.0	16.2	8.6	9.50	6.2	7.18	5.29	5.8	2.15	12.0	7.30	21.4	29.0	28	20.5
Ni	µg/g	150	--	20	--	--	--	--	--	--	2.9	--	33	130	410	410	--
Ga	µg/g	0.18	--	--	--	--	--	2.17	--	2.16	1.2	1.46	1.9	--	--	1.04	0.51
Ba	µg/g	--	--	--	--	--	--	53	--	--	39	45.4	31	18	21	--	8.25
La	µg/g	0.063	0.009	0.40	0.18	0.58	0.49	5.08	2.39	2.58	3.83	4.79	1.53	1.55	1.61	1.39	0.68
Ce	µg/g	--	--	0.50	--	--	1.8	13.7	6.8	--	9.9	12.0	5.62	3.1	4.0	--	1.67
Sm	µg/g	0.059	0.004	0.367	0.16	0.35	0.407	3.15	1.42	1.48	2.32	2.78	0.88	0.99	1.01	0.54	0.42
Eu	µg/g	0.011	0.002	0.110	0.36	0.33	0.44	0.782	0.56	0.61	0.71	0.70	0.504	0.33	0.34	0.32	0.17
Gd	µg/g	0.24	--	--	--	--	--	--	--	2.3	--	3.4	1.35	--	1.3	1.25	0.54
Tb	µg/g	--	--	0.11	--	0.07	0.14	0.73	0.40	0.60	0.54	0.66	0.25	0.25	0.24	0.29	0.1
Dy	µg/g	0.21	--	--	--	0.6	--	5.05	2.6	3.2	3.7	4.2	1.75	--	--	1.26	0.66
Ho	µg/g	0.059	--	--	--	--	--	1.13	--	0.42	--	0.97	0.46	--	0.35	0.23	0.16
Yb	µg/g	0.17	0.030	0.64	0.42	0.39	0.58	2.90	1.55	1.72	2.40	2.61	1.32	0.98	1.00	0.89	0.49
Lu	µg/g	0.027	0.006	0.088	0.075	0.066	0.090	0.40	0.25	0.28	0.35	0.36	0.20	0.150	0.16	0.14	0.073
Hf	µg/g	--	--	0.31	--	0.14	0.57	2.34	1.17	1.3	1.61	2.08	1.33	0.68	0.69	0.6	0.33
Ta	ng/g	--	--	50	--	80	20	500	140	120	181	300	190	100	110	100	42
Ir	ng/g	6.4	--	--	--	--	--	--	--	27	0.083	--	--	3.8	21	20	--
Au	ng/g	1.7	--	--	--	--	--	--	2.5	7.9	1.5	0.27	1.4	--	8.6	6.8	0.45
Th	ng/g	--	--	--	--	--	110	600	--	--	440	--	320	110	230	--	--
U	ng/g	2.8	--	--	--	--	--	160	--	89	140	163	70	--	--	51	22

(1, 11, 16) Wänke et al. (1977); (2) Mittlefehldt (1994); (3, 6, 13) Mittlefehldt and Lindstrom (1993), (4) Mittlefehldt (1979); (5, 8) Palme et al. (1978); (7) Palme et al. (1988); (9, 15) Wänke et al. (1972b); (10) Warren and Jerde (1987); (12) Palme et al. (1983); (14) Laul and Gosselin (1990).
*average matrix

Major and minor element composition. Diogenites are very uniform in bulk major and minor element composition, with the exception of Cr_2O_3. Variation in Cr_2O_3 undoubtedly reflects variation in the amount of chromite in the meteorites. This partially reflects the mineralogical nature of the diogenites, and is not entirely a problem of sampling these coarse-grained rocks; analyses of some diogenites always contain more Cr_2O_3 than typical. For example, 10 analyses for Cr_2O_3 in Shalka whole-rock samples range from 1.1 to 2.4 wt %, while for Johnstown, 29 analyses range from 0.7 to 1.1 wt %. As mentioned above, some diogenites are slightly more magnesian or ferroan than the typical diogenite. Nevertheless, the compositions of these meteorites are not very different from the typical diogenite; for example compare magnesian diogenite Manegaon (MgO 26.5 wt %, FeO 14.3 wt %) and ferroan diogenite Garland (MgO 25.0 wt %, FeO 18.5 wt %) with the typical diogenites Johnstown and Shalka (MgO 25.5 to 25.8 wt %, FeO 15.9 to 16.3 wt %). The Yamato Type B diogenites are exceptional, being quite distinct in bulk composition from other diogenites, as expected from their distinct mineralogies (Table 34).

The cumulate eucrites show a wider range in bulk major and minor element composition. In part this reflects compositional differences among the rocks, but it is also complicated by difficulties in adequately sampling these coarse-grained, modally heterogeneous lithologies. Serra de Magé is particularly difficult to adequately sample; reliable measurements of Al_2O_3 in this rock vary from 12.7 to 20.9 wt %, reflecting differences in plagioclase content in the samples. The mg# of the cumulate eucrites will be less sensitive to sampling problems, as it is essentially defined by the pyroxene in the rock. The cumulate eucrites vary in mg# from ~65 for Binda to ~44 for Y-791195. The compatible element Cr generally reflects this variation in mg#, and is high in Binda and low in Y-791195. However, EET 87548 is exceptional in having the highest Cr content, yet a mg# in the mid-range of cumulate eucrites (Warren et al. 1996).

The basaltic eucrites are very uniform in composition. Most plot within a very limited range in mg#, CaO, Al_2O_3, TiO_2 or Cr_2O_3 contents. Figure 43 is a TiO_2 vs. mg# plot for basaltic eucrites, a variant of a diagram first used by Stolper (1977) to discuss their petrogenesis. Many basaltic eucrites plot within a small region of mg# ~ 38-40, TiO_2 ~ 0.6-0.7 wt %. These are frequently referred to as the main-group eucrites. Some eucrites plot within this same mg# band, but at higher TiO_2 contents. These are the Stannern-trend eucrites. Some eucrites have both higher TiO_2 contents and lower mg#, and are referred to as Nuevo Laredo-trend eucrites. Figure 44 shows histograms of CaO and Cr_2O_3 contents for basaltic eucrites, where the uniformity in bulk compositions of these samples becomes obvious.

Figure 43. TiO_2 vs. mg# diagram for basaltic eucrites. The Stannern-trend (down arrow) is likely a trend of increasing partial melting. Most eucrites are members of the main-group. Their origin is controversial; they may either be primary partial melts or residual melts. The Nuevo Laredo-trend (left arrow) is a fractional crystallization trend. Anomalous eucrites are ALHA81001, Ibitira and Pomozdino. The data are averages of all available literature determinations.

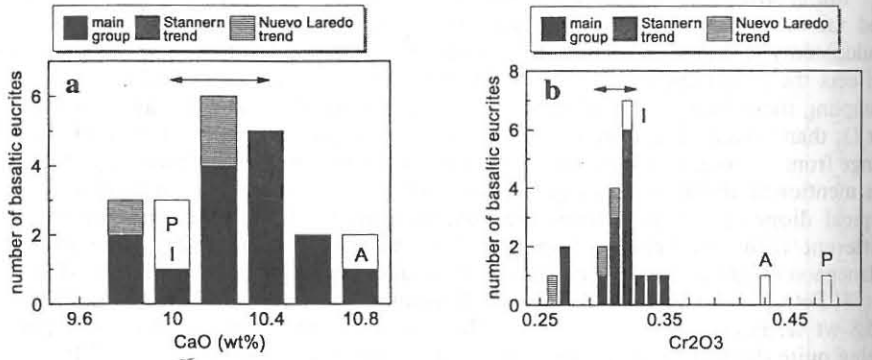

Figure 44. Histograms of (a) CaO and (b) Cr_2O_3 for basaltic eucrites. Both CaO and Cr_2O_3 have narrow ranges in basaltic eucrites, and the latter in particular has been taken as evidence for buffering by residual spinel in the eucrite source region, and hence a partial melting origin (Jurewicz et al. 1993). Arrows show the ranges in experimental, low temperature equilibrium partial melts of Murchison determined by these authors. Anomalous eucrites as in Figure 43.

The extreme heterogeneity in bulk major and minor element composition of the polymict breccias contrasts sharply with the uniformity seen for the igneous lithologies. For all intents and purposes, the polymict breccias are intermediate in composition between the diogenites and basaltic eucrites, and span wide ranges in composition. Figure 45 shows the relationship between CaO and MgO contents for polymict breccias compared to monomict basaltic eucrites and diogenites. The linear relationship displayed in this figure is consistent with the petrographic evidence that the polymict breccias are dominated by basalt clasts similar to the basaltic eucrites and orthopyroxene clasts similar to the diogenites. With few exceptions (see below), the polymict breccias would plot between basaltic eucrites and diogenites on any element-element plot (Fig. 46). Note that the single meteorite type, the howardites, spans a wide range in CaO and MgO contents, in contrast to what is observed for basaltic eucrites and diogenites (Fig. 45). This heterogeneity can also occur within individual howardites; seven analyses each of CaO and MgO for Kapoeta range from 3.1 to 9.9 and 8.1 to 22.2 wt %, respectively. This likely reflects differential sampling of basaltic and orthopyroxenitic clasts and matrix. Four matrix samples of Bholghati only vary from 6.7 to 7.2 wt % and 15.7 to 17.6 wt % for CaO and MgO, respectively (Laul and Gosselin 1990).

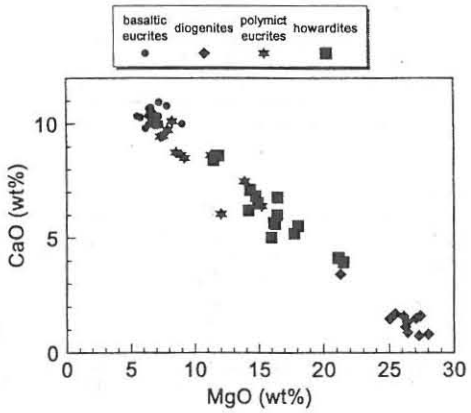

Figure 45. CaO vs. MgO for HED meteorites showing the mixing relationship between basaltic eucrites and diogenites to form the polymict eucrites and howardites. Although other components are present in the polymict breccias, they are dominantly composed of eucrite-like basalts and diogenite-like orthopyroxenes.

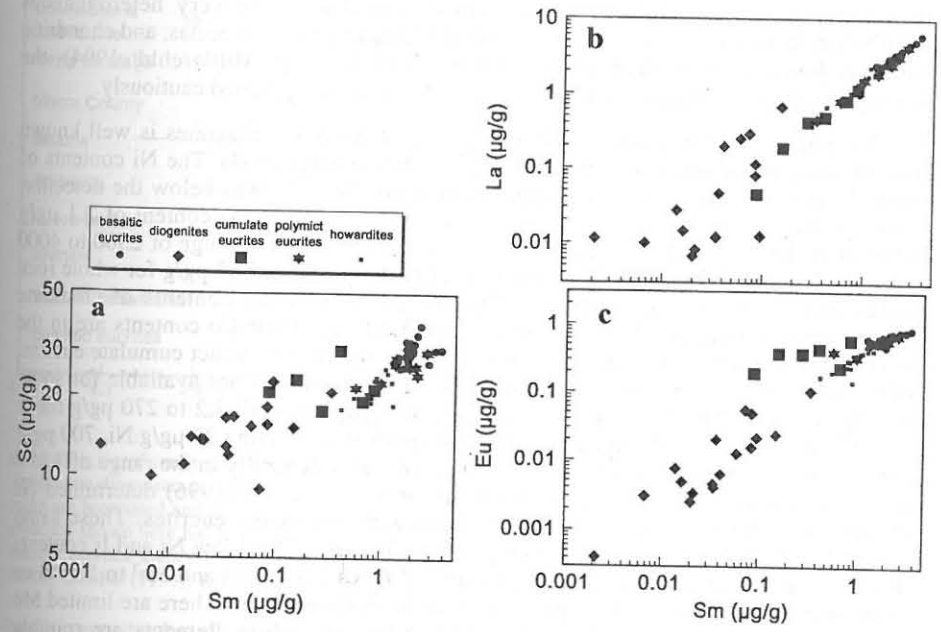

Figure 46. Scandium vs. Sm (a), La vs. Sm (b) and Eu vs. Sm diagrams for HED meteorites show the extreme variations in highly incompatible elements (La, Sm, Eu) in the HED suite compared to a moderately incompatible (bulk distribution coefficient near unity) element, Sc. The polymict breccias, howardites and polymict eucrites, are intermediate in trace element contents between basaltic eucrites and diogenites. The scatter in La and Sm content in diogenites and cumulate eucrites is due to the strong control of a trapped melt component on highly incompatible element contents in igneous cumulates. The "flattened" Eu-Sm trend between cumulate and basaltic eucrites is due to Eu becoming more compatible once plagioclase becomes a liquidus phase.

Trace lithophile element composition. Excluding the polymict breccias for the moment, the trace incompatible lithophile elements show systematic distributions related to rock type (Fig. 46). The contents of Sc, La, Sm and Eu, for example increase in the sequence diogenite, cumulate eucrite, basaltic eucrite. The La content varies by a factor of ~2000 in this suite, whereas Sc varies by only a factor of ~3. The trace incompatible elements are not uniform in the diogenites and the cumulate eucrites. For highly incompatible elements such as La and Sm, these meteorite types show wide ranges in content; the diogenites show a range of a factor of ~30 in La content, for example. The moderately incompatible element Sc exhibits much narrower ranges in content. For the basaltic eucrites, both the highly incompatible and moderately incompatible lithophile elements have narrow ranges, although the former are more variable than CaO, an incompatible major element. In some cases, the content of highly incompatible elements in whole-rock samples of diogenites are higher than observed in separated clasts. This suggests that even the monomict diogenites may contain incompatible element-rich debris in the matrix (Mittlefehldt 1994).

Siderophile element composition. Siderophile elements are strongly depleted in HED meteorites, and are generally higher in the polymict breccias than in the monomict breccias and unbrecciated samples. The Co and Ni contents of HED meteorites are fairly well known, but the contents of other siderophile elements are poorly known. In part this is due to there being relatively few analyses (e.g. Mo, W), in part due to the susceptibility

to anthropogenic contamination (Au), and in part due to the very heterogeneous distribution in the rocks (e.g. Ir). Because most HED samples are breccias, and chondritic debris is found even in supposedly monomict breccias (e.g. Mittlefehldt 1994), the siderophile element content of any HED sample needs to be evaluated cautiously.

The content of Co, a compatible siderophile element, in diogenites is well known through analyses of separated clasts, 6-38 μg/g (Mittlefehldt 1994). The Ni contents of these clasts range from 20 to 110 μg/g, but in many clasts Ni was below the detection limit. An analysis of a whole-rock sample of Shalka yielded a Ni content of 2.1 μg/g (Chou et al. 1976). For a few clast samples, Ir contents are in the range of 2500 to 4000 pg/g (Mittlefehldt 1994), whereas Chou et al. (1976) report 8 and 63 pg/g for whole rock Shalka and Tatahouine, respectively. The siderophile element contents of cumulate eucrites are generally poorly known due to few analyses. Their Co contents are in the lower end of the range of diogenites, ~6 to 10 μg/g. Binda, a polymict cumulate eucrite, is exceptional with ~16 μg/g. A few analyses for Ni, Ir and Au are available for some cumulate eucrites. The ranges observed are 1.2 to 13 μg/g for Ni, 3.2 to 270 pg/g for Ir and 0.038 to 1 ng/g for Au. Again, Binda is exceptional, containing 21 μg/g Ni, 700 pg/g Ir and 2.5 ng/g Au. The Co content of basaltic eucrites is generally in the range of 3 to 8 μg/g. Nickel contents appear to be much lower. Warren et al. (1996) determined Ni contents of ~0.5 to 1.5 μg/g for a suite of Antarctic monomict eucrites. These same authors determined Ir contents in the range 0.5 to 6.5 pg/g. These low Ni and Ir contents are significant because they put firm upper limits of ~10^{-2} to 10^{-3} % and 10^{-3} to 10^{-4} % on the amount of chondritic contamination that can be in the breccias. There are limited Mo and W data on basaltic eucrites. These refractory siderophile elements are roughly correlated with refractory incompatible lithophile elements such as La in basaltic eucrites, but are depleted compared to CI abundances by factors of 30 for W/La and 570 for Mo/La (Newsom 1985, Newsom and Drake 1982).

Noble gases. Some howardites are enriched in noble gases compared to other HED meteorites. Excluding decay products and cosmogenic gases, these howardites contain two noble gas components, planetary- and solar-type gases (e.g Mazor and Anders 1967). Early in the study of noble gases in howardites it was believed that these gases were brought in by a carrier phase (Mazor and Anders 1967, Müller and Zähringer 1966). The characterization of carbonaceous chondrite fragments in howardites (Wilkening 1973) led to the identification of these clasts as the carriers of the planetary-type gases (Wilkening 1976). Mazor and Anders (1967) noted that the planetary- and solar-type gas contents were correlated, and thus believed that they were brought in by the same carrier. However, subsequent experiments have shown that the solar-type gases are a surface correlated component of mineral and glass fragments of the howardites themselves, not just of the chondritic materials (Black 1972, Padia and Rao 1989, Rao et al. 1991). These solar-type gases represent solar wind and solar flare gases implanted in the outer few μm of grains in the breccias, and show that these howardites were part of the regolith of their parent body.

Ages

It has long been known that the HED suite of meteorites is very old, not much younger than the chondrites. This was established by analyses of whole-rock suites (e.g. Birck and Allègre 1978, Papanastassiou and Wasserburg 1969), on individual meteorites (e.g. Allègre et al. 1975, Tera et al. 1997) and on igneous clasts from the polymict breccias (Nyquist et al. 1986) using the long-lived Rb-Sr, Sm-Nd and/or Pb-Pb chronometers, as well as by evidence for the decay products of the short-lived nuclides ^{129}I and ^{244}Pu (e.g. Rowe 1970). The best estimate of the age of magmatism for the

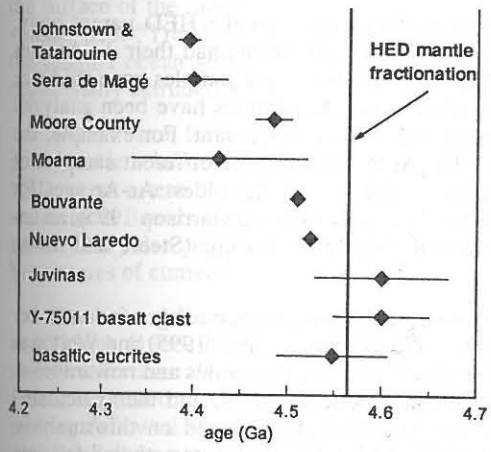

Figure 47. The age of magmatism on the HED parent body. The narrow band labeled HED mantle fractionation is the time of major parent body differentiation determined by Mn-Cr chronometry, and the width of the band includes the uncertainty on this age. The best estimate for the age of eucrite formation is given by the datum labeled basaltic eucrites. The ages of the brecciated basaltic eucrite Juvinas and the least metamorphosed basalt clast from Y-75011 are compatible with these age estimates. The brecciated basaltic eucrites Bouvante and Nuevo Laredo are significantly younger, but this could be due to impact metamorphism. The unbrecciated cumulate eucrites Moama, Moore County and Serra de Magé are significantly younger than the inferred HED mantle fractionation, and Serra de Magé is significantly younger than the basaltic eucrites best age estimate. The age of the Johnstown and Tatahouine diogenites are also significantly younger than the inferred HED differentiation time, but these rocks are brecciated and shocked, respectively, casting uncertainty on the meaning of their young age. The evidence shown here has been taken to indicate that the cumulate eucrites are ~100 Ma younger than the basaltic eucrites. Data are from Birck and Allègre (1981), Lugmair and Shukolyukov (1997), Nyquist et al. (1986), Smoliar (1993), Takahashi and Masuda (1990), Tera et al. (1997).

basaltic eucrites based on these data is in the range 4.51 Ga (Pb-Pb, Bouvante and Nuevo Laredo, Tera et al. 1997) to 4.60 Ga (Rb-Sr, Juvinas and Y-75011,84B least metamorphosed basalt clast, Allègre et al. 1975, Nyquist et al. 1986). Smoliar (1993) has examined all available Rb-Sr data on eucrites, and derived his best estimate for their formation age of 4.548±0.058 Ga. Recently, evidence for the presence of very short-lived ^{53}Mn ($t_{1/2}$ 3.7 Ma) and ^{60}Fe ($t_{1/2}$ 1.5 Ma) at the time of formation of basaltic eucrites has been found (Lugmair et al. 1994a,b; Shukolyukov and Lugmair 1993a,b). Lugmair and Shukolyukov (1997) have determined a Mn-Cr isochron for diogenite and basaltic eucrite samples, and combined this with a precise Pb-Pb age and Mn-Cr isotopic systematics for the angrite LEW 86010 to derive an estimate for the time of differentiation of the HED parent body of 4.5648±0.0009 Ga. Lugmair and Shukolyukov (1997) were careful to describe this time as "a time of HED mantle fractionation," rather than the time of formation of the diogenites and basaltic eucrites.

Age information on cumulate eucrites suggests that they are younger than basaltic eucrites. Tera et al. (1997) determined Pb-Pb ages for Moama, Moore County and Serra de Magé, all unbrecciated cumulate eucrites. These ages are, respectively, 4.426±0.094, 4.484±0.019 and 4.399±0.035 Ga, and are within the uncertainty of Sm-Nd ages determined on the same meteorites by Jacobson and Wasserburg (1984), Tera et al. (1997) and Lugmair et al. (1977). None of these ages overlaps the estimated time of HED parent-body differentiation given above within the stated 2σ uncertainty envelopes (Fig. 47). Takahashi and Masuda (1990) determined a Rb-Sr isochron for the diogenites Johnstown and Tatahouine of 4.394±0.011 Ga; again, this is outside the error envelope of the estimated HED parent-body differentiation time (Fig. 47). In this case, the difference is plausibly due to secondary processes as Johnstown is a breccia and Tatahouine has suffered shock damage.

Metamorphic and impact ages are best determined using the ^{39}Ar-^{40}Ar method, and Bogard (1995) has recently summarized these studies. He demonstrated that almost every eucrite and howardite studied by Ar-Ar chronometry contains evidence for significant Ar

degassing, and argued that this was due to heating events on the HED parent body. Bogard (1995) further showed that most eucrites and howardites had their Ar-Ar ages reset within the time period of ~4.1 to 3.4 Ga ago; relatively few samples gave evidence for older or younger Ar-Ar ages. In cases where multiple samples have been analyzed from the same meteorite, the Ar-Ar ages are not always concordant. For example, the results compiled by Bogard (1995) show that Ar-Ar resetting of different samples of Kapoeta vary from ~3.44 to 4.48 Ga. Paradoxically, one of the oldest Ar-Ar ages for HED meteorites is the 4.495±0.015 Ga age for Ibitira (Bogard and Garrison 1995), an unbrecciated, highly metamorphosed eucrite with hornfelsic texture (Steele and Smith 1976).

Noble gas studies geared toward determining cosmic-ray exposure ages for a number of HED meteorites have recently been done by Eugster and Michel (1995) and Welton et al. (1997). The former authors used their results on eucrites, diogenites and howardites to determine composition and shielding dependent production rates, and then calculated cosmic-ray exposure ages for their data plus literature data. Based on this analysis, Eugster and Michel (1995) suggested that 81% of all HED meteorites studied fell into five exposure age clusters; 6±1, 12±2, 21±4, 38±8 and 73±3 Ma. Welton et al. (1997) determined the noble gas contents of diogenites, and calculated exposure ages for them. They found that 70% of the diogenites have ages consistent with the 21 and 38 Ma age clusters. Using these data and literature data on eucrites and howardites, Welton et al. (1997) performed statistical analysis to determine that the 21 and 38 Ma exposure age clusters are statistically significant, while the 12 Ma cluster is not. The 6 and 73 Ma clusters are the smallest identified by Eugster and Michel (1995) and so presumably they are also not statistically significant. Both the 21 and the 38 Ma age clusters contain the range of petrologic types; eucrites, polymict eucrites, diogenites and howardites.

HED meteorite petrogenesis

The earliest petrogenetic model for asteroidal differentiation was that of Mason (1962). He noted that the lithologies in the HED group could plausibly represent a fractional crystallization sequence from early orthopyroxenites, through increasing plagioclase content to the basaltic eucrites. Mason (1962) suggested that a chondritic body depleted in Na was totally melted, a metallic core segregated, and the silicate melt solidified via fractional crystallization. The eucrites were thus the residual liquid products of an extensive sequence of crystallization. In this model, the crust of the asteroid from top down was composed of eucrites, howardites and diogenites. Mason (1962) considered howardites a brecciated igneous rock type, not a mixture of lithologies.

Stolper (1977) presented an alternative model for eucrite petrogenesis in which the basaltic eucrites represent primary partial melts of their parent body. Stolper based his arguments on the results of melting experiments on basaltic eucrites in which he found conditions of temperature and oxygen fugacity at which the eucrites are multiply saturated with pyroxene, plagioclase, olivine, metal and spinel. Because this is a plausible mineral assemblage for a chondritic parent body, Stolper (1977) concluded that eucrites are primary partial melts of their parent body. In Stolper's model, the parent body undergoes minimal heating as total melting is not envisioned.

The Mason and Stolper models represent end member models, and several intermediate or hybrid models have been developed. Ikeda and Takeda (1985) developed a magma ocean model for HED petrogenesis. They invoke an accretional energy source to cause total melting of the outer portion of the parent asteroid, producing a thin magma ocean. The magma ocean undergoes fractional crystallization and volatile loss, producing first dunites and then orthopyroxenites (diogenites). At some point during crystallization, the surface of the magma ocean became a stable, crystalline "scum" layer composed of volatile-poor "Trend A" eucrites like Juvinas and Nuevo Laredo. The lower portions of the magma ocean suffered less volatile loss, and melts from this lower region were occasionally extruded as more volatile-rich "Trend B" magmas like Stannern.

Warren and Jerde (1987) presented a hybrid model of the Mason and Stolper petrogenetic schemes, in which members of the Stannern-trend are partial melts of the HED parent asteroid, while the Nuevo Laredo-trend eucrites and the main-group eucrites are residual liquids from melts that first produced the diogenite cumulates. Warren and Jerde (1987) also suggested that the main-group and Nuevo Laredo-trend eucrites might be mixtures of cumulus grains and residual liquid.

Hewins and Newsom (1988) recognized the two eucrite trends, A and B, of Ikeda and Takeda (1985) but suggested that these trends are the result of two distinct parent melts, rather than divergent evolution of a single magma ocean. Hewins and Newsom (1988) suggested that magnesian parent melts that were formed by high degrees of partial melting followed fractional crystallization paths to produce an incompatible-element-poor trend and an incompatible-element-rich trend (equivalent to trends A and B of Ikeda and Takeda 1985, respectively). The Hewins and Newsom (1988) scenario posits that magnesian parental melts were produced on the HED parent body, and they suggest that two clasts from polymict breccias are candidates for these melts. More recently, Mittlefehldt and Lindstrom (1997) studied two additional magnesian basalt clasts from howardites, and reviewed existing data on the other two. These authors concluded that all four magnesian basalt clasts so far identified are more likely impact melts of the parent body surface. In their opinion, there is no petrologic evidence for the existence of primary magnesian basalt clasts in HED meteorites. The reality of separate "A" and "B" trends in the basaltic eucrite suite is open to question.

The central issue in all these models is whether main-group eucrites are primary partial melts or residual liquids. Experimental studies of chondritic materials have been done to attempt to resolve this issue. Jurewicz et al. (1993, 1995a) performed melting experiments on CM, CV, H and LL chondrites. Volatile elements like Na were allowed to escape from the system in these experiments. Jurewicz et al. (1993, 1995a) showed that there is a close match between the low-temperature melting fraction of volatile-poor CM chondrites and the main-group eucrites suggested by Stolper (1977) to be primary partial melts. Consequently these authors favored Stolper's model for eucrite petrogenesis. One potential problem with these experimental studies is that a volatile-poor, CM chondrite-like source has insufficient pyroxene to produce orthopyroxene cumulates in abundance. This seems at odds with the HED meteorite suite, in which diogenites and orthopyroxene clasts in polymict breccias are modally significant. The problem is compounded by melting experiments on LL chondrites which do contain sufficient pyroxene to easily explain diogenites, but produce minimum melts unlike eucrites (Jurewicz et al. 1995a).

The partial melt vs. residual melt origin for main-group eucrites remains an unsettled problem in the meteoritical community. Indeed, a recent series of publications has resulted in a range of models for eucrite petrogenesis. Jones et al. (1996) consider that the eucrites Bouvante, Stannern, Chervony Kut, Cachari and Sioux County are primary partial melts. Ruzicka et al. (1997) believe basaltic eucrites, excluding Bouvante and Stannern, formed from a magma ocean that first fractionally crystallized dunites and orthopyroxenites, and then crystallized under conditions approaching equilibrium to produce the suite of basaltic eucrites. Righter and Drake (1997) suggested the eucrite parent body was totally molten, separated a core, and then underwent equilibrium crystallization to form dunites and orthopyroxenites. A basaltic residual liquid then underwent fractional crystallization to form the main-group basaltic eucrite suite, while

Bouvant and Stannern represent other residual melts. Note that Ruzicka et al. (1997) and Righter and Drake (1997) come to opposite conclusions as to which igneous rocks require equilibrium vs. fractional crystallization to form them. Warren (1997) presented an updated version of the Warren and Jerde (1987) model for eucrite petrogenesis. He suggested that the HED suite formed from a large magma system, probably a global magma ocean. Diogenite cumulates formed early while the system was rapidly crystallizing. The rate of cooling, and thus crystallization, slowed down and high mg# cumulate eucrites were produced. During this period of slow crystallization, the residual melt was repeatedly tapped to produce the basaltic eucrite suite. At the end of magmatism, low mg# cumulate eucrites are formed from the last dregs of the magma system. Clearly, we are not converging on a consensus opinion for eucrite petrogenesis.

The petrogenesis of diogenites is more clear cut, at least to a first order; these coarse-grained rocks are cumulates from a fractionally crystallizing magma. The nature of their parent magma is uncertain, however. Stolper (1977) suggested that they may have crystallized from a melt of essentially orthopyroxene composition. Recent study of minor element distributions in the pyroxenes, trace element study of bulk orthopyroxene separates and SIMS study of pyroxenes have tended to support this model (Fowler et al. 1994, 1995; Mittlefehldt 1994). Both bulk samples and pyroxene grains show wide ranges in incompatible element contents, suggesting a wide range in fractional crystallization, yet they have a very restricted range in mg# and mineralogy, suggesting a very narrow range in crystallization. The uniformity in mg# could be due to metamorphic equilibration (Fowler et al. 1994, 1995; Mittlefehldt 1994), but the nearly monomineralic nature of diogenites implies either a restricted range in crystallization or a parent melt very rich in orthopyroxene component (Mittlefehldt 1994). The former is at odds with the wide range in incompatible element abundances. Fowler et al. (1995) suggested that the diogenites may have been derived from a suite of parent mafic melts with different incompatible element contents, rather than a single orthopyroxenitic melt. Shearer et al. (1997) have concluded that diogenites did not form from highly orthopyroxene normative magmas. Rather, they suggest that the major and trace element systematics of the diogenite suite can be modeled as cumulates arising via small amounts (10-20%) of fractional crystallization of a suite of distinct basaltic magmas formed either by fractional melting of a homogeneous source, or equilibrium melting of heterogeneous sources.

Sack et al. (1991) suggested that two diogenites are unusually olivine-rich, and represent melting residues (restites) from the HED parent body rather than cumulates. Mittlefehldt (1994) argued that those two diogenites were not unusually olivine-rich, based on modal data provided by R. Hewins and on a bulk composition for one of them. Fowler et al. (1995) and Mittlefehldt (1994) showed that these two diogenites are not unusual in minor and trace element composition compared to other diogenites, and that a restite origin for them seems unlikely.

The cumulate eucrites are cumulates from a fractionally crystallizing mafic melt. Stolper (1977) demonstrated that the cumulate eucrites are too iron-rich to have crystallized from basaltic eucrites. Liquidus pyroxenes for Sioux County have an mg# of 71-72 (Stolper 1977), while the most magnesian cumulate eucrite Binda contains pyroxenes with a bulk mg# of 67 (Takeda et al. 1976). Using the data in Stolper (1977), one can infer that liquidus pyroxene in Nuevo Laredo or Lakangaon, the most ferroan basaltic eucrites, would have an mg# of ~59, compared with bulk pyroxene mg# of 58 and 56 for Moama and Serra de Magé, respectively (Harlow et al. 1979, Lovering 1975). Several researchers have suggested that the parent melt of the cumulate eucrites was unusual in that it had a LREE-enriched pattern. This was originally based on calculations using bulk analyses of mineral separates from Moore County and Serra de Magé, and

mid-1970s vintage partition coefficients (Ma and Schmidt 1979, Ma et al. 1977), and has recently been reiterated by Hsu and Crozaz (1997) based on SIMS analyses of pyroxenes and plagioclase in Moama and Moore County and modern partition coefficients. These latter authors concluded that subsolidus redistribution did not affect the REE they measured, and that therefore the cumulate eucrites most likely were formed from melts with fractionated REE patterns which do not seem to be genetically related to the basaltic eucrites. Pun and Papike (1995) similarly found that nominal parent melts for the cumulate eucrites Binda, Moama, Moore County and Serra de Magé, calculated through inversion of mineral REE data obtained by SIMS, showed LREE-enriched patterns. These authors cautioned that unusual parent melts provided only one possible explanation of the result, and that subsolidus redistribution of the REE or inappropriate partition coefficients could be the cause of the unusual calculated patterns. Treiman (1997) showed that the cumulate eucrites Moore County and Serra de Magé can be modeled for major and trace elements as mixtures of cumulus minerals and trapped melt from parent melts similar to basaltic eucrites. He suggested that subsolidus redistribution of the REE causes parent melts calculated by inversion of SIMS data to have unusual REE patterns.

Thermal metamorphism of the HED parent body crust

As discussed above, almost all HED meteorites show textural evidence for extensive thermal annealing in the form of Fe-Mg equilibration and exsolution of pyroxenes and mineral grain recrystallization. Detailed study of the pyroxene textures led to the observation that the mg# and textural features were roughly correlated; more magnesian lithologies (diogenites, cumulate eucrites) are more annealed than are more ferroan lithologies (basaltic eucrites). As the former are intrusive rocks and the latter surficial rocks, this observation led to development of a layered-crust model for the HED parent body by H. Takeda and colleagues (e.g. Miyamoto and Takeda 1977, Takeda 1979, Takeda et al. 1976). In this model, the extent of pyroxene exsolution and inversion is related to the depth of formation of the rock, and the pyroxene textures are largely caused by slow cooling from the magmatic stage (Takeda 1979). It was recognized that some eucrites do not fit the overall trend, and later metamorphism was also noted as an important process in some cases (e.g. Takeda and Graham 1991). One possibility is that impact heating was an important agent of metamorphism, and this has been used to explain the textural differences between basalt clasts in polymict breccias and monomict eucrites (e.g. Nyquist et al. 1986, Takeda and Graham 1991). Heating by subsequent flows or intrusions is another possible metamorphism agent (Takeda and Graham 1991).

Other researchers have argued that impact heating (Keil et al. 1997) and contact metamorphism by later intrusions/extrusions (Yamaguchi et al. 1996) cannot possibly explain the great preponderance of metamorphosed lithologies in the HED suite. Yamaguchi et al. (1996, 1997) have addressed the issue of why thermal metamorphism was so prevalent among the basaltic eucrites, which presumably were extrusive flows on the HED parent body. These authors suggest that a high eruption rate on the parent body could bury early form basalts rapidly enough that heat conducted up from the mantle through the crust would be sufficient to anneal eucrites. Reestablishment of the parent body thermal gradient thus causes global thermal metamorphism in the crust. In this model, the earliest formed basalts would be the most highly metamorphosed, and the latest extrusions would be unmetamorphosed. This model can easily accommodate vesicular yet highly recrystallized eucrites such as Ibitira which must have been extruded onto the surface and yet suffered extensive metamorphism.

4 Vesta, the HED parent body?

The HED meteorite group is the only such group, excluding lunar and martian

meteorites, for which we have a strong candidate for the parent body, the asteroid 4 Vesta. McCord et al. (1970) first showed that the reflectance spectrum of Vesta in the wavelength region from 0.3 to 1.1 μm was matched by the laboratory spectrum of a basaltic eucrite, Nuevo Laredo. Subsequently, Consolmagno and Drake (1977) argued that Vesta was indeed the parent body of the HED meteorites. Wasson and Wetherill (1979) discussed the dynamical problems of moving material from Vesta to Earth-crossing orbits where they could be sampled as meteorites. Basically, Vesta is far from orbital resonances such that only energetic events could propel material into regions where they would have a reasonable probability of evolving into Earth-crossing orbits. Such material is expected to be heavily shocked, in contrast to most HED meteorites. The yield of material from Vesta should be much smaller than from other, presumably differentiated asteroids more suitably placed in orbital-element space (Wasson and Wetherill 1979).

Hostetler and Drake (1978) proposed that the material ejected from Vesta was originally in fragments large enough to shield most of the mass from cosmic-ray bombardment. Some of these bodies evolved into Earth-crossing orbits, and collisions in space liberated the smaller pieces that now fall as meteorites, with cosmic-ray exposure ages of 5-75 Ma. Recently, Cruikshank et al. (1991) determined that three asteroids of ~1-3 km diameter in Earth-approaching orbits have spectral characteristics very similar to those of Vesta and the HED meteorites. These authors suggested that these three asteroids are the immediate sources of many of the HED meteorites. Cruikshank et al. (1991) did not favor Vesta as the ultimate source for the Earth-approaching asteroids. They were led by the oxygen-isotopic similarity of HED meteorites and main-group pallasites into a belief that the parent body of these meteorites was one and the same, and must therefore have been totally disrupted to liberate pallasites from the core-mantle boundary. Binzel and Xu (1993) surveyed numerous small asteroids in orbits similar to Vesta's and found 20 with diameters between 4 and 10 km that have spectra similar to that of Vesta. These small asteroids form a "trail" in orbital-element space from near Vesta to near the 3:1 resonance. Binzel and Xu (1993) proposed that these small asteroids are spalls from collisions on Vesta, and that some of their brethren reached the 3:1 resonance, had their orbits perturbed into Earth-crossing or Earth-approaching orbits, and ultimately delivered HED meteorites to the Earth.

Wasson and Chapman (1996) have argued that Vesta is not the HED parent body. They suggested that there must have been many asteroids with basaltic crusts, based on the number of differentiated parent bodies inferred from the meteorite record. They further suggested that space weathering has altered the reflectance spectra of most of these bodies to resemble S asteroids, and that one of these asteroids in a more favorable orbit is the parent body for HED meteorites. In their view, Vesta stands out as being like HEDs only because it was recently resurfaced, exposing fresh material. The controversy over whether Vesta is indeed the HED parent body will likely only be resolved by petrological and geochemical analysis of returned Vesta samples.

The geology of the surface of Vesta has come under increasing scrutiny through both ground- and space-based telescopic study. Based on this work, Vesta is known to harbor regions rich in orthopyroxene and regions more basalt-like (Binzel et al. 1997, Gaffey 1997). There is a general hemispheric dichotomy, with one hemisphere being richer in magnesian pyroxenes (more diogenite-like) than the other (Binzel et al. 1997). This hemisphere also gives spectral evidence for the presence of substantial olivine (Binzel et al. 1997, Gaffey 1997).

ANGRITES

The angrite grouplet consists of four meteorites, Angra dos Reis, LEW 86010, LEW 87051 and Asuka 881371. These rocks, while petrologically distinct, have identical oxygen-isotopic compositions (Clayton and Mayeda 1996), have similar unusual mineralogies (e.g. McKay et al. 1988a, 1990; Prinz et al. 1977, Yanai 1994) and share a number of geochemical characteristics (Mittlefehldt and Lindstrom 1990, Warren et al. 1995) that suggest that they originated on a common parent body. Although the angrites share a narrow region of O-isotope space with the HED meteorites, mesosiderites and brachinites (Fig. 1d), the unusual mineralogies and compositions of the angrites suggest that they are not closely related to any of these other meteorite groups. The angrites are crustal igneous rocks of generally basaltic composition, although Angra dos Reis is mineralogically and compositionally quite unusual.

Mineralogy and petrology

Angra dos Reis. The most detailed description of this rock was given by Prinz et al. (1977), and the synopsis given here is derived from this source unless otherwise noted. Angra dos Reis is a medium- to coarse-grained igneous rock composed dominantly of aluminian-titanian-diopside, with minor olivine, spinel and troilite, and accessory magnesian kirschsteinite, celsian, whitlockite, titanian magnetite, baddeleyite and metal. The pyroxenes occur in two textures; a groundmass of small xenomorphic grains on the order of 100 μm in size, and larger, poikilitic grains on the order of 1 mm in size. Pyroxene grains in the former join at triple junctures. The small groundmass grains are enclosed in the poikilitic grains, and occur along the margins of the large grains where they are partially enclosed. Olivine occurs as grains within the groundmass, or as aggregates of small equidimensional grains joining at triple junctures. Wasserburg et al. (1977) noted that olivine is heterogeneously distributed in the meteorite. Spinel occurs as xenomorphic grains "dispersed throughout" pyroxene. Whitlockite occurs as mm-sized grains dispersed throughout the rock, although again, Wasserburg et al. (1977) note that it is heterogeneously distributed. Magnesian kirschsteinite occurs as inclusions in olivine. Celsian and titanomagnetite are found in the groundmass. The compositions of olivine and kirschsteinite are given in Table 36, pyroxene in Table 37, spinel and titanomagnetite in Table 38, and celsian in Table 39.

Plagioclase has also been reported, but has not been found in thin section. Prinz et al. (1977) found a few grains of plagioclase in mineral separates prepared by Wasserburg et al. (1977). The composition of this plagioclase is given in Table 39. Lugmair and Marti (1977) report small amounts of feldspar in one subsample of Angra dos Reis prepared by Wasserburg et al. (1977), but did not characterize it. Störzer and Pellas (1977) found feldspar in subsamples they prepared for track work. These authors did not characterize the feldspar, but noted that two distinct types were present. The majority of the grains required etching conditions like those used to reveal tracks in bytownite, while one grain required etching conditions like those used to reveal tracks in albite-oligoclase (Störzer and Pellas 1977). The composition of plagioclase measured by Prinz et al. (1977) for Angra dos Reis is quite distinct from that in the other angrites (Table 39), but like those in HED meteorites (Table 33). Because plagioclase has not been found in thin section in Angra dos Reis, there is the possibility that the grains measured by Prinz et al. (1977) represent contaminants introduced during sample processing. Eucrites were being actively studied in Wasserburg's lab during the time period that Angra dos Reis was being prepared (Wasserburg et al. 1977). Both types of feldspar found by Störzer and Pellas (1977) have identical cosmic-ray track records, indicating identical exposure histories.

Table 36. Representative olivine and kirschsteinite analyses for angrites.

	Angra dos Reis (1)	Angra dos Reis (2)	LEW 86010 (3)	LEW 86010 (4)	Asuka 881371 (5)	Asuka 881371 (6)	Asuka 881371 (7)	Asuka 881371 (8)	Asuka 881371 (9)	Asuka 881371 (10)	Asuka 881371 (11)
					Chemical Composition (wt %)						
SiO_2	36.3	34.6	32.5	32.4	39.9	33.3	39.6	34.2	37.6	30.6	31.0
Al_2O_3		0.33	0.03	0.01	0.04	0.02	0.06	0.06	0.04	0.04	-
FeO	38.3	26.2	50.6	32.2	10.3	43.1	13.5	43.5	28.6	53.4	43.3
MgO	24.3	8.90	13.4	4.93	47.5	20.5	45.4	19.6	32.8	0.35	2.30
MnO	0.60	0.42	0.62	0.39	0.18	0.48	0.16	0.50	0.34	0.77	0.64
Cr_2O_3	0.03	0.02	0.01	0.02	0.17	-	0.34	0.08	0.07	-	-
CaO	1.29	28.9	2.16	29.2	0.06	1.92	0.28	1.89	0.85	13.5	21.6
Total	100.82	99.37	99.32	99.15	98.15	99.32	99.34	99.83	100.30	98.66	98.84
					Cation Formula Based on 4 Oxygens						
Si	1.0170	1.0154	0.9985	0.9913	0.9994	0.9816	0.9956	1.0012	1.0070	1.0068	0.9894
Al	0.0000	0.0114	0.0011	0.0004	0.0012	0.0007	0.0018	0.0021	0.0013	0.0016	0.0000
Fe	0.8974	0.6430	1.3002	0.8239	0.2158	1.0625	0.2839	1.0650	0.6406	1.4694	1.1558
Mg	1.0146	0.3892	0.6136	0.2248	1.7732	0.9006	1.7011	0.8551	1.3092	0.0172	0.1094
Mn	0.0142	0.0104	0.0161	0.0101	0.0038	0.0120	0.0034	0.0124	0.0077	0.0215	0.0173
Cr	0.0007	0.0005	0.0002	0.0005	0.0034	0.0000	0.0068	0.0019	0.0015	0.0000	0.0000
Ca	0.0387	0.9087	0.0711	0.9573	0.0016	0.0606	0.0075	0.0593	0.0244	0.4760	0.7387
Total Cations	2.9826	2.9786	3.0008	3.0083	2.9984	3.0180	3.0001	2.9970	2.9917	2.9925	3.0106
					*Cation Ratios Larnite (La), Fosterite (Fo), Fayalite (Fa), Fe/Mn and mg# (100*Mg/(Mg+Fe))*						
La	2.0	46.8	3.6	47.7	0.1	3.0	0.4	3.0	1.2	24.3	36.9
Fo	52.0	20.1	30.9	11.2	89.1	44.5	85.4	43.2	66.3	0.9	5.5
Fa	46.0	33.1	65.5	41.1	10.8	52.5	14.2	53.8	32.4	74.9	57.7
Fe/Mn	63	62	81	82	56	89	83	86	83	68	67
mg#	53.1	37.7	32.1	21.4	89.2	45.9	85.7	44.5	67.1	1.2	8.6

(1) Average of olivine analyses (Prinz et al., 1977); (2) Average of kirschsteinite analyses (Prinz et al., 1977); (3) Average of olivine analyses (Crozaz and McKay, 1990); (4) Average of kirschsteinite analyses (Crozaz and McKay, 1990); (5, 6) Large, magnesian olivine core and rim, respectively (Yanai, 1994); (7, 8) Large, olivine xenocryst core and rim, respectively (Mikouchi et al., 1996); (9, 10) Groundmass olivine core and rim, respectively (Mikouchi et al., 1996); (11) Groundmass kirschsteinite (Yanai, 1994).

Table 37. Representative pyroxene analyses for angrites.

	Angra dos Reis (1)	LEW 86010 (2)	LEW 86010 (3)	LEW 86010 (4)	LEW 86010 (5)	LEW 86010 (6)	Asuka 881371 (7)	Asuka 881371 (8)	Asuka 881371 (9)	Asuka 881371 (10)	Asuka 881371 (11)
					Chemical Composition (wt %)						
SiO_2	45.9	48.5	44.8	43.2	42.3	41.8	46.5	41.4	45.6	44.5	40.7
Al_2O_3	10.0	5.85	9.11	11.0	11.8	11.7	7.82	6.63	9.13	3.91	8.26
TiO_2	2.16	0.83	2.21	2.71	3.14	3.39	1.78	3.90	1.58	2.42	4.75
Cr_2O_3	0.21	0.67	0.35	0.17	0.13	0.16	0.38	bd	0.60	-	-
FeO	6.70	7.69	9.58	9.84	10.4	10.9	12.1	26.1	9.90	27.4	25.2
MnO	0.06	0.09	0.10	0.09	0.09	0.10	0.17	0.16	0.06	0.24	0.06
MgO	10.6	12.0	9.23	8.39	7.56	7.18	8.19	0.05	8.90	0.10	-
CaO	24.1	24.1	24.4	24.4	24.2	24.1	23.1	21.5	23.0	21.1	21.7
Na_2O	nd	nd	nd	nd	nd	nd	-	0.04	0.03	nd	0.15
Total	99.73	99.73	99.78	99.80	99.62	99.33	100.04	99.78	98.80	99.67	100.82
					Cation Formula Based on 8 Oxygens (Ideal Plagioclase = 5 Cations per 8 Oxygens)						
Si	1.7185	1.8233	1.7073	1.6501	1.6237	1.6149	1.7751	1.7072	1.7460	1.8359	1.6537
^{iv}Al	0.2815	0.1767	0.2927	0.3499	0.3763	0.3851	0.2249	0.2928	0.2540	0.1641	0.3463
Total tet*	2.0000	2.0000	2.0000	2.0000	2.0000	2.0000	2.0000	2.0000	2.0000	2.0000	2.0000
Ti	0.0608	0.0235	0.0633	0.0778	0.0906	0.0985	0.0511	0.1209	0.0455	0.0751	0.1451
^{vi}Al	0.1598	0.0825	0.1165	0.1453	0.1576	0.1477	0.1270	0.0295	0.1581	0.0260	0.0493
Cr	0.0062	0.0199	0.0105	0.0051	0.0039	0.0049	0.0115	--	0.0182	--	--
Fe	0.2098	0.2418	0.3053	0.3143	0.3339	0.3522	0.3863	0.9001	0.3170	0.9454	0.8563
Mn	0.0019	0.0029	0.0032	0.0029	0.0029	0.0033	0.0055	0.0056	0.0019	0.0084	0.0021
Mg	0.5915	0.6723	0.5242	0.4776	0.4325	0.4134	0.4659	0.0031	0.5079	0.0061	--
Ca	0.9668	0.9708	0.9963	0.9986	0.9953	0.9977	0.9449	0.9500	0.9436	0.9328	0.9447
Na	--	--	--	--	--	--	--	0.0032	0.0022	--	0.0118
Total Cations	3.9968	4.0137	4.0193	4.0216	4.0167	4.0177	3.9922	4.0124	3.9944	3.9938	4.0093
					*Cation Ratios Ca:Mg:Fe, Fe/Mn and mg# (100*Mg/(Mg+Fe))*						
Ca	54.7	51.5	54.6	55.8	56.5	56.6	52.6	51.3	53.4	49.5	52.5
Mg	33.5	35.7	28.7	26.7	24.6	23.4	25.9	0.2	28.7	0.3	0.0
Fe	11.9	12.8	16.7	17.6	19.0	20.0	21.5	48.6	17.9	50.2	47.5
Fe/Mn	110	83	95	108	115	107	70	161	167	113	408
mg#	73.8	73.5	63.2	60.3	56.4	54.0	54.7	0.3	61.6	0.6	0.0

(1) Average of analyses (Prinz et al., 1977); (2-6) Individual analyses (Crozaz and McKay, 1990); (7, 8) Mikouchi et al. (1996); (9-11) Individual analyses (Yanai, 1994).

Table 38. Representative oxide analyses for angrites.

	Angra dos Reis (1)	Angra dos Reis (2)	LEW 86010 (3)	LEW 86010 (4)	Asuka 881371 (5)	Asuka 881371 (6)
Chemical Composition (wt %)						
TiO_2	0.65	21.9	0.78	27.0	1.48	27.3
Al_2O_3	54.5	3.50	56.9	4.86	37.8	2.42
Cr_2O_3	3.30	1.02	1.21	1.11	20.9	0.01
V_2O_3	0.07	0.26	--	--	0.60	0.08
Fe_2O_3	3.40	18.5	1.86	40.2	--	--
FeO	28.4	48.8	32.2	25.8	31.4	68.4
MgO	8.00	1.18	5.87	1.16	6.98	0.02
MnO	0.18	1.17	0.17	0.36	0.26	0.22
CaO	0.76	1.21	0.07	0.06	0.13	0.09
SiO_2	0.51	1.23	0.05	0.06	0.25	0.10
Total	99.77	98.77	99.11	100.61	99.80	98.64
Cation Formula Based on 4 Oxygens (Ideal Spinel = 3 Cations per 4 Oxygens)						
Ti	0.0137	0.6052	0.0166	0.6786	0.0337	0.7960
Al	1.7990	0.1516	1.8985	0.1914	1.3492	0.1106
Cr	0.0731	0.0296	0.0271	0.0293	0.5004	0.0003
V	0.0016	0.0077	--	--	0.0146	0.0025
Fe^{3+}	0.0717	0.5116	0.0396	1.0110	--	--
Fe^{2+}	0.6652	1.4997	0.7623	0.7211	0.7952	2.2179
Mg	0.3339	0.0646	0.2476	0.0578	0.3150	0.0012
Mn	0.0043	0.0364	0.0041	0.0102	0.0067	0.0072
Ca	0.0228	0.0476	0.0021	0.0021	0.0042	0.0037
Si	0.0143	0.0452	0.0014	0.0020	0.0076	0.0039
Total Cations	2.9996	2.9992	2.9993	2.7035	3.0266	3.1433
*Cation Ratios Fe/Mn, mg# (100*Mg/(Mg+Fe)) and cr# (100*Cr/(Cr+Al))*						
Fe/Mn	156	41	187	71	119	307
mg#	33.4	4.1	24.5	7.4	28.4	0.1
cr#	3.9	16.4	1.4	13.3	27.1	0.3

(1) Average of spinel analyses (Prinz et al., 1977); (2) Average of titanomagnetite analyses (Prinz et al., 1977) (3) Average of hercynite analyses (McKay et al., 1988a); (4)) Average of titanomagnetite analyses (McKay et al., 1988a); (5) Spinel (Mikouchi et al., 1996); (6) Ulvöspinel (Mikouchi et al., 1996).

LEW 86010. Sadly, petrologic details for LEW 86010 are lacking, and brief descriptions only are available in numerous abstracts. LEW 86010 is composed primarily of aluminian-titanian-diopside, plagioclase and olivine, with minor kirschsteinite and troilite, and accessory whitlockite, hercynitic spinel, titanomagnetite and Fe,Ni metal (McKay et al. 1988a, Prinz et al. 1988b). Different authors describe the texture variously as "gabbroic or granular" (Delaney and Sutton 1988), "cumulate" (Goodrich 1988) or "subophitic to poikilitic" (Prinz et al. 1988b), but it can best be described as hypidiomorphic-granular (McKay et al. 1988a) (Fig. 48). Aluminian-titanian-diopsides are generally anhedral grains on the order of 2-3 mm in size and are zoned from mg# of 70-75 to about 50, with lower TiO_2 and Al_2O_3, and higher Cr_2O_3 in the cores (Delaney and Sutton 1988, Goodrich 1988, McKay et al. 1988a, Prinz et al. 1988b). Plagioclase grains are subhedral to euhedral, on the order of 1 to 2.5 mm in size and are virtually end-member anorthite in composition (Goodrich 1988, McKay et al. 1988a). Olivine occurs as anhedral to subhedral grains roughly 1 to 2.5 mm in size and containing exsolution lamellae of kirschsteinite up to 20 μm in width (Delaney and Sutton 1988, Goodrich 1988, McKay et al. 1988a, Mikouchi et al. 1995). Olivine is uniform in composition with a mg# of 32-33 and a CaO content of 1.5 to 2.2 wt % (Crozaz and McKay 1990, McKay et al. 1988a, Prinz et al. 1988b). The compositions of olivine and kirschsteinite for LEW 86010 are given in Table 36, pyroxene in Table 37, spinel and titanomagnetite in Table 38, and plagioclase in Table 39.

Table 39. Representative plagioclase and celsian analyses for angrites.

	Angra dos Reis (1)	Angra dos Reis (2)	LEW 86010 (3)	Asuka 881371 (4)
Chemical Composition (wt %)				
SiO_2	46.2	33.6	43.3	43.8
Al_2O_3	33.6	28.0	36.7	35.4
FeO	0.21	0.43	0.23	0.37
MgO	--	--	0.03	0.19
CaO	17.2	1.20	20.5	20.2
Na_2O	1.47	0.15	0.03	0.04
K_2O	0.11	0.05	--	0.01
BaO	--	38.2	--	--
Total	98.79	101.63	100.79	100.01
Cation Formula Based on 8 Oxygens (Ideal Plagioclase = 5 Cations per 8 Oxygens)				
Si	2.1500	2.0135	1.9940	2.0316
^{IV}Al	1.8431	1.9778	1.9921	1.9354
Total tet*	3.9931	3.9913	3.9861	3.9670
Fe	0.0082	0.0216	0.0089	0.0144
Mg	--	--	0.0021	0.0131
Ca	0.8577	0.0771	1.0116	1.0040
Na	0.1326	0.0174	0.0027	0.0036
K	0.0065	0.0038	--	0.0006
Ba	--	0.8971	--	--
Total Cations	4.9981	5.0083	5.0114	5.0027
*Cation Ratios 100*Mg/(Mg+Fe) (mg#) and Molecular Proportion of Orthoclase (Or), Albite (Ab), Anorthite (An) and Celsian (Cs)*				
mg#	--	--	18.9	47.8
Or	0.7	0.4	--	0.1
Ab	13.3	1.8	0.3	0.4
An	86.0	7.7	99.7	99.5
Cs	--	90.1	--	--

(1) Average of plagioclase from mineral separates (Prinz et al., 1977); (2) Average of celsian analyses (Prinz et al., 1977); (3) Average of plagioclase analyses (Crozaz and McKay, 1990); (4) Plagioclase (Mikouchi et al., 1996).

A-881371 and LEW 87051. Asuka 881371 and Lewis Cliff 87051 are similar rocks. They are porphyritic-textured rocks containing large, subhedral to euhedral grains of magnesian olivine set in an ophitic textured groundmass of euhedral laths of anorthite intergrown with euhedral to subhedral, highly zoned aluminian-titanian-diopside and ferroan olivine (Fig. 49). Kirschsteinite and traces of titanomagnetite, spinel, whitlockite, troilite and Fe,Ni metal are also present (McKay et al. 1990, 1995; Mikouchi et al. 1996, Prinz and Weisberg 1995, Prinz et al. 1990, Yanai 1994).

The coarse olivines are variable in size and composition. Prinz et al. (1990) reported sizes from 0.15 to 1 mm for LEW 87051 with core compositions ranging from Fo_{73} to Fo_{90}, with the largest olivine being the most magnesian. The coarse olivines in A-881371 are up to about 2 mm in size, and core compositions have a narrower range of Fo_{81} to Fo_{89} (McKay et al. 1995, Mikouchi et al. 1996, Prinz and Weisberg 1995, Yanai 1994). The larger of the coarse olivines have very homogeneous cores with strongly zoned rims, while the smaller of the coarse olivines show zoning in the cores which is distinct from that in the rims (Mikouchi et al. 1996). Mikouchi et al. (1996) suggested that the zoning

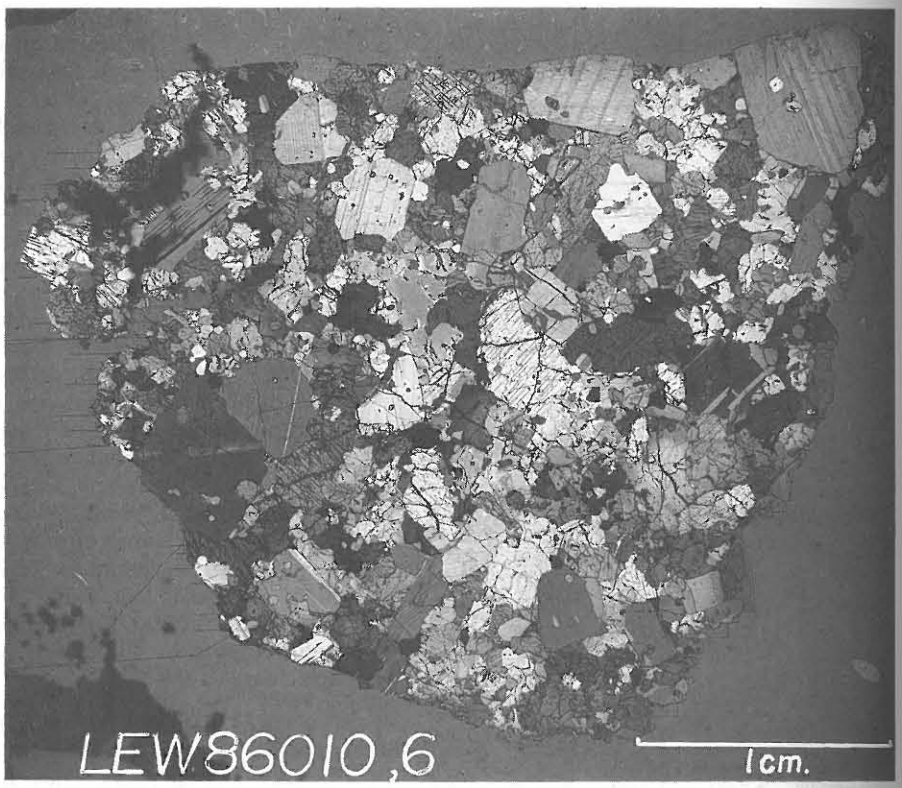

Figure 48. Photomicrograph of LEW 86010 in transmitted light, partially crossed nichols, showing heterogeneous, hypidiomorphic texture. Major phases are anorthite (twinned), olivine (unzoned, exsolution lamellae) and Al-Ti-diopside (zoned). NASA/JSC photo S88 28784 courtesy of G. McKay.

observed in the smaller olivine cores was an artifact of off-center cuts through large olivine grains with zoned rims. The cores of the large olivine grains have high Cr_2O_3 contents, ~0.34 wt %, compared to the cores of groundmass olivine grains, 0.07 wt % (Mikouchi et al. 1996). The rims on the coarse olivines and the groundmass grains are strongly zoned to Fe- and Ca-rich compositions. Cores of groundmass olivines have compositions of about Fo_{66-70}, with roughly 1 mol % of the larnite (La) component, Ca_2SiO_4, and are zoned out to ~Fo_0, ~La_{20-25} (McKay et al. 1990, 1995; Mikouchi et al. 1996, Prinz and Weisberg 1995, Warren and Davis 1995, Yanai 1994). The larnite content of the rims of groundmass olivine grains is difficult to determine because of fine-scale intergrowth with kirschsteinite (e.g. McKay et al. 1990). Representative analyses of olivine and kirschsteinite grains for A-881371 are given in Table 36.

The aluminian-titanian-diopside grains are strongly zoned in Fe-Mg, but have nearly constant CaO content (McKay et al. 1990, Yanai 1994), while Al_2O_3 and TiO_2 are complexly zoned. Both Al_2O_3 and TiO_2 are high in the magnesian cores and initially drop with decreasing mg#, but as mg# continues to decrease, Al_2O_3 is roughly constant or increases slightly, while TiO_2 increases significantly (e.g. McKay et al. 1990, Warren and Davis 1995). Representative analyses of pyroxene grains for A-881371 are in Table 37.

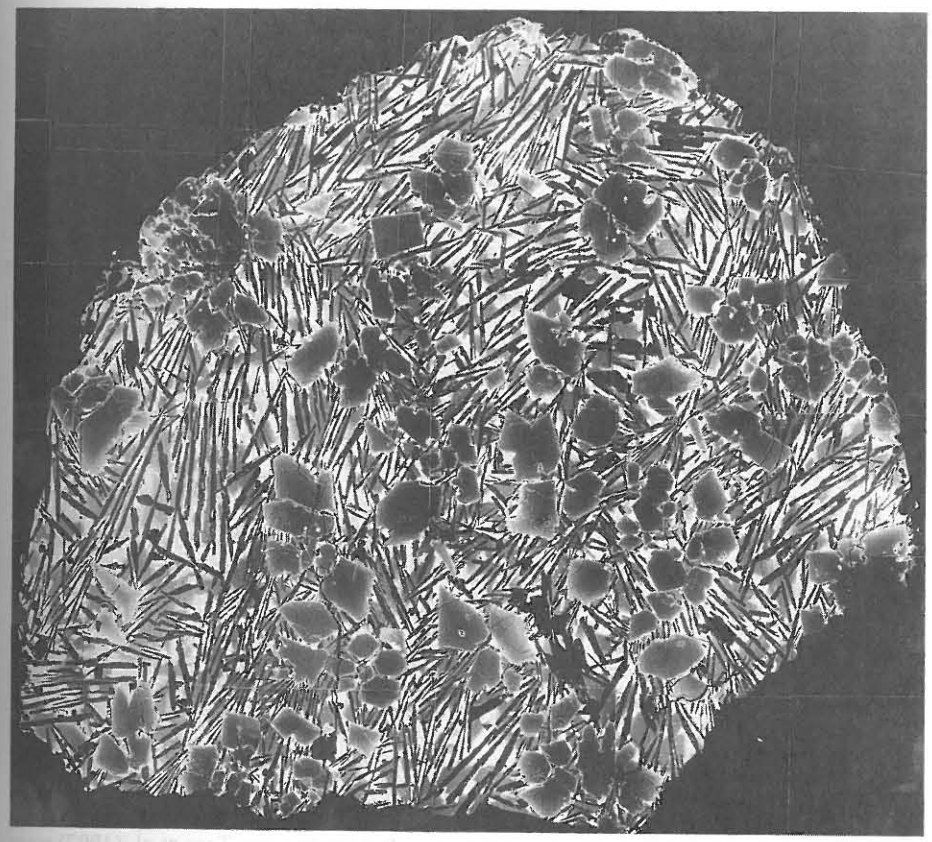

Figure 49. BSE image of LEW 87051 showing euhedral to anhedral olivine xenocrysts in a groundmass of anorthite (dark laths) and Al-Ti-diopside. Image is about 4.8 mm across. NASA/JSC photo S88 28784 courtesy of G. McKay.

Plagioclase in A-881371 and LEW 87051 are essentially pure anorthite. Representative analyses of plagioclase grains are given in Table 39. Representative analyses of spinel grains for A-881371 and LEW 87051 are given in Table 38.

Composition

The angrites are roughly basaltic in composition, although they are unlike any other known basalt in the solar system in that they are the most alkali-depleted. This is expressed by their very low Na_2O and K_2O contents (Table 40), and by their very low contents of the trace alkali elements, Li, Rb and Cs (e.g. Tera et al. 1970). Angrites also have low abundances of the moderately volatile element Ga, and they have lower Ga/Al ratios than any achondrite, lunar sample or martian meteorite (e.g. Warren et al. 1995). Paradoxically, however, angrites are not notably depleted in the highly volatile/mobile elements Br, Se, Zn, In and Cd compared to lunar basalts and eucrites (Warren et al. 1995). Figure 50 shows CI- and Sm-normalized moderately volatile and volatile element abundances for the angrites compared to the basaltic eucrites Sioux County, Juvinas and Ibitira. Also shown for comparison are the ranges in CI- and U-normalize volatile/mobile element abundances for 7 basaltic eucrite falls analyzed by Paul and Lipschutz (1990). (Both Sm and U are highly incompatible, refractory elements, and to first order, CI-

Table 40. Representative whole rock compositions of angrites.

		Angra dos Reis (1)	LEW 86010 (1)	LEW 87051 (1)	Asuka 881371 (2)
Bulk Major Element Composition					
SiO_2	wt%	43.7	39.6	40.4	37.3
TiO_2	wt%	2.05	1.15	0.73	0.88
Al_2O_3	wt%	9.35	14.1	9.19	10.1
Cr_2O_3	wt%	0.22	0.12	0.16	0.13
Fe_2O_3	wt%				0.63
FeO	wt%	9.8	18.2	19.4	23.4
MnO	wt%	0.10	0.20	0.24	0.20
MgO	wt%	10.8	7.0	19.4	14.8
CaO	wt%	23.1	18.4	10.4	12.5
Na_2O	wt%	0.0301	0.0211	0.0234	0.022
P_2O_5	wt%	0.13	0.13	0.08	0.17
S	wt%				0.59
Total		99.28	98.92	100.02	100.72
*Cation Ratios Fe/Mn and 100*Mg/(Mg+Fe) (mg#)*					
Fe/Mn		97	90	80	116
mg#		66.3	40.7	64.1	53.0
Whole Rock Trace Element Contents					
Sc	µg/g	49.6	56.7	36.0	32.9
Co	µg/g	21.3	21.8	27.4	
Ni	µg/g	58	39	45	
Zn	µg/g	1.73	1.8	0.89	
La	µg/g	6.14	3.38	2.32	2.34
Ce	µg/g	19.2	10.1	6.2	5.9
Sm	µg/g	5.76	2.68	1.48	1.39
Eu	µg/g	1.78	0.978	0.536	0.53
Tb	µg/g	1.39	0.66	0.36	
Yb	µg/g	4.82	2.64	1.52	1.38
Lu	µg/g	0.686	0.386	0.239	0.21
Hf	µg/g	2.79	2.21	1.17	1.03
Ta	ng/g	350	260	110	
Ir	ng/g	0.07	7.1	0.180	2.4
Th	ng/g	640	480	220	

(1) Data taken from Mittlefehldt and Lindstrom (1990), except Ni, Zn and Ir from Warren et al. (1995). All iron reported as FeO; (2) Major element data except Na_2O from Yanai (1994). Trace element data and Na_2O from Warren et al. (1995). Data identified by Warren et al. (1995) as having unusually high uncertainties not listed.

normalized element/Sm and element/U ratios are equivalent.) The angrites are depleted in the moderately volatile lithophile elements Li, Mn, Rb, K and Na, and lithophile/siderophile Ga compared to basaltic eucrites (Fig. 50), but within the ranges exhibited by basaltic eucrites for the more volatile/mobile elements, and moderately volatile siderophile elements. Note that volatile lithophile Cs in Angra dos Reis is more than an order of magnitude depleted relative to the narrow range exhibited by basaltic eucrites.

The Pb data displayed in Figure 50 are CI-normalized 1/µ (≡ $^{204}Pb/^{238}U$) as determined by chronologic studies of angrites and eucrites. For Angra dos Reis and Ibitira, the measured µ values of Wasserburg et al. (1977) were used. For LEW 86010, the conservatively low, inferred source region μ_1 of Lugmair and Galer (1992) was used. For the basaltic eucrite range, the inferred source μ_1 values for Bereba, Bouvante and Nuevo Laredo from Tera et al. (1997) were used. These data show that the angrite parent body was depleted in volatile/mobile Pb relative to the eucrite parent body (Lugmair and Galer 1992).

The angrites exhibit a range of fractionated refractory lithophile element patterns compared to basaltic eucrites (Fig. 51). A-881371, LEW 86010 and LEW 87051 show generally similar patterns, while Angra dos Reis is distinct. All angrites have superchondritic Ca/Al ratios, with Angra dos Reis showing extreme fractionation (Mittlefehldt and Lindstrom 1990), and compared to basaltic eucrites, have higher Ti/Hf ratios (Fig. 52a). The Antarctic angrites have generally flat REE patterns while Angra dos Reis has a fractionated pattern with depletions in the light and heavy REE compared to the middle REE, and only Angra dos Reis has a significant Eu anomaly (e.g. Ma et al. 1977, Mittlefehldt and Lindstrom 1990, Warren et al. 1995, see Fig. 51). The Antarctic angrites have higher Sc/Sm ratios than basaltic eucrites (Fig. 52b). Angra dos Reis has a lower Sc/Sm ratio, but this is because of its higher REE content. The Sc content of Angra dos Reis is substantially greater than that of basaltic eucrites (compare Table 40, Table 35). The pyroxene of Angra dos Reis contains ~200 ppb U (~25 times CI), roughly the same concentration as found in chondritic phosphates (Störzer and Pellas 1977).

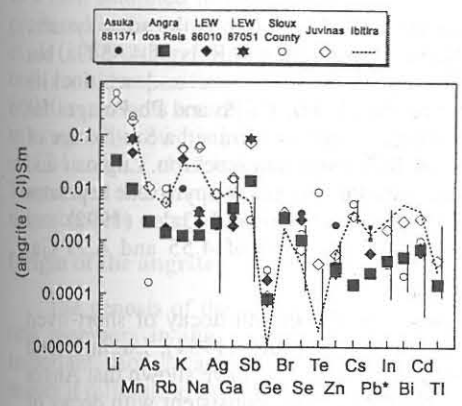

Figure 50. CI- and Sm-normalized moderately volatile and volatile elements in angrites plotted in order of decreasing nebular 50% condensation temperature. Data for the basaltic eucrites Sioux County, Juvinas and Ibitira are shown for comparison. Angrites are severely depleted in moderately volatile lithophile elements. The Pb data are CI-normalized $^{204}Pb/^{238}U$ ratios (see text). The K datum for LEW 86010 likely represents contamination acquired while in Antarctica. Angrite data are means of data from Laul et al. (1972), Lugmair and Galer (1992), Ma et al. (1977), Mittlefehldt and Lindstrom (1990), Nyquist et al. (1994), Schnetzler and Philpotts (1969), Tera et al. (1970), Warren et al. (1995), Wasserburg et al. (1977), Yanai (1994). The vertical line are ranges of CI-normalized volatile/U ratios for 7 basaltic eucrite falls from Paul and Lipschutz (1990).

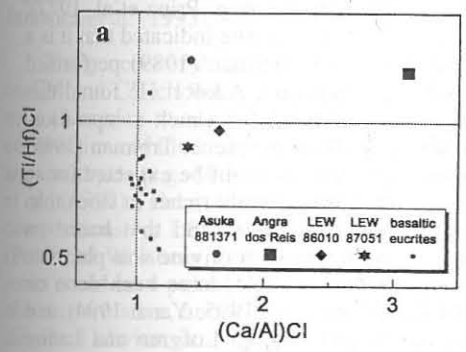

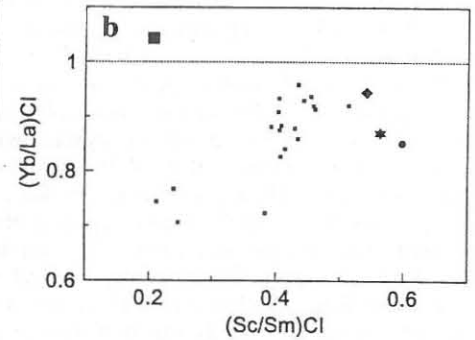

Figure 52. CI-normalized element ratio for angrites compared to basaltic eucrites. (a) Angrites have systematically higher Ca/Al and Ti/Hf than basaltic eucrites. The sole eucrite with $(Ti/Hf)_{CI} > 1$ is Ibitira, for which only single analyses of Ti and Hf are available. (b) The antarctic angrites have systematically higher Sc/Sm ratios than eucrites. Angra dos Reis is distinct from the other angrites in its refractory lithophile element ratios. Angrite data are from the sources listed in Figure 50.

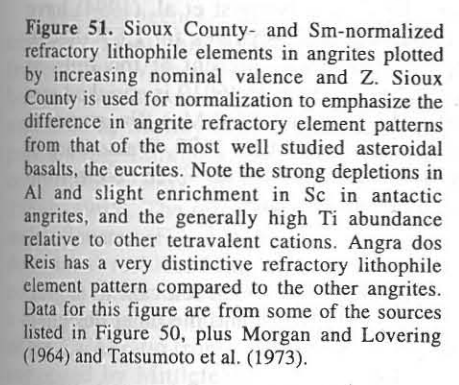

Figure 51. Sioux County- and Sm-normalized refractory lithophile elements in angrites plotted by increasing nominal valence and Z. Sioux County is used for normalization to emphasize the difference in angrite refractory element patterns from that of the most well studied asteroidal basalts, the eucrites. Note the strong depletions in Al and slight enrichment in Sc in antactic angrites, and the generally high Ti abundance relative to other tetravalent cations. Angra dos Reis has a very distinctive refractory lithophile element pattern compared to the other angrites. Data for this figure are from some of the sources listed in Figure 50, plus Morgan and Lovering (1964) and Tatsumoto et al. (1973).

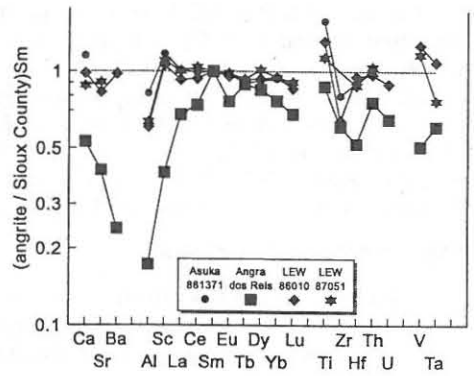

Ages

Chronologic studies show that the angrites are virtually as old as the solar system. Lugmair and Marti (1977) determined a Sm-Nd age for Angra dos Reis of 4.55 Ga, but this was essentially a two-point "isochron" defined by pyroxene and whitlockite separates. Wasserburg et al. (1977) reported concordant U-Pb, Th-Pb and Pb-Pb ages for Angra dos Reis of 4.54 Ga. Jacobsen and Wasserburg (1984) determined a Sm-Nd age of 4.56 Ga for Angra dos Reis, but again, this is virtually a two-point isochron. Lugmair and Galer (1992) have determined very precise concordant Pb-Pb ages for pyroxene separates for Angra dos Reis and LEW 86010 of 4.5578 Ga. Lugmair and Galer (1992) and Nyquist et al. (1994) have determined Sm-Nd isochron ages of 4.55 and 4.53 Ga, respectively, for LEW 86010.

The angrites contain isotope anomalies caused by the in situ decay of short-lived nuclides, further indicating old ages. Jacobsen and Wasserburg (1984), Lugmair and Marti (1977), Lugmair and Galer (1992) and Nyquist et al. (1994) have shown that Angra dos Reis and LEW 86010 have anomalies in $^{142}Nd/^{144}Nd$ ratios consistent with decay of short-lived ^{146}Sm ($t_{1/2}$ 103 Ma). Lugmair et al. (1992) and Nyquist et al. (1994) have measured anomalies in Cr isotopic composition of mineral separates for LEW 86010 which demonstrate that short-lived ^{53}Mn ($t_{1/2}$ 3.7 Ma) was present at the time of crystallization of this angrite. Xenon in Angra dos Reis and LEW 86010 is enriched in a heavy component derived from fission of short-lived ^{244}Pu ($t_{1/2}$ 81.8 Ma) (Eugster et al 1991, Hohenberg 1970, Hohenberg et al. 1991, Lugmair and Marti 1977, Wasserburg et al. 1977). Although Xe from fission of refractory ^{244}Pu is present, no ^{129}Xe excess from the decay of short-lived, volatile ^{129}I ($t_{1/2}$ 16 Ma) has been measured.

Experimental petrology studies

Two basic types of petrologic experiments have been performed relevant to angrite genesis; one designed to determine the origin of Angra dos Reis, and the other designed to infer the genesis of partial melts on the angrite parent body.

Angra dos Reis was originally considered to be a cumulate (e.g. Prinz et al. 1977), but Treiman (1989) suggested rather that the texture of this meteorite indicated that it is a metamorphosed porphyry, and nearly a melt composition. Treiman (1989) performed melting experiments on an Angra dos Reis analog composition, AdoR1. He found that the liquidus of AdoR1 was at a plausible temperature, 1246°C, for a melt composition, and that the composition AdoR1 crystallized to nearly 100% pyroxene. Treiman (1989) could not demonstrate that AdoR1 was saturated in olivine, as might be expected for an asteroidal basalt. He argued that his analog composition was slightly richer in silica than Angra dos Reis which would suppress the olivine phase field, and that based on experiments done by others in similar systems, co-saturation with olivine was plausible for Angra dos Reis. Subsequently, several measurements of SiO_2 have been done on Angra dos Reis (Mittlefehldt and Lindstrom 1990, Warren et al. 1995, Yanai 1994), and the results are essentially identical to that of the AdoR1 analog. Lofgren and Lanier (1991) performed dynamic crystallization experiments on two Angra dos Reis analog compositions to see if the texture of this meteorite could be duplicated without recourse to mineral accumulation. Lofgren and Lanier (1991) found that under the appropriate crystallization conditions, textures like that of Angra dos Reis could be duplicated. However, they also found that olivine did not crystallize in amounts as high as that observed in Angra dos Reis.

McKay et al. (1988b) performed melting experiments on analog compositions of LEW 86010 in order to determine whether this rock could represent a melt composition.

They found that LEW 86010 contains slight excesses of olivine and plagioclase relative to a melt saturated in these phases plus calcic-pyroxene. The compositions of pyroxene produced in the experiments closely matched those measured in LEW 86010, and McKay et al. (1988b) therefore concluded that LEW 86010 crystallized from a melt close to the bulk rock composition. However, they suggested that this could mean either that LEW 86010 represents a melt composition, or that it was formed by accumulation of minerals in essentially cotectic proportions. Jurewicz et al. (1993) performed melting experiments on CM and CV chondrites at oxygen fugacity conditions relevant to angrite petrogenesis. They found that minimum melts in these chondrites were "angritic" in the sense that they resembled the composition of LEW 86010, although there were differences in detail.

Origin of the angrites

The genesis of the angrites is not well understood. In part this is because there are few members in the grouplet, so magmatic trends are not well represented. More important, though, are the differences between various members of the grouplet which makes it difficult to determine the relationships among them.

The petrogenesis of LEW 86010 seems relatively well understood. The bulk composition of this rock is similar to that produced by partial melting of CM or (especially) CV chondrites at oxygen fugacities of about 1 log unit above the iron-wüstite buffer (Jurewicz et al. 1993). The oxygen fugacity used for these experiments was that estimated by McKay et al. (1994) based on their experiments on the effects of f_{O_2} on Eu partitioning. Similarly, the results of melting experiments on synthetic LEW 86010 compositions show that this rock could represent a melt composition (McKay et al. 1988b, 1995). The refractory incompatible element pattern of LEW 86010 is relatively unfractionated (Fig. 51), and plausibly that of a partial melt extracted from an olivine-dominated residue. Finally, variations in trace element contents with major element zoning in minerals in LEW 86010 are consistent with closed crystallization of a melt with a composition like that of the bulk rock (Crozaz and McKay 1990). Minor fractionation of the Ca/Al ratio from chondritic may be due to minor hercynitic spinel in the residue, as suggested by Mittlefehldt and Lindstrom (1990) and demonstrated experimentally by Jurewicz et al. (1993).

The genesis of Asuka 881371 and LEW 87051 is less certain. Melting experiments on CM and CV chondrites suggest that LEW 87051 could be a high temperature partial melt (Jurewicz et al. 1993). However, olivine-melt equilibrium experiments and the compositions of the large olivines in A-881371 and LEW 87051 show that these olivines are xenocrysts (e.g. McKay et al. 1995, Mikouchi et al. 1996), as first suggested by Prinz et al. (1990). Thus, these meteorites are hybrid rocks. The measured groundmass compositions for LEW 87051 and A-881371 are similar to LEW 86010 in composition (Prinz and Weisberg 1995, Prinz et al. 1990). Hence, the groundmass fraction of these rocks could be a partial melt of the angrite parent body. The groundmass is still highly olivine normative, and Mikouchi et al. (1996) suggested that the groundmass contains a dissolved olivine xenocryst component. These meteorites may represent contaminated partial melts (e.g. Mittlefehldt and Lindstrom 1990), or possibly, they are impact melts (Jurewicz et al. 1993, Mikouchi et al. 1996).

The origin of Angra dos Reis is unknown. Although the texture and major element composition allow this rock to represent a melt composition (e.g. Treiman 1989), its fractionated trace element pattern is not easily understood as being that of a melt (Mittlefehldt and Lindstrom 1990). Jones (1982) suggested that Angra dos Reis was a mesocumulate, a cumulate with a significant fraction of trapped intercumulus melt. Mittlefehldt and Lindstrom (1990) calculated that a mixture of about 60% cumulus

pyroxene and 40% melt could reproduce the REE pattern of Angra dos Reis. However, the melt would be very REE-rich, and they found no way to relate this melt to plausible partial melts of the angrite parent body, for example LEW 86010. The angrite parent body is extremely depleted in the moderately volatile elements Na, K, Rb and Ga compared to even the volatile-depleted eucrites (e.g. Mittlefehldt and Lindstrom 1990, Tera et al. 1970, Warren et al. 1995). Warren et al. (1995) have suggested that this does not extend to the most volatile elements, such as Cd and In. However, the estimated μ ($^{238}U/^{204}Pb$) for the angrite parent body does appear to be roughly a factor of 5 greater than that of the eucrite parent body (e.g. Lugmair and Galer 1992, Tera et al. 1997), suggesting a lower content of volatile Pb. It remains enigmatic how volatile depleted parent bodies were formed in the solar nebula. See discussion in Mittlefehldt (1987) and Humayun and Clayton (1995).

Angrites and eucrites represent the products of basaltic magmatism on asteroids, and it is instructive to compare them. Angrites are critically undersaturated in silica while eucrites are hypersthene normative, and thus mimic the dichotomy of alkaline and tholeiitic basalts on Earth (Mittlefehldt and Lindstrom 1990). Melting experiments on chondrites show that this difference can simply be due to differences in oxygen fugacity; melting under high f_{O_2} conditions yields melts critically undersaturated in silica, while melting under low f_{O_2} conditions yields melts that are hypersthene normative (Jurewicz et al. 1993, 1995b). The higher Ca/Al ratio for angrites compared to eucrites (Fig. 52a) is due to stabilization of hercynitic spinel in the residual source at high f_{O_2} causing a slight depletion in Al in the melt (Jurewicz et al. 1993, Mittlefehldt and Lindstrom 1990). Excluding Angra dos Reis, angrites also have slightly higher Sc/Sm ratios than eucrites (Fig. 52b) indicating that the residual source region for eucrites did contain some pyroxene. Based on melting experiments, the residual source region of LEW 86010 did not contain pyroxene (e.g. McKay et al. 1995).

MESOSIDERITES

Mesosiderites form one of the two major types of stony irons, and they are more enigmatic than the other group, the pallasites. Whereas pallasites are composed of materials logically expected for the core-mantle boundary region of a differentiated asteroid, the mesosiderites are composed of metal mixed in with mostly basaltic, gabbroic and pyroxenitic lithologies, and only minor olivine. Hence, mesosiderites seem to be mixtures of core material and crustal material, with little of the intervening mantle being present. This curious mix has fueled many imaginative scenarios for the formation of mesosiderites (see review by Hewins 1983) since the time of Prior (1918), who suggested that mesosiderites were formed by the invasion of a eucrite magma by a pallasite magma. Table 41 (below) gives a petrologic synopsis of all well-classified mesosiderites.

Bulk textures and classification

The silicate phase of mesosiderites is a brecciated mixture of igneous lithologies. The overall silicate texture is of mineral and lithic clasts in a fine-grained fragmental to igneous matrix (Floran 1978, Powell 1971). Large lithic clasts include basalts, gabbros, anorthosites, orthopyroxenites, and dunites. The basalts, gabbros and orthopyroxenites dominate, while dunites are subordinate and anorthosites are rare. Hence, the lithic clasts are dominantly from the crust of a differentiated asteroid, and are broadly similar to eucrites and diogenites. Mineral clasts consist mostly of coarse-grained orthopyroxene fragments up to at least 10 cm in size. Coarse-grained olivine clasts, up to at least 10 cm in size (McCall 1966), are less abundant, whereas coarse-grained plagioclase fragments a few mm in size are the least common. All-in-all, the silicate assemblage in mesosiderites

is very similar to that in the howardites; with the exception of the lack of coarse-grained olivine in the latter (Prior 1918).

Mesosiderite petrologic classification has been organized similarly to that of chondrites, where compositional and textural features are used to form a grid of types (Van Schmus and Wood 1967). The mesosiderites are divided into three petrologic groups based on the orthopyroxene content (Hewins 1984, 1988; see Fig. 53). Compositional class A mesosiderite silicates are relatively basaltic in composition, containing more plagioclase and clinopyroxene. The compositional class B mesosiderite silicates contain a greater proportion of orthopyroxene, and are therefore more ultramafic. A unique mesosiderite from Antarctica, RKPA79015, contains almost exclusively orthopyroxene as its silicate phase (Prinz et al. 1982a), and is the sole member of compositional class C (Hewins 1988). There is no apparent relationship between the compositional classes of mesosiderites and the amount of metal and/or troilite they contain. The metal content varies from about 17-90 wt % and troilite from <1-14 wt % (Table 41). Many new mesosiderites have not yet been formally classified, so additional petrologic-compositional types may exist. Chaunskij, for example, is unusual in containing cordierite, a mineral not previously reported in mesosiderites, more metal and a higher level of shock damage in the metal than typical (Petaev et al. 1993), and a very different composition of metal (Wasson et al. 1998a).

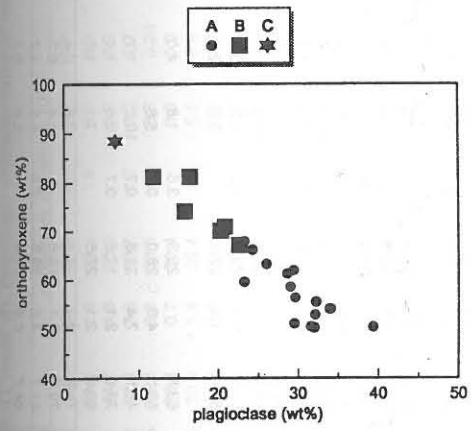

Figure 53. Orthopyroxene wt % vs. plagioclase wt % for mesosiderites showing the generally greater basaltic component, indicated by plagioclase, in the compositional class A mesosiderites compared to the more ultramafic-rich B mesosiderites. Data are from the summary in Table 41.

In addition to compositional distinctions based on the ratio of basaltic-gabbroic to orthopyroxenitic material in the breccias, mesosiderites have been further subdivided based on silicate textures. This is analogous to separation of chondrites into petrologic types 1 through 6. Like the chondrite sequence, the mesosiderite textural classification was originally thought to reflect increasing metamorphic equilibration of the silicates (Powell 1971). The lowest metamorphic grade (1) is characterized by a fine-grained fragmental matrix. Successively higher grades (2 and 3) are characterized by recrystallized matrixes, while the highest grade (4) mesosiderites are melt-matrix breccias (Floran et al. 1978b). Both compositional classes A and B mesosiderites contain members of textural grades 1 through 4 and the sole compositional class C mesosiderite is of textural grade 2.

This textural classification is somewhat too simplistic. Textures are variable in some mesosiderites; different samples of Estherville, for example, show textures indicating grades 3 and 4 (Hewins 1984). Also, Floran (1978) noted that even some textural grade 1 mesosiderites contain some igneous textured matrix material. One problem with the

Table 41. Petrologic characteristics of mesosiderites

Name	class	metal	troil	silicate	norm/mode silicates to 100%								notes
		wt%	wt%	wt%	opx	cpx	plag	oliv	trid	mer	cm	ilm	
ALHA77219	1B				76.0	1.4	12.9	4.1	2.9	1.3	1.4		mode
....					72.4	4.8	18.7		1.6	0.59	1.5	0.50	norm
....					70.0	6.0	18.8		3.4	1.8			matrix mode
....ALHA81059	1B				67.4	3.8	23.1		4.2	1.2	0.4		matrix mode, paired with ALHA77219
....ALHA81098	1B				72.8	2.2	22.1		0.3	0.2	2.3		matrix mode, paired with ALHA77219
ALHA81208	2B?				97.5					0.3	2.2		probably clast from one of above
Barea (f)	1A	56.6	1.6	41.8	63.6		27.3		6.2	2.9	1.2	0.7	norm
....					53.5	3.2	30.6	2.2	6.7	2.3	1.5		mode
....					53.9	2.9	34.4		7.4	1.4			matrix mode
Bondoc	3B(+)	43.7	0.68	55.62	81.3	0.5	16.5	0.5	0.2	0.2	0.8		mode, no corona
Budulan	3B(+)	70			70.2	2.6	20.3		4.1	1.8	1.0		mode
Chaunskij	?	90			46		34.2		5.9	4.7	1.2	0.9	mode, opx = total pyx, cordierite = 7.1%
....					46.8		34.7		7.6	5.2	0.8	0.8	norm, opx = total pyx, cordierite = 4.1%
Chinguetti	1B	80			81.3		11.8	2.1	2.1	1.7	1.0		mode
....					89.0		6.1		1.1	3.8			matrix mode
Clover Springs	2A	37			50.3	5.5	32.0	0.8	8.6	2.1	0.7		mode
....					47.9	1.1	37.5	0.3	10.6	2.3	0.3		matrix mode
Crab Orchard	1A	54.6	0.76	44.64	50.4	2.8	39.3	1.1	5.0	0.8	0.6		mode
....					49.3	2.7	33.5		11.3	2.9	0.3		matrix mode
Dalgaranga	A				54.1	1.7	33.9	2.5	4.1	3.4	0.3		mode
Donnybrook	3B(+)												
Dyarrl Island (f)	1A	17.5	2.3	80.2	61.6	9.0	22.8		2.4	0.7	1.0	2.1	norm
....					51.3	4.5	36.5		5.9	1.5	0.3		mode
Emery	3A	50.2	7.3	42.5	54.8		30.8		9.6	4.0	1.2	0.9	norm
....					46.2	2.5	32.5	3.8	9.8	3.7	1.5		mode
....					38.0	2.0	40.6		13.7	4.9	0.7	0.2	matrix mode
Estherville (f)	3/4A	56.4	3.40	40.2	59.3	3.6	27.1	2.2	5.5	1.5	0.8		mode
....					76.5		19.4		1.7	0.7	1.2	0.5	norm
....					53.2	3.7	29.5		11.9	1.3	0.4		matrix mode
Hainholz	4A	53.4	4.30	42.3	59.2	0.1	29.7	1.5	5.3	3.5	0.7		mode, no corona
....		53.3	2.00	44.7	63.4	1.7	27.4		3.9	2.0	1.4	0.19	norm
Harvard University	4A												
Lamont	3B				63.8		25.3	3.6	1.8	4.0	1.5	tr	matrix mode
Lowicz (f)	3A	59.6	0.61	39.79	63.3	4.0	26.0	0.7	5.6		0.4		mode
....					46.9	7.4	31.8	0.7	10.5	1.7	1.0		matrix mode
Mincy	3B(+)				73.6	2.1	17.8	0.7	2.6	1.4	1.8		mode
....					60.9	2.1	27.5		7.1	1.3	1.0		mode, coarse-grained
....					74.9	3.3	18.1		3.4	0.2	0.1		mode, fine-grained
....					79.5	3.1	15.6		1.4	0.3			matrix mode
Morristown	3A	49.8	0.66	49.54	51.1	4.2	29.5	6.0	6.5	1.7	1.0		mode
....					54.7	6.8	31.4		5.8	0.7	0.5		matrix mode

Table 41 (cont'd). Petrologic characteristics of mesosiderites

Name	class	metal	troil	silicate	norm/mode silicates to 100%								notes
		wt%	wt%	wt%	opx	cpx	plag	oliv	trid	mer	cm	ilm	
Mount Padbury	1A	49.8	7.6	42.6	59.6	2.6	23.2	1.9	8.5	3.3	0.9		mode
		57			44.7	4.3	35.0		13.0	2.9	0.2		matrix mode
Patwar (f)	1A	33.2	9.07	57.73	52.8	3.3	30.7	1.7	9.0	2.2	0.3		mode
		38.05	11.89	50.05	58.2	3.2	33.6		3.3	0.33	0.77	0.61	norm
					58.3	0.7	30.4		5.0	5.0	0.7		matrix mode
Pinnaroo	4A	64.08	7.76	28.16	50.9	1.4	35.4	1.8	6.5	3.6	0.2		mode, no corona
		54.6	13.9	31.5	57.3	3.5	32.5		3.1	2.0	0.69	0.93	norm
RKPA79015	2C(+)												
....RKPA80229	2C(+)												paired with RKPA79015
....RKPA80246	2C(+)												paired with RKPA79015
....RKPA80258	2C(+)				89.3	2.4	5.1	1.8		1.5			mode, paired with RKPA79015
....					87.7	2.8	9.0		0.2				matrix mode
....RKPA80263	2C(+)												paired with RKPA79015
Simondium	4A	42.7	8.8	48.5	63.8	1.2	27.7		3.7	1.2	1.8	0.48	norm
....					60.3	0.3	31.2	0.4	4.4	2.1	1.3		mode, no corona
Vaca Muerta	1A	47.3	12.63	40.07	52.9	2.0	32.1	1.4	8.0	3.0	0.6		mode
....					52.3	0.3	30.0		12.8	4.3	0.2		matrix mode
Veramin (f)	2B(+)	48.6	0.60	50.8	71.0	tr	20.8	5.7		1.0	1.5		mode, no corona
....					75.0	0.3	18.0	2.0	2.5	2.3			matrix mode
West Point	3A				66.2	3.5	24.2		4.3	1.8	tr		mode, Morristown?

Poorly characterized mesosiderites (paired meteorites listed in parentheses after the parent):

A-882023, Acfer 063, Acfer 265, EET 87500 (EET 87501, EET 92001), Eltanin (recovered in deep sea cores, USNS Eltanin), Ilafegh 002, LEW 86210, LEW 87006, MAC 88102, Murchison Downs, Pennyweight Point, QUE 86900 (QUE 93001, QUE 93002, QUE 93126, QUE 93150, QUE 93517, QUE 93575, QUE 93584, QUE 93586, QUE 94614, QUE 94639, QUE 94299), Um-Hadid, Weiyuan

References:

Classification: Floran (1978), Hewins (1984, 1988). Classifications indicated with (+) are considered petrologic grade 4 by Hewins (1984, 1988).

Wt % metal-trolite-silicate: Alderman (1940) - Pinnaroo; Floran (1978) - Hainholz, Pinnaroo, Simondium; Jarosewich and Mason (1969) - Patwar; Mason and Jarosewich (1973) - Barea, Budulan, Chinguetti, Clover Springs, Dyarrl Island, Emery, Mount Padbury; McCall (1966) - Mount Padbury; Powell (1971) - Bondoc, Crab Crchard, Estherville, Hainholz, Lowicz, Morristown, Patwar, Vaca Muerta, Veramin.

Modes: Hewins (1988) - ALHA81208, RKPA80258; Hewins and Harriott (1986) - Mincy; Petaev et al. (1993) - Chaunskij; Prinz et al. (1982) - RKPA79015, Prinz et al. (1980) - rest.

Matrix modes: Boesenberg et al. (1997) - Lamont; Hewins (1988) - ALHA77219, -81059, -81098; RKPA80258; Delaney et al. (1981) - rest.

Norms: Alderman (1940) - Pinnaroo; Floran (1978) - Hainholz, Pinnaroo, Simondium; Jarosewich and Mason (1969) - Patwar; Mason and Jarosewich (1973) - Barea, Budulan, Chinguetti, Clover Springs, Dyarrl Island, Emery, Mount Padbury; Nelen - Mason (1972) - Estherville; Marvin and Mason (1980) - ALHA77219; Petaev et al. (1993) - Chaunskij.

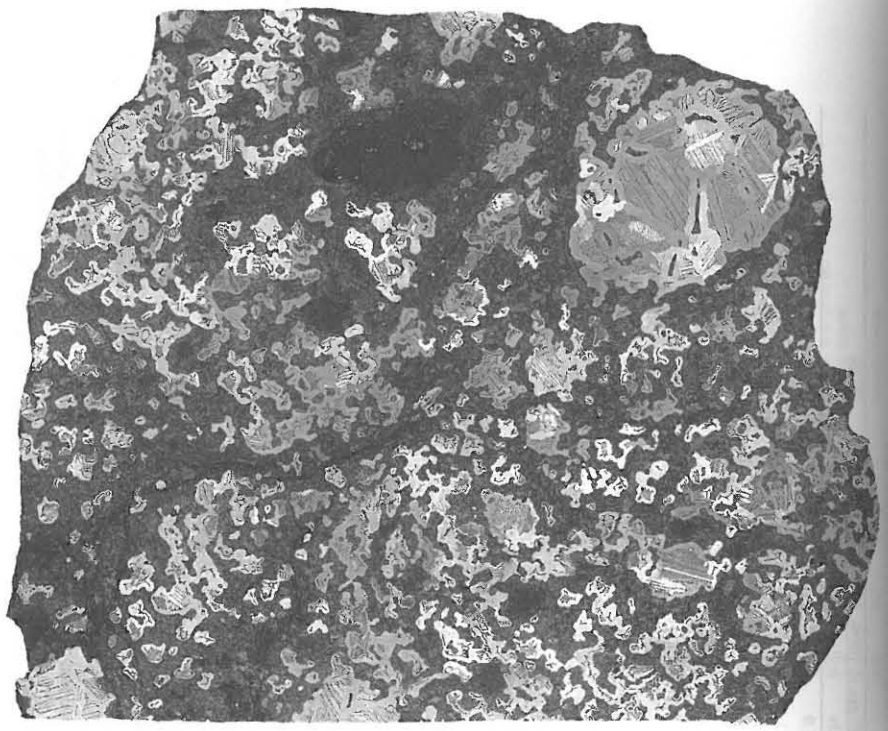

Figure 54. Polished and etched slab of Pinnaroo, a type 4A mesosiderite. Note the general coarse segregation of metal and silicate, the large silicate clast (upper center) and large metal clast, and the highly embayed borders between metal and silicate. This slab is 13 cm across. (Photograph courtesy of the Smithsonian Institution).

textural classification of mesosiderites is that it is frequently difficult to decide what is and what is not true matrix. Because of the pervasive, intervening metal plus troilite, it can be difficult to distinguish between true matrix material and small, fine-grained breccia or impact melt clasts. Finally, Hewins (1984, 1988) has shown that the type 2B, 2C and 3B mesosiderites have some igneous textured matrix, and so could be reclassified as petrologic grade 4. This is shown in Table 41 where their classification is given as, e.g. 3B(+), indicating possible classification as melt-matrix mesosiderites.

No systematic study of the metal-silicate textures at the macro-scale, similar to that done on pallasites, has been done for mesosiderites. There may be a correlation between silicate texture type and macro-scale metal-silicate textures. Both Pinnaroo (Fig. 54) and some parts of Estherville are classified as melt-matrix breccias (type 4A) and exhibit cm-scale separation of metal and silicate. The Patwar, Mount Padbury (Fig. 55) and Vaca Muerta fragmental matrix breccias (type 1A) exhibit fine-scale homogeneous distribution of metal and silicate. Some mesosiderites have anomalous metal-silicate textures, RKPA79015 (Fig. 56) being one example.

Mesosiderite matrix

Matrix textures. Mesosiderites exhibit essentially a continuum in particle sizes from large lithic and mineral clasts down to fine matrix grains, making the distinction between

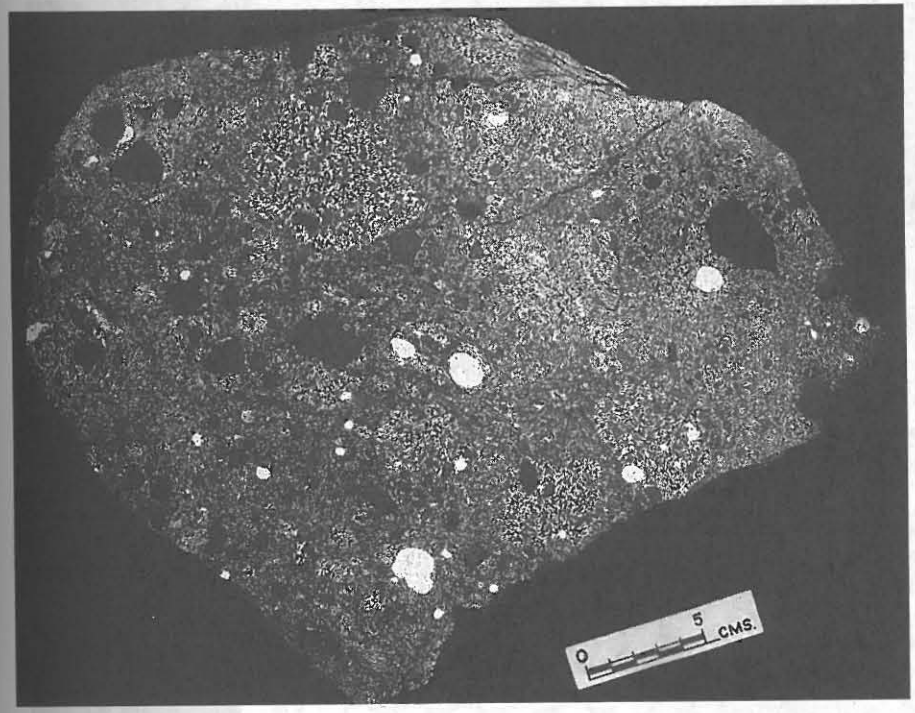

Figure 55. Polished slab of Mount Padbury, a type 1A mesosiderite. Numerous cm-sized silicate and metal clasts are dispersed in a finely divided metal-silicate matrix. Note metal-rich areas, some of which are metal-rich breccia clasts. (Photograph courtesy of the Smithsonian Institution).

matrix and clast arbitrary at some level. Because silicate textural domains are commonly bordered by troilite and/or metal, it is very difficult to distinguish matrix from fine-grained clasts in mesosiderites. Table 41 includes matrix modes for many of the mesosiderites, including members of all types except 4A and 4B. (A matrix mode is given for Estherville, but Delaney et al. (1981) did not indicate the textural type, 3A or 4A, corresponding to the Estherville thin section used for modal determination.)

According to Powell (1971) mesosiderites of textural grade 1 are characterized by clearly distinguishable cataclastic texture, with highly angular mineral and lithic fragments of all sizes. The fine-grained matrix contains much material of size <10 μm. Silicate-silicate grain boundaries in the matrix are not intergrown. These mesosiderites are texturally heterogeneous even on the microscopic scale.

Powell (1971) defined mesosiderites of textural grade 2 as still exhibiting a clearly cataclastic texture, but that the angularity is mostly confined to the larger lithic fragments. The matrix material is coarser-grained, and most grains are >10 μm in size. Contacts between small silicate grains may be sutured, and small grains may be intergrown with larger silicate fragments. Textural grade 2 mesosiderites are still texturally heterogeneous on a microscopic scale, but this is less pronounced than in grade 1.

Powell (1971) originally defined textural grade 3 as his highest metamorphic grade. Subsequent workers have shown that mesosiderites of textural class 3 display characteristic textures that are related to compositional type. Textural grade 3

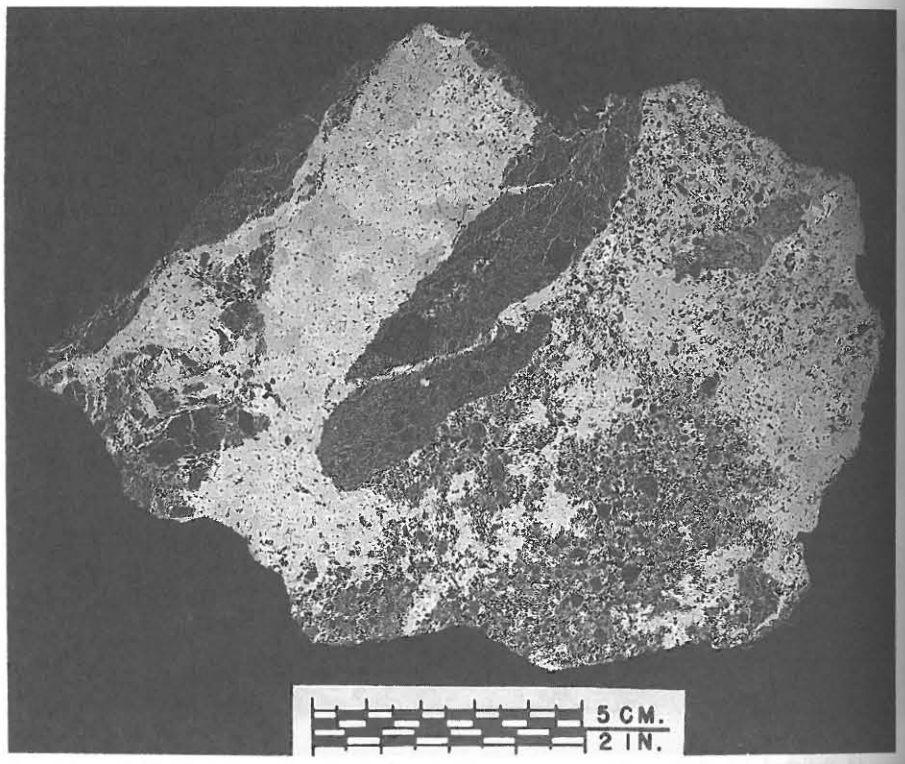

Figure 56. The type 2C mesosiderite RKPA79015 has an unusual texture, with silicate-free metal regions several cm in size. (Photograph courtesy of the Smithsonian Institution).

mesosiderites were originally split into the pyroxene poikiloblastic and plagioclase poikiloblastic textures for compositional class A and B, respectively (Floran 1978). Hewins (1984) reinterpreted the type 3B mesosiderite matrix to have an igneous texture, and therefore the texture of these mesosiderites will be referred to as plagioclase poikilitic. The plagioclase poikilitic matrix is characterized by plagioclase grains several mm in size enclosing numerous rounded to euhedral orthopyroxene grains on the order of 100 μm in size. As described by Floran (1978), the pyroxene poikiloblastic texture is characterized by large, inclusion-poor, low-Ca pyroxene grains, up to cm-size, with optically continuous overgrowths enclosing anhedral grains of plagioclase, tridymite, silica, troilite and metal. There are also optically continuous low-Ca pyroxene grains in the matrix enclosing a similar suite of minerals.

Mesosiderites of textural grade 4 exhibit igneous-textured matrixes. As originally defined by Floran et al. (1978b), these mesosiderites have fine- to medium-grained, intergranular textures composed of orthopyroxene granules between a network of subhedral, lath-shaped plagioclase grains. Minor to accessory minerals found between orthopyroxene and plagioclase grains include tridymite, augite, troilite, chromite, whitlockite and metal.

A unique texture found in mesosiderites is the corona texture developed around olivine grains (Delaney et al. 1981, Nehru et al. 1980, Powell 1971, Ruzicka et al. 1994).

Table 42. Compositions of pyroxene grains from representative mesosiderites.

	Mount Padbury		Chinguetti	Emery			Donnybrook					Mincy
	(1)	(2)	(3)	(4)	(5)	(6)	(7)	(8)	(9)	(10)	(11)	(12)
Chemical Composition (wt %)												
SiO_2	53.1	52.6	54.7	52.9	53.2	52.6	54.8	54.7	54.6	54.0	54.0	53.9
Al_2O_3	0.58	0.97	1.33	0.68	0.66	1.14	0.44	0.62	0.92	1.35	1.20	1.36
TiO_2	0.40	0.64	0.09	0.50	0.40	0.66	0.08	0.10	0.16	0.21	0.28	0.22
Cr_2O_3	0.29	0.46	0.71	0.33	0.29	0.60	0.13	0.16	0.28	0.46	0.39	0.80
FeO	20.7	9.27	15.5	19.9	19.2	10.4	15.8	15.2	14.8	15.5	13.2	13.0
MnO	0.96	0.48	0.58	1.01	0.89	0.53	0.70	0.76	0.73	0.70	0.60	0.54
MgO	23.2	15.3	26.5	23.1	23.9	15.0	27.6	28.0	27.5	27.4	26.1	27.9
CaO	1.25	20.2	1.09	1.80	1.55	19.8	0.14	0.41	0.96	0.18	4.14	1.52
Total	100.48	99.92	100.50	100.22	100.09	100.73	99.69	99.95	99.95	99.80	99.91	99.24
Cation Formula Based on 6 Oxygens												
Si	1.9641	1.9599	1.9671	1.9593	1.9631	1.9525	1.9838	1.9728	1.9687	1.9538	1.9531	1.9479
"Al	0.0253	0.0401	0.0329	0.0297	0.0287	0.0475	0.0162	0.0264	0.0313	0.0462	0.0469	0.0521
Total tet*	1.9894	2.0000	2.0000	1.9890	1.9918	2.0000	2.0000	1.9992	2.0000	2.0000	2.0000	2.0000
Ti	0.0111	0.0179	0.0024	0.0139	0.0111	0.0184	0.0022	0.0027	0.0043	0.0057	0.0076	0.0060
"Al	0.0000	0.0025	0.0235	0.0000	0.0000	0.0024	0.0026	0.0000	0.0078	0.0114	0.0043	0.0058
Cr	0.0085	0.0136	0.0202	0.0097	0.0085	0.0176	0.0037	0.0046	0.0080	0.0132	0.0112	0.0229
Fe	0.6403	0.2889	0.4662	0.6164	0.5925	0.3229	0.4784	0.4585	0.4463	0.4690	0.3993	0.3929
Mn	0.0301	0.0151	0.0177	0.0317	0.0278	0.0167	0.0215	0.0232	0.0223	0.0215	0.0184	0.0165
Mg	1.2789	0.8496	1.4203	1.2751	1.3143	0.8298	1.4890	1.5050	1.4777	1.4775	1.4069	1.5027
Ca	0.0495	0.8065	0.0420	0.0714	0.0613	0.7875	0.0054	0.0158	0.0371	0.0070	0.1604	0.0589
Total Cations	4.0078	3.9941	3.9923	4.0072	4.0073	3.9953	4.0028	4.0090	4.0035	4.0053	4.0081	4.0057
*Cation Ratios Ca:Mg:Fe, Fe/Mn and mg# (100*Mg/(Mg+Fe))*												
Ca	2.5	41.5	2.2	3.6	3.1	40.6	0.3	0.8	1.9	0.4	8.2	3.0
Mg	65.0	43.7	73.6	65.0	66.8	42.8	75.5	76.0	75.4	75.6	71.5	76.9
Fe	32.5	14.9	24.2	31.4	30.1	16.6	24.2	23.2	22.8	24.0	20.3	20.1
Fe/Mn	21	19	26	19	21	19	22	20	20	22	22	24
mg#	66.6	74.6	75.3	67.4	68.9	72.0	75.7	76.6	76.8	75.9	77.9	79.3

(1, 2) impact melt matrix pyroxenes; (3) fragmental matrix pyroxene; (4, 6, 7, 8) matrix pyroxenes; (5) corona structure pyroxene; (9, 10, 11, 12) chadacrysts enclosed in poikilitic plagioclase; all data from Mittlefehldt, unpublished.

Many olivine grains in mesosiderites are surrounded by a zoned sequence containing, in order of abundance, orthopyroxene, plagioclase, whitlockite, chromite, clinopyroxene (type not identified) and ilmenite. Against the olivine, the corona mineralogy is dominantly orthopyroxene and chromite, with or without whitlockite. A middle zone still has orthopyroxene as the major mineral, but plagioclase makes up about 1/3 of the zone, whitlockite is variable in abundance from a few percent up to about 20%, and minor amounts of chromite are present. The outer zone is similar to the matrix in mineralogy, except that this zone is devoid of tridymite and metal.

Matrix mineral compositions. There are relatively few published analyses of matrix minerals in mesosiderites, and for many analyses in the literature, it is often difficult to determine what textural type of material has been analyzed. We will therefore rely heavily on unpublished data by one of us (DWM). We will not discuss the composition small olivine grains here, as the development of corona textures and the abundance of tridymite in the matrix indicates that these are basically small mineral clasts which could not have substantially reacted with the matrix. There are few, if any, analyses of matrix plagioclase available in the literature. Hence, we will focus on pyroxene in the matrix. We include in this category overgrowths on larger silicate grains.

Representative analyses of matrix pyroxene grains are given in Table 42, and Figure 57 shows the molar Fe/Mg vs. molar Fe/Mn relationships for mesosiderite pyroxenes. For the type 1A mesosiderite Mount Padbury, low-Ca pyroxene and calcic clinopyroxenes from impact melt matrix have low molar Fe/Mn ratios, 21 and 19, respectively, and are

Table 42 (cont'd). Compositions of pyroxene grains from representative mesosiderites.

	Mincy	Budulan	Pinnaroo					Chinguetti		Mincy		
	(13)	(14)	(15)	(16)	(17)	(18)	(19)	(20)	(21)	(22)	(23)	(24)
Chemical Composition (Weight Percent)												
SiO_2	53.5	53.1	53.1	52.5	51.8	53.9	52.4	55.0	54.2	53.7	53.5	53.2
Al_2O_3	0.95	0.77	0.63	0.57	0.95	0.81	0.92	0.60	0.80	0.73	1.53	0.99
TiO_2	0.34	0.24	0.27	0.20	0.35	0.13	0.29	0.09	0.12	0.13	0.36	0.39
Cr_2O_3	0.52	0.56	0.49	0.42	0.53	0.62	0.54	0.43	0.26	0.49	0.45	0.50
FeO	16.9	18.5	21.6	22.4	22.0	17.0	20.7	15.3	14.9	17.0	17.1	17.2
MnO	0.78	0.76	0.79	0.89	0.91	0.57	0.84	0.52	0.57	0.64	0.79	0.84
MgO	26.0	24.2	21.8	20.5	19.5	25.5	19.9	27.5	27.4	25.3	25.4	25.4
CaO	1.32	1.60	1.68	2.84	3.90	1.46	4.72	1.14	1.08	1.39	0.76	1.05
Total	100.31	99.73	100.36	100.32	99.94	99.99	100.31	100.58	99.33	99.38	99.89	99.57
Cation Formula Based on 6 Oxygens												
Si	1.9482	1.9608	1.9749	1.9701	1.9566	1.9668	1.9620	1.9743	1.9681	1.9716	1.9523	1.9534
^{IV}Al	0.0408	0.0335	0.0251	0.0252	0.0423	0.0332	0.0380	0.0254	0.0319	0.0284	0.0477	0.0428
Total tet*	1.9890	1.9943	2.0000	1.9953	1.9989	2.0000	2.0000	1.9997	2.0000	2.0000	2.0000	1.9962
Ti	0.0093	0.0067	0.0076	0.0056	0.0099	0.0036	0.0082	0.0024	0.0033	0.0036	0.0099	0.0108
^{VI}Al	0.0000	0.0000	0.0025	0.0000	0.0000	0.0016	0.0026	0.0000	0.0023	0.0032	0.0181	0.0000
Cr	0.0150	0.0164	0.0144	0.0125	0.0158	0.0179	0.0160	0.0122	0.0075	0.0142	0.0130	0.0145
Fe	0.5147	0.5713	0.6719	0.7030	0.6950	0.5188	0.6482	0.4593	0.4525	0.5220	0.5219	0.5282
Mn	0.0241	0.0238	0.0249	0.0283	0.0291	0.0176	0.0266	0.0158	0.0175	0.0199	0.0244	0.0261
Mg	1.4110	1.3318	1.2083	1.1465	1.0977	1.3867	1.1105	1.4712	1.4828	1.3843	1.3814	1.3900
Ca	0.0515	0.0633	0.0670	0.1142	0.1578	0.0571	0.1894	0.0438	0.0420	0.0547	0.0297	0.0413
Total Cations	4.0146	4.0076	3.9966	4.0054	4.0042	4.0033	4.0015	4.0044	4.0079	4.0019	3.9984	4.0071
*Cation Ratios Ca:Mg:Fe, Fe/Mn and mg# (100*Mg/(Mg+Fe))*												
Ca	2.6	3.2	3.4	5.8	8.1	2.9	9.7	2.2	2.1	2.8	1.5	2.1
Mg	71.4	67.7	62.1	58.4	56.3	70.7	57.0	74.5	75.0	70.6	71.5	70.9
Fe	26.0	29.1	34.5	35.8	35.6	26.4	33.3	23.3	22.9	26.6	27.0	27.0
Fe/Mn	21	24	27	25	24	29	24	29	26	26	21	20
mg#	73.3	70.0	64.3	62.0	61.2	72.8	63.1	76.2	76.6	72.6	72.6	72.5

(13, 14) chadacrysts enclosed in poikilitic plagioclase; (15, 16, 17, 18, 19) impact melt matrix pyroxenes; (20, 21) and (22, 23) core-rim pairs for large pyroxenes; (24) rim on large pigeonite; all data from Mittlefehldt, unpublished.

relatively magnesian, with mg# of 66.6 and 74.7, respectively. For the type 1B mesosiderite Chinguetti, a small fragmental low-Ca pyroxene grain from the matrix has a higher molar Fe/Mn of 26 than the Mount Padbury impact-melt matrix grains, and is quite magnesian with a mg# of 75.3.

For the type 3A, pyroxene poikiloblastic mesosiderite Emery, low-Ca pyroxene and calcic clinopyroxene analyses for matrix grains, plus low-Ca pyroxene from the corona around an olivine grain have low molar Fe/Mn, 19-21, and are magnesian, with mg# of 67.4 to 72.0. For type 3B mesosiderites, the plagioclase poikilitic textural grade, low-Ca pyroxene chadacrysts (mineral grains completely enclosed in a single host crystal) from poikilitic plagioclase show a range of compositions. Donnybrook pyroxene chadacrysts with similar mg# (75.9 to 77.9) can show a range of CaO contents from ~0.2 to ~4.1 wt % (Table 42). Mincy and Budulan have generally more ferroan chadacrysts with a narrower range in CaO contents. Note that for each of these mesosiderites, only one thin section was studied, so sample heterogeneity cannot be established. Hewins and Harriott (1986) found a limited range in CaO of chadacrysts in a thin section from a different specimen of Budulan than studied here. Also shown in Table 42 are representative analyses of matrix pyroxene grains from Donnybrook, and analyses of rims on large low-Ca pyroxene cores for Budulan and Mincy.

A range of pyroxene analyses are given for the type 4A mesosiderite Pinnaroo. These grains range from magnesian, low-Ca pyroxenes with molar Fe/Mn of ~27 to 30,

Table 42 (cont'd). Compositions of pyroxene grains from representative mesosiderites.

	Budulan		Patwar				Mount Padbury	Vaca Muerta				
	(25)	(26)	(27)	(28)	(29)	(30)	(31)	(32)	(33)	(34)	(35)	(36)
Chemical Composition (wt %)												
SiO_2	53.2	53.6	50.9	52.2	51.4	51.8	50.3	52.4	52.5	50.6	51.6	53.2
Al_2O_3	0.92	0.60	1.15	0.99	0.62	0.69	0.66	0.75	0.56	0.30	1.24	0.21
TiO_2	0.26	0.13	0.83	0.48	0.40	0.42	0.44	0.46	0.35	0.23	0.60	0.18
Cr_2O_3	0.52	0.47	0.44	0.36	0.34	0.47	0.24	0.41	0.29	0.18	0.41	0.27
FeO	19.2	18.2	10.5	22.2	14.4	22.3	29.5	9.75	23.6	30.1	8.48	21.2
MnO	0.70	0.74	0.64	0.89	0.70	0.92	0.88	0.47	0.98	1.19	0.47	0.84
MgO	24.1	24.6	14.0	21.7	12.7	21.4	11.0	14.7	21.1	17.2	14.2	22.9
CaO	1.46	1.44	20.6	1.24	19.6	1.72	7.97	21.4	1.22	0.80	21.6	0.82
Total	100.36	99.78	99.06	100.06	100.16	99.72	100.99	100.34	100.60	100.60	98.60	99.62
Cation Formula Based on 6 Oxygens												
Si	1.9563	1.9722	1.9346	1.9540	1.9585	1.9526	1.9717	1.9565	1.9665	1.9592	1.9523	1.9849
^{IV}Al	0.0399	0.0260	0.0515	0.0437	0.0278	0.0307	0.0283	0.0330	0.0247	0.0137	0.0477	0.0092
Total tet*	1.9962	1.9982	1.9861	1.9977	1.9863	1.9833	2.0000	1.9895	1.9912	1.9729	2.0000	1.9941
Ti	0.0072	0.0036	0.0237	0.0135	0.0115	0.0119	0.0130	0.0129	0.0099	0.0067	0.0171	0.0051
^{VI}Al	0.0000	0.0000	0.0000	0.0000	0.0000	0.0000	0.0022	0.0000	0.0000	0.0000	0.0076	0.0000
Cr	0.0151	0.0137	0.0132	0.0107	0.0102	0.0140	0.0074	0.0121	0.0086	0.0055	0.0123	0.0080
Fe	0.5905	0.5601	0.3338	0.6950	0.4589	0.7030	0.9671	0.3045	0.7393	0.9747	0.2683	0.6615
Mn	0.0218	0.0231	0.0206	0.0282	0.0226	0.0294	0.0292	0.0149	0.0311	0.0390	0.0151	0.0265
Mg	1.3207	1.3490	0.7930	1.2106	0.7212	1.2022	0.6426	0.8180	1.1779	0.9925	0.8007	1.2734
Ca	0.0575	0.0568	0.8389	0.0497	0.8002	0.0695	0.3348	0.8562	0.0490	0.0332	0.8757	0.0328
Total Cations	4.0090	4.0045	4.0093	4.0054	4.0109	4.0133	3.9963	4.0081	4.0070	4.0245	3.9968	4.0014
*Cation Ratios Ca:Mg:Fe, Fe/Mn and mg# (100*Mg/(Mg+Fe))*												
Ca	2.9	2.9	42.7	2.5	40.4	3.5	17.2	43.3	2.5	1.7	45.0	1.7
Mg	67.1	68.6	40.3	61.9	36.4	60.9	33.0	41.3	59.9	49.6	41.2	64.7
Fe	30.0	28.5	17.0	35.5	23.2	35.6	49.7	15.4	37.6	48.7	13.8	33.6
Fe/Mn	27	24	16	25	20	24	33	20	24	25	18	25
mg#	69.1	70.7	70.4	63.5	61.1	63.1	39.9	72.9	61.4	50.5	74.9	65.8

(25, 26) core-rim pair for large pyroxene; (27, 28) impact melt clast pyroxenes; (29, 30) polygenic basalt clast RV-02 pyroxenes; (31) monogenic basalt clast RV-05 pyroxene; (32, 33, 34) gabbro clast RC-07 pyroxenes; (35, 36) pyroxene inclusions in tridymite, gabbro clast RC-07 ; all data from Mittlefehldt, unpublished except (31) from Mittlefehldt (1978).

to more calcic pyroxenes with molar Fe/Mn of 24 to 25. Some of these grains may not be true matrix grains. The low-Ca pyroxenes with the higher molar Fe/Mn are similar in composition to large low-Ca pyroxene clasts in the igneous matrix, suggesting that the smaller grains are simply smaller clasts.

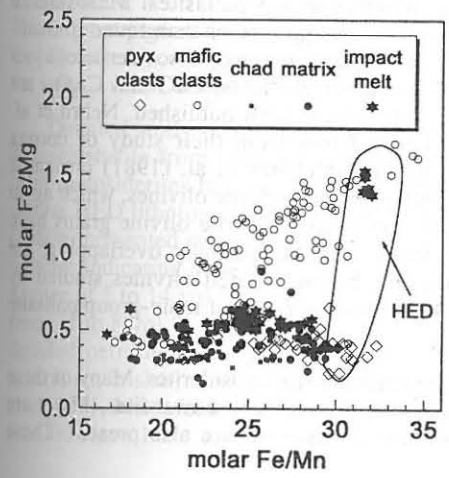

Figure 57. Molar Fe/Mg vs. Fe/Mn for mesosiderite pyroxenes compared to the field for HED meteorites. The HED field shows the effect of igneous processes; both partial melting and fractional crystallization result in relatively constant Fe/Mn but varying Fe/Mg. Mesosiderite mafic clasts show primarily the effects of FeO reduction; both Fe/Mn and Fe/Mg decrease during this process. Most mesosiderite matrix and impact melt pyroxenes, and pyroxene chadacrysts in plagioclase poikilitic mesosiderites form a band of roughly constant Fe/Mg but varying Fe/Mn. Data are from Mittlefehldt (1990 and unpublished).

Table 43. Compositions of olivine grains from representative mesosiderites.

	ALHA 77219	Crab Orchard	Emery			Hainholz		Mincy				Pinnaroo	Veramin
	(1)	(2)	(3)	(4)	(5)	(6)	(7)	(8)	(9)	(10)	(11)	(12)	(13)
Chemical Composition (wt %)													
SiO_2	37.5	36.3	39.3	39.0	37.4	37.4	40.8	39.5	39.4	41.9	38.8	42.1	39.3
FeO	27.3	32.2	17.6	20.6	25.4	22.8	8.5	13.3	13.4	9.90	24.8	8.01	18.5
MgO	35.0	30.7	43.8	40.9	36.0	39.0	51.7	46.0	46.0	50.7	37.9	51.6	41.7
MnO	0.65	0.80	0.39	nd	0.64	0.63	0.21	0.32	0.32	nd	nd	0.20	0.50
Cr_2O_3	nd	0.04	nd	nd	nd	0.04	0.04	0.04	0.06	nd	nd	nd	0.03
CaO	0.05	0.08	nd	nd	nd	0.07	0.04	0.07	0.01	nd	nd	nd	0.03
Total	100.50	100.12	101.09	100.5	99.44	99.94	101.29	99.23	99.19	102.50	101.5	101.91	100.06
Cation Formula Based on 4 Oxygens													
Si	0.9960	0.9939	0.9891	0.9988	0.9958	0.9800	0.9830	0.9933	0.9917	0.9998	1.0024	1.0026	1.0031
Fe	0.6064	0.7373	0.3705	0.4412	0.5656	0.4997	0.1713	0.2797	0.2821	0.1976	0.5359	0.1595	0.3949
Mg	1.3855	1.2527	1.6429	1.5611	1.4285	1.5231	1.8563	1.7239	1.7256	1.8029	1.4593	1.8313	1.5863
Mn	0.0146	0.0186	0.0083	--	0.0144	0.0140	0.0043	0.0068	0.0068	--	--	0.0040	0.0108
Cr	--	0.0009	--	--	--	0.0008	0.0008	0.0008	0.0012	--	--	--	0.0006
Ca	0.0014	0.0023	--	--	--	0.0020	0.0010	0.0019	0.0003	--	--	--0.0008	Total
Cations	3.0039	3.0057	3.0108	3.0011	3.0043	3.0196	3.0167	3.0064	3.0077	3.0003	2.9976	2.9974	2.9965
*Cation Ratios Fe/Mn and mg# (100*Mg/(Mg+Fe))*													
Fe/Mn	41	40	45	--	39	36	40	41	41	--	--	40	37
mg#	69.6	62.9	81.6	78.0	71.6	75.3	91.6	86.0	85.9	90.1	73.1	92.0	80.1

(1) large olivine (Prinz et al., 1980); (2, 6, 7, 13) olivines from corona structures (Nehru et al. 1980); (3, 4, 5, 10, 12) large olivines (Mittlefehldt 1980); (11) small olivine (Mittlefehldt 1980); (8, 9) core and rim of large olivine (Mittlefehldt unpublished).

Mineral and lithic clasts

The igneous mineral and lithic clasts in mesosiderites are superficially similar to igneous clasts in howardites, eucrites and diogenites. However, many of them have subtle to stark differences with HED materials and are distinct igneous materials.

Ultramafic mineral clasts. Coarse-grained olivine clasts are commonly found in mesosiderites, but are absent in HED meteorites. These olivine clasts are typically rounded, single crystal fragments of cm size, although some brecciated clasts may have had polycrystalline precursors (McCall 1966, Mittlefehldt 1980). Texturally, many of them are very similar to the rounded olivine grains found in pallasites, and this led to the initial suggestion that mesosiderites were formed by mixing eucrite and pallasite magmas (Prior 1918). Table 43 presents representative analyses of mesosiderite olivine grains, and Figure 58 compares them to olivines from main-group pallasites. Mesosiderite olivines extend from more magnesian to more ferroan compositions than found in main-group pallasites (Fig. 58). No complete analyses of coarse-grained mesosiderite olivines are available in the literature, so the contents of minor elements, CaO and Cr_2O_3, are unknown, and only a few analyses containing MnO have been published. Nehru et al. (1980a) presented complete analyses for a few olivines from their study of corona textures, but these may be small mineral fragments. Delaney et al. (1981) presented partial analyses determined by Nehru et al. (1980a) for mesosiderite olivines, which again may be for small grains. Their data indicate that most mesosiderite olivine grains have FeO/MnO ratios in the range of ~30 to 42, lower than, but partially overlapping, the range for main-group pallasites. A few bona fide coarse-grained olivines studied by Mittlefehldt (1980) have FeO/MnO of 40 to 45, within the range of main-group pallasite olivines.

Coarse-grained low-Ca pyroxene clasts are common in mesosiderites. Many of these clasts are similar to diogenites and to orthopyroxenite clasts in howardites. Many are single crystal fragments, although polycrystalline pyroxenites are also present. These

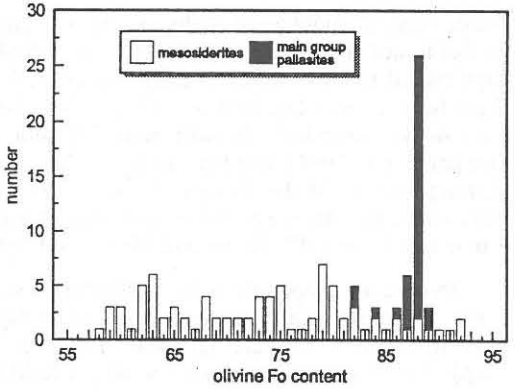

Figure 58. Histogram of olivine forsterite contents for individual mesosiderite olivine grains compared to average olivine compositions for main-group pallasites. Main-group pallasite olivines do not vary in composition within a given meteorite, except for minor zoning near the rims. Mesosiderite olivines show a wide range. Sources of pallasite data given in Figure 17. Mesosiderite data are from Agosto et al. (1980), Delaney et al. (1980), Mittlefehldt (1980 and unpublished), Nehru et al. (1980), Prinz et al. (1980).

clasts range in size up to about 10 cm. Coarse-grained orthopyroxenes are the most magnesian pyroxenes contained in mesosiderites, while coarse-grained pigeonites are among the most magnesian clinopyroxenes (Powell 1971). Systematics of pyroxene textural-compositional relationships are not well known. Powell (1971) determined that orthopyroxenes range from about Fs_{20} to Fs_{40}, and that in the mesosiderites Lowicz, Mincy and Morristown, orthopyroxenes more ferroan than about Fs_{30} were inverted from original pigeonite. This is similar to what is observed in the HED suite. Pyroxenes in typical diogenites ($Fs_{\sim 25}$) crystallized as orthopyroxene, while that in the ferroan Yamato Type B diogenites ($Fs_{\sim 32}$) crystallized as pigeonite. Table 42 gives representative coarse-grained low-Ca pyroxene analyses for mesosiderites.

Mafic lithic clasts. Mesosiderites contain basaltic and gabbroic clasts that are petrologically similar to basaltic and gabbroic eucrites and to mafic clasts in howardites (Ikeda et al. 1990, Kimura et al. 1991, McCall 1966, Mittlefehldt 1979, Rubin and Jerde 1987, 1988; Rubin and Mittlefehldt 1992). The original textures of these clasts vary from subophitic to ophitic for the finer-grained examples, to hypidiomorphic granular for the coarser-grained varieties. Many of them have been modified by shock metamorphism, which has caused granulation of minerals, recrystallization, formation of veins, impact melting and micro-faulting. These clasts are composed of original ferroan pigeonite and anorthitic plagioclase as the major phases, with minor to accessory silica (generally tridymite), whitlockite, augite, chromite and ilmenite. They typically contain metal and troilite, but it is difficult to determine whether these phases were added later by shock. The original pigeonite has undergone exsolution to form augite lamellae in either a lower Ca pigeonite or orthopyroxene host. Pyroxene textures in mesosiderites have not received the same level of detailed study accorded HED pyroxenes.

Detailed study of mesosiderite clasts has shown that many of the mafic clasts are distinguishable from similar HED meteorite materials. In general, basalts and gabbros from mesosiderites have higher modal proportions of tridymite and whitlockite than do similar HED lithologies (Nehru et al. 1980b, Rubin and Mittlefehldt 1992). Nehru et al. (1980b) presented summary data on basalt and gabbro clasts found in mesosiderite thin sections indicating a mean tridymite content of about 11 vol % for the basalt clasts, with a range of 5 to 14 vol %, while basaltic eucrites contain variable amounts of silica phases from ~1 to 8 vol % with a mean of about 4 vol % (Delaney et al. 1984). More recently, detailed petrologic study has been done on large basaltic and gabbroic clasts (up to several cm in size) mostly from the mesosiderite Vaca Muerta (Ikeda et al. 1990, Kimura et al. 1991, Mittlefehldt 1990, Rubin and Jerde 1987, Rubin and Mittlefehldt 1992). The basaltic clasts have a wider range of silica contents from about 0.4 to 13 vol % with a

lower mean of about 5 vol % than found by Nehru et al. (1980b). This large clast mean is probably not significantly different from that of the basaltic eucrites. Nevertheless, the high modal silica contents of many mesosiderite basalt clasts serve to distinguish them from basaltic eucrites. Nehru et al. (1980b) also noted that mesosiderite basaltic clasts have modal chromite > ilmenite, unlike basaltic eucrites which have chromite < ilmenite (Delaney et al. 1984). But here again, studies of larger basaltic clasts remove some of the distinctiveness. Of the 19 large basaltic clasts with modal chromite and ilmenite data, only about half have chromite significantly greater than ilmenite (Kimura et al. 1991, Rubin and Jerde 1987, Rubin and Mittlefehldt 1992).

Pyroxene compositions in mesosiderite mafic clasts also tend to be distinct from those of eucrites in that the former generally have lower FeO contents and lower FeO/MnO ratios (Mittlefehldt 1990). Figure 57 is a diagram of molar Fe/Mg vs. molar Fe/Mn for mesosiderite pyroxenes, with a field for HED meteorite pyroxenes shown for comparison. Some mesosiderite mafic clasts have pyroxenes with Fe/Mg-Fe/Mn similar to those of HED mafic rocks, for example Mount Padbury clast RV-05 of Mittlefehldt (1979). However, pyroxenes in many mesosiderite mafic clasts have generally lower Fe/Mg and Fe/Mn, and these types of pyroxenes are not found among HED samples. Many coarse orthopyroxene and magnesian pigeonite clasts in mesosiderites have Fe/Mg-Fe/Mn characteristics indistinguishable from those of their HED meteorite counterparts. Representative pyroxene analyses for mesosiderite mafic clasts are presented in Table 42.

Plagioclase grains in mafic clasts are typically anorthitic, An_{95-88}, with orthoclase contents of about 0.1 to 0.7 mol %; very similar to that of plagioclase in eucrites and howardites. Table 44 gives representative plagioclase analyses for basalt and gabbro clasts.

Silicate compositions

Bulk silicate compositions. Mesosiderite silicates are broadly similar to howardites in bulk composition, as would be expected for breccias composed of similar minerals. Table 45 gives representative major element compositions for several mesosiderite bulk silicates, which can be compared with similar data for howardites in Table 34. One problem with mesosiderite silicate analyses is that it is impossible to remove all the metal, and even more so all the troilite, from the silicate prior to analysis. Hence, the abundance of "FeO" in mesosiderite silicates by techniques such as XRF are always too high and need adjustment. Because of this, we have favored the wet chemical analyses from a reputable analyst (E. Jarosewich), which give true FeO contents. We have also used some XRF analyses if S and Ni have been determined which allow us to make adjustments for both metal and troilite. One major difference between mesosiderite silicates and howardites is the generally lower FeO in the former, resulting in a systematically lower FeO/MnO ratio for mesosiderite silicates (Simpson and Ahrens 1977). Mesosiderite silicates are also quite enriched in P_2O_5 compared to howardites. There is a systematic variation in bulk silicate composition with mesosiderite type; compositional class A mesosiderites have higher CaO and Al_2O_3 and lower MgO and Cr_2O_3 than compositional class B mesosiderites, consistent with the differences in basaltic and ultramafic components between the compositional classes.

Selected lithophile minor and trace elements for representative mesosiderites are presented in Table 46, which can be compared with similar data for howardites in Table 35. Mesosiderites generally contain lower contents of the most incompatible trace elements, such as the light rare-earth-elements, than do howardites. There are also systematic differences between compositional classes A, B and C mesosiderites. Compositional class A mesosiderites generally contain higher contents of the most

Table 44. Compositions of plagioclases from representative mesosiderites.

	Pinnaroo	Patwar				Clover Springs	
	(1)	(2)	(3)	(4)	(5)	(6)	(7)
	Chemical Composition w (wt %)						
SiO_2	45.3	46.2	46.0	45.3	45.5	45.6	45.2
Al_2O_3	34.8	34.9	34.5	34.8	34.8	35.2	35.7
FeO	0.34	0.35	0.19	0.23	0.24	0.16	0.17
CaO	19.0	18.4	18.3	18.7	18.4	18.5	18.8
Na_2O	0.83	0.95	0.95	0.90	0.95	0.89	0.77
K_2O	0.07	0.09	0.07	0.12	0.11	0.07	0.03
Total	100.34	100.89	100.01	100.05	100.00	100.42	100.67
	Cation Formula Based on 8 Oxygens (Ideal Plagioclase = 5 Cations per 8 Oxygens)						
Si	2.0873	2.1109	2.1182	2.0911	2.0988	2.0930	2.0714
^{IV}Al	1.8900	1.8795	1.8726	1.8935	1.8921	1.9043	1.9284
Total tet	3.9773	3.9904	3.9908	3.9846	3.9909	3.9973	3.9998
Fe	0.0131	0.0134	0.0073	0.0089	0.0093	0.0061	0.0065
Ca	0.9381	0.9008	0.9029	0.9249	0.9094	0.9098	0.9231
Na	0.0742	0.0842	0.0848	0.0806	0.0850	0.0792	0.0684
K	0.0041	0.0052	0.0041	0.0071	0.0065	0.0041	0.0018
Total Cations	5.0068	4.9940	4.9899	5.0061	5.0011	4.9965	4.9996
	Molecular Proportion of Orthoclase (Or), Albite (Ab), Anorthite (An)						
Or	0.4	0.5	0.4	0.7	0.6	0.4	0.2
Ab	7.3	8.5	8.6	8.0	8.5	8.0	6.9
An	92.3	91.0	91.0	91.3	90.9	91.6	92.9

(1) impact melt matrix plagioclase; (2) impact melt clast RV-01 plagioclase; (3) plagioclase in monogenic basalt (?) clast contained in impact melt clast RV-01; (4); polygenic basalt clast RV-02 plagioclase (5); gabbro clast RC-05 plagioclase (6) gabbro clast RC-01 plagioclase; (7) gabbro clast RC-01 plagioclase inclusion in tridymite; all data from Mittlefehldt (1978) except (7) from Mittlefehldt (unpublished).

incompatible elements than do compositional class B mesosiderites, and the sole mesosiderite of compositional class C is poorest in these elements. There is overlap in trace element composition between compositional classes A and B, however, and howardites can show considerable variation in trace element content from one sample to another. Therefore, caution must be used in interpreting variations in trace element contents with compositional class among mesosiderites.

Ultramafic mineral clast compositions. There are relatively few bulk analyses for coarse-grained olivine and orthopyroxene clasts from mesosiderites. Mittlefehldt (1980) presented an analysis for a Fo_{82} olivine clast from Emery and a Fo_{92} olivine clast from Pinnaroo done by INAA, with comparative data for Brenham pallasite olivine (Fo_{88}). For both of the mesosiderite clasts, the INAA Cr content was about a factor of 10 higher than electron microprobe analyses, indicating that chromite inclusions are present. Cobalt and Ni contents of the mesosiderite olivines were substantially higher than in the Brenham olivine, suggesting metal inclusions are present in the mesosiderite olivines. The Sc and Sm contents of the Emery olivine are much higher than those of Brenham olivine (Mittlefehldt 1980), or pallasite olivines in general.

Orthopyroxene clast analyses were presented for Emery and Patwar by Mittlefehldt (1979) and for Bondoc by Rubin and Mittlefehldt (1992). In addition, Kimura et al. (1991) presented results for an orthopyroxene breccia clast and an olivine-orthopyroxene

Table 45. Bulk chemical analyses of representative mesosiderites.

	Barea 1A		Patwar 1A		ALHA 77219 1B		Lowicz 3A		Mincy 3B		Patwar 1A		Mount Padbury 1A
	(1)	(1*)	(1)	(1*)	(1)	(1*)	(2)	(2*)	(2)	(2*)	(3)	(4)	(5)
						Composition (wt %)							
SiO_2	21.71	51.9	25.76	51.5	32.27	52.5	50.12	53.6	47.46	52.7	50.3	48.8	48.4
TiO_2	0.11	0.26	0.16	0.32	0.16	0.26	0.342	0.37	0.263	0.29	0.58	0.48	0.72
Al_2O_3	4.01	9.58	5.86	11.71	3.93	6.40	10.58	11.32	6.69	7.43	13.5	13.4	12.5
Cr_2O_3	0.37	0.88	0.26	0.52	0.63	1.03	0.767	0.82	1.474	1.64	0.44	0.43	0.36
Fe_2O_3	--	--	--	--	8.87	--	--	--	--	--	--	--	--
FeO	5.61	13.4	6.86	13.7	7.86	12.8	13.36	8.2	16.78	9.6	16.5	18.2	20.4
MnO	0.24	0.57	0.31	0.62	0.41	0.67	0.533	0.57	0.530	0.59	0.53	0.59	0.56
MgO	6.62	15.8	6.88	13.7	12.56	20.4	13.85	14.8	18.27	20.3	6.97	7.32	6.54
CaO	2.54	6.07	3.63	7.25	3.14	5.11	7.97	8.53	5.29	5.87	10.5	9.47	9.53
Na_2O	0.12	0.29	0.19	0.38	0.15	0.24	0.31	0.33	0.22	0.24	0.36	0.33	0.44
K_2O	0.01	0.02	--	--	0.03	0.05	0.017	0.02	0.008	0.01	--	0.02	--
P_2O_5	0.52	1.24	0.14	0.28	0.30	0.49	1.325	1.42	1.243	1.38	--	--	--
Fe	50.24	--	33.70	--	23.63	--	--	--	--	--	--	--	--
Ni	6.19	--	4.20	--	2.86	--	0.35	--	0.47	--	--	--	--
Co	0.12	--	0.13	--	0.10	--	--	--	--	--	--	--	--
P	--	--	0.02	--	--	--	--	--	--	--	--	--	--
FeS	1.62	--	11.89	--	1.10	--	--	--	--	--	--	--	--
S	--	--	--	--	--	--	0.246	--	0.544	--	--	--	--
Total	100.03	--	99.99	--	98.00	--	99.770	--	99.242	--	99.68	99.04	99.45
						*Cation Ratios Fe/Mn and mg# (100*MgO/(MgO+FeO))*							
Fe/Mn	23	--	22	--	19	--	25	14	31	16	31	30	36
mg#	67.8	--	64.1	--	74.0	--	64.9	76.3	66.0	79.0	42.9	41.7	36.4

(1) Wet chemistry analyses of bulk meteorite (Jarosewich, 1990). The Fe_2O_3 is from rusted metal, and not the silicate fraction. (1*) Analyses renormalized on a metal- and trolite-free basis to 100%. (2) XRF analyses of bulk non-magnetic fraction (Simpson 1982). (2*) Analyses with measured FeO corrected for metal and troilite contamination using measured Ni and S, and renormalized on a metal- and trolite-free basis to 100%. (3) Electron microprobe analyses of fused-glass bead (Mittlefehldt 1979) on basaltic impact melt clast, (4,5) Average of metal-troilite corrected INAA on bulk sample and electron microprobe analyses of fused-glass bead (Mittlefehldt 1979) on polygenic basalt clast (4), and monogenic basalt clast (5).

breccia clast from Vaca Muerta. We will not consider these latter breccia clasts here because of the possibility of contamination by other silicate materials. In general, the mesosiderite orthopyroxenites are similar in composition to diogenites (Mittlefehldt 1979). Although Mittlefehldt (1979) pointed out some trace element compositional differences between the Patwar orthopyroxenite and diogenites, subsequent recoveries of diogenites from Antarctica have largely removed the distinction. The Bondoc orthopyroxenite is more magnesian than that in typical diogenites (mg# 81 vs. ~74-76) (Rubin and Mittlefehldt 1992), but is within the range of individual orthopyroxene grains found in the diogenite EETA79002, mg# 73-82 (Mittlefehldt, unpublished).

Mafic lithic clast compositions. Both the basalt and the gabbro clasts in mesosiderites show much wider ranges in trace element compositions than do petrographically similar materials in the HED suite, and some of them have slightly unusual major element compositions. Representative major element compositions for basalt clasts are given in Table 45, and selected trace-element analyses are given in Table 46. These should be compared to basaltic eucrite analyses given in Tables 34 and 35. All of the mesosiderite clasts have high Ni and Co contents indicating that metal is present. The Ni and Co contents of mesosiderite metal was used to estimate the true FeO contents of the samples. Some of the analyses also have high Se contents indicative of high modal troilite. In the absence of information on the troilite Se content, a correction to FeO for troilite was done assuming troilite has a cosmic S/Se ratio. The mg# and molar Fe/Mn ratios discussed below are based on these corrected FeO contents.

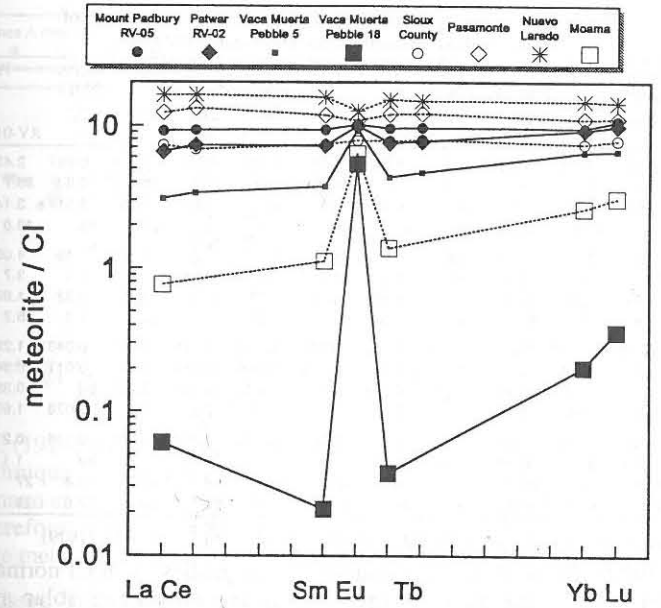

Figure 59. Rare earth element diagram for mesosiderite mafic clasts compared to select basaltic and cumulate eucrites. Mount Padbury RV-05 is a monogenic basalt, Patwar RV-02 a polygenic basalt, Vaca Muerta Pebble 5 an impact melt of cumulate gabbro(s), Vaca Muerta Pebble 18 an extremely fractionated cumulate gabbro (see Rubin and Mittlefehldt 1992 for classification). Data from Mittlefehldt (1979), Rubin and Jerde (1987), Rubin and Mittlefehldt (1992), Warren and Jerde (1987).

Some mesosiderite basalts are virtual clones of basaltic eucrites, for example, Mount Padbury clast RV-05 (Mittlefehldt 1979). This clast has a mg# of ~36, in the range of basaltic eucrites (33 to 41; see Table 34), a molar Fe/Mn of ~36, like that of basaltic eucrites, and a flat rare-earth-element (REE) pattern at about 9 to 10 × CI chondrite abundances. However, many of the basaltic clasts are distinct in major element composition. For example, Patwar basalt clast RV-02 (Mittlefehldt 1979) has a mg# of ~42, higher than that of basaltic eucrites, and a molar Fe/Mn of ~30, lower than that of basaltic eucrites. This clast also has a LREE-depleted pattern with a positive Eu anomaly, a pattern unknown among basaltic eucrite falls. Figure 59 shows REE patterns for mesosiderite basalt and gabbro clasts compared to basaltic and cumulate eucrites.

As is the case for the basalt clasts, some of the mesosiderite gabbro clasts are similar to cumulate eucrite gabbros in bulk major and/or trace element contents. Cumulate eucrites are more heterogeneous in major and trace element compositions than are basaltic eucrites, and there are fewer of them, so it is difficult to decide whether a given mesosiderite gabbro clast is distinct from the eucrite counterparts. The mesosiderite clast most similar to cumulate eucrites in major and trace element composition is Vaca Muerta Pebble 5, but this clast is texturally an impact melt (Rubin and Jerde 1987). Several mesosiderite gabbro clasts have trace element contents similar to those of cumulate eucrites (Mittlefehldt et al. 1992). However, many of the mesosiderite gabbroic clasts show extreme depletions in the most incompatible elements, such as the LREE, when compared to cumulate eucrites (Mittlefehldt 1979, Rubin and Mittlefehldt 1992). Extremes in this case are Vaca Muerta Pebbles 6 and 18, which have Sm abundances of 0.03 and 0.021 × CI chondrites, respectively (Rubin and Jerde 1987, Rubin and

Table 46. Trace element analyses of the non-magnetic fraction of representatitive mesosiderites and select mafic clasts.

		Barea	Mount Padbury	Patwar	Clover Springs	Esther-ville	Lowicz	Pinnaroo	Chin-guetti	Veramin	Mincy	RKPA 79015	Patwar		Mount Padbury
		IA	IA	IA	2A	3A	3A	4A	IB	2B	3B	2C	IA		IA
		wr	wr	wr	wr	wr	wr	wr	wr	wr	wr	wr	RV-01	RV-02	RV-05
Na	mg/g	1.53	1.52	1.33	1.46	1.83	1.25	1.31	0.502	0.929	0.787	0.067	2.45	2.33	3.14
Sc	µg/g	17.9	19.4	18.1	19.9	19.9	17.5	15.8	12.8	11.2	19.8	9.04	28.7	30.8	31.4
Cr	mg/g	5.18	3.58	7.75	8.87	6.08	5.08	5	6.72	6.68	5.03	3.31	3.14	3.05	2.40
Co	µg/g	52.6	113	43.8	72.1	39.5	51	320	79.4	108	138	95	48.0	63.0	22.2
Ni	mg/g	1.29	4.2	1.8	2.52	1.04	2.1	5.44	16.4	2.8	3.28	7.49	4.00	2.18	0.60
Se	µg/g	3.3	14.4	19.5	0.9	2.5	3.3	21.3	19.7	2.2	2.9	15.5	3.7	2.9	bd
La	µg/g	5.86	1.39	0.82	2.16	1.78	0.49	0.58	1.05	0.16	0.42	0.32	1.98	1.53	2.15
Ce	µg/g	12	3.4	2.3	10	4.5	1.6	bd	2.58	bd	bd	1.2	5.2	4.4	5.6
Sm	µg/g	0.364	0.386	0.479	0.272	0.703	0.327	0.323	0.138	0.075	0.295	0.0431	1.28	1.06	1.38
Eu	µg/g	0.23	0.23	0.24	0.23	0.32	0.18	0.2	0.068	0.044	0.15	0.011	0.54	0.56	0.57
Tb	µg/g	0.098	0.086	0.11	0.08	0.15	0.094	0.07	0.042	0.031	0.058	bd	0.39	0.28	0.35
Yb	µg/g	0.46	0.5	0.63	0.42	0.73	0.52	0.42	0.22	0.11	0.4	0.078	1.60	1.50	1.55
Lu	µg/g	0.07	0.08	0.08	0.067	0.1	0.075	0.068	0.03	0.027	0.063	0.014	0.23	0.24	0.26
Hf	µg/g	0.23	0.28	0.27	0.14	0.42	0.33	0.43	0.11	0.11	0.23	bd	1.1	0.87	0.88
Ir	ng/g	20.6	60.6	14.6	66.2	bd	9.9	bd	24.8	bd	bd	3.8	27	bd	bd
Au	ng/g	14.3	49.1	13.7	30.2	10.4	16	bd	33.6	bd	bd	57.6	21	17	bd

All analyses by INAA; whole rock by Mittlefehldt (unpublished), clasts by Mittlefehldt (1979).

Mittlefehldt 1992). These clasts have extreme Eu anomalies, with CI normalized Eu/Sm ratios of 220 to 260, the most extreme ratios known among solar system rocks (Mittlefehldt et al. 1992). In spite of these unusual trace element contents, these clasts have mg# and Fe/Mn ratios within the range of cumulate eucrites.

Mesosiderite metallic phase

Metallography. Powell (1969) provided the first comprehensive study of the metal phase of mesosiderites, although he primarily discussed the compositions and cooling rates of the metal. Like the silicates, metal occurs on a variety of scales and textural settings in mesosiderites from large, cm-sized clasts, to veins penetrating silicates, to matrix metal grains a few microns in size. An exceptional mesosiderite is RKPA79015 (Fig. 56), which contains large, several cm-sized areas of polycrystalline metal free of silicates (Clarke and Mason 1982). The boundaries between metal and silicate are generally irregular, with silicate grains commonly penetrating metal regions, and metal embays, penetrates, or veins, silicates (Powell 1969, 1971). Even the boundaries of the larger metal clasts exhibit fine-scale embayments with the silicate phase (Kulpecz and Hewins 1978, Powell 1969). Widmanstätten texture is developed in at least some of the larger metal clasts, but in general, kamacite occurs along metal-silicate and metal-metal boundaries, with taenite in the cores of the metal particles (Powell 1969). Tetrataenite has been observed rimming taenite cores in kamacite (Clarke and Mason 1982).

Troilite is common in mesosiderites, and makes up between <1 to about 14 wt % of the meteorites (Table 41). There are relatively few bulk sample modes or norms, so it is not possible to know how representative these values might be. In many cases, troilite occurs between silicate-rich and metal-rich regions in thin section. Schreibersite occurs included within kamacite, or at the metal-silicate grain boundaries of matrix metal particles (Kulpecz and Hewins 1978, Powell 1971).

Composition. The composition of the metal phase of mesosiderites was first extensively studied by Powell (1969) for bulk Ni content, by Wasson et al. (1974) for Ni, Ga, Ge and Ir, and by Begemann et al. (1976) for Fe, Ni and cosmogenic nuclides. Powell (1969) prepared his samples by grinding large surface areas of mesosiderite slabs, and therefore his analyses are of metal of all textural types; from clast to matrix metal.

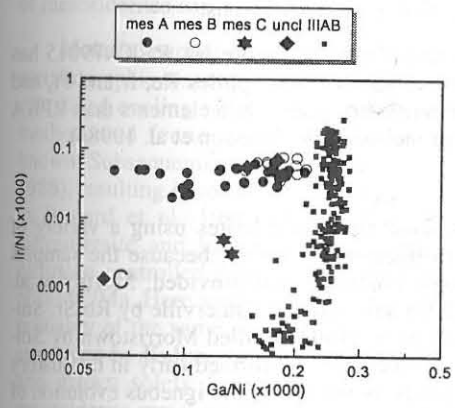

Figure 60. Comparison of mesosiderite metal and IIIAB irons on a plot of Ir/Ni vs. Ga/Ni. Mesosiderite metal does not exhibit the magmatic siderophile element trend shown by the IIIAB irons. Note that all low Ga/Ni mesosiderites are of compositional class A, and that duplicate analyses of the only compositional class C mesosiderite show its metal to be anomalous. The unclassified, anomalous mesosiderite Chaunsky (C) has a very unusual metal composition. Mesosiderite data are from Wasson et al. (1974, 1998a), Hassanzadeh et al. (1990); IIIAB iron data are from the compilation in Wasson (1974), plus more recent data from Esbensen et al. (1982), Kracher et al. (1980), Malvin et al. (1984), Scott and Wasson (1976), Wasson et al. (1989, 1998a).

Wasson et al. (1974) analyzed some of Powell's powders, powders they produced using the same technique, grains obtained by crushing and magnetic separation, and metal clasts. Begemann et al. (1976) prepared their metal separates by dry milling the samples, and they therefore included metal of all textural types. Hassanzadeh et al. (1990) analyzed large metal clasts from 15 mesosiderites for a suite of 11 siderophile elements.

As discussed by Wasson et al. (1974) and Hassanzadeh et al. (1990), and as is evident in the data of Begemann et al. (1976), the metal samples are invariably contaminated with silicates and oxides, and likely troilite as well. In addition, Wasson et al. (1974) and Hassanzadeh et al. (1990) have argued that the Ga and Fe, and possibly other siderophile element contents of the original metal may have been changed by interaction with the silicates. Hence, differences in the contents of Ni or other siderophile elements between different mesosiderites, or between different samples of the same mesosiderite, are difficult to interpret.

Using the original Powell (1971) classification for mesosiderites, Wasson et al. (1974) showed that textural grade 1 mesosiderites tended to be lower in Ga, Ge and Ir content than other mesosiderites. Using the current classification, it is clear that it is the compositional class A mesosiderites that tend to have the lower Ga, Ge and Ir contents. Figure 60 shows Ir/Ni vs. Ga/Ni for mesosiderite metal determined by Hassanzadeh et al. (1990) and Wasson et al. (1974, 1998a) compared with IIIAB irons. The compositional class B mesosiderites are all clustered at the high end of the Ga/Ni range, while the compositional class A mesosiderites span the range from the highest to lowest Ga/Ni ratios.

Hassanzadeh et al. (1990) divided mesosiderite metal compositions into three types; low-AuNi, intermediate-AuNi and high-AuNi on the basis of cluster analysis. They noted that all compositional class B mesosiderites except Chinguetti are in the low-AuNi group. They further argued that the classification of Chinguetti was not well known because only a small area was used for the modal analysis. One unusual feature of mesosiderite metal is the very small range in Ir contents compared to that found for igneous iron meteorite groups. Mesosiderite metal ranges in Ir from 1.7 to 6.3 µg/g, excluding the anomalous Chaunskij and RKPA79015 (Hassanzadeh et al. 1990, Wasson et al. 1974, 1998a). In contrast, IIIAB irons range in Ir from 0.011 to 19 µg/g (Wasson 1974). This difference is clearly shown in Figure 60, where IIIAB irons span three orders of magnitude in Ir/Ni whereas mesosiderite metal varies by only about a factor of four, excluding two anaomalous mesosiderites. The range in Ni content for mesosiderites,

excluding Chaunskij is essentially the same as that of the IIIAB irons.

As noted by Hassanzadeh et al. (1990) and shown in Figure 60, RPKA79015 has anomalous metal composition. It is low in the refractory siderophiles Re, Ir and Pt, and slightly low in W. Ghaunskij is even lower in refractory siderophile elements than RPKA 79001 and has higher Ni and Cu than any other mesosiderite (Wasson et al. 1998a).

Ages

Modern age determinations have been done on mesosiderites using a variety of techniques. Some of the data are difficult to interpret, however, because the samples analyzed are polymict breccias and petrologic control is not provided. Murthy et al. (1977) and Brouxel and Tatsumoto (1990, 1991) have studied Estherville by Rb-Sr, Sm-Nd and U-Th-Pb chronometry, and Prinzhofer et al. (1992) studied Morristown by Sm-Nd. Other than indicating that the mesosiderite silicates were formed early in the history of the solar system and later metamorphosed, little is learned of the igneous evolution of the mesosiderite parent body from these studies.

A limited amount of chronometry has been done on igneous clasts from mesosiderites. Ireland and Wlotzka (1992) reported ion microprobe analyses for U-Pb on zircons. Zircon VM-2, which occurs in a "eucritic clast," is concordant in the U-Pb system and yielded a $^{207}Pb/^{206}Pb$ age of 4.563±0.015 Ga (Ireland and Wlotzka 1992). Petrologic details of this clast were not given, so it is not known whether it is a basalt that is petrologically equivalent to basaltic eucrites, or one of the magnesian, low Fe/Mn basalts with unusual REE patterns. Either way, this result indicates that magmatic processes occurred very early on the mesosiderite parent body. Stewart et al. (1994) performed Sm-Nd analyses of three igneous clasts from Vaca Muerta that had previously been studied by petrography and bulk composition (Rubin and Jerde 1987, Rubin and Mittlefehldt 1992), and a clast from Mount Padbury. The Sm-Nd isochron age of the Mount Padbury clast is 4.52±0.04 Ga. The ages of the Vaca Muerta clasts are 4.48±0.09 Ga for a basalt clast, 4.48±0.19 Ga for a gabbro clast and 4.42±0.02 Ga for an impact-melt clast.

Numerous mesosiderites have been studied using the ^{39}Ar-^{40}Ar technique in order to investigate the metamorphic and impact history of their parent body. Bogard and Garrison (1998) and Bogard et al. (1990) have determined Ar-Ar ages for 20 samples from 14 different mesosiderites, including whole rock and igneous clast samples. Most of the samples show stepwise release profiles with only modest increases in calculated age with extraction temperature. The average Ar-Ar age for these samples is about 3.9 Ga. (The published ages of Bogard et al. (1990) are in error due to a round-off error in the ^{40}K decay constant used (Bogard and Garrison 1998). The average age given here incorporates a correction for this error.)

Cosmic-ray exposure ages have been calculated from ^{36}Ar and ^{36}Cl measurements of the metal phase of several mesosiderites (Begemann et al. 1976). The calculated ages vary from 9 to 162 Ma, and there is no correlation with petrologic type. The calculated cosmic-ray exposure ages for type 1A mesosiderites vary from 9 to 133 Ma, for type 3B mesosiderites from 36 to 162 Ma, and for type 3A mesosiderites from 33 to 134 Ma.

Cooling rates

Cooling rates of mesosiderites have been an enigma ever since Powell (1969) demonstrated that they are among the lowest known. Cooling rates have been determined by a variety of techniques on both the silicate and metallic fractions. These cooling rate estimates are generally for different temperature regimes, so details of the thermal history

of mesosiderites can be inferred.

Metallographic cooling rates. The larger metal clasts in mesosiderites have metallographic textures that allow cooling rates to be calculated. Powell (1969) originally calculated cooling rates for the temperature interval of ~500° to 350°C using the Wood method, and found rates of the order of 0.1°C/Ma, among the lowest cooling rates known. Subsequently, Ni diffusivity in Fe,Ni metal was revised (Saikumar and Goldstein 1988), resulting in recalculated cooling rates for mesosiderites of 1°C/Ma (see discussion in Bogard et al. 1990). Kulpecz and Hewins (1978) measured the Ni content in schreibersite and kamacite in the Emery mesosiderite, and used a non-isothermal, diffusion-controlled growth model for schreibersite in kamacite to calculate a cooling rate of 0.1°C/Ma. Here again, the more recent diffusivity data would require revision upward, probably of the same order as for the Wood method. However, in order for the method employed by Kulpecz and Hewins (1978) to be valid, schreibersite must have nucleated and grown solely from kamacite. Taenite and tetrataenite are typically present in mesosiderite metal particles, and even though they were not found in the grains studied by Kulpecz and Hewins (1978), it is likely that they were present out of the plane of the thin section, invalidating the calculated cooling rates (Agosto et al. 1980). Haack et al. (1996b) have reexamined the cooling rates of mesosiderites by modeling the Ni content of the centers of wide taenite lamellae and by modeling the central Ni content of kamacite using Powell's original data, and the phase diagram and diffusion constants of Saikumar and Goldstein (1988). Haack et al. (1996b) obtained very low cooling rates of ~0.01° to 0.03°C/Ma for several mesosiderites. Although there is uncertainty in the value of the low temperature cooling rate of mesosiderites, it seems clear that this value is very low, probably ≤1°C/Ma. Haack et al. (1996b) summarized metal phase compositional evidence that qualitatively argue that mesosiderite cooling rates are lower than those of other metal-bearing meteorites.

Silicate-based cooling rates. Estimates of cooling rates on the silicate fraction has been done by modeling element distributions in the minerals and by modeling Ar diffusion from bulk silicates. Delaney et al. (1981) measured steep Fe-Mg compositional profiles in pyroxene overgrowths on orthopyroxene cores for 4 mesosiderites, and suggested that these reflect cooling rates of 1° to 100°C per annum at temperatures in the range of 900° to 1150°C. Because diffusivity data for pyroxenes were lacking, they used data for olivines in this calculation. It is now known that Fe-Mg diffusion in pyroxenes is substantially slower than in olivine, and the cooling rates inferred for these pyroxene overgrowths should be much lower. Jones (1983) estimated values of ~2°C per annum for the highest rate given by Delaney et al. (1981), still ~10^6 to 10^8 times that estimated from the metal phase for low temperatures. Ganguly et al. (1994) reexamined the zoning profiles determined by Delaney et al. (1981) for Clover Springs and Lowicz overgrowths using updated diffusion data and more sophisticated cooling models. They calculated cooling rates of ~14°C/Ka at 1150°C and 5°C/Ka at 600°C. Ruzicka et al. (1994) modeled zoning profiles in overgrowths on plagioclase grains in corona structures, and estimated cooling rates of ≥100°C/Ka for temperatures of about 1100°C. Bogard et al. (1990) showed that the Ar-Ar release profiles and ages of mesosiderites were consistent with slow cooling at low temperature (500° to 350°C) as given by the metallographic cooling rates. Ganguly et al. (1994) estimated that the cooling rate at 250°C based on cation ordering in orthopyroxene was ≤1°C/Ma, similar to that determined on the metal phase for low temperatures.

Mesosiderite formation

As described above, the silicate fraction of mesosiderites is broadly similar to the

HED meteorites. Nevertheless, there are numerous differences in detail in their petrology and chemistry. Mesosiderites and HED meteorites show evidence for impact mixing on the surfaces of their parent bodies. Because mixing on asteroidal bodies is expected to be parent body-wide (e.g. Housen et al. 1979), Mittlefehldt (1979, 1990), Mittlefehldt et al. (1979) and Rubin and Mittlefehldt (1993) argued that mesosiderites and HEDs were formed on different parent bodies.

Because mesosiderites are composed of crustal silicates and iron metal presumed to represent core material of an asteroid, the formation of these meteorites requires complex processes. This complexity is compounded by estimates for cooling rates on the metal which indicate slow cooling, and hence deep burial (Powell 1969), while the textures and compositional zoning of the silicates give evidence for surficial processing and rapid cooling at high temperatures (Ganguly et al. 1994, Ruzicka et al. 1994). Indeed, the silicate textures and mineralogies of the mesosiderites indicate that these meteorites are polymict breccias formed by impact processes on the surface of a differentiated asteroid (Powell 1971). Rubin and Mittlefehldt (1993) presented a synopsis of the evolutionary history of mesosiderites, and what follows has been developed from this source and more recent work on mesosiderites.

Some of the igneous and meta-igneous clasts in mesosiderites are similar to the same materials found in the HED meteorite suite; they have essentially identical mg#, molar Fe/Mn, and trace element contents as eucrites and diogenites. Because of this, the earliest, post-accretion history of the mesosiderite parent body was likely similar to that of the HED parent body; parent body-wide igneous processes produced a mafic crust, a depleted ultramafic mantle and a metallic core. Just as there is active debate between partial melting vs. fractional crystallization models for formation of the HED parent body crust, this same uncertainty applies to the mesosiderite parent body crust. Age determinations on igneous and meta-igneous clasts have shown that the original mesosiderite parent body crust was formed about 4.56 Ga ago (e.g. Ireland and Wlotzka 1992). This is essentially the same as the time of formation of the HED meteorites, and shortly after the formation of chondritic meteorites (e.g. see Rubin and Mittlefehldt 1993). The presence of metal-poor breccia clasts in mesosiderites suggests that the parent body surface was gardened by impacts prior to metal-silicate mixing.

Metal-silicate mixing was the next major event (or events) on the mesosiderite parent body. A variety of models have been advanced to explain the metal-silicate mixing event including both internal and external mixing models (see review by Hewins 1983). Almost all models assume that the metallic and silicate fractions of mesosiderites originated in distinct regions, the core and crust, respectively, of either a single asteroid, or of two asteroids. The most plausible model is that of Wasson and Rubin (1985) and Hassanzadeh et al. (1990). These authors posit that an asteroidal core, stripped of its silicates by impacts except for some mantle olivine, accreted at low velocity to the mesosiderite parent body. Because the metal in mesosiderites appears to be undifferentiated, as indicated by the small range in Ir/Ni ratios (Fig. 60), these authors have suggested that the core was undifferentiated and therefore still largely molten at the time it was accreted. Hassanzadeh et al. (1990) further argued that metal-silicate mixing was responsible for the compositional distinction between compositional class A and B mesosiderites. They argued that all mesosiderites were originally of compositional class A, and that the region where the B mesosiderites were formed accreted more olivine with the metal. Through reduction of FeO and reaction with tridymite, this olivine was converted to orthopyroxene. The presence of metal-rich breccia clasts in mesosiderites suggests, but does not prove, that impacts gardened the surface of the parent body after metal-silicate mixing, and hence the proto-mesosiderite material remained on the parent body surface for some period of time.

Mittlefehldt (1979, 1990) and Rubin and Mittlefehldt (1992) have shown that many of the basalt and gabbro clasts in mesosiderites have undergone remelting after metal-silicate mixing. These are the clasts that are more magnesian than their eucrite counterparts, have low molar Fe/Mn ratios, LREE-depleted patterns with positive Eu anomalies, and high modal abundances of tridymite and/or whitlockite. This mineralogical and mineral compositional data shows that the mafic magmas were reduced by P from the metal phase (Mittlefehldt 1990). The LREE-depleted patterns and trace element signatures of some basaltic clasts indicate they are mixtures of basalts and cumulates (Mittlefehldt 1990, Rubin and Mittlefehldt 1992), and the extreme Eu/Sm fractionation of some gabbros indicate multiple melting and fractional crystallization steps (Mittlefehldt 1979, 1990; Mittlefehldt et al. 1992, Rubin and Mittlefehldt 1992). Because many of the mafic clasts in mesosiderites were remelted, it appears that a large fraction of the mesosiderite crust may have been remelted after metal-silicate mixing.

The overgrowths on pyroxene and plagioclase clasts and grains give evidence for rapid cooling at moderately high temperatures. The pyroxene overgrowths certainly must have formed at the time the mesosiderites were lithified into their current form, as these overgrowths can extend to cm size and poikilitically include all other minerals in the matrix (e.g. Floran 1978). Therefore, the evidence suggests that after the mesosiderites were assembled in their current form, they were still located near the surface of their parent body. Subsequently, the mesosiderites must have been put in a low-temperature environment where the cooling rate was many orders of magnitude lower, as indicated by the metallographic cooling rates and the cation ordering in orthopyroxene. Bogard et al. (1990) suggested that this was caused by a catastrophic disruption and reassembly of the mesosiderite parent body about 4.2 Ga ago, as indicated by the Ar-Ar ages. (We have adjusted the age quoted by Bogard et al. (1990) to correct for the computational error discovered by Bogard and Garrison (1998).) This event resulted in the mesosiderites being deeply buried in the parent body, where slow cooling at low temperatures caused Ar degassing. Haack et al. (1996b) have argued that break-up and reassembly did not occur on the mesosiderite parent body; instead they suggest that the cooling rates and petrology can be explained by essentially a single process: metal-silicate mixing by a large impact formed the mesosiderite breccias as we see them and led to the evidence for rapid cooling at high temperature. Continuing accretion of debris from the impact built up an insulating regolith. This gradually lowered the cooling rate at the mesosiderite location, leading to the low metallographic cooling rates at low temperature and Ar degassing. This model appears inconsistent with the petrologic and geochemical data on mesosiderite mafic clasts which suggest that melting and crystallization of much of the parent body crust occurred after metal-silicate mixing (Rubin and Mittlefehldt 1993).

MISCELLANEOUS NON-CHONDRITIC ASTEROIDAL METEORITES

A number of meteorites do not fit into well-defined groups on the basis of mineralogy, petrology or oxygen-isotopic compositions. In some cases, these meteorites formed by processes unknown from the main groups. In other cases, their origin was similar to that of a well-defined group, although probably representing another parent asteroid. Here we discuss several of these meteorites.

Bocaiuva

Bocaiuva is a unique silicate-bearing iron meteorite that was recovered as a single mass of 64 kg in 1947. The meteorite was studied by Desnoyers et al. (1985) and Malvin

et al. (1985) and information given below is taken from these sources.

Bocaiuva is dominated by Fe,Ni metal (~85 vol %) which exhibits a Widmanstätten pattern in some portions. The width of the kamacite bands indicates the Bocaiuva is a finest octahedrite. Bocaiuva contains 8.49 wt % Ni in the metal, but a remarkably high Ge/Ga ratio (Malvin et al. 1985). The Ge/Ga ratio suggests that Bocaiuva may be related to IIF iron meteorites, Eagle Station pallasites, or a small number of ungrouped irons. Detailed comparison of the metal compositions suggests that none of these are closely related, however, and they may not have formed on the same parent body.

Silicates in Bocaiuva occur as nodules or aligned stringers up to 1 cm in maximum dimension. They are composed of olivine ($Fa_{7.7}$), orthopyroxene ($Fs_{7.6}$), minor plagioclase (An_{49}) and clinopyroxene ($Fs_{4.5}$, Wo_{42}) in approximately chondritic abundances. The mafic silicate compositions are similar to those in IAB irons, while the plagioclase is alkali-poor compared to plagioclase in IAB irons.

The oxygen-isotopic composition of Bocaiuva silicates is closest to that of the Eagle Station pallasites (Fig. 1a) and the CO and CV chondrites, suggesting that the parent bodies of all of these meteorites may have formed from a similar reservoir.

Malvin et al. (1985) argued for an origin by impact, largely because of the analogy with IAB irons (see section on silicate-bearing IAB irons) and the occurrence of apparently-aligned stringers of silicates indicative of flow. Desnoyers et al. (1985) noted that only a small part of the 64 kg mass had been sampled and suggested that more work was in order.

Divnoe

Divnoe is an ultramafic achondrite whose relationship to other groups has been debated. Divnoe has been studied by McCoy et al. (1992) and Weigel et al. (1996) who reported their work in abstracts and Petaev and Brearley (1994) and Petaev et al. (1994) who provided a more comprehensive study. The information given here is taken from those papers.

Divnoe consists predominantly of olivine (74.6 vol %, $Fa_{20\text{-}28}$) which occurs as mm-sized elongate grains with a strong preferred orientation. Olivine in Divnoe is unusual in containing exsolution lamellae of slightly more and less ferroan olivine, with differences in composition of 2 to 4 mol % Fa. Orthopyroxene ($Fs_{20\text{-}28}$) is also common throughout the meteorite, comprising 14.3 vol % of the bulk. Large clinopyroxene grains often poikilitically enclose other grains. The meteorite has been heavily shocked, dispersing melted Fe,Ni metal and troilite droplets into the surrounding rock. Plagioclase is depleted relative to chondrites, comprising 1.5 vol % of the bulk with a composition ranging from $An_{32\text{-}45}$. The oxygen-isotopic composition for Divnoe is similar to that for brachinites and HED meteorites in $\Delta^{17}O$, although Divnoe has higher $\delta^{18}O$ and $\delta^{17}O$ than these other meteorite groups (Fig. 1c). Divnoe is similar to the brachinites ALH 84025 and Brachina in its major element composition. However, Divnoe is strongly depleted in the highly incompatible lithophile elements compared to brachinites, and in this is more similar to lodranites. Refractory siderophile elements are enriched in Divnoe compared to brachinites. Divnoe and Brachina also contain the same trapped Xe isotopic pattern.

The relationship between Divnoe and other groups of meteorites is not clear. McCoy et al. (1992) argued that Divnoe might represent an extension of the correlation between Fa and $\Delta^{17}O$ observed in lodranites, although it is much more oxidized ($Fa_{20\text{-}28}$) than the most oxidized lodranite (Fa_{13}). Petaev et al. (1994) agreed that Divnoe and the lodranites shared a number of similarities and, at the minimum, formed through similar processes.

However, these authors concluded that Divnoe is a unique meteorite not genetically related to any other known meteorite. The more recent work of Weigel et al. (1996), however, provides evidence for a link between Divnoe and brachinites. Future recoveries of more brachinites and lodranites, both of which are small groups whose ranges are incompletely understood, will likely be necessary before this issue can be resolved.

Enon

Enon is a unique stony-iron meteorite find, but little is known about it. Its oxygen-isotopic composition is near the field defined by the differentiated meteorite groups (Clayton and Mayeda 1996), the IIIAB irons, main-group pallasites, HED meteorites, mesosiderites, angrites, and it plots near two of the four brachinites (Fig. 1d).

A brief description of Enon was given by Bunch et al. (1970), and what follows was taken from that source. Enon is composed of roughly equal amounts of Fe,Ni metal and silicates having a texture similar to mesosiderites. Silicates in Enon are olivine ($Fo_{91.1}$), orthopyroxene ($Wo_{1.9}En_{87.6}Fs_{10.5}$), clinopyroxene ($Wo_{43.7}En_{51.9}Fs_{4.4}$) and plagioclase ($Ab_{78.9}An_{14.7}Or_{6.4}$). The silicates in Enon are quite reduced as shown by the magnesian nature of the ferromagnesian minerals. The sodic plagioclase is similar to those in chondritic meteorites. Enon also contains chromite, whitlockite, troilite and schreibersite. Bunch et al. (1970) suggested that the silicate mineral assemblage of Enon is in, or near, equilibrium.

Major and trace element analysis by INAA/RNAA was reported by Kallemeyn and Wasson (1985), who also published an earlier analysis by Bild (1976). Niemeyer (1983) reported K, Cl, Te, I and U concentrations for an acid-washed silicate fraction of Enon. Enon has a chondritic lithophile element signature. With the exceptions of V, Cr and La, the Mg- and CI-normalized refractory and moderately volatile lithophile elements are at CI abundances. The slight depletions in V and Cr are plausibly due to undersampling of chromite. Refractory siderophile elements and the moderately volatile siderophile elements Au and As are enriched 10 to 20 × CI abundances relative to Mg, whereas the three most volatile siderophile elements analyzed, Ga, Sb and Ge, have lower abundances of 2 to 6 × CI. Enon has slightly low refractory siderophile element/Ni ratios, which Kallemeyn and Wasson (1985) attribute to shock mobilization of metal. The most volatile elements studied by Bild (1976) and Kallemeyn and Wasson (1985), Br, Se, Zn and Cd, show depletions relative to CI abundances. The compositional characteristics of Enon are thus those of a metal-rich chondrite. Kallemeyn and Wasson (1985) state that differential melt-solid transport resulting from shock melting is a plausible cause for the high metal and troilite content and texture of Enon.

Niemeyer (1983) did an Ar-Ar and I-Xe study of Enon. He determined an Ar-Ar age of 4.59 Ga for Enon, and found no evidence for loss of radiogenic Ar at low temperature. This suggests that Enon has not been disturbed by thermal events essentially since it was formed. No I-Xe age could be determined, but the Xe data suggested that short-lived ^{244}Pu was present in Enon at levels greater than typical for chondrites at the time of closure for Xe loss, indicating that Enon is an ancient object.

Enon appears to be a highly metamorphosed, metal-rich, reduced chondrite. Its silicates are distinct from those of the brachinites with similar O-isotopic composition. Enon is much more reduced with an olivine mg# 91 vs. 65-70 for brachinites, and molar FeO/MnO of 19 vs. 63-68 (Nehru et al. 1983, Warren and Kallemeyn 1989a).

Guin

The Guin iron meteorite was recovered as a single 34.5 kg mass in 1969. Guin is an

ungrouped iron with similarities to IIE irons, but with enough significant differences to suggest that it samples yet another parent body. Guin has been studied by Rubin et al. (1986) and the description given here is taken from that work.

Guin is a coarse octahedrite with an unusually high Ni content. It is similar in composition to the iron meteorite groups IAB and IIICD, but is not a member of these groups. Guin contains ~6 vol % of silicate inclusions which are similar to silicate inclusions in the IIE irons Colomera, Kodaikanal and Elga. The largest inclusion consists of shock-melted plagioclase-rich matrix (~65 wt %, $Ab_{\sim 87}$) surrounding large, partly-melted augite grains (~20 wt %, $Fs_{10.4}Wo_{41.4}$) with minor low-Ca pyroxene ($Fs_{20.9}Wo_{3.7}$). The oxygen-isotopic composition of Guin is similar to that of L or LL chondrites, and differs dramatically from that of IIE irons (Fig. 1b).

Rubin et al. (1986) discussed two possible origins for Guin (1) fractional crystallization in a deep-seated magma chamber and (2) shock-melting of chondritic material from near the parent body surface. These models have been discussed in the section on IIE irons and shall not be repeated here. However, Guin is an important meteorite since it suggests that whichever process formed Guin and the IIE irons operated on more than a single parent body.

LEW 88763

This small achondrite was originally classified as a brachinite (AMN 14-2). Nehru et al. (1992) presented a brief characterization of brachinites, and noted that LEW 88763 had an anomalous oxygen-isotopic composition compared to other brachinites (see Fig. 1c). Nakamura and Morikawa (1993) determined a number of lithophile element concentrations on LEW 88763, and noted that it has a composition very similar to that of Brachina, and a chondritic REE pattern. Swindle et al. (1998) did a detailed study of LEW 88763, and concluded that it is not a brachinite, but a unique achondrite. The description that follows is from Swindle et al. (1998).

LEW 88763 is an ultramafic rock composed of 71% olivine, 7% pigeonite and augite, 10% plagioclase, 6% opaque phases including taenite, troilite, chromite and ilmenite, 7% unidentified material and accessory whitlockite. It is a fine-grained rock with equigranular texture of mostly anhedral grains <1 mm in size. Compositions of the major minerals are: olivine Fo_{63-64}, pigeonite $Wo_4En_{67}Fs_{29}$, augite $Wo_{38}En_{46}Fs_{16}$ and plagioclase $Or_{2-7}Ab_{55-74}An_{19-44}$. Chromite has an mg# of 12 to 15. Fe-Mg have equilibrated in the mafic silicates; no Fe-Mg zoning was detected in augite, and olivine and pigeonite are close to Fe-Mg equilibrium. Compared to brachinites, olivine in LEW 88763 is slightly more ferroan, and at lower modal abundance (compare with Table 18).

LEW 88763 has a chondritic bulk composition. Refractory lithophile elements including both compatible and incompatible elements are in chondritic ratios, indicating that igneous processes have not altered the bulk composition. The REE patterns of three samples analyzed show small positive Eu anomalies and variable Ce anomalies, which Swindle et al. (1998) suggest may be due to terrestrial weathering. There is a slight depletion in moderately volatile and volatile elements consistent with nebular fractionation. Siderophile elements are in chondritic abundance in LEW 88763, with slight depletions in the most volatile siderophile elements measured. Swindle et al. (1998) suggest LEW 88763 shows a slight depletion in Se, which they attribute to loss of sulfide from the rock. However, Se is the most volatile element they measured and it seems the Se depletion could equally well be nebular in origin.

No ages have been determined for LEW 88763, but Swindle et al. (1998) infer that its K-Ar age is ≥ 4.5 Ga based on K and Ar measurements made on different splits. They found no evidence for ^{129}Xe excess from the decay of ^{129}I. The isotopic composition of Xe in LEW 88763 is identical to chondritic Xe.

Based on mineralogy, bulk composition and noble gas data, LEW 88763 is an ultra-metamorphosed chondrite of unique type.

Puente del Zacate

Puente del Zacate is a IIIAB iron with 8.2% Ni in its metallic host. This meteorite is unusual, however, in containing a silicate inclusion, which was studied by Olsen et al. (1996). The inclusion is 7 mm in diameter and contained within a troilite nodule. The inclusion itself is composed olivine (23 wt %, Fa_4), low-Ca pyroxene (14 wt %, Fs_6Wo_1), chromium diopside (15 wt %, Fs_3Wo_{47}), plagioclase (15 wt %, $An_{14}Or_4$), graphite (27 wt %), and traces of troilite, chromite, daubreelite and Fe,Ni metal. The bulk mineralogy is similar to chondrites. The bulk REE pattern calculated from mineral compositions and abundances is flat at about 2.5 × CI abundances. The bulk oxygen-isotopic composition of the clast is similar to phosphates and chromites in other IIIAB irons (Clayton and Mayeda 1996; see Fig. 1c). The petrography, mineralogy and mineral compositions within the silicate inclusion of Puente del Zacate are similar to those in IAB irons, although differences in oxygen-isotopic composition and composition of the metallic host preclude formation of these two groups on a common parent body.

The origin of Puente del Zacate is unclear. Unlike IAB irons, IIIAB irons display fractional crystallization trends consistent with formation in a single core of an asteroid. If this is, in fact, the case, the incorporation of an undifferentiated silicate inclusion is difficult to understand. This is especially true considering the link between IIIAB irons and main-group pallasites, which contain silicates formed by magmatic processes. Olsen et al. (1996) argued that IAB and IIIAB irons may represent a continuum in the degree of partial melting they experienced, with IAB irons forming from a parent body with a very small degree of partial melting and IIIABs representing a higher degree of partial melting, but with some undifferentiated regions remaining in the mantle. Again, this seems at odds with the IIIAB-main-group pallasite connection inferred from geochemical data, and the likely origins of these groups. The reader is referred to the sections iron meteorite groups, the IAB iron silicates and pallasites above.

Sombrerete

Further evidence supporting formation of IIE-like meteorites on other parent bodies comes from the Sombrerete meteorite. Sombrerete is an ungrouped iron with 10.0 wt % Ni in the metallic host (Malvin et al. 1984).

Sombrerete contains ~7 vol % of silicate inclusions, which were studied by Prinz et al. (1982b). The inclusions are 1 to 5 mm in size and rounded. Quench-textured albitic glass is the dominant phase and may contain needles of apatite and orthopyroxene, as well as microphenocrysts of orthopyroxene. The inclusions consist of orthopyroxene (14.7%, En_{68}), albitic glass (66.7%), quench plagioclase (9.0%), chlorapatite (8.0%) and traces of kaersutite, tridymite, chromite, ilmenite and rutile. The silicate inclusions are broadly similar to those in the IIE irons Weekeroo Station and Miles, although substantially enriched in Al_2O_3, Na_2O and P_2O_5. The oxygen-isotopic composition of Sombrerete silicates lies below the terrestrial mass fractionation line on a three-isotope oxygen plot (Fig. 1b), substantially different from IIE irons and Guin (Clayton and Mayeda 1996).

As in the case of the IIE irons and Guin, the origin of Sombrerete is not clear (see

section on IIE irons). However, the existence of these meteorites suggests that at least three parent bodies experienced similar processes.

Tucson

The Tucson meteorite, with its striking ring shape, may be the most famous, and in many ways the most enigmatic, meteorite on Earth. The most complete petrologic study of Tucson was conducted by Nehru et al. (1982) and the information given here is from that work and sources referenced therein.

Tucson is an anomalous iron meteorite with 0.8 wt % Si and 2200 μg/g Cr in the metallic host and is chemically uniform. Small (0.1-2 mm) silicate inclusions comprise 8 vol % of the meteorite, are arranged in curved lines with flow orientation, and are elongate parallel to the direction of flow. The inclusions are composed of olivine (66.4 vol % of the silicate fraction; Fo_{99-100}), enstatite (30 vol %; 0.5-21 wt % Al_2O_3), diopside (3 vol %; 5-18 wt % Al_2O_3), minor plagioclase or glass and traces of spinel and brezinaite. Some of the pyroxenes are the most aluminous known in nature.

The compositions and textures of both the metal and silicate assemblages suggest that Tucson was essentially quenched from high temperature (1300-1500°C). The incorporation of aluminum into pyroxene resulted from the difficulty in nucleating feldspar. Nehru et al. (1982) favored a model for the origin of Tucson in which the silicate assemblage represented an impactor which mixed with the metal phase. The impact mixing caused melting of the silicates and rapid quenching of the metal and silicate, producing the quench textures of the silicates, the homogeneous composition of the metal and the flow alignment of silicates within metal.

It is interesting to note that the preferred scenario for the formation of Tucson bears a strong similarity to that suggested for the origin of Shallowater. However, the oxygen-isotopic composition of Tucson (Fig. 1a) differs dramatically from the enstatite meteorite clan which lie along the terrestrial fractionation line (Clayton et al. 1976b). Thus, Tucson may represent another example of a highly-reduced meteorite parent body which experienced processes similar to those postulated for formation of the Shallowater aubrite.

ACHONDRITIC CLASTS IN CHONDRITES

Some chondrites contain achondritic inclusions. In some cases, petrologic and geochemical study shows that they are obviously impact melts of the chondrite parent body (e.g. Keil et al. 1980). These are discussed in Chapter 3, not here. However, some achondritic clasts are obviously not impact melts of the parent body as they have distinct oxygen-isotopic compositions, mineralogies unlike bulk chondritic silicates and fractionated trace element abundances (e.g. Hutchison et al. 1988). These inclusions are of uncertain origin; they are not obviously nebular materials, nor are they easily understood in terms of parent-body igneous processes (e.g. Mittlefehldt et al. 1995) and hence are fascinating objects that deserve more study. Only a few of them have been studied in any detail, and surveys have been done on several others. Here we summarize what is known about these clasts. Bridges and Hutchison (1997) have done a survey of clasts in ordinary chondrites, and found that they occur in roughly 4% of ordinary chondrites. Of the 24 clasts they categorized, 10 are chemically fractionated and differ substantially from chondrules, and 8 could not be categorized.

Troctolites

Three clasts that can be classified as troctolites have been described from the L6 chondrites Barwell, Y-75097 and Y-793241. All of these inclusions have H chondrite O-isotopic compositions (Hutchison et al. 1988, Nakamura et al. 1994). The petrographic descriptions of these clasts are summarized from Hutchison et al. (1988), Sack et al. (1994), Yanai and Kojima (1993) and Yanai et al. (1983). These inclusions are dominated by olivine of varying grain sizes. The grains are subhedral to euhedral from <0.3 to >1.0 mm in size. Modal and normative data indicate that olivine makes up roughly 70 to 80% of the inclusions. Interstitial to the olivine is plagioclase or maskelynite, which makes up most of the remainder of the inclusion. Generally, fine-grained chromite is a minor component. Chlorapatite is a trace component in the Barwell and Y-793241 inclusions, whereas whitlockite makes up ~6% of the Y-75097 inclusion. Only a small surface area of the Y-793241 inclusion was available for study by Sack et al. (1994), so the modal data probably are not representative. Significantly, no pyroxene is reported from any of these inclusions. Yanai and Kojima (1993) report a barred olivine chondrule in the core of the Y-793241 inclusion, but petrographic details are not given.

Olivine compositions from all of these inclusions are within uncertainty the same as olivines from the host L chondrite (Hutchison et al. 1988, Sack et al. 1994). Plagioclase compositions are variable. In the Barwell inclusion, plagioclase in the core of the inclusion is very calcic, up to An_{74-70}, while near the margins of the inclusion they are more sodic, An_{20} (Hutchison et al. 1988). In the Y-75097 inclusion, plagioclase is only slightly more calcic than that in the host chondrite, and no mention is made of compositional variation within the inclusion (Sack et al. 1994). In the Y-793241 inclusion, plagioclase is much more calcic than that in the host chondrite, An_{61-44} vs. An_{19} (Sack et al. 1994).

Lithophile and siderophile element data are available for all of these inclusions. Two analyses have been done of the Barwell inclusion, one each of the interior and exterior (Hutchison et al. 1988). The LREE are slightly enriched and the HREE are depleted relative to CI chondrites, and there is a slight positive Eu anomaly. The patterns resemble that of plagioclase, which must be dominating the REE budget in the samples analyzed. The Barwell inclusion is depleted in siderophile elements, consistent with the low metal content. The Y-75097 inclusion has a highly fractionated lithophile element composition, but because of the heterogeneous nature of this inclusion (Nakamura et al. 1994, Sack et al. 1994), it is difficult to estimate a bulk inclusion composition. Many analyses of the inclusion display a common REE pattern with Eu at roughly chondritic abundance, moderate depletions in the LREE and HREE, and large depletions in the middle REE (e.g. Mittlefehldt et al. 1995, Nakamura et al. 1994, Warren and Kallemeyn 1989a). This type of pattern appears to represent that portion of the inclusion slightly interior of the margin with the host (Mittlefehldt et al. 1995). That part of the inclusion nearest the host has a REE pattern intermediate between this highly fractionated pattern and that of the host. The portion of the inclusion that may be the most interior (the original size and shape of the inclusion are unknown) is highly enriched in REE, with LREE at ~25 times CI abundances, HREE ~12 × CI and a negative Eu anomaly (Mittlefehldt et al. 1995). This portion of the inclusion has a high modal abundance of phosphates, which are controlling the REE content. Mittlefehldt et al. (1995) showed that all samples analyzed had Na contents higher than, and Sc contents lower than, those of H chondrites, and inferred therefore that the bulk inclusion could not have H chondrite composition. Analyses of the Y-793241 inclusion yield REE patterns similar to those of the intermediate regions of the Y-75097 inclusion (Mittlefehldt et al. 1995, Nakamura et al. 1994), but it is not known whether these analyses are representative.

The origin of these inclusions is unknown, but considering their general petrologic similarity, it is plausible they were all formed by the same process. Hutchison et al.

(1988) ascribed the origin of the Barwell clast to an unspecified planetary process, and they ruled out either nebular or impact processes. Mittlefehldt et al. (1995) pointed out the difficulties of producing pyroxene-free troctolites on asteroidal-sized bodies. Low pressure phase relationships do not yield olivine-plagioclase cumulates without recourse to ad hoc models; olivine-pyroxene, pyroxene and/or plagioclase-pyroxene rocks would be expected. Mittlefehldt et al. (1995) also discussed the difficulties of a nebular origin for these inclusions. No nebular materials, such as chondrules, proposed chondrule precursors, or matrix material, appear to be compositionally like the inclusions, and again, ad hoc models would be required to explain their genesis in the solar nebula. The origin of these clasts remains a conundrum.

"Norite"

Nakamura et al. (1990) and Misawa et al. (1992) describe a clast from the Hedjaz L3 chondrite which they classify as a norite. Based on the descriptions given and the photomicrographs, the major mafic mineral in this clast is olivine, and hence this is not a norite. The clast is small, only about 15 mg in mass, and yet the bulk lithophile element composition is not far removed from chondritic. Misawa et al. (1992) showed that Mg, Sc, Sr and Eu were slightly high compared to the range of L chondrites, while the moderately volatile Na, K and Rb were depleted. These authors suggested that impact melt processes could explain the unusual compositional features. Because of the small size of the sample, making representative sampling difficult, and its general similarity in bulk composition to L chondrites, we suspect that it is indeed impact melt material and will not discuss it further here.

Orthopyroxene-silica clasts

Ruzicka et al. (1995) described a silica-rich orthopyroxenite clast from the Bovedy L3 chondrite. The clast is composed of about 84% fine-grained orthopyroxene in equant to elongate grains showing normal igneous zoning with core mg# ~ 92 and rim mg# ~ 76. Tridymite and plagioclase make up about 6% each of the clast. Tridymite occurs as equant to elongate grains, generally interstitial to orthopyroxene. Plagioclase is interstitial to orthopyroxene and tridymite, and is An_{77-66} in composition. Plagioclase is associated with sodic glass (about 3% of the clast). There is minor pigeonite (~1%) that occurs at the rims of orthopyroxene. Chromite, augite, metal and sulfide are accessory to trace phases.

This clast has a distinctive O-isotopic composition, plotting well away from the region of ordinary chondrites. It lies on a mass fractionation line from H chondrites, about 3.8 ‰ heavier in ^{18}O than the H chondrite mean. The bulk composition is distinct from average L chondrites for some elements. The moderately volatile alkali elements Na, K and Rb are all depleted relative to L chondrites, while volatile Cs is not. The refractory incompatible lithophile trace elements (Sc, Ti, Sr, REE, Hf, Th) are all depleted, but in general are not fractionated from each other. Aluminum is slightly depleted, Si slightly enriched and Mg, Ca, V, Cr and Mn are at roughly L chondrite abundances. Siderophile element abundances are depleted in the clast to ~0.2 × CI for refractory siderophile elements and to ~0.01 × CI for Ni, Co, Au and the chalcophile element Se. Iron is also depleted in the clast at ~0.5 × CI.

Ruzicka et al. (1995) suggested that this clast was formed by a complicated igneous process on its parent body involving melting and separation of low temperature metallic and silicate partial melts, melting at higher temperature, either as a continuation of magmatism or a second melting event, separating this high temperature melt from residual metal, olivine and orthopyroxene. Ruzicka et al. (1995) suggested that other silica-rich clasts and chondrules studied by other researchers (e.g. Bischoff et al. 1993, Brigham et al. 1986, Wlotzka et al. 1983) may have had a magmatic origin. Some of these authors favored nebular, or at least non-igneous, origins for the clasts studied (Brigham et al. 1986, Wlotzka et al. 1983). Bischoff et al. (1993) could not choose between igneous processes, or thermal or impact metamorphism as the origin of the silica-alkali-rich clasts they studied. The very small sizes of the clasts studied by Bischoff et al. (1993), ~100-700 μm across, makes determining their petrogenesis difficult.

Nakamura et al. (1990) described a small (5 mg) orthopyroxene-silica clast from Hedjaz that may be similar to the Bovedy clast, but there is insufficient detailed information to make comparisons.

SUMMARY

The research discussed in this chapter summarizes past research and current thinking about the genesis of a wide diversity of meteorites which were affected by a common process—extensive heating on asteroidal bodies. An underlying theme of much of the current research on these rocks is the complexity of this process. Far from the simplistic ideas of whole body melting with lighter, basaltic components rising to the surface, a denser metallic component forming a core and depleted ultramafic components forming the mantle, modern meteorite research recognizes that a wide range of parameters can influence the final product. Clearly, non-chondritic meteorites were derived from a wide range of precursor chondrites, probably a wider range than is currently sampled by chondritic meteorites. Non-chondritic meteorite precursors had a wide range in volatile and moderately volatile element abundances (compare angrites, IVB irons with IAB iron metal and silicates, acapulcoites). Oxygen fugacities clearly differed by many orders of magnitude among the precursors, yielding the range from reduced aubrites to oxidized angrites. Possible variations in metal/silicate ratios and refractory lithophile/Mg ratios have been obscured by the extensive differentiation that produced many of these meteorites. The rocks were heated by a potentially diverse suite of heat sources, whose identification remains elusive (see however, Wood and Pellas 1991). The heat sources were apparently flexible enough to generate the wide range in heating observed. The degree of partial melting experienced by a parent body also varied dramatically, from very low degrees of partial melting producing acapulcoites and winonaites to very high degrees of partial melting to produce some iron meteorites and possibly the HED suite. Evidence from mesosiderites further suggests that differentiated crustal rocks were remelted and slowly crystallized on a scale larger than seems plausible for simple impact melting. Although the highly differentiated parent bodies may have had similar stratigraphies, the individual meteorites represent vastly different depths within the parent body, from metallic cores to the basaltic crust.

One interesting complexity, however, is that olivine-rich mantle rocks expected from differentiation of a chondritic precursor are surprisingly uncommon. Ureilites are potential mantle samples of their parent body, being basalt-depleted ultramafic rocks whose origin was probably as residues from partial melting. However, the O-isotopic heterogeneity, noble gas contents and siderophile element abundances of ureilites suggest that they may not have come from a parent body that underwent large-scale differentiation. The "dunite problem" has been discussed by several authors (e.g. Bell et al. 1989) and the solution likely has an explanation in asteroidal fragmentation and sampling, rather than in our understanding of melting and differentiation. Magmatic iron meteorites generally have very long cosmic-ray exposure histories compared to stony meteorites, suggesting that the mantle dunites stripped off iron meteorite cores could have been largely destroyed long ago. A second complexity is the lack of complementary basalts for the iron meteorites and the aubrite, lodranite and ureilite achondrites.

Collisional destruction may explain the lack of basalts to match the number of cores, as is generally invoked for the lack of dunites. However, the lack of basalts that can be associated with the depleted ultramafic achondrites is curious. This is especially true for the ureilites, as the polymict ureilites would be expected to contain a mixture of material from the parent body surface, including basalts.

Impact was a clear influence in the history of meteorite parent bodies. In some cases, impacts mixed lithologies from the same parent body (e.g. IAB and IIE irons) or from different parent bodies (e.g. mesosiderites). In many cases, stony achondrites experienced mixing of lithologies after solidification and cooling. These polymict brecciated achondrites vastly improve our sampling of these parent bodies, but also complicate our efforts to understand their petrogenesis. There are many unique irons, stony-irons or stones which are the only recognized representatives of their parent bodies. The full elucidation of the history of these parent bodies will almost certainly have to await further recoveries. It seems future research will likely serve to increasingly emphasize the complexity of asteroidal heating processes. Answers to many of our questions about the genesis of these rocks will be found through continued meteorite research. However, many of the most vexing problems will only be solved through eventual study of asteroidal materials in situ during planetary missions and on Earth using samples returned to our laboratories.

ACKNOWLEDGMENTS

We would like to thank several people for support and/or help in providing information used in this chapter: J.L. Berkley, G. Crozaz, C.R. Goodrich, J.N. Grossman, J.H. Jones, M. Prinz, T.D. Swindle, A.H. Treiman, D. Walker and J.T. Wasson. Reviews by the Pacific Rim review team of A.E. Rubin, H. Takeda and P.H. Warren resulted in great improvements in the manuscript, and we thank them for their Herculean efforts. The senior author rues the day he picked up the phone and heard J. Papike on the other end of the line, and vows never again to agree to produce a major manuscript under deadline pressure. He suspects the co-authors similarly wish they had not answered the phone when the senior author called. Support for D.W. Miitlefehldt came from NASA RTOP #152-13-40-21 to M.M. Lindstrom. Support for T.J. McCoy came from NASA grant NAG5-4490.

REFERENCES

Agosto WN, Hewins RH, Clarke RS Jr (1980) Allan Hills A77219, the first Antarctic mesosiderite. Proc Lunar Planet Sci Conf 11:1027-1045

Alserman AR (1940) A siderolite from Pinnaroo, South Australia. Trans Roy Soc S Aust 64:109-113

Allègre CJ, Birck JL, Fourcade S, Semet MP (1975) Rubidium-87/Strontium-87 age of Juvinas basaltic achondrite and early igneous activity in the solar system. Science 187:436-438

Anders E, Grevasse N (1989) Abundances of the elements: Meteoritic and solar. Geochim Cosmochim Acta 53:197-214

Aylmer D, Bonanno V, Herzog GF, Weber H, Klein J, Middleton R (1988) ^{26}Al and ^{10}Be production in iron meteorites. Earth Planet Sci Lett 88:107-118

Baba T, Takeda H, Saiki K (1993) Mineralogy of three EUROMET ureilites including an orthopyroxene-augite achondrite. Meteoritics 28:319

Begemann F, Weber HW, Vilcsek E, Hintenberger (1976) Rare gases and ^{36}Cl in stony-iron meteorites: cosmogenic elemental production rates, exposure ages, diffusion losses and thermal histories. Geochim Cosmochim Acta 40:353-368

Bell JF, Davis DR, Hartmann WK, Gaffey MJ (1989) Asteroids: The Big Picture. *In* Asteroids II, RP Binzel, T. Gehrels, MS Matthews (eds) Univ Arizona Press, 921-945

Bence AE, Burnett BS (1969) Chemistry and mineralogy of the silicates and metal of the Kodaikanal meteorite. Geochim Cosmochim Acta 33:387-407

Benedix GK, McCoy TJ, Keil K, Bogard DD, Garrison DH (1998a) A petrologic and isotopic study of winonaites: Evidence for early partial melting, brecciation, and metamorphism. Geochim Cosmochim Acta, in press

Benedix GK, McCoy TJ, Love SG, Keil K (1998b) A petrologic study of IAB irons: Constraints on the formation of the IAB-winonaite parent body. Geochim Cosmochim Acta (submitted)

Berkley JL (1986) Four Antarctic meteorites: Petrology and observations on ureilite petrogenesis. Meteoritics 21:169-189

Berkley JL (1990) Petrology of newly recovered orthopyroxene-bearing Antarctic meteorites: A new ureilite type? Lunar Planet Sci 21:69-70

Berkley JL, Boynton NJ (1992) Minor/major element variation within and among diogenite and howardite orthopyroxenite groups. Meteoritics 27:387-394

Berkley JL, Jones JH (1982) Primary igneous carbon in ureilites: Petrological implications. Proc Lunar Planet Sci Conf 13th, J Geophys Res 87:A353-A364

Berkley JL, Brown HG, Keil K, Carter NL, Mercier J-CC, Huss G (1976) The Kenna ureilite: An ultramafic rock with evidence for igneous, metamorphic and shock origin. Geochim Cosmochim Acta 40:1429-1437

Berkley JL, Taylor GJ, Keil K, Harlow GE, Prinz M (1980) The nature and origin of ureilites. Geochim Cosmochim Acta 44:1579-1597

Berkley JL, Goodrich CA, Keil K (1985) The unique ureilite, ALHA82106-82130: Evidence for progressive reduction during ureilite magmatic differentiation. Meteoritics 20:607-608

Bevan AWR, Grady MM (1988) Mount Morris (Wisconsin): A fragment of the IAB iron Pine River? Meteoritics 23:349-352

Bevan AWR, Bevan JC, Francis JG (1977) Amphibole in the Mayo Belwa meteorite: First occurrence in an enstatite achondrite. Mineral Mag 41:531-534

Bhandari N, Shah VG, Graham A (1981) The Lahrauli ureilite. Meteoritics 16:185-191

Bild RW (1976) A study of primitive and unusual meteorites. PhD thesis, Univ of California at Los Angeles, 234 p

Bild RW (1977) Silicate inclusions in group IAB irons and a relation to the anomalous stones Winona and Mt. Morris (Wis.). Geochim Cosmochim Acta 41:1439-1456

Bild RW, Wasson JT (1976) The Lodran meteorite and its relationship to the ureilites. Mineral Mag 40:721-735

Bild RW, Wasson JT (1977) Netschaëvo: A new class of chondritic meteorite. Science 197:58-62

Binns RA (1969) A chondritic inclusion of unique type in the Cumberland Falls meteorite. *In* Meteorite Research, PM Millman (ed) Reidel, Dordrecht, Netherlands, p 695-704

Binz CM, Ikramuddin M, Lipschutz ME (1975) Contents of eleven trace elements in ureilite achondrites. Geochim Cosmochim Acta 39:1576-1579

Binzel RP, Xu S (1993) Chips off of asteroid 4 Vesta: Evidence for the parent body of basaltic achondrite meteorites. Science 260:186-191

Binzel RP, Gaffey MJ, Thomas PC, Zellner BH, Storrs AD, Wells EN (1997) Geologic mapping of Vesta from 1994 Hubble Space Telescope images. Icarus 128:95-103

Birck JL, Allègre CJ (1978) Chronology and chemical history of the parent body of basaltic achondrites studied by the ^{87}Rb-^{87}Sr method. Earth Planet Sci Lett 39:37-51

Birck J-L, Allègre CJ (1988) Manganese-chromium isotope systematics and the development of the early solar system. Nature 331:579-584

Bischoff A, Geiger T, Palme H, Spettel B, Schultz L, Scherer P, Schlüter J, Lkhamsuren J (1993) Mineralogy, chemistry, and noble gas contents of Adzhi-Bogdo—an LL3-6 chondritic breccia with L-chondritic and granitoidal clasts. Meteoritics 28:570-578

Black DC (1972) On the origin of trapped helium, neon and argon isotopic variations in gas-rich meteorites, lunar soil and breccia. Geochim Cosmochim Acta 36:347-375

Bland P, Pillinger CT, Hutchison R (1992) A new ureilite from the Sahara—Acfer 277. Lunar Planet Sci 23:119

Boesenberg JS, Prinz M, Weisberg MK, Davis AM, Clayton RN, Mayeda TK, Wasson JT (1995) Pyroxene-pallasites: A new pallasite grouplet. Meteoritics 30:488-489

Boesenberg JS, Delaney JS, Prinz M (1997) Magnesian megacrysts and matrix in the mesosiderite Lamont. Lunar Planet Sci 28:125-126

Bogard DD (1995) Impact ages of meteorites: A synthesis. Meteoritics Planet Sci 30:244-268

Bogard DD, Garrison DH (1994) ^{39}Ar-^{40}Ar ages of four ureilites. Lunar Planet Sci 25:137-138

Bogard DD, Garrison DH (1995) ^{39}Ar-^{40}Ar age of the Ibitira eucrite and constraints on the time of pyroxene equilibration. Geochim Cosmochim Acta 59:4317-4322

Bogard DD, Garrison DH (1998) ^{39}Ar-^{40}Ar ages and thermal history of mesosiderites. Geochim Cosmochim Acta, in press

Bogard D, Burnett D, Eberhardt P, Wasserburg GJ (1967) ^{40}Ar-^{40}K ages of silicate inclusions in iron meteorites. Earth Planet Sci Lett 3:275-283
Bogard DD, Burnett DS, Wasserburg GJ (1969) Cosmogenic rare gases and the ^{40}K-^{40}Ar age of the Kodaikanal iron meteorite. Earth Planet Sci Lett 5:273-281
Bogard DD, Gibson EK, Moore DR, Turner NL, Wilken RB (1973) Noble gas and carbon abundances of the Haverö, Dingo Pup Donga, and North Haig ureilites. Geochim Cosmochim Acta 37:547-557
Bogard DD, Nyquist LE, Johnson P, Wooden J, Bansal B (1983) Chronology of Brachina. Meteoritics 18:269-270
Bogard DD, Garrison DH, Jordan JL, Mittlefehldt D (1990) ^{39}Ar-^{40}Ar dating of mesosiderites: Evidence for major parent body disruption <4 Ga ago. Geochim Cosmochim Acta 54:2549-2564
Bottke W F Jr., M C Nolan, R Greenberg, R A Kolvoord (1994) Velocity distributions among colliding asteroids. Icarus 107:255-268
Bowman LE, Spilde MN and Papike JJ (1997) Automated energy dispersive spectrometer modal analysis applied to the diogenites. Meteoritics Planet Sci 32:869-875
Boynton WV, Hill DH (1993) Trace-element abundances in several new ureilites. Lunar Planet Sci 24:167-168
Boynton WV, Starzyk PM, Schmitt RA (1976) Chemical evidence for the genesis of the ureilites, the achondrite Chassigny and the nakhlites. Geochim Cosmochim Acta 40:1439-1447
Brearley AJ, Prinz M (1992) CI chondrite-like clasts in the Nilpena polymict ureilite. Implications for aqueous alteration processes in CI chondrites. Geochim Cosmochim Acta 56:1373-1386
Brett R, Keil K (1986) Enstatite chondrites and enstatite achondrites (aubrites) were not derived from the same parent body. Earth Planet Sci Lett 81:1-6
Bridges JC, Hutchison R (1997) A survey of clasts and large chondrules in ordinary chondrites. Meteoritics Planet Sci 32:389-394
Brigham CA, Yabuki H, Ouyang Z, Murrell MT, El Goresy A, Burnett DS (1986) Silica-bearing chondrules and clasts in ordinary chondrites. Geochim Cosmochim Acta 50:1655-1666
Brouxel M, Tatsumoto M (1990) U-Th-Pb systematics of the Estherville mesosiderite. Proc Lunar Planet Sci Conf 20:309-319
Brouxel M, Tatsumoto M (1991) The Estherville mesosiderite: U-Pb, Rb-Sr, and Sm-Nd isotopic study of a polymict breccia. Geochim Cosmochim Acta 55:1121-1133
Buchanan PC, Reid AM (1996) Petrology of the polymict eucrite Petersburg. Geochim Cosmochim Acta 60:135-146
Buchanan PC, Zolensky ME, Reid AM (1993) Carbonaceous chondrite clasts in the howardites Bholghati and EET87513. Meteoritics 28:659-669
Buchwald VFB (1975) Handbook of iron meteorites. 3 vol. Berkeley: University of California Press
Buchwald VF (1977) The mineralogy of iron meteorites. Phil Trans Royal Soc London A286:453-491
Buchwald VF, Scott ERD (1971) First nitride (CrN) in iron meteorites. Nature Phys Sci 233:113-114
Bunch, TE (1975) Petrography and petrology of basaltic achondrite polymict breccias (howardites). Proc Lunar Sci Conf 6:469-492
Bunch TE, Fuchs LH (1969) A new mineral: brezinaite, Cr_3S_4, and the Tucson meteorite. Am Mineral 54:1509-1518
Bunch TE, Keil K (1971) Chromite and ilmenite in non-chondritic meteorites. Am Mineral 56:146-157
Bunch TE, Olsen E (1968) Potassium feldspar in Weekeroo Station, Kodaikanal, and Colomera iron meteorites. Science 160:1223-1225
Bunch TE, Keil K, Olsen E (1970) Mineralogy and petrology of silicate inclusions in iron meteorites. Contrib Mineral Petrol 25:297-240
Bunch TE, Keil K, Huss GI (1972) The Landes meteorite. Meteoritics 7:31-38
Burghle A, Dreibus G, Palme H, Rammensee W, Spettel B, Weckworth G, Wänke H (1983) Chemistry of shergottites and Shergottite Parent Body (SPB): Further evidence for the two component model for planet formation. Lunar Planet Sci 14:80-81
Burnett DS, Wasserburg GJ (1967a) Evidence for the formation of an iron meteorite at 3.8×10^9 years. Earth Planet Sci Lett 2:137-147
Burnett DS, Wasserburg GJ (1967b) ^{87}Rb-^{87}Sr ages of silicate inclusions in iron meteorites. Earth Planet Sci Lett 2:397-408
Buseck PR (1977) Pallasite meteorites-mineralogy, petrology, and geochemistry. Geochim Cosmochim Acta 41:711-740
Buseck PR, Goldstein JI (1969) Olivine compositions and cooling rates of pallasitic meteorites. Geol Soc Amer Bull 80:2141-2158
Buseck PR, Holdsworth E (1977) Phosphate minerals in pallasite meteorites. Mineral Mag 41:91-102
Carter NL, Raleigh CB, DeCarli P (1968) Deformation of olivine in stony meteorites. J Geophys Res 73:5439-5461

Casanova I (1992) Osbornite and the distribution of titanium in enstatite meteorites. Meteoritics 27: 208-209
Casanova I, Keil K, Newsom HE (1993a) Composition of metal in aubrites: Constraints on core formation. Geochim Cosmochim Acta 57:675-682
Casanova I, McCoy TJ, Keil K (1993b) Metal-rich meteorites from the aubrite parent body. Lunar Planet Sci 24:259-260
Casanova I, Graf T, Marti K (1995) Discovery of an unmelted H-chondrite inclusion in an iron meteorite. Science 268:469-608
Chase MW, Davies CA, Downing JR, Frurip DJ, McDonald RA, Syverud AN (1985) JANAF thermochemical tables. J Phys Chem Ref Data 14, Suppl. 1
Chen JH, Wasserburg GJ (1990) The isotopic composition of Ag in meteorites and the presence of ^{107}Pd in protoplanets. Geochim Cosmochim Acta 54:1729–1743
Chikami J, Mikouchi T, Takeda H, Miyamoto M (1997a) Mineralogy and cooling history of the calcium-aluminum-chromium enriched ureilite, Lewis Cliff 88774. Meteoritics Planet Sci 32:343-348
Chikami J, Mikouchi T, Miyamoto M, Takeda H (1997b) Mineralogical comparison of Hammadah Al Hamra 126 with some ureilites. Antarctic Meteorite Res 10:389-399
Choi B-G, Ouyang X, Wasson JT (1995) Classification and origin of IAB and IIICD iron meteorites. Geochim Cosmochim Acta 59:593-612
Chou C-L, Boynton WV, Bild RW, Kimberlin J, Wasson JT (1976) Trace element evidence regarding a chondritic component in howardite meteorites. Proc Lunar Sci Conf 7:3501-3518
Christophe Michel-Levy M, Bourot-Denise M, Palme H, Spettel B, Wänke H (1987) L'eucrite de Bouvante: chimie, pétrologie et minéralogie. Bull Minéral 110:449-458
Clarke, RS Jr., Mason B (1982). A new metal-rich mesosiderite from Antarctica, RKPA79015. Natl Inst Polar Res (Japan) Spec Issue 25:78-85
Clarke RS Jr, Scott ERD (1980) Tetrataenite—ordered FeNi, a new mineral in meteorites. Am Mineral 65:624-630
Clayton RN (1993) Oxygen-isotopes in meteorites. Ann Rev Earth Planet Sci 21:115-149
Clayton RN, Mayeda TK (1978) Genetic relations between iron and stony meteorites. Earth Planet Sci Lett 40:168-174
Clayton RN, Mayeda TK (1983) Oxygen-isotopes in eucrites, shergottites, nakhlites, and chassignites. Earth Planet Sci Lett 62:1-6
Clayton RN, Mayeda TK (1988) Formation of ureilites by nebular processes. Geochim Cosmochim Acta 52:1313-1318
Clayton RN, Mayeda TK (1996) Oxygen-isotope studies of achondrites. Geochim Cosmochim Acta 60:1999-2018
Clayton RN, Grossman L, Mayeda TK (1973) A component of primitive nuclear composition in carbonaceous chondrites. Science 181:485-487
Clayton RN, Mayeda TK, Onuma N, Shearer J (1976a) Oxygen-isotopic composition of minerals in the Kenna ureilite. Geochim Cosmochim Acta 40:1475-1476
Clayton RN, Onuma N, Mayeda TK (1976b) A classification of meteorites based on oxygen-isotopes. Earth Planet Sci Lett 30:10-18
Clayton RN, Mayeda TK, Rubin AE (1984) Oxygen-isotopic compositions of enstatite chondrites and aubrites. Proc Lunar Planet Sci Conf 15:C245-C249
Clayton RN, Mayeda TK, Nagahara H (1992) Oxygen-isotope relationships among primitive achondrites. Lunar Planet Sci 23:231-232
Consolmagno GJ, Drake MJ (1977) Composition and evolution of the eucrite parent body: evidence from rare earth elements. Geochim Cosmochim Acta 41:1271-1282
Crozaz G, Lundberg LL (1995) The origin of oldhamite in unequilibrated enstatite chondrites. Geochim Cosmochim Acta 59:3817-3831
Crozaz G, McKay G (1990) Rare earth elements in Angra dos Reis and Lewis Cliff 86010, two meteorites with similar but distinct magma evolutions. Earth Planet Sci Lett 97:369-381
Crozaz G, Pellas P (1983) Where does Brachina come from? Lunar Planet Sci 14:142-143
Cruikshank DP, Tholen DJ, Hartmann WK, Bell JF, Brown RH (1991) Three basaltic earth-approaching asteroids and the source of the basaltic meteorites. Icarus 89:1-13
Davis AM (1977) The cosmochemical history of the pallasites. Ph.D dissertation, Yale University, 285 p
Davis AM, Olsen EJ (1991) Phosphates in pallasite meteorites as probes of mantle processes in small planetary bodies. Nature 353:637-640
Davis AM, Prinz M, Laughlin JR (1988) An ion microprobe study of plagioclase-rich clasts in the North Haig polymict ureilite. Lunar Planet Sci 19:251-252
Dean DC, Goldstein JI (1986) Determination of interdiffusion coefficients in the Fe-Ni and Fe-Ni-P systems below 900°C. Metall Trans 17A:1131-1138

Delaney JS, Sutton SR (1988) Lewis Cliff 86010, an ADORable Antarctican. Lunar Planet Sci 19:265-266
Delaney JS, Nehru CE, Prinz M (1980) Olivine clasts from mesosiderites and howardites: Clues to the nature of achondritic parent bodies. Proc Lunar Planet Sci 11:1073-1087
Delaney JS, Nehru CE, Prinz M, Harlow GE (1981) Metamorphism in mesosiderites. Proc Lunar Planet Sci 12B:1315-1342
Delaney JS, Takeda H, Prinz M, Nehru CE, Harlow GE (1983) The nomenclature of polymict basaltic achondrites. Meteoritics 18:103-111
Delaney JS, Prinz M, Takeda H (1984) The polymict eucrites. Proc 15th Lunar Planet Sci Conf Part 1, J Geophys Res 89 Supl:C251-C288
Desnoyers C (1982) L'olivine dans les howardites: origine, et implications pour le corps parent de ces météorites achondritiques. Geochim Cosmochim Acta 46:667-680
Desnoyers C, Christophe Michel-Levy M, Azevedo IS, Scorzelli RB, Danon J, da Silva EG (1985) Mineralogy of the Bocaiuva iron meteorite: A preliminary study. Meteoritics 20:113-124
Dickinson TL, Lofgren GE (1992) Melting relations for Indarch (EH4) under reducing conditions. Lunar Planet Sci 23:307-308
Dickinson TL, McCoy TJ (1997) Experimental rare-earth-element partitioning in oldhamite: Implications for the igneous origin of aubritic oldhamite. Meteoritics Planet Sci 32:395-412
Dollase WA (1967) The crystal structure at 220°C of orthorhombic high tridymite from the Steinbach meteorite. Acta Cryst 23:617-623
Dreibus G, Palme H, Rammensee W, Spettel B, Weckworth G, Wänke H (1982) Composition of the Shergottite Parent Body: Further evidence of a two component model of planet formation. Lunar Planet Sci 13:186-187
Duke MB (1965) Metallic iron in basaltic achondrites. J Geophys Res 70:1523-1527
Duke MB, Silver LT (1967) Petrology of eucrites, howardites and mesosiderites. Geochim Cosmochim Acta 31:1637-1665
Dymek RF, Albee AL, Chodos AA, Wasserburg GJ (1976) Petrography of isotopically-dated clasts in the Kapoeta howardite and petrologic constraints on the evolution of its parent body. Geochim Cosmochim Acta 40:1115-1130
Ebihara M, Shinonaga T, Takeda H (1990) Trace element compositions of Antarctic ureilites and some implications to their origin. Meteoritics 25:359-360
Ebihara M, Ikeda Y, Prinz M (1997) Petrology and chemistry of the Miles IIE iron. II: Chemical characteristics of the Miles silicate inclusions. Antarctic Meteorite Res 10:373-388
Ehlers EC (1972) The Interpretation of Geological Phase Diagrams. San Francisco: WH Freeman and Co, 327 p
Esbensen KH, Buchwald VF, Malvin DJ, Wasson JT (1982) Systematic compositional variations in the Cape York iron meteorite. Geochim Cosmochim Acta 46:1913-1920
Eugster O, Michel T (1995) Common asteroid break-up events of eucrites, diogenites, and howardites and cosmic-ray production rates for noble gases in achondrites. Geochim Cosmochim Acta 59:177-199
Eugster O, Michel Th, Niedermann S (1991) ^{244}Pu-Xe formation and gas retention age, exposure history, and terrestrial age of angrites LEW86010 and LEW87051: Comparison with Angra dos Reis. Geochim Cosmochim Acta 55:2957-2964
Evensen NM, Hamilton PJ, Harlow GE, Klimentidis R, O'Nions RK, Prinz M (1979) Silicate inclusions in Weekeroo Station: Planetary differentiates in an iron meteorite. Lunar Planet Sci 10:376-378
Fioretti AM, Molin G (1996) Petrography and mineralogy of FRO93008 ureilite: Evidence for pairing with FRO90054 ureilite. Meteoritics 31:A43-A44
Fioretti AM, Molin G, Brandstätter F, Kurat G (1996) Schreibersite, metal, and troilite in ureilites FRO90054 and FRO93008. Meteoritics 31:A44
Floran RJ (1978) Silicate petrography, classification, and origin of the mesosiderites: Review and new observations. Proc Lunar Planet Sci Conf 9:1053-1081
Floran RJ, Prinz M, Hlava PF, Keil K, Nehru CE, Hinthorne JR (1978a) The Chassigny meteorite: a cumulate dunite with hydrous amphibole-bearing melt inclusions. Geochim Cosmochim Acta 42:1213-1229
Floran RJ, Caulfield JBD, Harlow GE, Prinz M (1978b) Impact origin for the Simondium, Pinnaroo, and Hainholz mesosiderites: Implications for impact processes beyond the earth-moon system. Proc Lunar Planet Sci Conf 9:1083-1114
Floran RJ, Prinz M, Hlava PF, Keil K, Spettel B, Wänke H (1981) Mineralogy, petrology, and trace element geochemistry of the Johnstown meteorite: a brecciated orthopyroxenite with siderophile and REE-rich components. Geochim Cosmochim Acta 45, 2385-2391
Floss C, Crozaz G (1993) Heterogeneous REE patterns in oldhamite from the aubrites: Their nature and origin. Geochim Cosmochim Acta 57:4039-4057
Floss C, Strait MM, Crozaz G (1990) Rare earth elements and the petrogenesis of aubrites. Geochim Cosmochim Acta 57:4039-4057
Fogel RA (1994) Aubrite basalt vitrophyres: High sulfur silicate melts and a snapshot of aubrite formation. Meteoritics 29:466-467
Fogel RA (1997) A new aubrite basalt vitrophyre from the LEW 87007 aubrite. Lunar Planet Sci 28:369-370
Fogel RA, Hess PC, Rutherford MJ (1988) The enstatite chondrite-achondrite link. Lunar Planet Sci 19:342-343
Fogel RA, Weisberg MK, Prinz M (1996) The solubility of CaS in aubrite silicate melts. Lunar Planet Sci 27:371-372
Folco L (1992) Meteorites from the 1990/'91 expedition to the Frontier Mountains, Antarctica. Meteoritics 27:221-222
Foshag WF (1940) The Shallowater meteorite; a new aubrite. Am Mineral 25:279-286
Fowler GW, Papike JJ, Spilde MN, Shearer CK (1994) Diogenites as asteroidal cumulates: Insights from orthopyroxene major and minor element chemistry. Geochim Cosmochim Acta 58:3921-3929
Fowler GW, Shearer CK, Papike JJ, Layne GD (1995) Diogenites as asteroidal cumulates: Insights from orthopyroxene trace element chemistry. Geochim Cosmochim Acta 59:3071-3084
Fredriksson K (1982) The Manegaon diogenite. Meteoritics 17:141-144
Frondel C, Marvin UB (1967) Lonsdaleite, a hexagonal polymorph of diamond. Nature 214:587-589
Fuchs LH (1966) Djerfisherite, alkali copper-iron sulfide, a new mineral from the Kota-Kota and St. Mark's enstatite chondrites. Science 153:166-167
Fuchs LH (1969) The phosphate mineralogy of meteorites. *In* Meteorite Research (ed. PM Millman), p 683-695. Reidel
Fuchs LH (1974) Glass inclusions of granitic compositions in orthopyroxene from three enstatite achondrites. Meteoritics 9:342
Fuhrman M, Papike JJ (1981) Howardites and polymict eucrites: Regolith samples from the eucrite parent body. Petrology of Bholgati, Bununu, Kapoeta, and ALHA76005. Proc. Lunar Planet Sci 12B:1257-1279
Fukuoka T, Kimura M (1990) Chemistry of Y-74063, -74357 and ALH-78230 unique meteorites. Papers presented 15th Symp Antarctic Meteorites, NIPR, Tokyo, 99-100
Fukuoka T, Ma M-S, Wakita H, Schmitt RA (1978) Lodran: The residue of limited partial melting of matter like a hybrid between H and E chondrites. Lunar Planet Sci 9:356-358
Gaffey MJ (1990) Thermal history of the asteroid belt: Implications for accretion of the terrestrial planets. In Origin of the Earth (HE Newsom, JH Jones, eds) Oxford Univ Press p 17-28
Gaffey MJ (1997) Surface lithologic heterogeneity of asteroid 4 Vesta. Icarus 127:130-157
Ganguly J, Yang H, Ghose S (1994) Thermal history of mesosiderites: Quantitative constraints from compositional zoning and Fe-Mg ordering in orthopyroxenes. Geochim Cosmochim Acta 58: 2711-2723
Garcia DJ, Prinz M (1978) The Binda orthopyroxene cumulate eucrite: A slightly polymict brecciated melanorite. Meteoritics 13:473
Garrison DH, Bogard DD (1995) ^{39}Ar-^{40}Ar ages of silicates from IIE iron meteorites. Meteoritics 30:508
Gibson EK (1976) Nature of the carbon and sulfur phases and inorganic gases in the Kenna ureilite. Geochim Cosmochim Acta 40:1459-1464
Göbel R, Ott U, Begemann F (1978) On trapped noble gases in ureilites. J Geophys Res 83:855-867
Goldstein JI, Ogilvie RE (1965) The growth of the Widmannstätten pattern in metallic meteorites. Geochim Cosmochim Acta 29:893-920
Gomes CB and Keil K (1980) Brazilian Stone Meteorites. Univ New Mexico Press, 162 p
Goodrich CA (1986a) Trapped primary silicate liquid in ureilites. Lunar Planet Sci 17:273-274
Goodrich CA (1986b) Y73140: A ureilite with cumulus augite. Meteoritics 21:373-374
Goodrich CA (1988) Petrology of the unique achondrite LEW86010. Lunar Planet Sci 19:399-400
Goodrich CA (1992) Ureilites: a critical review. Meteoritics 27:327-252
Goodrich CA (1997a) Preservation of a nebular mg-Δ^{17}O correlation during partial melting of ureilites. Lunar Planet Sci 28:435-436
Goodrich CA (1997b) Iron-manganese-magnesium relations and mg-Δ^{17}O correlations in ureilites, lodranites, Allende chondrules, and ordinary chondrites: Nebular or planetary? Meteoritics Planet Sci 32:A49-A50
Goodrich CA (1997c) The chondrite-achondrite transition: Decoupling of oxygen-isotopic and geochemical changes. *In* Workshop on Parent-Body and Nebular Modification of Chondritic Materials. Zolensky ME, Krot AN, Scott ERD (eds) LPI Tech Report 97-02 Part 1, 15-17
Goodrich CA (1998) A ureilite (Hughes 009) with an unusual shock texture: Implications for the origin of metal in ureilites? Lunar Planet Sci 29:1123
Goodrich CA, Berkley JL (1986) Primary magmatic carbon in ureilites: Evidence from cohenite-bearing

spherules. Geochim Cosmochim Acta 50:681-691
Goodrich CA, Lugmair GW (1991) PCA82506: a ureilite with LREE-enriched component and a whole-rock Sm-Nd model age of 4.55 Ga. Lunar Planet Sci 22:467-468
Goodrich CA, Lugmair GW (1992) Addition of LREE-enriched material to a ureilite at 4.23 Ga: Evidence for episodic metasomatism? Lunar Planet Sci 23:429-430
Goodrich CA, Lugmair GW (1995) Stalking the LREE-enriched component in ureilites. Geochim Cosmochim Acta 59:2609-2620
Goodrich CA Keil K, Berkley JL, Laul JC, Smith MR, Wacker JF, Clayton RN, Mayeda TK (1987a) Roosevelt County 027: A low-shock ureilite with interstitial silicates and high noble-gas concentration. Meteoritics 22:191-218
Goodrich CA, Jones JH, Berkley JL (1987b) Origin and evolution of the ureilite parent magmas: Multi-stage igneous activity on a large parent body. Geochim Cosmochim Acta 51:2255-2273
Goodrich CA, Patchett PJ, Lugmair GW, Drake MJ (1991) Sm-Nd and Rb-Sr isotopic systematics of ureilites. Geochim Cosmochim Acta 55:829-848
Goodrich CA, Lugmair GW, Drake MJ, Patchett PJ (1995) Comment on "U-Th-Pb and Sm-Nd isotopic systematics of the Goalpara ureilite: Resolution of terrestrial contamination" by N Torigoye-Kita, K Misawa, and M Tatsumoto. Geochim Cosmochim Acta 59:4083-4085
Gooley R (1972) The chemistry and mineralogy of the diogenites. Ph.D dissertation, Arizona State University 198 p
Gooley R, Moore CB (1976) Native metal in diogenite meteorites. Am Mineral 61:373-378
Göpel C, Manhès G, Allègre CJ (1985) Concordant 3,676 Ma U-Pb formation age for the Kodaikanal iron meteorite. Nature 317:341-344
Göpel Ch., Manhès G, Allègre CJ (1992) U-Pb study of the Acapulco meteorite. Meteoritics 27:226
Grady MM, Pillinger CT (1986) The ALHA 82130 ureilite: Its light element stable isotope composition and relationship to other ureilites. Meteoritics 21:375-376
Grady MM, Pillinger CT (1987a) The EET83309 polymict ureilite: Its relationship to other ureilites on the basis of stable isotope measurements. Lunar Planet Sci 18:353-354
Grady MM, Pillinger CT (1987b) Unusual nitrogen isotopic composition of polymict ureilites. Meteoritics 22:394-395
Grady MM, Pillinger CT (1993) EUROMET ureilite consortium: A preliminary report on carbon and nitrogen geochemistry. Lunar Planet Sci 24:551-552
Grady MM, Wright IP, Swart PK, Pillinger CT (1985a) The carbon and nitrogen isotopic composition of ureilites: Implications for their genesis. Geochim Cosmochim Acta 49:903-915
Grady MM, Pillinger CT and Wacker J F (1985b) Carbon isotopes in HF/HCL residues of the unshocked ureilite ALHA78019. Meteoritics 20:652-653
Grossman JN (1994) Meteoritical Bulletin. Meteoritics 29:100-143
Guan Y, Crozaz G (1995a) The quest for the elusive LREE carrier in ureilites: An ion microprobe study. Lunar Planet Sci 26:527-528
Guan Y, Crozaz G (1995b) Rare-earth-element distribution in Elephant Morraine and the "missing" basaltic component associated with ureilites. Meteoritics 30:514-515
Guan Y, Crozaz G (1997) Rare earth elements in some lithic and mineral clasts of polymict ureilites and petrogenetic implications. Lunar Planet Sci 28:485-486
Haack H, Scott ERD (1993) Chemical fractionations in Group IIIAB iron meteorites: Origin by dendritic crystallization of an asteroidal core. Geochim Cosmochim Acta 57:3457-3472
Haack H, Rasmussen KL, Warren PH (1990) Effects of regolith/megaregolith insulation on the cooling histories of differentiated asteroids. J Geophys Res 95:5111-5124
Haack H, Scott ERD, Love SG, Brearley AJ, McCoy TJ (1996a) Thermal histories of IVA stony-iron and iron meteorites: Evidence for asteroid fragmentation and reaccretion. Geochim Cosmochim Acta 60:3103-3113
Haack H, Scott ERD, Rasmussen KL (1996b) Thermal and shock history of mesosiderites and their large parent asteroid. Geochim Cosmochim Acta 60:2609-2619
Haramura H, Kushiro I, Yanai K (1983) Chemical compositions of Antarctic meteorites I Proc Symp Antarctic Meteorites 8:109-121, NIPR, Tokyo
Harlow GE, Nehru CE, Prinz M, Taylor GJ, Keil K (1979) Pyroxenes in Serra de Magé: Cooling history in comparison with Moama and Moore County. Earth Planet Sci Lett 43:173-181
Haskin L, Warren P (1991) Chapter 8: Lunar Chemistry. *In* Lunar Sourcebook: A User's Guide to the Moon (G Heiken, D Vaniman, BM French, eds) Cambridge Univ Press, Cambridge, UK
Hassanzadeh J, Rubin AE, Wasson JT (1990) Compositions of large metal nodules in mesosiderites; links to iron meteorite group IIIAB and the origin of mesosiderite subgroups. Geochim Cosmochim Acta 54:3197-3208
Herpfer MA, Larimer JW, Goldstein JI (1994) A comparison of metallographic cooling rate methods used

in meteorites. Geochim Cosmochim Acta 58:1353-1366
Hess HH, Henderson EP (1949) The Moore County meteorite: A further study with comment on its primordial environment. Am Mineral 34:494-507
Hewins RH (1983) Impact versus internal origins for mesosiderites. Proc 14th Lunar Planet Sci Conf, Part 1: J Geophys Res 88:B257-B266
Hewins RH (1984) The case for a melt matrix in plagioclase-POIK mesosiderites. Proc 15th Lunar Planet Sci Conf, Part 1: J Geophys Res 89 Suppl, C289-C297
Hewins RH (1988) Petrology and pairing of mesosiderites from Victoria Land, Antarctica. Meteoritics 23:123-129
Hewins RH, Harriott TA (1986) Melt segregation in plagioclase-poikilitic mesosiderites. Proc 16th Lunar Planet Sci Conf, Part 2: J Geophys Res 91:D365-D372
Hewins RH, Klein LC (1978) Provenance of metal and melt rock textures in the Malvern howardite. Proc Lunar Planet Sci Conf 9:1137-1156
Hewins RH, Newsom HE (1988) Igneous activity in the early solar system. *In* Meteorites and the Early Solar System (JF Kerridge and MS Matthews, eds.) Univ Arizona Press, Tucson, AZ, 73-101
Higuchi H, Morgan JW, Ganapathy R, Anders E (1976) Chemical variation in meteorites—X Ureilites. Geochim Cosmochim Acta 40:1563-1571
Hiroi T, Bell JF, Takeda H, Pieters CM (1993) Spectral comparison between olivine-rich asteroids and pallasites. Proc NIPR Symp Antarctic Meteorites 6:234-245
Hohenberg CM (1970) Xenon from the Angra dos Reis meteorite. Geochim Cosmochim Acta 34:185-191
Hohenberg CM, Bernatowicz TJ, Podosek FA (1991) Comparative xenology of two angrites. Earth Planet Sci Lett 102:167-177
Honda M (1988) Statistical estimation of the production of cosmic-ray-induced nuclides in meteorites. Meteoritics. 23:3-12
Horan MF, Smoliar MI, Walker RJ (1998) ^{182}W and ^{187}Re-^{187}Os systematics of iron meteorites: Chronology for melting, differentiation, and crystallization in asteroids. Geochim Cosmochim Acta 62:545-554
Hostetler CJ, Drake MJ (1978) Quench temperatures of Moore County and other eucrites: residence time on eucrite parent body. Geochim Cosmochim Acta 42:517-522
Housen KR, Wilkening LL, Chapman CR, Greenberg RJ (1979) Asteroidal regoliths. Icarus 39:317-352
Hsu W, Crozaz G (1997) Mineral chemistry and the petrogenesis of eucrites: II. Cumulate eucrites. Geochim Cosmochim Acta 61:1293-1302
Hsu W, Huss GR, Wasserburg GJ (1997) Mn-Cr systematics of differentiated meteorites . Lunar Planet Sci 28:609-610
Humayun M, Clayton RN (1995) Potassium isotope cosmochemistry: Genetic implications of volatile element depletion. Geochim Cosmochim Acta 59:2131-2148
Hutcheon ID, Olsen E (1991) Cr isotopic composition of differentiated meteorites: A search for ^{53}Mn. Lunar Planet Sci 22:605-606
Hutchison R (1977) A crystalline ureilite from Oman. Meteoritics 12:263
Hutchison R, Williams CT, Din VK, Clayton RN, Kirschbaum C, Paul RL, Lipschutz ME (1988) A planetary, H-group pebble in the Barwell, L6, unshocked chondritic meteorite. Earth Planet Sci Conf 90:105-118
Ikeda Y, Prinz M (1996) Petrology of silicate inclusions in the Miles IIE iron. Proc NIPR Symp Antarctic Meteorites 9:143-173
Ikeda Y, Takeda H (1985) A model for the origin of basaltic achondrites based on the Yamato 7308 howardite. Proc Lunar Planet Sci Conf 15th; J Geophys Res 90:C649-C663
Ikeda Y, Ebihara M, Prinz M (1990) Enclaves in the Mt. Padbury and Vaca Muerta mesosiderites: Magmatic and residue (or cumulate) rock types. Proc NIPR Symp Antarctic Meteorites 3:99-131
Ikeda Y, Ebihara M, Prinz M (1997) Petrology of and chemistry of the Miles IIE iron. I: Description and petrology of twenty new silicate inclusions. Antarctic Meteorite Res 10:355-372
Imamura M, Shima M, Honda M (1980) Radial distribution of spallogenic K, Ca, Ti, V and Mn isotopes in iron meteorites. Z Naturforsch 35A:267-279
Ireland TR, Wlotzka F (1992) The oldest zircons in the solar system. Earth Planet Sci Lett 109:1-10
Jacobsen SB, Wasserburg GJ (1984) Sm-Nd isotopic evolution of chondrites and achondrites, II. Earth Planet Sci Lett 67:137-150
Janssens M-J, Hertogen J, Wolf R, Ebihara M, Anders E (1987) Ureilites: Trace element clues to their origin. Geochim Cosmochim Acta 51:2275-2283
Jaques AL, Fitzgerald MJ (1982) The Nilpena ureilite, an unusual polymict breccia: Implications for origin. Geochim Cosmochim Acta 46:893-900
Jarosewich E (1967) Chemical analysis of seven stony meteorites and one iron with silicate inclusions. Geochim Cosmochim Acta 31:1103-1106
Jarosewich E (1990) Chemical analyses of meteorites: A compilation of stony and iron meteorite analyses.

Meteoritics 25:323-337
Jarosewich E, Mason B (1966) Chemical analysis with notes on one mesosiderite and seven chondrites. Geochim Cosmochim Acta 33:411-416
Johnson JE, Scrymgour JM, Jarosewich E, Mason B (1977) Brachina meteorite—a chassignite from South Australia. Rec S Australia Mus 17:309-319
Jones JH (1982) The geochemical coherence of Pu and Nd and the $^{244}Pu/^{238}U$ ratio of the early solar system. Geochim Cosmochim Acta 46:1793-1804
Jones JH (1983) Mesosiderites: (1) reevaluation of cooling rates and (2) experimental results bearing on the origin of metal. Lunar Planet Sci 14:351-352
Jones JH (1994) Fractional crystallization of iron meteorites; constant versus changing partition coefficients. Meteoritics 29:423-426
Jones JH, Boynton WV (1983) Experimental geochemistry in very reducing systems: Extreme REE fractionation by immiscible sulfide liquids. Lunar Planet Sci 14:353-354
Jones JH, Drake MJ (1983) Experimental investigations of trace element fractionation in iron meteorites; II, The influence of sulfur. Geochim Cosmochim Acta 47:1199-1209
Jones JH, Malvin DJ (1990) A nonmetal interaction model for the segregation of trace metals during solidification of Fe-Ni-S, Fe-Ni-P, and Fe-Ni-S-P alloys. Met Trans B 21B:697-706
Jones JH, Treiman AH, Janssens M-J, Wolf R, Ebihara M (1988) Core formation on the eucrite parent body, the moon and the AdoR parent body. Meteoritics 23:276-277
Jones JH, Mittlefehldt DW, Jurewicz AJG, Lauer HV Jr, Hanson BZ, Paslick CR, McKay GA (1996) The origin of eucrites: An experimental perspective. *In* Workshop on Evolution of Igneous Asteroids: Focus on Vesta and the HED Meteorites, Mittlefehldt DW, Papike JJ, eds., LPI Tech Report 96-02, Part 1, 15
Jurewicz AJG, Mittlefehldt DW, Jones JH (1993) Experimental partial melting of the Allende (CV) and Murchison (CM) chondrites and the origin of asteroidal basalts. Geochim Cosmochim Acta 57:2123-2139
Jurewicz AJG, Mittlefehldt DW, Jones JH (1995a) Experimental partial melting of the St. Severin (LL) and Lost City (H) chondrites. Geochim Cosmochim Acta 59:391-408
Jurewicz AJG, Jones JH, Mittlefehldt DW, Longhi J(1995b) Making melts having 40%, 50% or 60% SiO_2 from chondritic materials: A synopsis of low-pressure, low-volatile, equilibrium melting relations. Lunar Planet Sci 26:707-708
Kallemeyn GW, Warren PH (1994) Geochemistry of LEW88774 and two other unusual ureilites. Lunar Planet Sci 25:663-664
Kallemeyn GW, Wasson JT (1985) The compositional classification of chondrites: IV Ungrouped chondritic meteorites and clasts. Geochim Cosmochim Acta 49:261-270
Keil K (1968) Mineralogical and chemical relationships among enstatite chondrites. J Geophys Res 73:6945-6976
Keil K (1989) Enstatite meteorites and their parent bodies. Meteoritics 24:195-208
Keil K, Brett R (1974) Heideite, $(Fe,Cr)_{1+x}(Ti,Fe)_2S_4$: A new mineral in the Bustee enstatite achondrite. Am Mineral 59:465-470
Keil K, Wilson L (1993) Explosive volcanism and the composition of cores of differentiated asteroids. Earth Planet Sci Lett 117:111-124
Keil K, Fodor RV, Starzyk PM, Schmitt RA, Bogard DD, Husain L (1980) A 3.6-b.y.-old impact-melt rock fragment in the Plainview chondrite: Implications for the age of the H-group chondrite parent body regolith formation. Earth Planet Sci Lett 51:235-247
Keil K, Berkley JL, Fuchs LH (1982) Suessite, Fe_3Si: A new mineral in the North Haig ureilite. Am Mineral 67:126-131
Keil K, Ntaflos Th., Taylor GJ, Brearley AJ, Newsom HE, Romig AD Jr. (1989) The Shallowater aubrite: Evidence for origin by planetesimal impact. Geochim Cosmochim Acta 53:3291-3307
Keil K, Stöffler D, Love SG, Scott ERD (1997) Constraints on the role of impact heating and melting in asteroids. Meteoritics Planet Sci 32:349-363
Kelly, W R, J W Larimer (1977) Chemical fractionation in meteorites-VII Iron meteorites and the cosmochemical history of the metal phase. Geochim Cosmochim Acta 41:93-111
Kimura M, Ikeda Y, Ebihara M, Prinz M (1991) New enclaves in the Vaca Muerta mesosiderite: Petrogenesis and comparison with HED meteorites. Proc NIPR Symp Antarctic Meteorites 4:263-306
Kimura M, Tsuchiyama A, Fukuoka T, Iimura Y (1992) Antarctic primitive achondrites, Yamato-74025, -75300, and -75305: Their mineralogy, thermal history, and the relevance to winonaite. Proc NIPR Symp Antarctic Meteorites 5:165-190
King EA, Jarosewich E, Daugherty FW (1981) Tierra Blanca: An unusual achondrite from West Texas. Meteoritics 16:229-237
Klein LC, Hewins RH (1979) Origin of impact melt rocks in the Bununu howardite. Proc Lunar Planet Sci

Conf 10:1127-1140
Kozul J, Hewins RH (1988) LEW 85300,02,03 polymict eucrites consortium—II: Breccia clasts, CM inclusion, glassy matrix and assembly history. Lunar Planet Sci 19:647-648
Kracher A (1974) Untersuchungen am Landes Meteorit. *In* Analyse extraterrestrischen Materials (W Kiesl and H Maliss, Jr., eds.), p 315-326. Springer
Kracher A (1982) Crystallization of a S-saturated Fe,Ni-melt, and the origin of the iron meteorite groups IAB and IIICD. Geophys Res Lett 9:412-415
Kracher A (1985) The evolution of partially differentiated planetesimal: evidence from iron meteorite groups IAB and IIICD. Proc Lunar Planet Sci Conf 15th, J Geophys Res 90:C689-C698
Kracher A, Wasson JT (1982) The role of S in the evolution of the parental cores of iron meteorites. Geochim Cosmochim Acta 46:2419-2426
Kracher A Willis J (1981) Composition and origin of the unusual Oktibbeha County iron meteorite. Meteoritics 16:239-246
Kracher A, Kurat G, Buchwald VF (1977) Cape York: The extraordinary mineralogy of an ordinary iron meteorite and its implications for the genesis of IIIAB irons. Geochem J 11:207-217
Kracher A, Willis J, Wasson JT (1980) Chemical classification of iron meteorites; IX, A new group (IIF), revision of IAB and IIICD, and data on 57 additional irons. Geochim Cosmochim Acta 44:773-787
Kring DA, Boynton WV (1992) The trace-element composition of Eagles Nest and its relationship to other ultramafic achondrites. Lunar Planet Sci 23:727-728
Kring DA, Boynton WV, Hill DH, Haag RA (1991) Petrologic description of Eagles Nest: A new olivine achondrite. Meteoritics 26:360
Krot A, Ivanova MA, Wasson JT (1993) The origin of chromatic chondrules and the volatility of Cr under a range of nebular conditions. Earth Planet Sci Lett 119:569-584
Kulpecz AA Jr, Hewins RH (1978) Cooling rate based on schreibersite growth for the Emery mesosiderite. Geochim Cosmochim Acta 42:1495-1500
Kurat G (1988) Primitive meteorites: An attempt towards unification. Phil Trans Royal Soc London A325:459-482
Kurat G, Zinner E, Brandstätter F (1992) An ion microprobe study of an unique oldhamite-pyroxenite fragment from the Bustee aubrite. Meteoritics 27:246-247
Labotka TC, Papike JJ (1980) Howardites: Samples of the regolith of the eucrite parent body: Petrology of Frankfort, Pavlovka, Yurtuk, Malvern, and ALHA 77302. Proc Lunar Planet Sci Conf 11:1103-1130
Laul J-C, Gosselin DC (1990) The Bholghati howardite: Chemical study. Geochim Cosmochim Acta 54:2167-2175
Lindner M, Leich RJ, Russ GP, Bazan JM, Borg RJ (1989) Direct determination of the half life of ^{187}Re. Geochim Cosmochim Acta 53:1597-1606
Lipschutz ME (1964) Origin of diamonds in the ureilites. Science 143:1431-1434
Lodders K (1996) An experimental and theoretical study of rare-earth-element partitioning between sulfides (FeS,CaS) and silicate and applications to enstatite achondrites. Meteoritics Planet Sci 31: 749-766
Lodders K, Palme H, Wlotzka F (1993) Trace elements in mineral separates of the Peña Blanca Spring aubrite: Implications for the evolution of the aubrite parent body. Meteoritics 28:538-551
Lofgren G, Lanier AB (1991) Dynamic crystallization experiments on the Angra dos Reis achondrite meteorite. Earth Planet Sci Lett 111:455-466
Lomena ISM, Touré F, Gibson EK Jr., Clanton US, Reid AM (1976) Aïoun el Atrouss: A new hypersthene achondrite with eucritic inclusions. Meteoritics 11:51-57
Lonsdale JT (1947) The Peña Blanca Spring meteorite, Brewster County, Texas. Am Mineral 32:354-364
Lovering JF (1964) Electron microprobe analysis of the metallic phase in basic achondrites. Nature 203:70
Lovering JF (1975) The Moama eucrite—A pyroxene-plagioclase adcumulate. Meteoritics 10:101-114
Lovering JF, Nichiporuk W, Chodos A, Brown H (1957) The distribution of gallium, germanium, cobalt, chromium, and copper in iron and stony-iron meteorites in relation to nickel content and structure. Geochim Cosmochim Acta 11:263-278
Lugmair GW, Galer SJG (1992) Age and isotopic relationships among the angrites Lewis Cliff 86010 and Angra dos Reis. Geochim Cosmochim Acta 56:1673-1694
Lugmair GW, Marti K (1977) Sm-Nd-Pu timepieces in the Angra dos Reis meteorite. Earth Planet Sci Lett 35:273-284
Lugmair GW, Shukolyukov A (1997) ^{53}Mn - ^{53}Cr isotope systematics of the HED parent body. Lunar Planet Sci 28:852-852
Lugmair GW, Scheinin NB, Carlson RW (1977) Sm-Nd systematics of the Serra de Magé eucrite. Meteoritics 12:300-301
Lugmair GW, MacIsaac C, Shukolyukov A (1994a) Small differences in differentiated meteorites recorded by the ^{53}Mn - ^{53}Cr chronometer. Lunar Planet Sci 24:813-814

Lugmair GW, MacIsaac C, Shukolyukov A (1994b) Small differences recorded in differentiated meteorites. Meteoritics 29:493-494
Ma M-S, Schmitt RA (1979) Genesis of the cumulate eucrites Serra de Magé and Moore County: A geochemical study. Meteoritics 14:81-89
Ma M-S, Murali AV, Schmitt RA (1977) Genesis of Angra dos Reis and other achondritic meteorites. Earth Planet Sci Lett 35:331-346
Malhotra PD (1962) A note on the composition of the Basti meteorite. Records Geol. Survey India 89: 479-481
Malvin DJ, Wang D, Wasson JT (1984) Chemical classification of iron meteorites; X, Multielement studies of 43 irons, resolution of group IIIE from IIIAB, and evaluation of Cu as a taxonomic parameter. Geochim Cosmochim Acta 48:785-804
Malvin DJ, Wasson JT, Clayton RN, Mayeda TK, Curvello WdS (1985) Bocaiuva—A silicate-inclusion bearing iron meteorite related to the Eagle-Station pallasites. Meteoritics 20:259-273
Malvin DJ, Jones JH, Drake MJ (1986) Experimental investigations of trace element fractionation in iron meteorites; III, Elemental partitioning in the system Fe-Ni-S-P. Geochim Cosmochim Acta 50:1221-1231
Marshall RR, Keil K (1965) Polymineralic inclusions in the Odessa iron meteorite. Icarus 4:461-479
Marvin U B, Wood JA (1972) The Haverö ureilite: Petrographic notes. Meteoritics 7:601-610
Marvin UB, Petaev MI, Croft WJ, Killgore M (1997) Silica minerals in the Gibeon IVA iron meteorite. Lunar Planet Sci 28:879-880
Mason B (1962) Meteorites. Wiley, NY 274 p
Mason B (1963) The hypersthene achondrites. Am Mus Novitates No. 2155, 13 p
Mason B, Jarosewich E (1973) The Barea, Dyarrl Island, and Emery meteorites, and a review of the mesosiderites. Mineral Mag 39:204-215
Mason B, Wiik HB (1966a) The composition of the Bath, Frankfort, Kakangari, Rose City, and Tadjera meteorites. Am Mus Novitates No. 2272, 24 p
Mason B, Wiik HB (1966b) The composition of the Barratta, Carraweena, Kapoeta, Mooresfort, and Ngawi meteorites. Am Mus Novitates No. 2273, 25 p
Matsuda J-I, Fukunaga K, Ito K (1988) On the vapor-growth diamonds formation in the solar nebula. Lunar Planet Sci 19:736-737
Matsuda J-I, Fukunaga K, Ito K (1991) Noble gas studies in vapor-growth diamonds: Comparison with shock-produced diamonds and the origin of diamonds in ureilites. Geochim Cosmochim Acta 55: 2011-2023
Matsuda J-I, Kusima A, Yajima H, Syono Y (1995) Noble gas studies in diamonds synthesized by shock loading in the laboratory and their implications on the origin of diamonds in ureilites. Geochim Cosmochim Acta 59:4939-4949
Mazor E, Anders E (1967) Primordial gases in Jodzie howardite and the origin of gas-rich meteorites. Geochim Cosmochim Acta 31:1441-1456
Mazor E, Heymann D, Anders E (1970) Nobles gases in carbonaceous chondrites. Geochim Cosmochim Acta 34:781-824
McCall GJH (1966) The petrology of the Mount Padbury mesosiderite and its achondrite enclaves. Mineral Mag 35:1029-1060
McCall GJH (1973) Meteorites and Their Origins. Wiley
McCall GJ, Cleverly WH (1968) New stony meteorite finds including two ureilites from the Nullarbor Plain, Western Australia. Mineral Mag 36:691-716
McCarthy TS, Ahrens LH, Erlank AJ (1972) Further evidence in support of the mixing model for howardite origin. Earth Planet Sci Lett 15:86-93
McCarthy TS, Erlank AJ, Willis JP (1973) On the origin of eucrites and diogenites. Earth Planet Sci Lett 18:433-442
McCarthy TS, Erlank AJ, Willis JP, Ahrens LH (1974) New chemical analyses of six achondrites and one chondrite. Meteoritics 9:215-221
McCord TB, Adams JB, Johnson TV (1970) Asteroid Vesta: Spectral reflectivity and compositional implications. Science 168:1445-1447
McCoy TJ (1995) Silicate-bearing IIE irons: Early mixing and differentiation in a core-mantle environment and shock resetting of ages. Meteoritics 30:542-543
McCoy TJ (1998) A pyroxene-oldhamite clast in Bustee: Igneous aubritic oldhamite and a mechanism for the Ti enrichment in aubritic troilite. Antarctic Meteorite Research 11:34-50
McCoy TJ, Scott ERD, Haack H (1993) Genesis of the IIICD iron meteorites: Evidence from silicate-bearing inclusions. Meteoritics 28:552-560
McCoy TJ, Keil K, Mayeda TK, Clayton RN (1992) Petrogenesis of the lodranite-acapulcoite parent body. Meteoritics 27:258-259

McCoy TJ, Ehlmann AJ, Benedix GK, Keil K, Wasson JT (1996a) The Lueders, Texas, IAB iron meteorite with silicate inclusions. Meteoritics Planet Sci 31:419-422
McCoy TJ, Keil K, Clayton RN, Mayeda TK, Bogard DD, Garrison DH, Huss GR, Hutcheon ID, Wieler R (1996b) A petrologic, chemical, and isotopic study of Monument Draw and comparison with other acapulcoites: Evidence for formation by incipient partial melting. Geochim Cosmochim Acta 60:2681-2708
McCoy TJ, Keil K, Clayton RN, Mayeda TK, Bogard DD, Garrison DH, Wieler R (1997a) A petrologic and isotopic study of lodranites: Evidence for early formation as partial melt residues from heterogeneous precursors. Geochim Cosmochim Acta 61:623-637
McCoy TJ, Keil K, Muenow DW, Wilson L (1997b) Partial melting and melt migration in the acapulcoite-lodranite parent body. Geochim Cosmochim Acta 61:639-650
McCoy TJ, Dickinson TL, Lofgren GE (1997c) Partial melting of Indarch (EH4) from 1000-1425°C: New insights into igneous processes in enstatite meteorites. Lunar Planet Sci 28:903-904
McCoy TJ, Dickinson TL, Lofgren GE (1997d) Experimental and petrologic studies bearing on the origin of aubrites. Papers presented to the 22nd Symp Antarctic Met, 103-105
McKay G, Lindstrom D, Yang S-R, Wagstaff J (1988a) Petrology of a unique achondrite Lewis Cliff 86010. Lunar Planet Sci 19:762-763
McKay G, Lindstrom D, Le L, Yang S-R (1988b) Experimental studies of synthetic LEW86010 analogs: Petrogenesis of a unique achondrite. Lunar Planet Sci 19:760-761
McKay G, Le L, Wagstaff J (1989) Is unique achondrite LEW86010 a crystallized melt? Lunar Planet Sci 20:675-676
McKay G, Crozaz G, Wagstaff J, Yang S-R, Lundberg L (1990) A petrographic, electron microprobe, and ion microprobe study of mini-angrite Lewis Cliff 87051. Lunar Planet Sci 21:771-772
McKay G, Le L, Wagstaff J, Crozaz G (1994) Experimental partitioning of rare earth elements and strontium: Constraints on petrogenesis and redox conditions during crystallization of Antarctic angrite Lewis Cliff 86010. Geochim Cosmochim Acta 58:2911-2919
McKay GA, Crozaz G, Mikouchi T, Miyamoto M (1995) Petrology of antarctic angrites LEW 86010, LEW 87051, and Asuka 881371. Antarc Meteorites 20:155-158
McSween HY, Labotka TC (1993) Oxidation during metamorphism of the ordinary chondrites. Geochim Cosmochim Acta 57:1105-1114
McSween HY Jr., Bennett ME III, Jarosewich E (1991) The mineralogy of ordinary chondrites and implications for asteroid spectrophotometry. Icarus 90:107-116
Metzler K, Bobe KD, Palme H, Spettel B, Stöffler D (1995) Thermal and impact metamorphism on the HED parent asteroid. Planet Space Sci 43:499-525
Mikouchi T, Takeda H, Miyamoto M, Ohsumi K, McKay GA (1995) Exsolution lamellae of kirschsteinite in magnesium-iron olivine from an angrite meteorite. Am Mineral 80, 585-592
Mikouchi T, Miyamoto M, McKay GA (1996) Mineralogical study of angrite Asuka-881371: Its possible relation to angrite LEW87051. Proc. NIPR Symp Antarctic Meteorites 9:174-188
Misawa K, Watanabe S, Kitamura M, Nakamura N, Yamamoto K, Masuda A (1992) A noritic clast from the Hedjaz chondritic breccia: implications for melting events in the early solar system. Geochem J 26:435-446
Mittlefehldt DW (1978) The differentiation history of small bodies in the solar system: The howardite and mesosiderite meteorite parent bodies. PhD dissertation, Univ California, Los Angeles, 208 p
Mittlefehldt DW (1979) Petrographic and chemical characterization of igneous lithic clasts from mesosiderites and howardites and comparison with eucrites and diogenites. Geochim Cosmochim Acta 43:1917-1935
Mittlefehldt DW (1980) The composition of mesosiderite olivine clasts and implications for the origin of pallasites. Earth Planet Sci Lett 51:29-40
Mittlefehldt D W (1986) Fe-Mg-Mn relations of ureilite olivines and pyroxenes and the genesis of ureilites. Geochim. Cosmochim. Acta 50:107-110
Mittlefehldt DW (1987) Volatile degassing of basaltic achondrite parent bodies: Evidence from alkali elements and phosphorus. Geochim Cosmochim Acta 51:267-278
Mittlefehldt DW (1990) Petrogenesis of mesosiderites: I Origin of mafic lithologies and comparison with basaltic achondrites. Geochim Cosmochim Acta 54:1165-1173
Mittlefehldt DW (1994) The genesis of diogenites and HED parent body petrogenesis. Geochim Cosmochim Acta 58:1537-1552
Mittlefehldt DW, Lindstrom MM (1990) Geochemistry and genesis of the angrites. Geochim Cosmochim Acta 54:3209-3218
Mittlefehldt DW, Lindstrom MM (1993) Geochemistry and petrology of a suite of ten Yamato HED meteorites. Proc NIPR Symp Antarctic Meteorites 6:268-292
Mittlefehldt DW, Lindstrom MM (1997) Magnesian basalt clasts from the EET 92014 and Kapoeta

howardites and a discussion of alleged primary magnesian HED basalts. Geochim Cosmochim Acta 61:453-462
Mittlefehldt DW, Lindstrom MM (1998) Black clasts from howardite QUE 94200—Impact melts, not primary magnesian basalts. Lunar Planet Sci 29:1832
Mittlefehldt DW, Meyers B (1991) Petrology and geochemistry of the EETA79002 diogenite . Meteoritics 26:373
Mittlefehldt, DW, Chou, C-L, Wasson JT (1979) Mesosiderites and howardites: igneous formation and possible genetic relationships. Geochim Cosmochim Acta 43:673-688
Mittlefehldt DW, Rubin AE, Davis AM (1992) Mesosiderite clasts with the most extreme positive europium anomalies among solar system rocks. Science 257:1096-1099
Mittlefehldt DW, Lindstrom MM, M-S Wang, ME Lipschutz (1995) Geochemistry and origin of achondritic inclusions in Yamato-75097, -793241 and -794046 chondrites. Proc NIPR Symp Antarctic Meteorites 8:251-271
Mittlefehldt DW, Lindstrom MM, Bogard DD, Garrison DH, Field SW (1996) Acapulco- and Lodran-like achondrites: Petrology, geochemistry, chronology and origin. Geochim Cosmochim Acta 60:867-882
Miyamoto M, Takeda H (1977) Evaluation ofa crust model of eucrites from the width of exsolved pyroxene. Geochem J 11:161-169
Miyamoto M, Takeda H (1994) Chemical zoning of olivine in several pallasites suggestive of faster cooling . Lunar Planet Sci 25:921-922
Miyamoto M, Takeda H, Yanai (1978) Yamato achondrite polymict breccias. Mem Natl Inst Polar Res (Japan) Spec Issue No 8:185-197
Miyamoto M, Toyoda H, Takeda H (1985) Thermal history of ureilite as inferred from mineralogy of Pecora Escarpment 82506. Lunar Planet Sci 16:567-568
Miyamoto M, Furuta T, Fujii N, McKay DS, Lofgren GE, Duke MB (1993) The Mn-Fe negative correlation in olivines in ALHA77257 ureilite. J Geophys Res 98:5301-5307
Morgan JW, Walker RJ, Grossman JN (1992) Rhenium-osmium isotope systematics in meteorites I: Magmatic iron meteorite groups IIAB and IIIAB. Earth Planet Sci Lett 108:191-202
Morgan JW, Horn MF, Walker RJ, Grossman JN (1995) Rhenium-osmium concentration and isotope systematics in group IIAB iron meteorites. Geochim Cosmochim Acta 59:2331-2344
Mori H, Takeda H (1981a) Thermal and deformational histories of diogenites as inferred from their microtextures of orthopyroxene. Earth Planet Sci Lett 53:266-274
Mori H, Takeda H (1981b) Evolution of the Moore County pyroxenes as viewed by an analytical transmission electron microprobe (ATEM). Meteoritics 16:362-363
Mori H, Takeda H (1983) An electron petrographic study of ureilite pyroxenes. Meteoritics 18:358-359
Mori H, Takeda H (1988) TEM observations of carbonaceous material in the Dyalpur ureilite. Lunar Planet Sci 19:808
Mori H, Takeda H, Toyoda H (1986) Mineralogy of pigeonites from the Allan Hills 82106 ureilites. Meteoritics 21:466-467
Müller HW, Zähringer J (1966) Chemische Unterschiede bei Uredelgashaltigen Steinmeteoriten. Earth Planet Sci Lett 1:25-29
Müller HW, Zähringer J (1969) Rare gases in stony meteorites. *In* Meteorite Research (ed. P Millman), p. 845. D Reidel, Hingham, Massachusetts
Murthy VR, Coscio MR Jr., Sabelin T (1977) Rb-Sr internal isochron and the initial $^{87}Sr/^{86}Sr$ for the Estherville mesosiderite. Proc Lunar Sci Conf 8:177-186
Murty SVS (1994) Interstellar vs. ureilitic diamonds: nitrogen and noble gas systematics. Meteoritics 29:507
Nagahara H (1992) Yamato-8002: Partial melting residue on the "unique" chondrite parent body. Proc NIPR Symp Antarctic Meteorites 5:191-223
Nagahara H, Ozawa K (1986) Petrology of Yamato-791493, "lodranite": Melting, crystallization, cooling history, and relationship to other meteorites. Mem NIPR Spec Issue No 41, 181-205
Nakamura N, Morikawa N (1993) REE and other trace lithophiles in MAC88177, LEW88280 and LEW88763. Lunar Planet Sci 24:1047-1048
Nakamura N, Misawa K, Kitamura M, Masuda A, Watanabe S, Yamamoto K (1990) Highly fractionated REE in the Hedjaz (L) chondrite: implications for nebular and planetary processes. Earth Planet Sci Lett 99:290-302
Nakamura N, Morikawa N, Hutchison R, Clayton RN, Mayeda TK, Nagao K, Misawa K, Okano O, Yamamoto K, Yanai K, Matsumoto Y (1994) Trace element and isotopic characteristics of inclusions in the Yamato ordinary chondrites Y-75097, Y-793241 and Y-794046. Proc NIPR Symp Antarctic Meteorites 7:125-143
Narayan C, Goldstein JI (1982) A dendritic solidification model to explain Ge-Ni variations in iron meteorite chemical groups. Geochim Cosmochim Acta 46:259-268

Narayan C, Goldstein JI (1985) A major revision of iron meteorite cooling rates; an experimental study of the growth of the Widmanstätten pattern. Geochim Cosmochim Acta 49:397-410
Nehru CE, Zucker SM, Harlow GE, Prinz M (1980a) Olivines and olivine coronas in mesosiderites. Geochim Cosmochim Acta 44:1103-1118
Nehru CE, Delaney JS, Harlow GE, Prinz M (1980b) Mesosiderite basalts and the eucrites . Meteoritics 15:337-338
Nehru CE, Prinz M, Delaney JS (1982) The Tucson iron and its relationship to enstatite meteorites. Proc 13th Lunar Planet Sci Conf, J Geophys Res B87, Suppl 1:A365-A373
Nehru CE, Prinz M, Delaney JS, Dreibus G, Palme H, Spettel B, Wänke H (1983) Brachina: A new type of meteorite, not a Chassignite. Proc Lunar Planet Sci Conf 14th J Geophys Res 88:B237-B244
Nehru CE, Prinz M, Weisberg MK, Ebihara ME, Clayton RN, Mayeda TK (1992) Brachinites: A new primitive achondrite group. Meteoritics 27:267
Nehru CE, Prinz M, Weisberg MK, Ebihara ME, Clayton RN, Mayeda TK (1996) A new brachinite and petrogenesis of the group. Lunar Planet Sci 27:943-944
Nelen J, Mason B (1972) The Estherville meteorite. Smithson Contrib Earth Sci 9:55-56
Neuvonen KJ, Ohlson B, Papuen TA, Hakli TA, Ramdohr P (1972) The Haverö ureilite. Meteoritics 7:515-531
Newsom HE (1985) Molybdenum in eucrites: Evidence for a metal core in the eucrite parent body. Proc 15th Lunar Planet Sci Conf, Part 2, J Geophys Res Suppl 90:C613-C617
Newsom HE, Drake MJ (1982) The metal content of the eucrite parent body: constraints from the partitioning behavior of tungsten. Geochim Cosmochim Acta 46:2483-2489
Newsom HE, Ntaflos Th., Keil K (1996) Dark clasts in the Khor Temiki aubrite: Not basalts. Meteoritics Planet Sci 31:146-151
Nichols RH, Jr., Hohenberg CM, Kehm K, Kim Y, Marti K (1994) I-Xe studies of the Acapulco meteorite: Absolute I-Xe ages of individual phosphate grains and the Bjurböle standard. Geochim Cosmochim Acta 58:2553-2561
Nielsen HP, Buchwald VF (1981) Roaldite, a new nitride in iron meteorites. Proc Lunar Planet Sci Conf 12, Geochim Cosmochim Acta, Suppl 16:1343-1348
Niemeyer S (1979a) I-Xe dating of silicate and troilite from IAB iron meteorites. Geochim Cosmochim Acta 43:843-860
Niemeyer S (1979b) ^{40}Ar-^{39}Ar dating of inclusions from IAB iron meteorites. Geochim Cosmochim Acta 43:1829-1840
Niemeyer S (1980) I-Xe and ^{40}Ar-^{39}Ar dating of silicate from Weekeroo Station and Netschaëvo iron meteorites. Geochim Cosmochim Acta 44:33-44
Niemeyer S (1983) I-Xe and ^{40}Ar-^{39}Ar analyses of silicate from the Eagle Station pallasite and the anomalous iron meteorite Enon. Geochim Cosmochim Acta 47:1007-1012
Nininger HH (1952) Out of the Sky. Dover
Nyquist LE, Takeda H, Bansal BM, Shih C-Y, Wiesmann H, Wooden JL (1986) Rb-Sr and Sm-Nd internal isochron ages of a subophitic basalt clast and a matrix sample from the Y75011 eucrite. J Geophys Res 91:8137-8150
Nyquist L, Bansal B, Wiesmann H, Shih C-Y (1994) Neodymium, strontium and chromium isotopic studies of the LEW86010 and Angra dos Reis meteorites and the chronology of the angrite parent body. Meteoritics 29:872-885
Ogata H, Takeda H, Ishii T (1987) Interstitial Ca-rich silicate materials in the Yamato ureilites with reference to their origin. Lunar Planet Sci 18:738-739
Ogata H, Mori H, Takeda H (1988) Mineralogy of interstitial rim materials of ureilites and their origin. Abstr Symp Antarctic Meteorites 13:138-141
Ogata H, Mori H, Takeda H (1991) Mineralogy of interstitial rim materials of the Y74123 and Y790981 ureilites and their origin. Meteoritics 16:195-201
Ohtani E (1983) Formation of olivine textures in pallasites and thermal history of pallasites in their parent body. Phys Earth Planet Interiors 32:182-192
Okada A, Keil K (1982) Caswellsilverite, $NaCrS_2$: A new mineral in the Norton County enstatite achondrite. Am Mineral 67:132-136
Okada A, Keil K, Taylor GJ, Newsom H (1988) Igneous history of the aubrite parent asteroid: Evidence from the Norton County enstatite achondrite. Meteoritics 23:59-74
Olsen E, Jarosewich E (1970) The chemical composition of the silicate inclusions in the Weekeroo Station iron meteorite. Earth Planet Sci Lett 8:261-266
Olsen E, Jarosewich E (1971) Chondrules: First occurrence in an iron meteorite. Science 174:583-585
Olsen EJ, Steele IA (1997) Galileiite: A new meteoritic phosphate mineral. Meteoritics Planet Sci 32: A155-A-156
Olsen E, Erlichman J, Bunch TE, Moore PB (1977) Buchwaldite, a new meteoritic phosphate mineral. Am

Mineral 62:362-364
Olsen E, Noonan A, Fredriksson K, Jarosewich E, Moreland G (1978) Eleven new meteorites from Antarctica, 1976-1977. Meteoritics 13:209-225
Olsen E, Dod BD, Schmitt RA, Sipiera PP (1987) Monticello: A glass-rich howardite. Meteoritics 22:81-96
Olsen EJ, Fredriksson K, Rajan S, Noonan A (1990) Chondrule-like objects and brown glasses in howardites. Meteoritics 25:187-194
Olsen E, Davis A, Clarke RS Jr., Schultz L, Weber HW, Clayton R, Mayeda T, Jarosewich E, Sylvester P, Grossman L, Wang M-S, Lipschutz ME, Steele IM, Schwade J (1994) Watson: A new link in the IIE iron chain. Meteoritics 29:200-213
Olsen EJ, Davis AM, Clayton RN, Mayeda TK, Moore CB and Steele IM (1996) A silicate inclusion in Puente del Zacate: A IIIA iron meteorite. Science 273:1365-1367
Osadchii Eu.G, Baryshnikova GV, Novikov GV (1981) The Elga meteorite: Silicate inclusions and shock metamorphism. Proc Lunar Planet Sci Conf 12B:1049-1068
Ott U, Begemann F, Löhr HP (1983) Noble gases in the Brachina and Chassigny meteorites. Lunar Planet Sci 14:586-587
Ott U, Löhr HP, Begemann F (1984) Ureilites: The case of the missing diamonds and a new neon component. Meteoritics 19:287-288
Ott U, Löhr HP, Begemann F (1985a) Noble gases and the classification of Brachina. Meteoritics 20:69-78
Ott U, Löhr HP, Begemann F (1985b) Trapped neon in ureilites—A new component. *In* Isotopic Ratios in the Solar System. (Ed. Centre National d'Etudes Spatiales), p 129-136. Cepadues-Editions; Toulouse, France
Ott U, Begemann F, Löhr HP (1987) Noble gases in ALH 84025: Like Brachina, unlike Chassigny. Meteoritics 22:476-477
Ott U, Löhr HP, Begemann F (1990) EET83309: A ureilite with solar noble gases. Meteoritics 25:396
Ott U, Löhr HP, Begemann F (1993) Solar noble gases in polymict ureilites and an update on ureilite noble gas data. Meteoritics 28:415-416
Padia JT, Rao MN (1989) Neon isotope studies of Fayetteville and Kapoeta meteorites and clues to ancient solar activity. Geochim Cosmochim Acta 53:1461-1467
Palme H, Baddenhausen H, Blum K, Cendales M, Dreibus G, Hofmeister H, Kruse H Palme C, Spettel B, Vilcsek E, Wänke H (1978) New data on lunar samples and achondrites and a comparison of the least fractionated samples from the earth, the moon and the eucrite parent body. Proc Lunar Planet Sci Conf 9:25-57
Palme H, Schultz L, Spettel B, Weber HW, Wänke H, Christophe Michel-Levy M, Lorin JC (1981) The Acapulco meteorite: Chemistry, mineralogy and irradiation effects. Geochim Cosmochim Acta 45:727-752
Palme H, Spettel B, Burghele A, Weckwerth G, Wänke H (1983) Elephant Moraine polymict eucrites: A eucrite-howardite compositional link. Lunar Planet Sci 14:590-591
Palme H, Wlotzka F, Spettel B, Dreibus G, Weber H (1988) Camel Donga: A eucrite with high metal content. Meteoritics 23:49-57
Palme H, Hutcheon ID, Kennedy AK, Sheng YJ, Spettel B (1991)Trace element distribution in minerals from a silicate inclusion in the Caddo IAB-iron meteorite. Lunar Planet Sci 22:1015-1016
Papanastassiou DA, Wasserburg GJ (1969) Initial strontium isotopic abundances and the resolution of small time differences in the formation of planetary objects. Earth Planet Sci Lett 5:361-376
Paul RL, Lipschutz ME (1990) Chemical studies of differentiated meteorites: I. Labile trace elements in Antarctic and non-Antarctic eucrites. Geochim Cosmochim Acta 54:3185-3196
Pellas P, Fiéni C, Trieloff M, Jessberger EK (1997) The cooling history of the Acapulco meteorite as recorded by the ^{244}Pu and ^{40}Ar-^{39}Ar chronometers. Geochim Cosmochim Acta 61:3477-3501
Petaev MI, Brearley AJ (1994) Exsolution in ferromagnesian olivine of the Divnoe meteorite. Science 266:1545-1547
Petaev MI, Clarke RS Jr, Olsen EJ, Jarosewich E, Davis AM, Steele IM, Lipschutz ME, Wang M-S, Clayton RN, Mayeda TK, Wood JA (1993) Chaunskij: The most highly metamorphosed, shock-modified and metal-rich mesosiderite. Lunar Planet Sci 24:1131-1132
Petaev MI, Barsukova LD, Lipschutz ME, Wang M-S, Arsikan AA, Clayton RN, Mayeda TK (1994) The Divnoe meteorite: Petrology, chemistry, oxygen-isotopes and origin. Meteoritics 29:182-199
Powell BN (1969) Petrology and chemistry of mesosiderites-I. Textures and composition of nickel-iron. Geochim Cosmochim Acta 33:789-810
Powell BN (1971) Petrology and chemistry of mesosiderites-II. Silicate textures and compositions and metal-silicate relationships. Geochim Cosmochim Acta 35:5-34
Prinz M, Weisberg MK (1995) Asuka 881371 and the angrites: Origin in a heterogeneous, CAI-enriched, differentiated, volatile-depleted body. Antarc Meteorites 20:207-210
Prinz M, Keil K, Hlava PF, Berkley JL, Gomes CB, Curvello WS (1977) Studies of Brazilian meteorites, III. Origin and history of the Angra dos Reis achondrite. Earth Planet Sci Lett 35:317-330

Prinz M, Nehru CE, Delaney JS, Harlow GE, Bedell RL (1980) Modal studies of mesosiderites and related achondrites, including the new mesosiderite ALHA 77219. Proc Lunar Planet Sci Conf 11:1055-1071
Prinz M, Nehru CE, Delaney JS (1982a) Reckling Peak A79015: An unusual mesosiderite. Lunar Planet Sci 13:631
Prinz M, Nehru CE, Delaney JS (1982b) Sombrerete: An iron with highly fractionated amphibole-bearing Na-P-rich silicate inclusions. Lunar Planet Sci 13:634-635
Prinz. M, Delaney JS, Nehru CE, Weisberg MK (1983a) Enclaves in the Nilpena polymict ureilite. Meteoritics 18:376-377
Prinz M, Nehru CE, Delaney JS, Weisberg M, Olsen E (1983b) Globular silicate inclusions in IIE irons and Sombrerete: Highly fractionated minimum melts. Lunar Planet Sci 14:618-619
Prinz M, Nehru CE, Delaney JS, Fredriksson K, Palme H (1984) Silicate inclusions in IVA iron meteorites. Meteoritics 19:291-292
Prinz M, Weisberg MK, Nehru CE, Delaney JS (1986a) ALHA84025: A second Brachina-like meteorite. Lunar Planet Sci 17:679-680
Prinz. M, Weisberg MK, Nehru CE (1986b) North Haig and Nilpena: Paired polymict ureilites with Angra dos Reis-related and other clasts. Lunar Planet Sci 17:681-682
Prinz M, Weisberg MK, Nehru CE, Delaney JS (1987) EET83309: a polymict ureilite:Recognition of a new group. Lunar Planet Sci 18:802-803
Prinz M, Weisberg MK, Nehru CE (1988a) Feldspathic components in polymict ureilites. Lunar Planet Sci 19:947-948
Prinz M, Weisberg MK, Nehru CE (1988b) LEW86010, a second angrite: Relationship to CAI's and opaque matrix. Lunar Planet Sci 19:949-950
Prinz M, Weisberg MK, Nehru CE (1990) LEW 87051, a new angrite: Origin in a Ca-Al-enriched eucritic planetesimal? Lunar Planet Sci 21:979-980
Prinz M, Weisberg MK, Nehru CE (1994) LEW88774: A new type of Cr-rich ureilite. Lunar Planet Sci 25:1107-1108
Prinzhofer A, Papanastassiou DA, Wasserburg GJ (1992) Samarium-neodymium evolution of meteorites. Geochim Cosmochim Acta 56:797-815
Prior GT (1918) On the mesosiderite-grahamite group of meteorites: with analyses of Vaca Muerta, Hainholz, Simondium, Powder Mill Creek. Mineral Mag 18:151-172
Pun A, Papike JJ (1995) Ion microprobe investigation of exsolved pyroxenes in cumulate eucrites: Determination of selected trace-element partition coefficients. Geochim Cosmochim Acta 59:2279-2289
Ramdohr P (1973) The opaque minerals in stony meteorites. Akademie Verlag, Berlin
Ramdohr P, Prinz M, El Goresy A (1975) Silicate inclusions in the Mundrabilla meteorite. Meteoritics 10:477-479
Randich E, Goldstein JI (1978) Cooling rates of seven hexahedrites. Geochim Cosmochim Acta 42: 221-234
Rao MN, Garrison DH, Bogard DD, Badhwar G, Murali AV (1991) Composition of solar flare noble gases preserved in meteorite parent body regolith. J Geophys Res 96:19321-19330
Rasmussen KL (1981) The cooling rates of iron meteorites; a new approach. Icarus 45:564-576
Rasmussen KL (1982) Determination of the cooling rates and nucleation histories of eight group IVA iron meteorites using local bulk Ni and P variation. Icarus 52:444-453
Rasmussen KL (1989) Cooling rates and parent bodies of iron meteorites from group IIICD, IAB, and IVB. Physica Scripta 39:410-416
Rasmussen KL, Malvin DJ, Buchwald VF, Wasson JT (1984) Compositional trends and cooling rates of group IVB iron meteorites. Geochim Cosmochim Acta 48:805-813
Rasmussen KL, Ulff-Møller F, Haack H (1995) The thermal evolution of IVA iron meteorites; evidence from metallographic cooling rates. Geochim Cosmochim Acta 59:3049-3059
Reed SJB, Scott ERD, Long JVP (1979) Ion microprobe analyses of olivine in pallasite meteorites for nickel. Earth Planet Sci Lett 43:5-12
Reid AM, Cohen AJ (1967) Some characteristics of enstatite from enstatite achondrites. Geochim Cosmochim Acta 31:661-672
Reid AM, Williams RJ, Takeda H (1974) Coexisting bronzite and clinobronzite and the thermal evolution of the Steinbach meteorites. Earth Planet Sci Lett 22:67-74
Reid AM, Buchanan P, Zolensky ME, Barrett RA (1990) The Bholghati howardite: Petrography and mineral chemistry. Geochim Cosmochim Acta 54:2161-2166
Reuter KB, Williams DB, Goldstein JI (1988) Low temperature phase transformations in the metallic phases of iron and stony-iron meteorites. Geochim Cosmochim Acta 52:617-626
Richter GR, Wolf R, Anders E (1979) Aubrites: Are they direct nebular condensates? Lunar Planet Sci

10:1028-1030
Righter K, Drake MJ (1997) A magma ocean on Vesta: Core formation and petrogenesis of eucrites and diogenites. Meteoritics Planet Sci 32:929-944
Righter K, Arculus RJ, Delano JW, Paslick C (1990) Electrochemical measurements and thermodynamic calculations of redox equilibria in pallasite meteorites: Implications for the eucrite parent body. Geochim Cosmochim Acta 54:1803-1815
Robinson KL, Bild RW (1977) Silicate inclusions from the Mundrabilla iron. Meteoritics 12:354-355
Rowe MW (1970) Evidence for decay of extinct Pu^{244} and I^{129} in the Kapoeta meteorite. Geochim Cosmochim Acta 34:1019-1025
Rubin AE (1990) Kamacite and olivine in ordinary chondrites: Intergroup and intragroup relationships. Geochim Cosmochim Acta 54:1217-1232
Rubin AE (1997) Mineralogy of meteorite groups. Meteoritics Planet Sci 32:231-247
Rubin AE, Jerde EA (1987) Diverse eucritic pebbles in the Vaca Muerta mesosiderite. Earth Planet Sci Lett 84:1-14
Rubin AE, Jerde EA (1988) Compositional differences between basaltic and gabbroic clasts in mesosiderites. Earth Planet Sci Lett 87:485-490
Rubin AE, Mittlefehldt DW (1992) Classification of mafic clasts from mesosiderites: Implications for endogenous igneous processes. Geochim Cosmochim Acta 56:827-840
Rubin AE, Mittlefehldt DW (1993) Evolutionary history of the mesosiderite asteroid: A chronologic and petrologic synthesis. Icarus 101:201-212
Rubin AE, Jerde EA, Zong P, Wasson JT, Westcott JW, Mayeda TK, Clayton RN (1986) Properties of the Guin ungrouped iron meteorite: The origin of Guin and of group-IIE irons. Earth Planet Sci Lett 76:209-226
Rubin AE, Wasson JT, Clayton RN, Mayeda TK (1990) Oxygen-isotopes in chondrules and coarse-grained chondrule rims from the Allende meteorite. Earth Planet Sci Lett 96:247-255
Ruzicka A, Boynton WV, Ganguly J (1994) Olivine coronas, metamorphism, and the thermal history of the Morristown and Emery mesosiderites. Geochim Cosmochim Acta 58:2725-2741
Ruzicka A, Kring DA, Hill DH, Boynton WV, Clayton RN, Mayeda TK (1995) Silica-rich orthopyroxenite in the Bovedy chondrite. Meteoritics Planet Sci 30:57-70
Ruzicka A, Snyder GA, Taylor LA (1997) Vesta as the howardite, eucrite and diogenite parent body: Implications for the size of a core and for large-scale differentiation. Meteoritics Planet Sci 32:825-840
Ryder, G (1982) Siderophiles in the Brachina meteorite: impact melting? Nature 299:805-807
Sack RO, Azeredo WJ, Lipschutz ME (1991) Olivine diogenites: The mantle of the eucrite parent body. Geochim Cosmochim Acta 55:1111-1120
Sack RO, Azeredo WJ, Lipschutz ME (1994a) Erratum to R.O. Sack, W.J. Azeredo, and M.E. Lipschutz (1991) "Olivine diogenites: The mantle of the eucrite parent body." Geochim Cosmochim Acta 55:1111-1120. Geochim Cosmochim Acta 58:1044
Sack RO, Ghiorso MS, Wang M-S, Lipschutz ME (1994b) Igneous inclusions from ordinary chondrites: High temperature cumulates and a shock melt. J Geophys Res 99:26029-26044
Saikumar V, Goldstein JI (1988) An evaluation of the methods to determine the cooling rates of iron meteorites. Geochim Cosmochim Acta 52:715-726
Saito J, Takeda H (1989) Mineralogical study of LEW85328 ureilite. Lunar Planet Sci 20:938-939
Saito J, Takeda H (1990) Information of elemental distributions in heavily shocked ureilites as a guide to deduce the ureilite formation process. Lunar Planet Sci 21:1063-1064
Sanz HG, Burnett DS, Wasserburg GJ (1970) A precise $^{87}Rb/^{87}Sr$ age and initial $^{87}Sr/^{86}Sr$ for the Colomera iron meteorite. Geochim Cosmochim Acta 34:1227-1239
Schaudy R, Wasson JT, Buchwald VF (1972) The chemical classification of iron meteorites: VI. A reinvestigation of irons with Ge concentrations lower than 1 ppm. Icarus 17:174-192
Schmitt R, Laul JC (1973) A survey of the selenochemistry of major, minor, and trace elements. The Moon 8:182-209
Schnetzler CC, Philpotts JA (1969) Genesis of the calcium-rich achondrites in light of rare-earth and barium concentrations. *In* Meteorite Research (P.M. Millman, ed.), Reidel, Dordrecht, Holland, 206-216
Schultz L, Palme H, Spettel B, Weber HW, Wänke H, Christophe Michel-Levy M, Lorin JC (1982) Allan Hills A77081—An unusual stony meteorite. Earth Planet Sci Lett 61:23-31
Scott ERD (1972) Chemical fractionation in iron meteorites and its interpretation. Geochim Cosmochim Acta 36:1205-1236
Scott ERD (1977a) Composition, mineralogy and origin of Group IC iron meteorites. Earth Planet Sci Lett 37:273-284
Scott ERD (1977b) Pallasites—metal composition, classification and relationships with iron meteorites. Geochim Cosmochim Acta 41:349-360

Scott ERD (1977c) Geochemical relationship between some pallasites and iron meteorites. Mineral Mag 41:265-272
Scott ERD (1977d) Formation of olivine-metal textures in pallasite meteorites. Geochim Cosmochim Acta 41:693-710
Scott ERD (1979a) Origin of anomalous iron meteorites. Mineral Mag 43:415-421
Scott ERD (1979b) Origin of iron meteorites. *In* "Asteroids," editor T Gehrels. Tucson, AZ:Univ Ariz Press, p 892-921
Scott ERD (1982) Origin of rapidly solidified metal-troilite grains in chondrites and iron meteorites. Geochim Cosmochim Acta. 46:813-823
Scott ERD, Bild RW (1974) Structure and formation of the San Cristobal meteorite, other IB irons and group IIICD. Geochim Cosmochim Acta 38:1379-1391
Scott ERD, Clarke RS Jr (1979) Identification of clear taenite in meteorites as ordered FeNi. Nature 281:360-362
Scott ERD, Wasson JT (1975) Classification and properties of iron meteorites. Rev Geophys Space Phys 13:527-546
Scott ERD, Wasson JT (1976) Chemical classification of iron meteorites—VIII Groups IC, IIE, IIIF and 97 other irons. Geochim Cosmochim Acta 40:103-115
Scott ERD, Wasson JT, Buchwald VF (1973) The chemical classification of iron meteorites; VII, A reinvestigation of irons with Ge concentrations between 25 and 80 ppm. Geochim Cosmochim Acta 37:1957-1983
Scott ERD, Taylor GJ, Keil K (1993) Origin of ureilite meteorites and implications for planetary accretion. Geophys Res Lett 20:415-418
Scott ERD, Haack H, McCoy TJ (1996) Core crystallization and silicate-metal mixing in the parent body of the IVA iron and stony-iron meteorites. Geochim Cosmochim Acta 60:1615-1631
Sears DW (1980) Formation of E-chondrites and aubrites—A thermodynamic model. Icarus 43:184-202
Sellamuthu R, Goldstein JI (1985) Analysis of segregation trends observed in iron meteorites using measured distribution coefficients. Proc 15th Lunar Planet Sci Conf, J Geophys Res 90 (Suppl):C677-C688
Sexton A, Franchi IA, Pillinger CT (1996) Hammadah al Hamra 126—A new Saharan ureilite. Lunar Planet Sci 27, 1173-1174
Shearer CK, Fowler GW, Papike JJ (1997) Petrogenetic models for magmatism on the eucrite parent body: Evidence from orthopyroxene in diogenites. Meteoritics Planet Sci 32:877-889
Shen JJ, Papanastassiou DA, Wasserburg GJ (1996) Precise Re-Os determinations and systematics of iron meteorites. Geochim Cosmochim Acta 60:2887-2900
Sherman SB ,Treiman AH (1989) The olivine-fassaite liquidus: Experiments and implications for angrite achondrites and Ca-Al chondrules. Lunar Planet Sci 20:998-999
Shimaoka TK, Shinotsuka K, Ebihara M, Prinz M (1995) Whole rock compositions of aubritic meteorites: Implications for their origin. Lunar Planet Sci 26:1291-1292
Shukolyukov A, Lugmair GW (1993a) Live iron-60 in the early solar system. Science 259:1138-1142
Shukolyukov A, Lugmair GW (1993b) ^{60}Fe in eucrites. Earth Planet Sci Lett 119:159-166
Shukolyukov A, Lugmair GW (1997) The ^{53}Mn-^{53}Cr isotope system in the Omolon pallasite and the half-life of ^{187}Re . Lunar Planet Sci 28:1315-1316
Simpson AB (1982) Aspects of the composition and origin of achondrites and mesosiderites. PhD Dissertation, Univ Cape Town, 629 p
Simpson AB, Ahrens LH (1977) The chemical relationship between howardites and the silicate fraction of mesosiderites. *In* Comets, Asteroids, Meteorites—Interpretations, Evolution and Origins. AH Delsemme, ed., U. Toledo Press, 445-450
Smales AA, Mapper D, Webb MSW, Webster RK, Wilson J.D. (1970) Elemental composition of lunar surface material. Proc Apollo 11 Lunar Sci Conf:1575-1581
Smoliar MI (1993) A survey of Rb-Sr systematics of eucrites. Meteoritics 28:105-113
Spitz AH (1991) Trace element analysis of ureilite meteorites and implications for their petrogenesis. PhD dissertation, University of Arizona. 232 p
Spitz AH (1992) ICP-MS trace element analysis of ureilites: Evidence for mixing of distinct components. Lunar Planet Sci 23:1339-1340
Spitz AH, Boynton WV (1991) Trace element analysis of ureilites: New constraints on their petrogenesis. Geochim Cosmochim Acta 55:3417-3430
Spitz AH, Goodrich CA (1987) Rare earth element tests of ureilite petrogenesis models. Meteoritics 21:515-516
Spitz AH, Goodrich CA, Crozaz G, Lundberg L (1988) Ion microprobe search for the LREE host phase in ureilite meteorites. Lunar Planet Sci 19:1111-1112
Stauffer H (1961) Primordial argon and neon in carbonaceous chondrites and ureilites. Geochim

Cosmochim Acta 24:70-82
Steele IM, Smith JV (1976) Mineralogy of the Ibitira eucrite and comparison with other eucrites and lunar samples. Earth Planet Sci Lett 33:67-78
Steele IM, Olsen E, Pluth J, Davis- AM (1991) Occurrence and crystal structure of Ca-free beusite in the El Sampal IIIA iron meteorite. Am Mineral 76:1985-1989
Stewart BW, Papanastassiou DA, Wasserburg GJ (1994) Sm-Nd chronology and petrogenesis of mesosiderites. Geochim Cosmochim Acta 58:3487-3509
Stewart B, Papanastassiou DA, Wasserburg GJ (1996) Sm-Nd systematics of a silicate inclusion in the Caddo IAB iron meteorite. Earth Planet Sci Lett 143:1-12
Stolper E (1977) Experimental petrology of eucrite meteorites. Geochim Cosmochim Acta 41:587-611
Störzer D, Pellas P (1977) Angra dos Reis: Plutonium distribution and cooling history. Earth Planet Sci Lett 35:285-293
Swartzendruber LJ, Itkin VP, Alcock CB (1991) The Fe-Ni (iron-nickel) system. J Phase Equil 12:288-312
Swindle TD, Burkland MK, Kring DA (1993) Noble gases in the Brachinites Eagles Nest and LEW88763. Meteoritics 28:445-446
Swindle TD, Kring DA, Burkland MK, Hill DH, Boynton WV (1998) Noble gases, bulk chemistry, and petrography of olivine-rich achondrites Eagles Nest and Lewis Cliff 88763: Comparison to brachinites. Meteoritics Planet Sci 33:31-48
Tagai T, Sadanaga R, Takeuchi Y, Takeda H (1977) Twinning in tridymite from the Steinbach meteorite. Min. Journal 8:382-400
Takahashi K, Masuda A (1990a) The Rb-Sr and Sm-Nd dating and REE measurements of ureilites. Meteoritics 25:413
Takahashi K, Masuda A (1990b) Young ages of two diogenites and their genetic implications. Nature 343:540-542
Takeda H (1979) A layered-crust model of a howardite parent body. Icarus 40:455-470
Takeda H (1986) Mineralogy of Yamato 791073 with reference to crystal fractionation of the howardite parent body. Proc Lunar Planet Sci Conf 16th, Part 2; J Geophys Res 91:D355-D363
Takeda H (1987) Mineralogy of Antarctic ureilites and a working hypothesis for their origin and evolution. Earth Planet Sci Lett 81:358-370
Takeda H (1989) Mineralogy of coexisting pyroxenes in magnesian ureilites and their formation conditions. Earth Planet Sci Lett 93:181-194
Takeda H (1991) Comparisons of Antarctic and non-Antarctic achondrites and possible origin of the differences. Geochim Cosmochim Acta 55:35-47
Takeda H, Graham AL (1991) Degree of equilibration of eucritic pyroxenes and thermal metamorphism of the earliest planetary crust. Meteoritics 26:129-134
Takeda H, Mori H (1985) The diogenite-eucrite links and the crystallization history of a crust of their parent body. Proc Lunar Planet Sci Conf 15th, Part 2; J Geophys Res 90:C636-C648
Takeda H, Yanai K (1978) A thought on the ureilite parent body as inferred from pyroxenes in Yamato-Y74659. Proc 11:189-194, Lunar Planet Symp Tokyo, Inst Space Aeronaut Sci, Univ Tokyo
Takeda H, Miyamoto M, Ishii T, Reid AM (1976) Characterization of crust formation on a parent body of achondrites and the moon by pyroxene crystallography and chemistry. Proc Lunar Sci Conf 7:3535-3548
Takeda H, Miyamoto M, Duke MB, Ishii T (1978a) Crystallization of pyroxenes in lunar KREEP basalt 15386 and meteoritic basalts. Proc Lunar Planet Sci Conf 9:1157-1171
Takeda H, Miyamoto M, Yanai K, Haramura H (1978) A preliminary mineralogical examination of the Yamato-74 achondrites. Mem Natl Inst Polar Res (Japan) Spec Issue 8, 170-184
Takeda H, Miyamoto M, Ishii T, Yanai K, Matsumoto Y (1979a) Mineralogical examination of the Yamato-75 achondrites and their layered crust model. Mem Nat'l Inst Polar Res Spec Issue 12:82-108
Takeda H, Duke M, Ishii T, Haramura H, Yanai K (1979b) Some unique meteorites found in Antarctica and their relation to asteroids. Mem Nat'l Inst Polar Res Special Issue 15:54-73
Takeda H, Mori H, Yanai K (1981) Mineralogy of the Yamato diogenites as possible pieces of a single fall. Mem Natl Inst Polar Res Spec Issue No 20:81-99
Takeda H, Tachikawa O, Toyoda H (1986) Mineralogy of augite-bearing ureilites and some hypotheses on the origin of ureilites. Lunar Planet Sci 17:863-864
Takeda H, Mori H, Ogata H (1988a) On the pairing of Antarctic ureilites with reference to their parent body. Proc NIPR Symp Antarctic Meteorites 1:145-172
Takeda H, Mori H, Ogata H (1988b) Mineralogy of magnesian and calcic groups of ureilites and formation condition of ureilites. Lunar Planet Sci 19:1173-1174
Takeda H, Mori H, Ogata H (1989) Mineralogy of augite-bearing ureilites and the origin of their chemical trends. Meteoritics 24:73-81
Takeda H, Babi T, Mori H (1992) Mineralogy of a new orthopyroxene-bearing ureilite LEW88201 and the

relationship between magnesian ureilites and lodranites. Lunar Planet Sci 23:1403-1404
Takeda H, Baba T, Saiki K, Otsuki M, Ebihara M (1993) A plagioclase-augite inclusion in Caddo County: Low-temperature melt of primitive achondrites. Meteoritics, 28:447
Takeda H, Mori H, Hiroi T, Saito J (1994a) Mineralogy of new Antarctic achondrites with affinity to Lodran and a model of their evolution in an asteroid. Meteoritics 29:830-842
Takeda H, Yamaguchi A, Nyquist LE, Bogard DD (1994b) A mineralogical study of the proposed paired eucrites Y-792769 and Y-793164 with reference to cratering events on their parent body. Proc NIPR Symp Antarctic Meteorites 7:73-93
Takeda H, Mori H, Bogard DD (1994c) Mineralogy and ^{39}Ar-^{40}Ar age of an old pristine basalt: Thermal history of the HED parent body. Earth Planet Sci Lett 122:183-194
Takeda H, Yugami K, Bogard D, Miyamoto M (1997a) Plagioclase-augite-rich gabbro in the Caddo County IAB Iron and the missing basalts associated with iron meteorites. Lunar Planet Sci 28:1409-1410
Takeda H, Ishii T, Arai T, Miyamoto M (1997b) Mineralogy of the Asuka 87 and 88 eucrites and the crustal evolution of the HED parent body. Antarctic Meteorite Res 10:401-413
Tera F, Eugster O, Burnett DS, Wasserburg GJ (1970) Comparative study of Li, Na, K, Rb, Cs, Ca, Sr and Ba abundances in achondrites and in Apollo 11 lunar samples. Proc. Apollo 11 Lunar Sci Conf: 1637-1657
Tera F, Carlson RW, Boctor NZ (1997) Radiometric ages of basaltic achondrites and their relation to the early history of the solar system. Geochim Cosmochim Acta 61:1713-1731
Tomeoka K, Takeda H (1989) Fe-S-Ca-Al-bearing carbonaceous veins in the Yamato-74130 ureilite: Evidence for the genetic link to carbonaceous chondrites. Lunar Planet Sci 20:1120-1121
Torigoye N, Yamamoto K, Misawa K, Nakamura N (1993) Compositions of REE, K, Rb, Sr, Ba, Mg, Ca, Fe and Sr isotopes in Antarctic "unique" meteorites. Proc NIPR Symp Antarctic Meteorites 6:100-119
Torigoye-Kita N, Misawa K, Tatsumoto M (1995a) U-Th-Pb and Sm-Nd isotopic systematics of the Goalpara ureilite: resolution of terrestrial contamination. Geochim Cosmochim Acta 59:381-390
Torigoye-Kita N, Misawa K, Tatsumoto M (1995b) Reply to the Comment by CA Goodrich, GW Lugmair, MJ Drake, and PJ Patchett on "U-Th-Pb and Sm-Nd isotopic systematics of the Goalpara ureilite: resolution of terrestrial contamination". Geochim Cosmochim Acta 59:4087-4091
Torigiye-Kita N, Tatsumoto M, Meeker GP, Yanai K (1995c) The 4.56 Ga age of the MET 78008 ureilite. Geochim Cosmochim Acta 59:2319-2329
Toyoda H, Haga N, Tachikawa O, Takeda H, Ishii T (1986) Thermal history of ureilite, Pecora Escarpment 82506 deduced from cation distribution and diffusion profile of minerals. Mem Nat'l Inst Polar Res Spec Issue 41:206-221
Treiman AH (1988) Angra dos Reis is not a cumulate igneous rock. Lunar Planet Sci 19:1203-1204
Treiman AH (1989) An alternate hypothesis for the origin of Angra dos Reis: Porphyry, not cumulate. Proc Lunar Planet Sci Conf 19:443-450
Treiman AH (1997) The parent magmas of the cumulate eucrites: A mass balance approach. Meteoritics Planet Sci 32:217-230
Treiman AH, Berkley JL (1994) Igneous petrology of the new ureilites Nova 001 and Nullarbor 010. Meteoritics 29:843-848
Treiman AH, Drake MJ, Janssens M-J, Wolf R, Ebihara M (1986) Core formation in the Earth and Shergottite Parent Body (SPB): Chemical evidence from basalts. Geochim Cosmochim Acta 50: 1071-1091
Treiman AH, Jones JH, Janssens M-J, Wolf R, Ebihara M (1988) Angra dos Reis: Complex silicate fractionations. Meteoritics 23:305-306
Ulff-Møller F, Rasmussen KL, Prinz M, Palme H, Spettel B, Kallemeyn GW (1995) Magmatic activity on the IVA parent body: Evidence from silicate-bearing iron meteorites. Geochim Cosmochim Acta 59:4713-4728
Ulff-Møller F, Tran J, Choi B-G, Haag R, Rubin AE, Wasson JT (1997) Esquel: Implications for pallasite formation processes based on the petrography of a large slab. Lunar Planet Sci 28:1465-1466
Ulff-Moller F (1998) Effects of liquid immiscibility on trace element fractionation in magmatic iron meteorites: A case study of group IIIAB. Meteoritics Planet Sci 33:207-220
Ulff-Moller F, Choi B-G, Rubin AE, Tran J, Wasson JT (1998) Paucity of sulfide in a large slab of Esquel: New perspectives on pallasite formation. Meteoritics Planet Sci 33:221-227
Van Schmus WR, Ribbe PH (1968) The composition and structural state of feldspar from chondritic meteorites. Geochim Cosmochim Acta 32:1327-1342
Van Schmus WR, Wood JA (1967) A chemical-petrologic classification for the chondritic meteorites. Geochim Cosmochim Acta 31:747-765
Vdovykin GP (1970) Ureilites. Space Sci Rev 10:483-510
Vogel R, Heumann T (1941) Das System Eisen-Eisensulfid-Kalziumsulfid. Archiv Eisenhüttenw 15:195-

199
Voshage H (1967) Bestrahlungsalter und Herkunft der Eisenmeteorite. Z Naturforsch 22a:477-506
Voshage H, Feldmann H (1979) Investigations on cosmic-ray-produced nuclides in iron meteorites; 3, Exposure ages, meteoroid sizes and sample depths determined by mass spectrometric analyses of potassium and rare gases. Earth Planet Sci Lett 45:293-308
Wacker J (1986) Noble gases in the diamond-free ureilite, ALHA78019: The roles of shock and nebular processes. Geochim Cosmochim Acta 50:633-642
Wadhwa M, Shukolyukov A, Lugmair GW (1998) ^{53}Mn-^{53}Cr systematics in Brachina: A record of one of the earliest phases of igneous activity on an asteroid. Lunar Planet Sci 29:1480
Wahl W (1952) The brecciated stony meteorites and meteorites containing foreign fragments. Geochim Cosmochim Acta 2:91.117
Wai CM, Wasson JT (1977) Nebular condensation of moderately volatile elements and their abundances in ordinary chondrites. Earth Planet Sci Lett 36:1-13
Wai CM, Wasson JT (1979) Nebular condensation of Ga, Ge and Sb and the chemical classification of iron meteorites. Nature 282:790-793
Walker D, Grove T (1993) Ureilite smelting. Meteoritics 28:629-636
Wänke H, Baddenhausen H, Spettel B, Teschke F, Quijano-Rico M, Dreibus G, Palme H (1972a) The chemistry of the Haverö ureilite. Meteoritics 7:579-590
Wänke H, Baddenhausen H, Balacescu A, Teschke F, Spettel B, Dreibus G, Palme H, Quijano-Rico M, Kruse H, Wlotzka F, Begemann F (1972b) Multielement analyses of lunar samples and some implications of the results. Proc Lunar Sci Conf 3rd:1251-1268
Wänke H, Baddenhausen H, Dreibus G, Jagoutz E, Kruse H, Palme H, Spettel B, Teschke F (1973) Multielement analyses of Apollo 15, 16 and 17 samples and the bulk composition of the moon. Proc 4th Lunar Sci Conf Geochim Cosmochim Acta Suppl 4:1461-1481
Wänke H, Baddenhausen H, Blum K, Cendales M, Dreibus G, Hofmeister H, Kruse H, Jagoutz E, Palme C, Spettel B, Thacker R, Vilcsek E (1977) On the chemistry of lunar samples and achondrites. Primary matter in the lunar highlands: A re-evaluation. Proc Lunar Sci Conf 8:2191-2213
Warren PH (1987) Mars regolith vs. SNC meteorites: Possible evidence for abundant crustal carbonates. Icarus 70:153-161
Warren PH (1997) Magnesium oxide-iron oxide mass balance constraints and a more detailed model for the relationship between eucrites and diogenites. Meteoritics Planet Sci 32:945-963
Warren PH, Davis AM (1995) Consortium investigation of the Asuka-881371 angrite: Petrographic, electron microprobe, and ion microprobe observations. Antarc Meteorites 20:257-260
Warren PH, Jerde EA (1987) Composition and origin of Nuevo Laredo trend eucrites. Geochim Cosmochim Acta 51:713-725
Warren PH, Kallemeyn GW (1989a) Allan Hills 84025: The second Brachinite, far more differentiated than Brachina, and an ultramafic achondritic clast from L chondrite Yamato 75097. Proc Lunar Planet Sci Conf 19:475-486
Warren PH, Kallemeyn GW (1989b) Geochemistry of polymict ureilite EET83309: and a partially-disruptive impact model for ureilite origin. Meteoritics 24:233-246
Warren PH, Kallemeyn GW (1991) Geochemistry of unique achondrite MAC88177: Comparison with polymict ureilite EET87720 and "normal" ureilites. Lunar Planet Sci 22:1467-1468
Warren PH, Kallemeyn GW (1992) Explosive volcanism and the graphite-oxygen fugacity buffer on the parent asteroid(s) of the ureilite meteorites. Icarus 100:110-126
Warren PH, Kallemeyn GW (1994) Petrology of LEW88774: An extremely Chromium-rich ureilite. Lunar Planet Sci 25:1465-1466
Warren PH, Jerde EA, Migdisova LF, Yaroshevsky AA (1990) Pomozdino: An anomalous, high-MgO/FeO, yet REE-rich eucrite. Proc Lunar Planet Sci Conf 20:281-297
Warren PH, Kallemeyn GW, Mayeda T (1995) Consortium investigation of the Asuka-881371 angrite: Bulk-rock geochemistry and oxygen-isotopes. Antarc Meteorites 20:261-264
Warren PH, Kallemeyn GW, Arai T, Kaneda K (1996) Compositional-petrologic investigations of eucrites and the QUE94201 shergottite. Antarctic Meteorites 21:195-197
Wasserburg GJ, Sanz HG, Bence AE (1968) Potassium-feldspar phenocrysts in the surface of Colomera, an iron meteorite. Science 161:684-687
Wasserburg GJ, Tera F, Papanastassiou DA, Huneke JC (1977) Isotopic and chemical investigations on Angra dos Reis. Earth Planet Sci Lett 35:294-316
Wasson JT (1967) The chemical classification of iron meteorites; I, A study of iron meteorites with low concentrations of gallium, germanium. Geochim Cosmochim Acta 31:161-180
Wasson JT (1969) The chemical classification of iron meteorites; III, Hexahedrites and other irons with germanium concentrations between 80 and 200 ppm. Geochim Cosmochim Acta 33:179-198
Wasson JT (1970) The chemical classification of iron meteorites; IV, Irons with Ge concentrations greater

than 190 ppm and other meteorites associated with group I. Icarus 12:407-423
Wasson JT (1972) Parent-body models for the formation of iron meteorites. Proc Intl Geol Cong 24: 161-168
Wasson JT (1974) Meteorites: Classification and Properties. Berlin and New York: Springer-Verlag, 316 p
Wasson JT (1985) Meteorites. Their Record of Early Solar-System History. New York: WH Freeman, 267 p
Wasson JT (1990) Ungrouped iron meteorites in Antarctica; origin of anomalously high abundance. Science 249:900-902
Wasson JT, Chapman CR (1996) Space weathering of basalt-covered asteroids: Vesta an unlikely source of the HED meteorites. *In* Workshop on Evolution of Igneous Asteroids: Focus on Vesta and the HED Meteorites, Mittlefehldt DW, Papike JJ, eds., LPI Tech Report 96-02, Part 1, 38-39
Wasson JT, Choi B-G, Jerde EA, Ulff-Moller F (1998a) Chemical classification of iron meteorites: XII. New members of the magmatic group. Geochim Cosmochim Acta 62:715-724
Wasson JT, Jerde E, Choi B-G, Ulff-Moller F (1998b) Chemical classification of iron meteorites: XIII. New ungrouped irons and members of the nonmagmatic groups. Geochim Cosmochim Acta 62, in press
Wasson JT, Kimberlin J (1967) The chemical classification of iron meteorites; II, Irons and pallasites with germanium concentrations between 8 and 100 ppm. Geochim Cosmochim Acta 31:149-178
Wasson JT, Rubin AE (1985) Formation of mesosiderites by low-velocity impacts as a natural consequence of planet formation. Nature 318:168-170
Wasson JT, Schaudy R (1971) The chemical classification of iron meteorites; V, Groups IIC and IIID and other irons with germanium concentrations between 1 and 25ppm. Icarus 14:59-70
Wasson JT, Wai CM (1970) Composition of the metal, schreibersite and perryite of enstatite achondrites and the origin of enstatite chondrites and achondrites. Geochim Cosmochim Acta 34:169-184
Wasson JT, Wai CM (1976) Explanation for the very low Ga and Ge concentrations in some iron meteorite groups. Nature 261:114-116
Wasson JT, Wang J (1986) A nonmagmatic origin of group-IIE iron meteorites. Geochim Cosmochim Acta 50:725-732
Wasson JT, Wetherill GW (1979) Dynamical, chemical and isotopic evidence regarding the formation locations of asteroids and meteorites. *In* Asteroids, T. Gehrels (ed) Univ Arizona Press, p 926-974
Wasson, JT, Schaudy R, Bild RW, Chou C-L (1974) Mesosiderites-I. Compositions of their metallic portions and possible relationship to other metal-rich meteorite groups. Geochim Cosmochim Acta 38:135-149
Wasson, JT, Chou C-L, Bild RW, Baedecker PA (1976) Classification of and elemental fractionation among ureilites. Geochim Cosmochim Acta 40:1449-1458
Wasson JT, Willis J, Wai CM, Kracher A (1980) Origin of iron meteorite groups IAB and IIICD. Z Naturforsch 35a:781-795
Wasson JT, Ouyang Xinwei, Jerde E (1989) Chemical classification of iron meteorites; XI, Multi-element studies of 38 new irons and the high abundance of ungrouped irons from Antarctica. Geochim Cosmochim Acta 53:735-744
Watters TR, Prinz M (1979) Aubrites: Their origin and relationship to enstatite chondrites. Proc Lunar Planet Sci Conf 10:1073-1093
Weber D, Bischoff A (1996) New meteorite finds from the Libyan Sahara. Lunar Planet Sci 27:1393-1394
Weber I, Bischoff A (1998) Mineralogy and chemistry of the ureilites Hammadah Al Hamra 064 and Jalanash. Lunar Planet Sci 29:1365
Weber HW, Hintenberger H, Begemann F (1971) Noble gases in the Haverö ureilite. Earth Planet Sci Lett 13:205-209
Weber, HW, Begemann F, Hintenberger H (1976) Primordial gases in graphite-diamond-kamacite inclusions from the Haverö ureilite. Earth Planet Sci Lett 29:81-90
Weigel A, Eugster O, Koeberl C and Krähenbühl U (1996) Primitive differentiated achondrite Divnoe and its relationship to brachinites. Lunar Planet Sci 27:1403-1404
Welten KC, Lindner L, van der Borg K, Loeken T, Scherer P, Schultz L (1997) Cosmic-ray exposure ages of diogenites and the recent collisional history of the howardite, eucrite and diogenite parent body/bodies. Meteoritics Planet Sci 32:891-902
Wheelock MM, Keil K, Floss C, Taylor GJ, Crozaz G (1994) REE geochemistry of oldhamite-dominated clasts from the Norton County aubrite: Igneous origin of oldhamite. Geochim Cosmochim Acta 58:449-458
Wiik HB (1969) On regular discontinuities in the composition of meteorites. Soc Fennica Commentationes Phys-Math 34:135-145
Wiik HB (1972) The chemical composition of the Haverö meteorite and the genesis of the ureilites. Meteoritics 7:553-557

Wilkening LL (1973) Foreign inclusions in stony meteorites-I. Carbonaceous chondrite xenoliths in the Kapoeta howardite. Geochim Cosmochim Acta 37:1985-1989
Wilkening LL (1976) Carbonaceous chondritic xenoliths and planetary-type noble gases in gas-rich meteorites. Proc Lunar Sci Conf 7:3549-3559
Wilkening LL, Anders E (1975) Some studies of an unusual eucrite: Ibitira. Geochim Cosmochim Acta 39:1205-1210
Wilkening LL, Marti K (1976) Rare gases and fossil particle tracks in the Kenna ureilite. Geochim Cosmochim Acta 40:1465-1473
Willis J (1980) The bulk composition of iron meteorite parent bodies. PhD Dissertation, University of California at Los Angeles, 208 p
Willis J, Goldstein JI (1982) The effects of C, P, and S on trace element partitioning during solidification in Fe-Ni alloys. Proc 13th Lunar Planet Sci Conf, J Geophys Res 87 (Suppl):A435-A445
Wilson L, Keil K (1991) Consequences of explosive eruptions on small solar system bodies: The case of the missing basalts from the aubrite parent body. Earth Planet Sci Lett 104:505-512
Wlotzka F (1993) Meteoritical Bulletin, No. 75, 1993 December. Meteoritics 28:692-703
Wlotzka F (1994) Meteoritical Bulletin, No. 77, 1994 November. Meteoritics 29:891-897
Wlotzka F, Jarosewich E (1977) Mineralogical and chemical compositions of silicate inclusions in the El Taco, Camp del Cielo, iron meteorite. Smithsonian Contrib Earth Sci 19:104-125
Wlotzka F, Palme H, Spettel B, Wänke H, Jarosewich E, Noonan AF (1983) Alkali differentiation in LL-chondrites. Geochim Cosmochim Acta 47:743-757
Wood JA (1964) The cooling rates and parent planets of several iron meteorites. Icarus 3:429-459
Wood JA (1981) On the nature of the pallasite parent body: Midcourse corrections. Lunar Planet Sci 12:1200-1202
Wood JA, Pellas P (1991) What heated the meteorite planets? *In* The Sun in Time, CP Sonnet, MS Giampapa, MS Matthews (eds) Univ Arizona, 740-760
Xue S, Herzog GF, Souzis A, Ervin MH, Lareau RT, Middleton R, Klein J (1995) Stable magnesium isotopes, ^{26}Al, ^{10}Be, and ^{26}Mg/^{26}Al exposure ages of iron meteorites. Earth Planet Sci Lett 136:397-406
Yajima H, Matsuda J (1989) Further study on noble gases in shock-produced diamonds. Mass Spect 37:331-342
Yamaguchi A, Takeda H, Bogard DD, Garrison D (1994) Textural variations and impact history of the Millillillie eucrite. Meteoritics 29:237-245
Yamaguchi A, Taylor GJ, Keil K (1996) Global crustal metemorphism of the eucrite parent body. Icarus 124:97-112
Yamaguchi A, Taylor GJ, Keil K (1997) Metemorphic history of the eucritic crust of 4 Vesta. J Geophys Res 102:13381-13386
Yanai K (1994) Angrite Asuka-881371: Preliminary examination of a unique meteorite in the Japanese collection of antarctic meteorites. Proc NIPR Symp Antarc Meteorites 7:30-41
Yanai K, Kojima H (1984) Meteorites News. National Institute of Polar Research, Tokyo, Japan. 58 p
Yanai K, Kojima H (1987) Photographic Catalog of the Antarctic Meteorites. National Institute of Polar Research, Tokyo, Japan. 298 p
Yanai K, Kojima H (1991) Yamato-74063: Chondritic meteorite classified between E and H chondrite groups. Proc NIPR Symp Antarctic Meteorites 4:118-130
Yanai K, Kojima H (1993) General features of some unique inclusions in Yamato ordinary chondrites. Papers Presented to the 18th Symp Antarctic Meteorites, 57-60
Yanai K, Kojima H (1995a) Yamato-8451: A newly identified pyroxene-bearing pallasite. Proc NIPR Symp Antarctic Meteorites 8:1-10
Yanai K, Kojima H (1995b) Catalog of Antarctic Meteorites. National Institute of Polar Research Tokyo, Japan
Yanai K, Matsumoto Y, Kojima H (1983) A Brachina-like inclusion in the Yamato-75097 L6 chondrite: A preliminary examination. Mem Nat'l Inst Polar Spec Issue 30:29-35
Yang C-W, Williams DB, Goldstein JI (1996) A revision of the Fe-Ni phase diagram at low temperatures (<400°C). J Phase Equilibria 17:522-531
Yang C-W, Williams DB, Goldstein JI (1997a) A new empirical cooling rate indicator for meteorites based on the size of the cloudy zone of the metallic phases. Meteoritics Planet Sci 32:423-429
Yang C-W, Williams DB, Goldstein JI (1997b) Low-temperature phase decomposition in metal from iron, stony-iron and stony meteorites. Geochim Cosmochim Acta 61:2943-2956
Yugami K, Miyamoto M, Takeda H, Hiroi T (1993) Mineralogy of ALH81187: A partly reduced acapulcoite. Papers Presented to the 18th Symp Antarctic Meteorites, 34-37
Yugami K, Takeda H, Kojima H, Miyamoto M (1997) Modal abundances of primitive achondrites and the endmember mineral assemblage of the differentiation trend. Papers presented to the 22nd Symp Antarctic Meteorites, 220-222

Yugami K, Takeda H, Kojima H and Miyamoto M (1996) Mineralogy of the new primitive achondrites Y8005 and Y8307 and their differentiation from chondritic materials. Papers presented to the 21st Symp Antarctic Meteorites, 216-218
Zhou Y, Steele IM (1993) Chemical zoning and diffusion of Ca, Al, Mn, and Cr in olivine of Springwater pallasite. Lunar Planet Sci 24:1573-1574
Zipfel J, Palme H (1993) Chemical composition of new acapulcoites and lodranites. Lunar Planet Sci 24:1579-1580
Zipfel J, Palme H, Kennedy AK, Hutcheon ID (1995) Chemical composition and origin of the Acapulco meteorite. Geochim Cosmochim Acta 59:3607-3627
Zolensky ME, Hewins RH, Mittlefehldt DW, Lindstrom MM, Xiao X, Lipschutz ME (1992) Mineralogy, petrology and geochemistry of carbonaceous chondritic clasts in the LEW 85300 polymict eucrite. Meteoritics 27:596-604
Zolensky ME, Weisberg MK, Buchanan PC, Mittlefehldt DW (1996) Mineralogy of carbonaceous chondrite clasts in HED achondrites and the moon. Meteoritics Planet Sci 31:518-537